The Impact of Spatial Variability of Precipitation on the Predictive Uncertainty of Hydrological Models

Von der Fakultät Bauingenieur- und Vermessungswesen der Universität Stuttgart
zur Erlangung der Würde eines Doktor-Ingenieurs (Dr.-Ing.)
genehmigte Abhandlung

Vorgelegt von
Tapash Das
aus Khantura, India

Hauptberichter: Prof. Dr. rer. nat. Dr.-Ing. András Bárdossy
Mitberichter: Prof. Dr.-Ing. Gerd H. Schmitz

Tag der mündlichen Prüfung: 20. November 2006

Institut für Wasserbau der Universität Stuttgart
Stuttgart 2006

Heft 154

The Impact of Spatial Variability of Precipitation on the Predictive Uncertainty of Hydrological Models

von
Dr.-Ing.
Tapash Das

Eigenverlag des Instituts für Wasserbau der Universität Stuttgart

D93 The Impact of Spatial Variability of Precipitation on the Predictive Uncertainty of Hydrological Models

CIP-Titelaufnahme der Deutschen Bibliothek

Das, Tapash:
The Impact of Spatial Variability of Precipitation on the Predictive Uncertainty of Hydrological Models / von Tapash Das. Institut für Wasserbau, Universität Stuttgart. – Stuttgart: Inst. für Wasserbau, 2006
(Mitteilungen / Institut für Wasserbau, Universität Stuttgart: H. 154)
Zugl.: Stuttgart, Univ., Diss., 2006
ISBN 3-933761-57-3
NE: Institut für Wasserbau <Stuttgart>: Mitteilungen

Gegen Vervielfältigung und Übersetzung bestehen keine Einwände, es wird lediglich um Quellenangabe gebeten.

Herausgegeben: 2006 vom Eigenverlag des Instituts für Wasserbau
Druck: Sprint-Digital-Druck GmbH, Stuttgart

Acknowledgment

This work was done as a doctoral student within the International Doctoral Program "Environment Water" (ENWAT), Universität Stuttgart and was supported by a scholarship program (IPSWaT) initiated by the German Federal Ministry of Education and Research (BMBF) which is gratefully acknowledged and I feel honored for the same.

First of all, I wish to express my deepest appreciation to Professor András Bárdossy, who accepted me as his doctoral student and provided me a precious opportunity to work on some of the most interesting problems in the area of Hydrology. In my endeavor for this work, I have been scrupulously trained by him, for which I am truly fortunate. Every discussion that I had with him has always been a pleasure, enlightening and educative, considering his wide knowledge and expertise in the subject. His enthusiasm and integral view on research has made a deep impression on me. This thesis would not have been what it is now but for his invaluable guidance, support, discussions and critical evaluation at each and every stage of my progress. I also express my sincere gratitude to Professor Gerd H. Schmitz for his willingness to co-supervise my work. The discussions that I had with him have been quite useful for successful completion of my work.

I would like to take this opportunity to thank Professor Erwin Zehe for his continuous supports in many aspects of research, fruitful discussions and continuous encouragement. I would also like to thank Dr.-Ing. Yeshewatesfa Hundecha Hipra, Dr.- Ing. Greta Moretti and Dr. S. J. Birkinshaw for their helpful discussions. Of course, this endeavor would not have been possible without the help of other colleagues and friends like, Jens Götzinger, Pawan Kumar Thapa, Jürgen Brommundt, Wei Hu, Sachin Patil, Yi He, Eloise Byrne and Jeff Tuhtan, as well as all other colleagues in our group and in the Institute of Hydraulic Engineering who helped me directly or indirectly in the course of my journey to complete this work. I would like to extend my heartfelt thanks to my colleague Ferdinand Beck for taking the pain to write the German version of the summary of my work. I would also like to acknowledge Krista Uhrmann and Andrea Bange for their always being very helpful. I also express my sincere thanks to Dr.-Ing. Arne Färber for providing warm working atmosphere and continuous supports through out my stay.

Finally, I am extremely grateful to my beloved parents, brothers, sisters and my wife who have always been a source of constant support and encouragement. I want to specially thank my brother, Palash and my wife, Mou for their moral support during hard days.

Table of contents

List of Figures

List of Tables

Abstract

Water is a precious natural resource which is vital for life, the health of people and the ecosystem and a basic requirement for the development of a country; and at the same time, the judicious management of water poses a complex situation. This complexity has further increased on account to the possible impacts due to projected climate change. Floods are the most dangerous hydrological phenomena, causing a considerable loss of human life and huge property damages every year throughout the world. Nearly one third of natural catastrophes belong to floods. The modern water resources management, no matter whether interested in the origin of the water, in its consumption, its use, or even in the possible consequences of human activity on the water cycle, can not neglect the new potentialities issued from the fast developing mathematical models. Hydrological models are simplified representations of a part of the hydrologic cycle. The estimation and representation of the input precipitation in hydrological models are crucial. Precipitation is governed by complicated physical processes which are inherently nonlinear and extremely sensitive. Precipitation is often significantly variable in space and time within a catchment. Indeed, the estimation of precipitation is very important in rainfall-runoff modeling since no model, however well founded in physical theory or empirically justified by past performance, will be able to predict adequate hydrographs if the model inputs do not characterize the rainfall inputs. The main aim of this dissertation was to investigate and quantify the impact of spatial variability of precipitation on the predictive uncertainty of hydrological model simulations. Given the importance to the role of the precipitation input in hydrological applications, the following research questions were addressed: (a) how does the spatial variability of precipitation influence the hydrological simulation results? (b) will a higher spatial resolution of model input data necessarily lead to a better model performance? (c) what is the impact on the simulated hydrographs of interpolated precipitation at different spatial resolutions through varying raingauge networks? (d) what is the benefit of using conditionally-simulated precipitation in hydrological modeling? (e) how does uncertainty in precipitation affect parameter identification of a conceptual model?

The modified rainfall-runoff model HBV was applied to investigate majority of the objectives. Based on the HBV model concept, four different structures namely, fully-lumped, semi-lumped, semi-distributed and distributed were developed. The main differences among the model structures lies on the scale of representation of forcing meteorological variables, the scale of different processes calculation and the scale of parameterization. The physically-based spatially-distributed modeling system SHETRAN was also used to investigate how does uncertainty in precipitation affect parameter identification of a conceptual model? The upper Neckar catchment (up to gauge

Plochingen, Neckar; approximately 4000 km^2), located in south-wast Germany, was selected as test catchment.

A number of simulation experiments were carried out in line with the objectives and scope of this study. The study aimed to investigate the influence of spatial variability of precipitation in a rainfall-runoff model indicated no significant differences in the model performance when the model was run using averaged precipitation at different spatial scales. However, there was clear deterioration in the model performance during the summer season. The results also highlights that there can be a significant deterioration in the model performance when the model calibrated using detailed precipitation is run using relatively less detailed input precipitation. When the level of main forcing precipitation input is different for the model simulation than that used for calibration, one should be cautious.

The study on the comparison of modeling performance using different representations of spatial variability indicates that for the present study catchment semi-distributed and semi-lumped model structures of the HBV model out-performs the distributed and fully-lumped model structures for the given level of information. The results highlight that using interpolated precipitation on finer resolution does not improve the simulation accuracy in either the calibration or validation periods at the subcatchments' outlets. Perhaps there is a higher compensation for the bias in the precipitation input over the calibration period for the relatively simple model structures. Also the error in representing spatial variability of precipitation in finer resolution is more and perhaps, dominating the bias compensation in the precipitation input by the calibration procedure for the distributed model structure, even with the scope of large number of parameters to be adjusted.

The study related to assess the impacts of raingauge density on the simulation results showed that the number and spatial distribution of raingauges affect the simulation results. It was found that the model performances worsen radically with an excessive reduction of raingauges. However, the performances were not significantly improved by increasing the number of raingauges more than a certain threshold number. The analysis also indicates that models using different raingauge networks might need their parameters recalibrated. Specifically, models calibrated with dense input precipitation information fail when run with sparse information. However, the models calibrated with sparse input precipitation information can perform well when run with dense information. Also the model calibrated with complete set of observed precipitation and being run with incomplete observed precipitation data in associated with the data estimated at the locations with missing measurements using multiple linear regression technique, performed well. This result offers an encouraging perspective for the implementation of such a procedure for an operational flood forecasting system.

Conditional spatial rainfall simulation indicates significantly more spatial variability in the simulated rainfall than the interpolated rainfall. The model performs better for modeling the peak discharges using conditionally-simulated rainfall than the model using interpolated rainfall. Thus conditional rainfall simulation is reasonable for flood modeling. Application of copulas for rainfall simulation was very encouraging. Non-Gaussian copulas can be used to generate conditionally-simulated rainfall as an alternative of the Gaussian copula. The analysis also indicates that inadequate representation of spatial variability of precipitation in modeling is partly responsible for modeling errors and also this leads to the problems in parameter estimation of a conceptual hydrological model. Thus spatial variability must be captured and used as an input to the hydrological model in order to eliminate the errors due to input rainfall data.

Kurzfassung

Einführung

Wasser ist eine wertvolle natürliche Ressource. Es ist die Grundlage des Lebens, der Gesundheit von Menschen und Ökosystemen und eine Grundbedingung für die wirtschaftliche Entwicklung eines Landes. Das vernünftige Haushalten mit der Ressource Wasser ist jedoch eine komplexe Aufgabe – und die Komplexität hat zugenommen durch die möglichen Folgen des prognostizierten Klimawandels. Es ist wahrscheinlich, dass der Wasserkreislauf sich durch den Klimawandel verändern wird (Stehlik und Bárdossy, 2000; Dibike und Coulibaly, 2005; Merritt et al., 2006). Die globalen Auswirkungen des menschlichen Handels wirken sich zusätzlich auf diese Entwicklung aus und werden die Probleme verstärken. Aus dem Wasserkreislauf ergeben sich schwierige Aufgaben; die Herausforderung, diese zu lösen, wird immer größer. Hochwasserereignisse sind das gefährlichste hydrologische Phänomen, dem jedes Jahr überall auf der Welt eine erhebliche Zahl an Menschen zu Opfer fallen und durch das sehr große Schäden zu beklagen sind. Fast ein Drittel aller Naturkatastrophen gehören zur Kategorie Hochwasser. Auch in Europe treten katastrophale Ereignisse immer häufiger auf. Vor allem in den letzten Jahren ereigneten sich auf den großen europäischen Flüssen einige Hochwasser. Die meisten Hochwasser sind das Ergebnis außergewöhnlicher meteorologischer Ereignisse wie außergewöhnlich intensiver und/oder außergewöhnlich langer Niederschläge. Vom Flood-Routing bis zur Regelung des Niedrigwasserabflusses, vom wachsenden Wasserbedarf der Industrie bis zur Überwachung der ökologischen Eigenschaften des Trinkwassers ist die nachhaltige Bewirtschaftung der knappen Ressource Wasser eines der Hauptprobleme des 21. Jahrhunderts.

Die moderne Wasserwirtschaft, egal ob sie sich für die Vorkommen des Wassers interessiert oder den Verbrauch oder gar für die möglichen Effekte menschlicher Eingriffe in den Wasserkreislauf, kann die neuen Möglichkeiten nicht vernachlässigen, die sich aus der schnellen Entwicklung mathematischer Modelle ergeben haben. Hydrologische Modelle sind vereinfachte Repräsentationen eines Teils des Wasserkreislaufs. Sie dienen einer Reihe verschiedener Ziele, werden aber vor allem zur hydrologischen Vorhersage eingesetzt und dafür, hydrologische Prozesse zu untersuchen und zu verstehen. Entscheidend für ein hydrologisches Modell ist die richtige Abschätzung und Abbildung des Modellinputs Niederschlag. Die Niederschlagsbildung wird von sehr komplexen physikalischen Prozessen bestimmt, die von Natur aus nichtlinear sind und sehr stark auf Veränderungen reagieren (Bárdossy und Plate, 1992). Niederschlag ist innerhalb eines Flusseinzugsgebiets zeitlich und räumlich sehr variabel und die richtige Abschätzung des Niederschlags ist sehr wichtig für die Niederschlags-Abfluss-Modellierung in hydrologischen

Modellen. Denn kein Modell, wie gut es auch immer in der physikalischen Theorie begründet ist und wie verlässlich es auch aufgrund der bisherigen Modellgüte zu sein scheint, kann präzise Vorhersagen der Abflussganglinie erzeugen, wen der Modellinput den Niederschlag nicht richtig abbildet (Beven, 2001). Darum ist die Zielsetzung dieser Dissertation zu untersuchen, wie sich die räumliche Variabilität des Niederschlags auf die Vorhersageunsicherheit hydrologischer Modelle auswirkt.

Aufgrund der beschriebenen Bedeutung, die der Niederschlag als Input für hydrologische Anwendungen hat, werden folgende Fragestellungen untersucht:

a. Wie beeinflusst die räumliche Variabilität des Niederschlags die Ergebnisse hydrologischer Simulierung?

b. Welchen Einfluss hat eine Variation des Messstationen Netzwerks bei der Interpolation des Niederschlags auf verschiedenen räumlichen Skalen auf simulierte Hydrographen?

c. Welchen Nutzen bietet die Verwendung bedingter Niederschlagssimulation in hydrologischer Modellierung?

d. Wird eine höhere räumliche Auflösung der Input-Daten eines Modells zwingender Weise zu einer besseren Modelleistung führen?

Die Hauptzielsetzung der Arbeit ist es, die genannten Fragestellungen zu beantworten. Weitere Ziele sind: (1) die Verlässlichkeit von Parametrisierungen zu untersuchen, die aus einer Kalibrierung mit Input Daten resultieren, die sich von den Daten unterscheiden, die im Modell verwendet werden. (2) die Unsicherheit zu analysieren, die sich aus den hydrologischen Parametern ergibt und die Abhängigkeit der Parameter untereinander zu identifizieren.

Die Mehrzahl der Fragestellung wurde anhand einer modifizierten Version des HBV Niederschlag-Abfluss Modells untersucht. Das HBV Modell beinhaltet konzeptionelle Routinen, um Schneeakkumulation und Schneeschmelze, Bodenfeuchtigkeit und Abflussgenerierung, die Abflusskonzentration im Untereinzugsgebiet und die Ganglinien des Abfluss im Flussnetz zu simulieren. Die Routine zur Schneeberechnung verfolgt den Grad-Tag-Ansatz. Die momentane Bodenfeuchtigkeit wird unter Berücksichtigung von Niederschlag und Evapotranspiration berechnet. Die Abflussgenerierung wird mit einer nicht-linearen Funktion der momentanen Bodenfeuchte und des Niederschlags berechnet. Die Dynamik der verschiedenen Abflusskomponenten auf der Raumskala des Untereinzugsgebiets wird konzeptionell mit zwei linearen Speichern repräsentiert. Basierend auf dem HBV Modellkonzept wurden vier verschiedene Strukturen entwickelt, das räumlich aggregierte, das halb-aggregierte, das halb-verteilte und das verteilte Model. Der Hauptunterschied zwischen den Modellstrukturen liegt in der maßgebenden Raumskala der Repräsentierung des Niederschlagsinputs.

Für eine Fragestellung wurde das physikalisch basierte, räumlich-verteilte Modellsystem SHETRAN verwendet. SHETRAN ist ein 3D finite Differenzen Modell mit Oberflächen/Untergrund Kopplung für Abfluss, Sedimenttransport verschiedener Korngrößen und dem Transport mehrerer löslicher reaktiver Substanzen im Einzugsgebiet. SHETRAN repräsentiert physikalische Prozesse anhand der physikalischen Gesetze, die auf ein 3D finite Differenzen Netz angepasst sind. In dieser Arbeit wird die Komponente zur Abflussberechnung des SHETRAN Model Systems verwendet (Version 4.3).

Die Arbeit dieser Dissertation hat ihren Fokus auf dem oberen Neckareinzugsgebiet (bis zum Pegel Plochingen, rund 4000 km^2).

Simulationsexperimente

Es wurde eine Vielzahl von Simulationsexperimenten durchgeführt, um die genannten Fragestellungen zu klären. Die angewandten Methoden und die erzielten Ergebnisse werden in den folgenden Abschnitten vorgestellt.

Das Kapitel 4 der Arbeit widmet sich der Untersuchung des Einflusses der räumlichen Niederschlagsaktivität auf die Vorhersageunsicherheit eines konzeptionellen Niederschlags-Abfluss-Modells. Die interpolierten Niederschlagsdaten von einer Regenmessstelle (Punktdaten) und gemittelte Niederschlagswerte über verschiedene räumliche Auflösungen wurden als zwingender Modellinput verwendet. Die räumliche Skala reicht von 1 km^2 bis 25 km^2. Die verteilte und halb-verteilte Modelstruktur des modifizierten HBV Modells wurden angepasst. Die simulierten Abflussganglinien unter Verwendung der originalen Niederschlagswerte und unter Verwendung der gemittelten Niederschlagswerte wurden untersucht. Es konnten keine signifikanten Unterschiede in der Leistung des kalibrierten Modells festgestellt werden, wenn ein 1 km x 1 km Niederschlagsraster verwendet wurde und gemittelte Niederschlagswerte auf verschiedenen räumlichen Skalen entweder einer verteilten oder einer halb-verteilten Modellstruktur als Input dienten. Geringe Unterschiede ergaben sich jedoch für die Abschätzung der Abflussspitzen.

Die Studie wurde dann erweitert, um die Verlässlichkeit der Parameter zu testen, die von der Kalibrierung mit einem Niederschlagsinput stammen, wenn sie auf ein anderes Set von Niederschlagsinput angewendet werden. Die Ergebnisse zeigen, dass es signifikante Störungen der Modellleistung gibt, wenn ein Modell, welches mit detaillierten Niederschlagsdaten kalibriert wurde, mit relativ dazu weniger detaillierten Niederschlagsdaten betrieben wird. Im Gegensatz dazu werden nur minimale Verbesserungen der Modellleistung erzielt, wenn ein Model, das mit weniger detaillierten Niederschlagsdaten kalibriert wurde mit im Vergleich dazu detaillierten Daten betrieben wird.

In Kapitel 5 wird eine Antwort auf die Frage gesucht, ob eine höhere räumliche Auflösung des Modellinputs auch zwingend zu einer besseren Modellleistung führen wird. Für die Beantwortung der Frage wurden die 4 Modellstrukturen des modifizierten HBV-Modells verglichen. Für die Reproduktion der räumlichen Variabilität der meteorologischen Input-Daten wird „External Drift Kriging“ angewandt. Damit wird die Interpolation vorhandener Punktmessungen über das gesamte Einzugsgebiet ermöglicht. Die Kalibrierungen der verschiedenen Modellstrukturen werden mit dem „simulated annealing“ Optimierungsalgorithmus durchgeführt. Die simulierten Abflussganglinien der verschiedenen Modellstrukturen, die sich am Ausfluss des Unter-Einzugsgebiets ergeben, werden unteruscht. Die Ergebnisse zeigen, dass die halb-verteilte- und die halb-aggregierte Modellstruktur den anderen beiden Strukturen bei einer gegebenen Anzahl an Beobachtungen überlegen sind. Es zeigt sich auch, dass die Verwendung detaillierter, vollständig verteilter Regendaten die Simulationsgenauigkeit weder in der Kalibrierungsperiode noch in der Validierungsperiode verbessert. Die Ergebnisse lassen den Schluss zu, dass eine höhere Auflösung der Eingangsdaten nicht immer besser ist und die Auswahl der Modellstruktur nach dem Prinzip der Einfachheit erfolgen und sich an der Verfügbarkeit beobachteter Daten orientieren sollte.

In Kapitel 6 werden die Auswirkungen von Veränderungen des Niederschlagsmessstationen-netzes für die Interpolation auf die simulierten Hydrographen untersucht. Die optimale räumliche Lage einer bestimmten Anzahl an Messstellen innerhalb eines Netzwerks wird mit „simulated annealing“ als kombinatorischen Optimierungsalgorithmus bestimmt. Die räumliche Repräsentierung des Niederschlags wird ausgehend von dem gewählten Netzwerk untersucht. Die verteilte- und halb-verteilte Modellstruktur des modifizierten HBV Modells werden dann dazu verwendet, den Effekt zu bestimmen, den die Anzahl an Regenstationen und ihre Lage auf die Vorhersageunsicherheit des jeweiligen Modells hat.

Die Analyse ergab, dass die Anzahl und die räumliche Verteilung der Regenmessstationen die Simulationsergebnisse durchaus beeinflusst. Es zeigte sich, dass sich die Modellleistung mit einer sinkenden Anzahl an Messstellen extrem verschlechtert. Andererseits jedoch wird die Modelleistung mit einer steigenden Anzahl an Messstationen nicht signifikant verbessert, sobald eine bestimmte Mindestanzahl überschritten wird. Der Einfluss des Netzwerks der Niederschlagsstationen auf die Modellkalibrierung und die Anwendung werden ebenfalls untersucht. Es soll bestimmt werden, ob eine Kalibrierung der Parameter mit Niederschlagsdaten von einem Typ des Messstationennetzes in der Lage ist, die Phänomene abzubilden, die den Niederschlags-Abfluss-Prozess bestimmen, wenn der Input dazu von einer anderen Konfiguration des Messstellennetzes kommt. Die halb-verteilte Modellstruktur des HBV Modells wird mit Niederschlägen kalibriert, die von verschiedenen Messnetzen stammen. Das kalibrierte Modell wird

dann für den Validierungszeitraum mit einem Messnetz betrieben, dass nicht zur Kalibrierung verwendet wurde. Die Analyse zeigt, dass für Modelle, die verschiedene Niederschlagsmessnetze verwenden, die Parameter nachkalibriert werden müssen. Vor allem versagen Modelle, die mit einem dichten Netzwerk an Niederschlagsmessstationen kalibriert wurden, wenn sie mit einem spärlichen Netzwerk betrieben werden. Modelle jedoch, die mit wenig Information kalibriert wurden, können sehr gute Resultate zeigen, wenn sie mit einem dichten Netzwerk betrieben werden. Des Weiteren wird geprüft, wie verlässlich es ist, fehlende Niederschlagsdaten bei der Kalibrierung mit Daten zu ergänzen, die durch multiple lineare Regression erzeugt werden. Das Modell wird dabei mit einer Kombination erzeugter und beobachteter Daten betrieben. Die Ergebnisse legen nahe, dass das Modell gute Ergebnisse liefert, ob es nun mit einem vollständigen Satz an beobachteten Niederschlagsdaten kalibriert wird oder mit einem unvollständigen Datensatz, der mit simulierten Daten ergänzt wird. In der Tat eröffnet dieses Ergebnis die ermutigende Perspektive, dass ein solches Verfahren in ein operationelles Hochwasservorhersagesystem implementiert werden könnte.

Eine letzte Reihe von Analysen wurde durchgeführt, um den Einfluss von Temperaturmessstellen auf die Simulationsergebnisse zu untersuchen, wenn man die Anzahl der Regenmessstellen konstant hält. Die Resultate zeigen, dass die Temperaturmessstellen die Simulationsergebnisse für das untersuchte Einzugsgebiet beeinflussen, insbesondere im Winter. Der Einfluss ist jedoch im Vergleich mit dem Einfluss des Niederschlagsmessstellennetzes sehr niedrig.

In Kapitel 7 wird der Nutzen von bedingter Simulation bei der Erzeugung der Niederschlagsdaten für hydrologische Modelle untersucht. Die halb-verteilte Modellstruktur des modifizierten HBV Modells wird mit interpolierten Niederschlägen kalibriert. Das kalibrierte Model wird mit interpolierten, durch bedingte Simulation erzeugten Niederschlagsdaten validiert. Die bedingte Simulation erfolgt über „Turning Bands“ Simulation und einer Gauss’schen Copula Methode. Die bedingten räumlichen Niederschlagssimulationen zeigen signifikant mehr Variabilität im Niederschlag, behalten aber die Hauptstrukturen bei. Darüber hinaus war im Vergleich zu den interpolierten Niederschlagsfeldern im Falle der „turning band“ Simulation die Modellleistung schlechter, wenn das Mittel der bedingten Simulation verwendet wurde, im Fall der auf Gauss’schen Copula basierenden Simulation war sie besser. Werden nicht der gesamte Zeitraum einer Untersuchung betrachtet, sondern nur Hochwasserereignisse, wird die Modellgüte für beide Arten bedingter Simulation besser als bei einen Modell mit interpolierten Niederschlagswerten.

Eine weitere Reihe an Versuchen beschäftigte sich mit dem Einfluss der räumlichen Repräsentierung des Niederschlagsinputs auf die Ergebnisse und die Unsicherheit der Simulation, die konzeptionellen Modellparameter zu identifizieren (Kapitel 8). Diese Untersuchung wurde mit

dem physikalisch basierten hydrologischen Model SHETRAN und dem konzeptionellen Niederschlag-Abfluss-Modell HBV durchgeführt. Konditionell simulierte Niederschläge mit auf Copula basierender Simulation, wurden als Niederschlagsinput für das SHETRAN bzw. das HBV Modell verwendet. Die simulierten Abflüsse, die aus verschiedenen Realisationen der konditionellen Simulation des Niederschlags resultieren, werden untersucht, um die Unsicherheit im resultierenden Abfluss zu quantifizieren. Die Studie wird dann erweitert, um die Unsicherheit bei der Parameterfestlegung des HBV Modells zu charakterisieren. Die simulierten Abflüsse des SHETRAN Modells werden dabei als eine Basis für die Kalibrierung des HBV Models unter Verwendung der interpolierten Niederschläge verwendet. Das SHETRAN Modell wird angenommen als die „wahre“ Repräsentation des herrschenden hydrologischen Regimes des untersuchten Einzugsgebiets.

Die Studie zeigt sehr deutlich, dass die räumliche Variabilität des Niederschlags zum Teil für Modellierungsfehler verantwortlich ist – was auch zu Problemen bei der Parameterabschätzung von konzeptionellen hydrologischen Modellen führt.

Zusammenfassung der Ergebnisse

Aus der Vielzahl an Untersuchungen können einige Hauptergebnisse gewonnen werden:

Es konnten keine signifikanten Unterschiede in der Modellleistung beobachtet werden, wenn das Modell mit gemittelten Niederschlägen verschiedener räumlicher Skalen betrieben wird. Es wird jedoch eine klare Störung der Modellleistung während des Sommers festgestellt. Die Ergebnisse zeigen ebenso, dass die Modellleistung signifikant gestört wird, wenn ein Modell, welches mit detaillierten Niederschlagsdaten kalibriert wurde, mit relativ schlechterem (wenig detailliertem) Niederschlagsinput betrieben wird. Dies ist eine Warnung an den Anwender, besonders vorsichtig zu sein, wenn die Art der Niederschlagsdaten als Modellinput eine andere ist als die, die für die Kalibrierung verwendet wurde.

Die Untersuchung des Vergleichs der Modellleistungen bei der Verwendung verschiedener räumlicher Variabilitäten des Niederschlags zeigt, dass die halb-verteilte und die halb- aggregierte Modellstruktur für das gegebene Untersuchungsgebiet der verteilten und der räumlich aggregierte Modellstruktur bei einem gegebenen Niveau an Inputinformation überlegen sind. Es wird deutlich, dass die Verwendung vollständig verteilter Daten die Genauigkeit der Simulation des Abflusses am Auslass des Untereinzugsgebietes weder für die Kalibrierungsperiode noch für die Validierungsperiode verbessert. Eventuell tritt bei relativ simplen Modellstrukturen eine höhere Kompensation des Bias in den Niederschlagsbeobachtungen während der Kalibrierungsperiode auf. Ebenso ist der Fehler bei der Repräsentierung der räumlichen Variabilität des Niederschlags bei einer feineren Auflösung höher. Möglicherweise dominiert er darum bei der verteilten

Modellstruktur die Kompensierung des Bias der Niederschlagsbeobachtungen bei der Durchführung der Kalibrierung. Dies ist eben auch in Anbetracht der großen Zahl an Parametern zu sehen, die angepasst werden müssen.

Die Anzahl der Regenmessstationen und deren räumliche Verteilung beeinflusst sehr stark die Simulationsergebnisse. Vermindert man die Anzahl an Regenmessstationen im Modell übermäßig, geht die Modellleistung extrem zurück. Umgekehrt jedoch, wenn man mehr Messstellen berücksichtigt, verbessert sich ab einem bestimmten Schwellenwert die Leistung des Modells nicht mehr signifikant. Es zeigt sich auch, dass Modelle, die mit verschiedenen Messstellennetzen betrieben werden, nachkalibriert werden müssen. Speziell versagen Modelle, die mit einer sehr hohen Informationsdichte kalibriert wurden, wenn Sie mit sehr wenig Information betrieben werden. Umgekehrt können Modelle, die mit wenig Niederschlagsinformation kalibriert wurden, gute Ergebnisse bringen, wenn sie mit hoher einer hohen Dichte an Inputinformation betrieben werden. Auch Modelle, die mit einem kompletten Satz an beobachteten Niederschlagsdaten kalibriert wurden funktionieren gut, wenn sie mit einem lückenhaften Satz an Beobachtungen betrieben werden, bei dem fehlende Werte mit multipler linearer Regression ersetzt wurden. Dieses Ergebnis eröffnet eine ermutigende Perspektive für den Einsatz solcher Verfahren in operationellen Hochwasservorhersagesystemen. Es ist allerdings noch Forschungsbedarf in dieser Hinsicht über deren praktische Anwendbarkeit.

Bedingte räumliche Niederschlagssimulation resultiert in einer signifikant höheren Variabilität in der Niederschlagsverteilung, behält jedoch die Hauptstruktur der Daten bei. Ein gewähltes hydrologisches Modell liefert bessere Simulationen der Spitzenabflüsse, wenn bedingt simulierte Niederschlagswerte anstatt interpolierter Werten verwendet werden. Der Einsatz bedingter Simulation des Niederschlags für die Hochwasser-modellierung ist demnach sehr sinnvoll. Sehr vielversprechend ist vor allem der Einsatz von Gauss'schen Copulas bei der räumlichen Niederschlagsverteilung. In weiterführenden Versuchen könnten auch nicht-Gauss'sche Copulas zur Erzeugung bedingt simulierter Niederschlagsdaten verwendet werden. Die Untersuchung zeigt auch, dass die räumliche Variabilität des Niederschlags zum Teil für Fehler in der Modellierung verantwortlich ist. Dies führt zu den Problemen bei der Abschätzung von Parametern konzeptioneller hydrologischer Modelle.

1 Introduction

1.1 Problems classification and motivation

Water is a precious natural resource which is vital for life, the health of people and the ecosystem and a basic requirement for the development of a country; and at the same time, the judicious management of water poses a complex situation. This complexity has further increased on account of the possible impacts due to projected climate change. The hydrological cycle is likely to be altered due to projected climate change (Stehlik and Bárdossy, 2000; Dibike and Coulibaly, 2005; Merritt et al., 2006). The modern human society and its globalization also influence the evolution of the problems incident to it. Nevertheless, water is still a challenge which has become even greater. Floods are the most dangerous hydrological phenomena, causing a considerable loss of human life and huge property damages every year throughout the world. Nearly one third of natural catastrophes belong to floods. Floods are also becoming more common natural disasters in most parts of Europe. Especially in recent years there were some large floods in major European rivers. Most of the floods resulted from climatic events such as excessively heavy and/or excessively prolonged rainfall. From flood routing to granting a low-water flow, from the growing demand of water for industrial use in a large sense to the maintenance of the ecological characteristics for consumption, the sustainable management of the scare resource water is one of the major challenges of the 21st century. Modern water resources management, no matter whether interested in the origin of the water, in its consumption or in its use or even in the possible consequences of human activity on the water cycle, can not neglect the potential of the fast developing mathematical models. Hydrological models are simplified representations of a part of the hydrologic cycle. They serve a range of purposes but they are primarily used for hydrological prediction and for understanding hydrological processes. The estimation and representation of the input precipitation in hydrological models are crucial. Precipitation is governed by complicated physical processes which are inherently nonlinear and extremely sensitive (Bárdossy and Plate, 1992). The estimation of precipitation is very important in rainfall-runoff modeling since no model, however well founded in physical theory or empirically justified by past performance, will be able to produce accurate hydrograph predictions if the inputs to the model do not characterize the precipitation inputs (Beven, 2001). Rainfall-runoff models have uncertainties arising from a number of sources, namely: (a) input data error and inadequate representativeness of the variability (Grayson and Blöschl, 2000) (b) model structure as the model itself is only an approximation of the hydrological reality (Beven, 2001) (c) model parameters (Wood, 1976; Seibert, 1997) and (d) output measurement error.

1.1.1 Influences of rainfall variability

The spatial variability of rainfall is often termed as the major source of error in investigations of rainfall-runoff processes and modeling (O'Loughlin et al., 1996; Syed et al., 2003). Precipitation is often significantly variable in space and time within a catchment. Many studies have dealt with the sensitivity of hydrological models together with other uncertainties related to spatial rainfall variability, i.e. with the spatial density of the raingauge network and with the interpolation methods (Kuczera and Williams, 1992; Goovaerts, 2000; St-Hilarie et al., 2003; Brath et al., 2004; Dong et al., 2005) and with rainstorm displacement (Niemczynowicz, 1991). These studies demonstrate that the spatial distribution of rainfall should be taken into account in any catchment area. It influences not only the runoff volumes and the peak flows, but also the time shift of hydrographs (Krajewski et al., 1991). Duncan et al., 2003 studied the effect of raingauge sampling density on the accuracy of river flow prediction for a rural catchemnt. They observed that gauge density has a very strong effect on the estimation accuracy of hydrograph parameters with the standard error generally falling off as a power law with increasing gauge density. Schilling and Fuchs (1986) also noted the dominant impact of spatial rainfall variability on runoff modeling.

Arnaud et al., (2002) observed a substantial effect of rainfall spatial averaging on the synthetic discharges simulated for four fictitious catchments of varying area. Zehe et al., (2005) observed reduction in model's predictive uncertainty when spatially averaged precipitation is used during parameter estimation. Finnerty et al., (1997) investigated runoff timing and volume biases when they were performing hydrological forecasting at space-time scales different from those at which the model parameters were calibrated. They observed that hydrological model parameters are inherently tied to the space-time scales at which they were calibrated.

Additionally, the need to accurately describe temporal rainfall variability for modeling small catchment response is relatively well-known (Beven, 2001). On a small catchment, Krajweski et al. (1991) found a higher sensitivity to the temporal resolution of precipitation than to the spatial resolution. Ogden and Julien (1994) performed tests that identified the period when spatial and temporal variability of precipitation was dominant. However, in large catchements, the spatial variation is generally more important than the temporal variation (Beven, 2001). At larger scales, the crucial importance of spatial rainfall pattern estimates for runoff modeling has also been demonstrated (Liang et al., 2004; Brath et al., 2004). For urban drainage design, the impact of spatial rainfall variability on runoff modeling has been shown to be important on catchments of decreasing size with increasing raingauge density (Schilling and Fuchs, 1986). At yet a smaller scale of eight raingauges in a 0.4 km^2 Swiss catchment, Mutzner (1991) found only one event from a set of 177 in which spatial rainfall variability was large enough to impact runoff modeling.

Moreover, it significantly increases uncertainty about the estimation of hydrological model parameters, and consequently estimation of the extreme quartiles (Kuczera and Williams, 1992).

Brath et al., (2004) observed that the performances of a spatially-distributed hydrological model did not considerably deteriorate for a medium sized catchment under the hypothesis of spatially uniform rainfall, provided that the mean areal rainfall intensity was reliably estimated based on sufficient number of raingauges. However, they noted that different case studies may provide fairly different results, depending on the geomorphologic and climatic characteristics of the catchment area, the scale of the catchment, the dominant runoff production mechanism and the period of the year.

On the other hand, Beven and Hornberger (1982) stated that rainfall patterns have only a secondary effect on runoff hydrographs, while a correct assessment of the global volume of rainfall input in a variable pattern is more important in simulating streamflow hydrographs.

It should be noted that the majority of these and other studies were based on synthetically generated precipitation and stream flow records. Usually, comparisons were made against a "reference" hydrograph generated by running the hydrologic model at the finest data resolution. Synthetically-generated data were often used due to the lack of appropriately long periods of observed data. Moreover, many of the studies emphasizing the importance of the spatial variability of precipitation used models containing the Hortonian runoff generation mechanism.

Obled et al. (1994) argued that numerical experiments in the literature were based on the use of models which may be only a simplified representation of reality. Furthermore, they argued that the actual processes at work in a catchment may not be those predicted by the model. Thus, the research in the literature may have shown the sensitivity of a particular model to the spatial variability of precipitation, and not the sensitivity of the actual catchment. Obled et al. (1994) examined the effects of the spatial variation of precipitation using observed precipitation and stream flow data. In addition, the model used in their studies focused on saturation excess runoff as the main runoff generation mechanism. In simulations against observed data, they were unable to prove the value of distributed inputs as they had intended. They showed that even if the simulated hydrographs exhibit different characteristics for uniform and distributed forcing, the performances are similar when compared with the actual observations. In their attempt to capture the spatial variability of precipitation, they observed that their model sometimes responded to a precipitation event which the catchment ignored or dampened. This study highlighted the problem of how well a model structure and parameters fit the real system when making conclusions from simulation studies. Furthermore, they noted that in medium-sized catchments (ranging from 100 to a few 1000 km^2) most evidence for the significance of the rainfall pattern was based on synthetic studies. They also

suggested that if the dominant runoff-generation process is of the Dunne type rather than Hortonian, then most of the rainfall infiltrates and will be smoothed out as the water is stored and delayed in the soil layers.

Winchell et al. (1998) noted that there has been a bias towards the use of infiltration-excess runoff mechanisms as opposed to the saturation excess type. Their work with both types of runoff generation mechanisms found that saturation excess and infiltration excess models respond differently to uncertainty in precipitation. They suggest that generalizations concerning the effects of rainfall variability on runoff generation cannot be made. Koren et al. (1999) indicated a similar conclusion based on simulation results from several different rainfall-runoff partitioning mechanisms. Shah et al., (1996) studied the spatial variability of rainfall on a small catchment having area of 10.55 km^2 for various levels of antecedent moisture conditions. They observed that spatial averaging of rainfall inputs provided adequate simulations under wet conditions. However, they observed higher errors when spatially-averaged rainfall fields were used with dry antecedent moisture conditions. This indicated a linkage between spatial variability of rainfall and the distribution of soil moisture which subsequently controls the generation of runoff.

From the above review, it is clear that the different case studies may provide fairly different results, depending on the geomorphologic and climatic characteristics of the catchment area, the scale of the catchment, the dominant runoff production mechanism and the period of the year.

1.1.2 Complexity and challenges in distributed hydrological modeling

Again, the question may arise how one can obtain highly spatially resolved precipitation data; weather radar and satellite precipitation may be the option. The development of radar rainfall measurement has allowed for a greater appreciation of the temporal and spatial variation of rainfall intensities than was previously possible from raingauge measurements alone. This would appear to be a very important development in the data available for rainfall-runoff modeling; indeed it is. But there are some important limitations that must be recognized (Collier, 1989; Ehret, 2003).

Today, spatially-distributed hydrological models are increasingly applied to account for spatial variability of the main forcing variables within the catchment (e.g., precipitation); landscape characteristics (e.g., soil, land use) and detailed process calculation (Götzinger and Bárdossy, 2005). Distributed models in hydrology have been developing rapidly since the first outline of a physically-based distributed model published by Freeze and Harlen (1969). The same models are also utilized to undertake impact assessment studies, land use changes, prediction in ungauged basins, climate change studies and investigation of the influence of the spatial variability of meteorological variables as well as basin characteristics. A major reason for the use of distributed rainfall-runoff models is the hypothesis that by accounting for the spatial variability of precipitation

and physical features within the catchment, better simulations can be achieved at the catchment outlet. One of the few studies that have carried out a systematic intercomparision of different model structures is documented by Refsgaard and Knudsen (1996). They compared three different models embodying three quite different model structures and degrees of spatial distribution using a systematic calibration and validation procedure. Farmer et al. (2003) and Atkinson et al. (2002, 2003) applied models of increasing complexity to investigate the trade-off between model complexity and prediction accuracy and to determine the physical controls on flow prediction. The different model structures investigated were conceptual rainfall-runoff models based on one or more simple storages, where increasing complexity was obtained by adding thresholds and more storages, etc.

Also, it is of concern that few of the studies have shown a direct comparison of distributed model's and lumped model's results with observed discharge data. The emergence of high resolution data sets, Geographical Information System capabilities, and rapidly increasing computer power have pushed distributed hydrological models to the forefront of research and development (Vieux, 2001). While the utility of distributed models to predict interior hydrological processes is well known (Uhlenbrook et al., 2004), few studies have specifically addressed the advantage of distributed models over lumped models for predicting catchemnt outflow hydrographs (Toth and Brath, 2003). Sieber and Uhlenbrook (2005) carried out sensitivity analyses of the complex process-oriented model TACD (tracer aided catchment model, distributed) to verify the model structure. Lee et al., (2005) attempted a study to identify relationships between suitable conceptual rainfall-runoff model structures and catchment types. They demonstrated an objective procedure for selection of model structures for use in model regionalization studies across UK catchments.

However, a higher spatial and temporal resolution of data and model application does not always lead to a better representation of the water fluxes for a given catchment (Reed et al., 2004). This depends on the variability and distribution of catchment properties. Results from the Distributed Model Intercomparison Project (DMIP) (Reed et al., 2004; Smith et al, 2004a,b) indicate that distributed modeling approaches may not always provide improved outlet simulations compared to lumped conceptual models. They suggested that there may be a trade-off between the complexity of the model descriptions necessary to represent the catchment processes, the accuracy and the representativeness of the input data available and the accuracy required to achieve reliable simulation results. Butts et al. (2004) evaluated impacts of different model structures on hydrological modeling uncertainty for streamflow simulation. They showed that model performance is strongly dependent on model structure. Nevertheless, they observed that distributed routing and

to a lesser extent distributed rainfall were the dominant processes controlling simulation accuracy in their study catchment.

It is worth mentioning that distributed modeling may play an important role in the future. However, the main disadvantage of this strategy is the increase in model complexity and parameters parallel to the increase in partitioning. For complex, highly parameterized models, as the number of hydrological units is increased, the calibration procedure quickly becomes intractable. Further, many of the parameters may not be identifiable by the information contained within the observed data, remotely sensed or otherwise. The hydrological modeling problem can be partitioned into three main components; hydrological model structure, model input data, any parameter estimation procedures. Successful development and application of any hydrological model requires careful consideration of each component and its relevance to the overall modeling problem.

Nevertheless, a large volume of research continues to emerge that addresses the possibility of improving lumped hydrologic simulations by using distributed and semi-distributed modeling approaches which account for the spatial variation not only of physiographic catchment features but of precipitation as well. Recently, the availability of high resolution precipitation estimates from weather radar or satellite has intensified this investigation. Most efforts have focused on event-based modeling, and mixed and somewhat surprising results have been realized compared to the numerical results discussed above. As a consequence, the hypothesis that higher resolution data will lead to more accurate hydrograph simulations remains largely unexamined.

Moreover, in practical hydrological applications, the existing model and data collection system must be compromised (Dong et al., 2005). Beven (1989) pointed out the limitations of the current generation of rainfall-runoff models and also argued that the possible way forward must be based on a realistic assessment of predictive uncertainty.

The reality is that most recording systems in use are still point-measuring raingauges. Point estimation of raingauge accumulations is distributed in space over the river basin by interpolation techniques (i.e., kriging, thiessen polygon, inverse distance method). However, hydrologists have long recognized the problems of interpolating point raingauge measurements to estimate spatial rainfall fields. Kriging as mostly used interpolation techniques provides idealized smooth rainfall fields and does not possess the same fluctuation pattern (Haddeland et al., 2002). However the variability of rainfall has a considerable impact in hydrological model's predictive uncertainty (Brath et al., 2004; Zehe et al., 2005). Simulations usually conditional on the observations preserve typical fluctuation patterns (Mantoglou and Wilson, 1982).

Nevertheless, the question may arise: what is the influence of such distributed precipitation on the uncertainty when estimating stream flows? And will a higher spatial resolution of model input

data necessarily, as most people assume, lead to a better model performance? Is there a compromise between model complexity and available information, i.e., an interaction between the resolution of input data and model structure itself, when generating model uncertainty?

This research work was thus initiated with the overall objective to better understand how spatial rainfall variability impacts the performance of a rainfall-runoff model for a meso-scale catchment.

1.2 Research questions and objectives

Given the importance to the role of the precipitation input in hydrological applications, the following research questions were addressed:

a. How does the spatial variability of precipitation influence the hydrological simulation results?

b. Will a higher spatial resolution of model input data necessarily lead to a better model performance?

c. What is the impact on the simulated discharges of interpolated precipitation at different spatial resolutions through varying raingauge networks?

d. Is there any benefit of using conditionally-simulated precipitation in hydrological modeling?

The main objective of this study is to answer the above research questions. Supplementary objectives are: (1) to investigate the reliability of the parameters obtained from calibration over input data different from those used in model simulations and (2) to study the uncertainty in identifying the model parameters of a conceptual model due to uncertain precipitation.

1.3 Structure of the dissertation

In line with the objectives and scope of this study, the dissertation consists of nine chapters. In Chapter 2, the data of the study catchment is discussed. A description of the model structure, modifications of the structure and automatic parameter estimation for the hydrological model applied in the study are given in Chapter 3. Chapter 4 focuses on the study to identify the influence of spatial variability of precipitation on the predictive uncertainty of the hydrological model. An attempt has been made in Chapter 5, to provide an answer to the question, ‘Will a higher spatial resolution of model input data necessarily lead to a better model performance?’ Chapter 6 explains the impact on the simulated hydrographs of interpolated precipitation at different spatial resolutions through varying raingauge networks. The possible benefits, of using conditionally simulated precipitation in hydrological modeling are illustrated in Chapter 7. ‘How does uncertainty in precipitation affect parameter identification of a conceptual model?’ is explored in Chapter 8. Chapter 9 presents a summary of the study and recommendations for further works.

2 Study area and data description

2.1 Introduction

The upper Neckar catchment, located in the region of Baden-Württemberg (south-west of Germany), was selected as the test catchment. The reason for the selection of the upper Neckar catchment for the study is that the rivers in the catchment are not affected by larger hydropower plants or other water management structures or navigations, which may influence the runoff characteristics of the catchment. Further, the upper Neckar catchment can be considered to be a typical example of a medium-sized catchment. In addition, data availability must be carefully considered before any modeling attempt is carried out. All the required data was provided by the German Weather Service (DWD) and the State Agency for Environmental Protection (LUBW, Baden-Württemberg). Due to the reasons stated above, it is worthy at the present stage of this research to have an overview of the relevant information available for the chosen study area. The description of the study area is partly based on the description of Bárdossy et al., 1999 and Samaniego, 2003.

2.2 General description of the study area

The study area is located to the south and south-east of Stuttgart, Germany (Figure 2.1). It comprises the upper catchment of the Neckar River upstream of the Plochingen gauging station covering an area of about 4000 km^2. The upper Neckar catchment was divided into 13 subcatchments depending on the available discharge gauges. Table 2.1 summarizes the sizes of the different subcatchments. The catchment area represents approximately 28% of the whole Neckar catchment. The Neckar is a right-bank tributary of the Rhine; it is 367 km long and flows 40% of its course in direction north and north-east within the study area. The upper Neckar is bounded by the north-western edge of the Swabian Jura on the right bank side of the Neckar and by the Black Forest on its left bank. Its elevation ranges from about 240 m a.s.l. to around 1010 m a.s.l., with a mean elevation of 548 m a.s.l.. Slopes are generally mild; approximately 90% of the area has slopes varying from 0^o to 15^o, although some areas of the Swabian Jura and the Black Forest may have values as high as 50^o.

The main geological formations in the upper Neckar catchment originated in the Triassic and Jurassic periods, both corresponding to the Mesozoic Era. The main formations are composed of altered keuper, claystone-jura, claystone-keuper, limestone-jura, loess, sandstone and shelly limestone (Muschelkalk). Conversely, the river bed of the Neckar and its tributaries are relatively

young compared with the previous formations. They are mainly composed of Quaternary sediments, originating mainly from the erosion of outcrops of the aforementioned rock types.

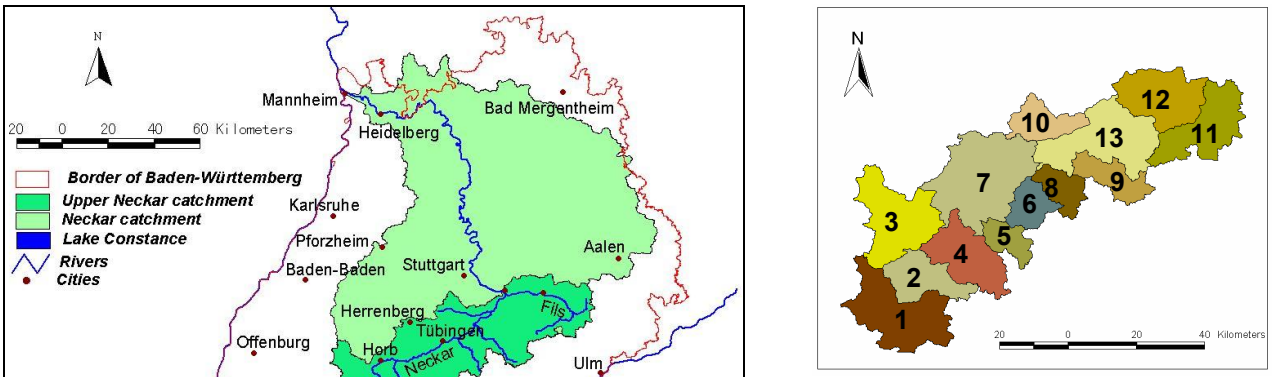

Figure 2.1: Study area: upper Neckar catchment in south-west Germany (upper-right: 13 subcatchments of the upper Neckar catchment).

Table 2.1: Summary of the sizes of the different subcatchments in the study catchment.

Subcatchments		Subcatchment size [km^2]	Drainage area [km^2]
1	Rottweil	454.65	454.65
2	Oberndorf	240.13	694.78
3	Horb	420.18	1114.96
4	Bad Imnau, Eyach	322.94	322.94
5	Rangendingen, Starzel	119.89	119.89
6	Tuebingen, Steinlach	140.21	140.21
7	Kirchentellinsfurt, Neckar	613.33	2311.33
8	Wannweil, Echaz	135.26	135.26
9	Riederich, Erms	169.84	169.84
10	Oberensingen, Aich	178.18	178.18
11	Suessen, Fils	345.74	345.73
12	Plochingen, Fils	349.09	694.83
13	Plochingen, Neckar	472.05	3961.49

The climate of the study area is characterized by warm-to-hot summers with generally mild winters, and is wet during all seasons. The coldest and hottest months in the study area are January and July respectively. The daily mean air temperature in the former is about -0.8^{o}C and in the latter is about 17^{o}C according to the daily mean temperature records available for the period 1961 to 1990. The annual variation of precipitation in the study area exhibits a multi-modal distribution. Precipitation-events may occur the whole year round, the wettest month being June and the driest one October with monthly means of 126 mm and 64 mm respectively, according to the daily amount of raingauge records available for the period 1961 to 1990. The mean annual precipitation observed during this period is 908 mm. Snowfall is an important parameter during the winter months, particularly in the upper parts of the catchment. With regard to land use, the study area has endured rapid land use transitions from crop land or grass land to built-up area or industrial usages in the last several decades.

2.3 Physical structure of study area

The physiographical factors considered in this study have been derived from different sources, mainly: (1) Digital Elevation Model (DEM) available for the study area with a spatial resolution of 30 m × 30 m; (2) a digitized soil map of the state of Baden-Württemberg at the scale 1:200 000; (3) a digitized geological map of the state of Baden-Württemberg at the scale 1:600 000. A detailed explanation of the relevance and calculation of these factors is provided below.

2.3.1 Topography

The upper Neckar catchment is characterised by strong variation in altitude between the foothills of the Black Forest in the west, the valley of the Neckar in the centre and again the steep ascent to the Swabian Alb in the east (Figure 2.2). The catchment consists of a number of narrow valleys.

The origin of the river Neckar is situated in the south-western part of the catchment near to the city of Schwenningen (‘Schwenninger Moos’), in an area called the Baar region, which is a small area between the Black Forest and the Swabian Alb. Starting at the city of Rottweil, the river Neckar digs a steep and impressive but narrow valley, with many meandering loops, into the Muschelkalk. In this area of the river Neckar (at the city of Horb) the river bed becomes smoother. At the city of Rottenburg the river leaves the narrow Muschelkalk valley and flows into a broad valley bottom to Plochingen. The slope of the Neckar catchment is illustrated in Figure 2.2 (right panel). Table 2.2 represents the topographic and slope characteristics of different subcatchments.

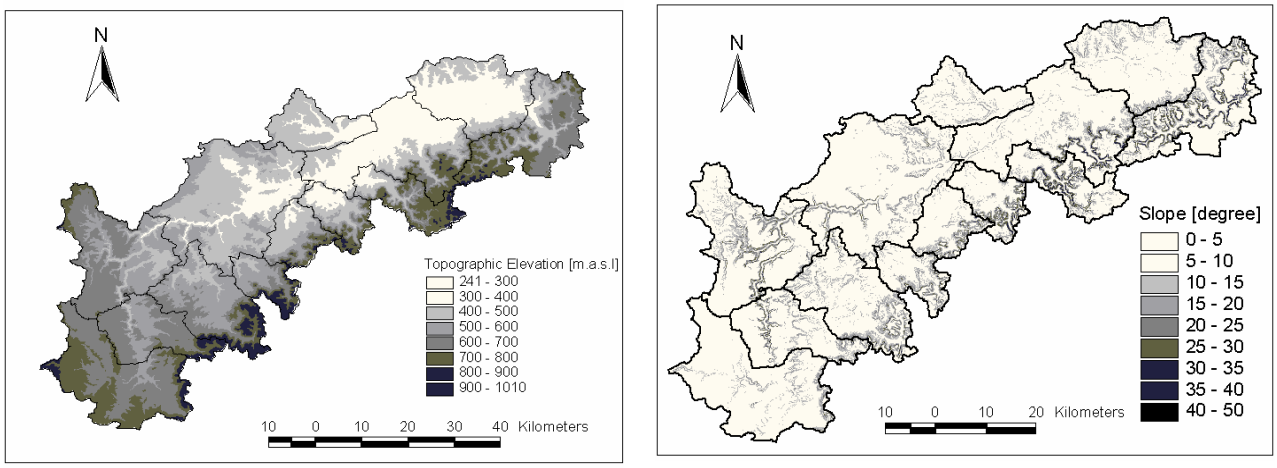

Figure 2.2: Digital Elevation Model (left panel) and Slope (right panel) of the upper Neckar catchment.

Table 2.2: Elevation and slope of the different subcatchments of the upper Neckar catchment.

Subcatchments	**Elevation (m)**				**Slope (degree)**			
	Min.	Max.	Mean	Std. dev.	Min.	Max.	Mean	Std. dev.
Rottweil	555.0	1010.0	700.0	59.9	0.0	34.2	4.4	4.0
Oberndorf	460.0	1004.0	651.7	86.4	0.0	44.2	6.1	6.1
Horb	383.0	841.0	597.1	79.1	0.0	48.9	6.4	6.4
Bad Imnau, Eyach	394.0	988.0	626.3	124.9	0.0	42.5	7.0	5.8
Rangendingen, Starzel	421.0	954.0	644.9	133.0	0.0	36.9	7.7	6.1
Tuebingen, Steinlach	341.0	882.0	541.4	127.5	0.0	38.8	7.0	6.6
Kirchentellinsfurt, Neckar	308.0	622.0	457.3	59.7	0.0	36.8	4.9	4.9
Wannweil, Echaz	309.0	862.0	5291.0	144.6	0.0	45.9	8.1	7.8
Riederich, Erms	317.0	865.0	629.7	149.1	0.0	49.4	9.2	8.4
Oberensingen, Aich	278.0	601.0	425.6	49.2	0.0	27.1	5.0	3.8
Suessen, Fils	359.0	859.0	625.2	107.5	0.0	49.3	9.2	8.6
Plochingen, Fils	252.0	785.0	396.5	68.7	0.0	39.7	5.7	4.8
Plochingen, Neckar	241.0	871.0	431.0	139.8	0.0	45.8	6.0	6.3
Whole Catchment	241.0	1010.0	548.8	144.0	0.0	49.4	6.3	6.2

2.3.2 Geology

The study area belongs to the ‘Süddeutsches Schichtstufenland’, a terraced landscape which was formed during the Mesozoic era (225 to 145 million years before). The area was flooded several times during that time leaving different sediment layers behind. The oldest formations are the variegated sandstones in the western part of the catchment, near the Black forest. These formations lay directly on the bedrock of the Black forest. This variegated sandstone is followed by Muschelkalk, Keuper and the Jurassic formations Lias, Dogger and Malm, which can be found in the Swabian Alb. The terraces are very narrow in the Baar region, due to the small distance between the Black forest and the Swabian Alb. The type of geological formations –along with their faults

and interstices- underneath a given basin have a special relevance to its water balance because they can act as groundwater reservoirs (i.e., aquifers), as well as pipelines for groundwater flow. In general, a catchment whose subsurface consists of proportions of karstic formations would present huge abnormalities in its water budget, and thus in its discharge regime. There are some karstic formations within the study area. Figure 2.3 (left panel) illustrates the main geological formations of the study area.

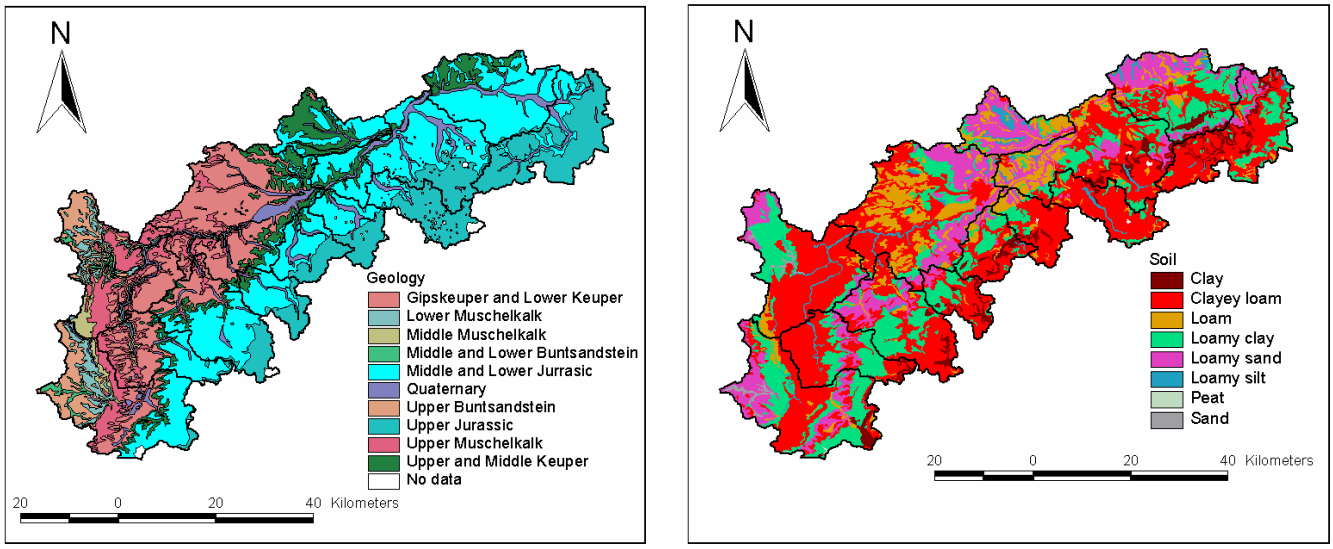

Figure 2.3: Main geological formations (left panel) and Soil map (right panel) of the upper Neckar catchment.

2.3.3 Soils

The variability in geological formations leads to variability in soil within the study catchment. In the western part of the catchment, the variegated sandstones were weathered to shallow podsols and grey brown podsolic soils, which are poor in minerals. The Muschelkalk area of the upper Gäu is mainly covered with a layer of fertile loess. In the Keuper area there are sandy as well as heavy clay soils. Despite not all of this area being covered with loess, it is still good for agriculture. Figure 2.3 (right panel) shows a soil map of the upper Neckar catchment. Table 2.3 represents the soil characterization of different subcatchments.

Table 2.3: Soil types of the different subcatchments of the upper Neckar catchment.

Soil types	Whole Catchment		Subcatchments											
			Rottweil		Oberndorf		Horb		Bad Imnau, Eyach		Rangendingen, Starzel		Tuebingen, Steinlach	
	Area (sq. km.)	Area (%)	Area (sq. km.)	Area (%)	Area (sq. km.)	Area (%)	Area (sq. km.)	Area (%)	Area (sq. km.)	Area (%)	Area (sq. km.)	Area (%)	Area (sq. km.)	Area (%)
Clay	156.20	3.95	17.09	3.76	5.88	2.45	*	*	10.06	3.12	13.36	11.08	14.91	15.55
Clayey loam	1569.98	39.66	143.72	31.61	136.44	56.83	243.25	57.87	134.77	41.73	62.92	52.20	19.68	20.53
Loam	446.59	11.28	22.16	4.87	2.11	0.88	18.62	4.43	15.57	4.82	1.19	0.99	12.98	13.54
Loamy clay	872.34	22.04	144.91	31.88	68.09	28.36	96.28	22.90	88.96	27.55	34.40	28.54	41.62	43.41
Loamy sand	637.13	16.10	97.53	21.45	20.70	8.62	40.62	9.66	56.34	17.45	7.82	6.49	5.54	5.78
Loamy silt	92.86	2.35	3.11	0.68	4.33	1.80	13.61	3.24	2.70	0.84	0.84	0.70	0.89	0.93
Peat	1.56	0.04	1.56	0.34	*	*	*	*	*	*	*	*	*	*
Sand	18.59	0.47	10.60	2.33	*	*	7.99	1.90	*	*	*	*	*	*
No data	163.08	4.12	13.93	3.06	2.53	1.05	*	*	14.55	4.51	*	*	0.26	0.27
Sum	3958.32	100.00	454.61	100.00	240.08	100.00	420.37	100.00	322.95	100.00	120.53	100.00	95.88	100.00

* indicates no area under that soil type

Table 2.3 (continued): Soil types of the different subcatchments of the upper Neckar catchment.

Soil types	Subcatchments													
	Kirchentellinsfurt, Neckar		Wannweil, Echaz		Riederich, Erms		Oberensingen, Aich		Suessen, Fils		Plochingen, Fils		Plochingen, Neckar	
	Area (sq. km.)	Area (%)	Area (sq. km.)	Area (%)	Area (sq. km.)	Area (%)	Area (sq. km.)	Area (%)	Area (sq. km.)	Area (%)	Area (sq. km.)	Area (%)	Area (sq. km.)	Area (%)
Clay	*	*	7.30	5.41	2.95	1.75	*	*	39.92	11.55	18.70	5.36	26.03	5.54
Clayey loam	209.61	34.18	62.13	46.04	132.17	78.19	1.28	0.71	183.62	53.11	42.45	12.16	153.39	32.63
Loam	160.83	26.22	18.61	13.79	6.93	4.10	54.62	30.15	11.09	3.21	33.81	9.69	91.06	19.37
Loamy clay	81.69	13.32	16.98	12.58	19.87	11.75	12.95	7.15	70.77	20.47	105.59	30.25	90.63	19.28
Loamy sand	127.38	20.77	4.21	3.12	0.98	0.58	91.37	50.43	23.71	6.86	100.63	28.83	60.41	12.85
Loamy silt	16.80	2.74	0.38	0.28	6.14	3.63	18.83	10.39	6.20	1.79	12.69	3.64	6.97	1.48
Peat	*	*	*	*	*	*	*	*	*	*	*	*	*	*
Sand	*	*	*	*	*	*	*	*	*	*	*	*	*	*
No data	17.01	2.77	25.33	18.77	*	*	2.14	1.18	10.45	3.02	35.21	10.09	41.67	8.86
Sum	613.32	100.00	134.94	100.00	169.04	100.00	181.19	100.00	345.76	100.00	349.08	100.00	470.16	100.00

* indicates no area under that soil type

2.3.4 Vegetation

There is a wide variety of vegetation in the study catchment. The differences of altitude, pedological, hydrological and other site relevant factors exhibit this variation. In the western part of the catchment, forest grows on acid soils which are poor in minerals. Spruce, fir and beech are the dominating trees. The wide plateau of the Gäu with its fertile soil is mostly arable. Vegetation on the sandy soils of the keuper area mainly consists of forest with spruce, fir and beech. The heavy clay soil is used as pasture and meadows. On the slopes of the southern part of the catchment, fruit and vines are cultivated.

The foreland between the keuper area and the Alb area has heavy clay soil and is used as arable land, pasture and meadows. On the slopes to the Alb, ash trees, beech, elm and lime trees grow. The barren soil on top of the Alb is covered with heath and juniper. Dry meadows, mesoxerophytic meadows with rare Orchids can also be found.

2.3.5 Land cover data

The land cover map available for this study is a LANDSAT TM scene for the year 1993 with a spatial resolution of 30 m × 30 m with 16 classes. Figure 2.4 illustrates the distribution of different land cover classes within the study area. The area under different land cover for different subcatchments is represented in Table 2.4.

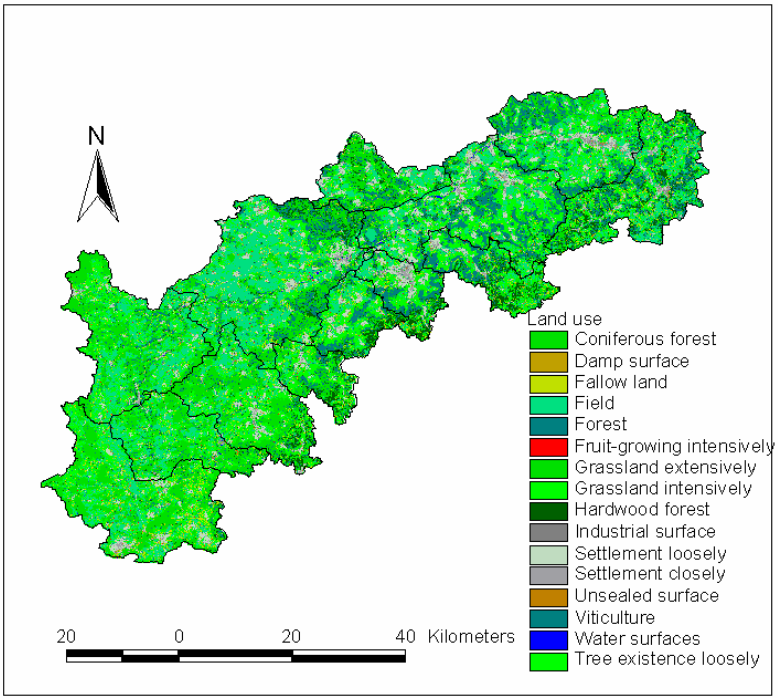

Figure 2.4: Land cover map of the upper Neckar catchment for the year 1993.

The land cover map was categorized into four major classes and latter used for modeling purposes. The land cove map for the year 1975 was also available. Figure 2.5 compares the spatial distribution of different classes for the year 1975 and 1993.

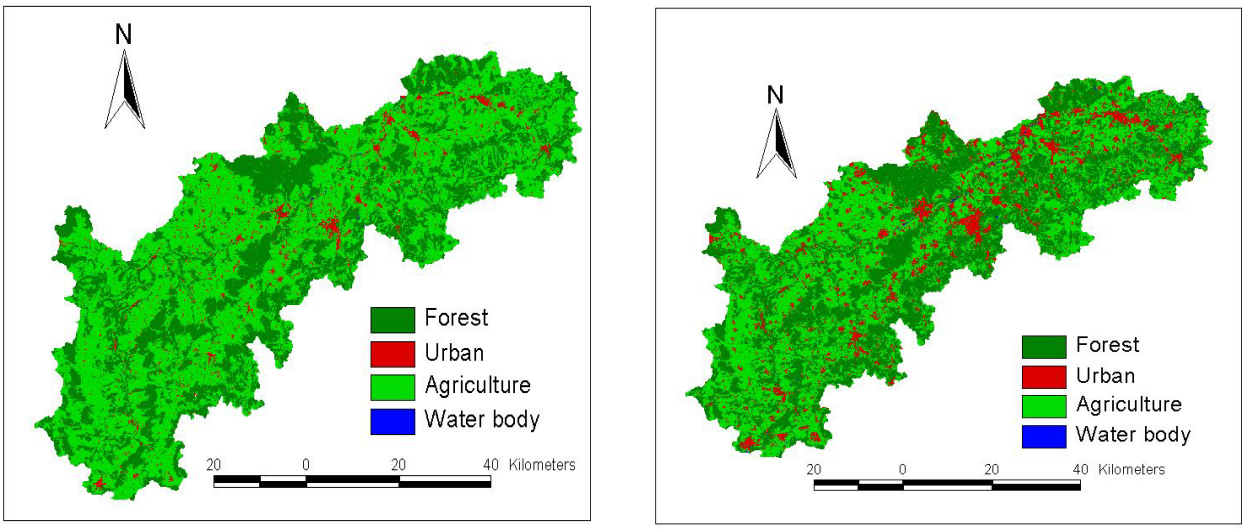

Figure 2.5: Reclassified land cover map of the upper Neckar catchment for the year 1975 (left panel) and for the year 1993 (right panel).

2.4 Climate

The study area's weather is influenced by both continental and oceanic climate systems. This is due to the prevailing westerly winds within the region and the impact of the Atlantic Ocean, which is relatively strong. The second major impact on the climate is the topography; the climate on a local scale differs due to variations in elevation.

For the Neckar catchment, a long time series of observed daily data is available for a large number of locations. Though only part of the network is located within the study catchment area, the information of locations in the surroundings of the catchment is still useful for analysis purposes and for improving the results of simulations and other calculations. The raingauges and temperature stations located within and around 30 km from the boundary of the catchment were used for the study (Figure 2.6).

Table 2.4: Land use types of the different subcatchments of the upper Neckar catchment.

LANDUSE	Whole Catchment		Subcatchments											
			Rottweil		Oberndorf		Horb		Bad Imnau, Eyach		Rangendingen, Starzel		Tuebingen, Steinlach	
	Area (sq. km.)	Area (%)	Area (sq. km.)	Area (%)	Area (sq. km.)	Area (%)	Area (sq. km.)	Area (%)	Area (sq. km.)	Area (%)	Area (sq. km.)	Area (%)	Area (sq. km.)	Area (%)
Field	797.45	20.13	88.19	19.41	52.35	21.80	98.46	23.46	44.95	13.92	11.39	9.51	20.36	14.52
Tree existence loosely	335.78	8.48	12.96	2.85	10.73	4.47	15.09	3.59	30.15	9.34	11.37	9.49	22.57	16.10
Fallow lands	164.32	4.15	34.19	7.53	9.44	3.93	12.66	3.02	13.55	4.20	6.37	5.32	6.93	4.94
Damp surfaces	2.98	0.08	0.92	0.20	0.16	0.07	0.06	0.02	0.12	0.04	0.07	0.06	0.03	0.02
Unsealed surfaces	13.44	0.34	2.08	0.46	1.03	0.43	1.23	0.29	0.88	0.27	0.36	0.30	0.32	0.23
Grassland extensively	46.43	1.17	1.03	0.23	2.75	1.15	0.83	0.20	5.12	1.59	3.48	2.90	2.36	1.68
Grassland intensively	724.03	18.28	112.98	24.87	53.03	22.08	110.13	26.24	60.77	18.82	21.81	18.20	20.63	14.71
Industrial surfaces	29.84	0.75	2.63	0.58	1.11	0.46	2.09	0.50	1.50	0.47	0.57	0.48	0.83	0.59
Hardwood forest Auwald	223.34	5.64	6.72	1.48	5.47	2.28	6.38	1.52	16.38	5.07	13.13	10.96	15.78	11.25
Coniferous forest	770.21	19.44	145.59	32.05	79.25	33.01	122.93	29.29	101.28	31.36	29.30	24.45	13.01	9.28
Fruit-growing intensively	5.46	0.14	0.69	0.15	0.16	0.07	0.49	0.12	0.28	0.09	0.11	0.09	0.14	0.10
Settlement closely	76.16	1.92	4.49	0.99	2.41	1.00	5.53	1.32	4.41	1.37	1.44	1.20	1.86	1.32
Settlement loosely	245.98	6.21	26.19	5.77	8.10	3.37	16.53	3.94	19.41	6.01	5.57	4.65	9.89	7.05
Forest other	468.86	11.84	8.69	1.91	11.19	4.66	22.78	5.43	19.73	6.11	13.65	11.39	23.71	16.91
Water surfaces	4.66	0.12	0.20	0.04	0.23	0.09	0.18	0.04	0.06	0.02	0.00	0.00	0.02	0.01
Viticulture	52.55	1.33	6.72	1.48	2.68	1.12	4.36	1.04	4.32	1.34	1.20	1.00	1.78	1.27
Sum	3961.57	100.00	454.27	100.00	240.10	100.00	419.74	100.00	322.92	100.00	119.82	100.00	140.20	100.00

* indicates no area under that land use type

Table 2.4 (continued): Land use types of the different subcatchments of the upper Neckar catchment.

LANDUSE	Subcatchments													
	Kirchentellinsfurt, Neckar		Wannweil_Bahn, Echaz		Riederich, Erms		Oberensingen, Aich		Suessen, Fils		Plochingen, Fils		Plochingen, Neckar	
	Area (sq. km.)	Area (%)	Area (sq. km.)	Area (%)	Area (sq. km.)	Area (%)	Area (sq. km.)	Area (%)	Area (sq. km.)	Area (%)	Area (sq. km.)	Area (%)	Area (sq. km.)	Area (%)
Field	207.94	33.93	15.04	11.12	17.89	10.54	28.99	16.30	65.52	18.96	57.13	16.38	88.79	18.82
Tree existence loosely	47.70	7.78	19.85	14.68	17.34	10.21	15.21	8.55	20.19	5.84	32.04	9.19	80.55	17.07
Fallow lands	21.12	3.45	5.52	4.08	8.14	4.80	5.13	2.89	20.25	5.86	7.08	2.03	13.75	2.91
Damp surfaces	0.14	0.02	0.04	0.03	0.06	0.04	0.04	0.02	0.99	0.29	0.25	0.07	0.06	0.01
Unsealed surfaces	1.95	0.32	0.81	0.60	0.94	0.55	0.33	0.19	0.50	0.14	1.33	0.38	1.68	0.36
Grassland extensively	0.61	0.10	2.36	1.75	8.74	5.15	0.17	0.10	13.82	4.00	1.35	0.39	3.68	0.78
Grassland intensively	62.20	10.15	15.36	11.36	29.22	17.21	19.95	11.22	63.98	18.51	75.79	21.73	77.68	16.46
Industrial surfaces	3.77	0.61	2.40	1.77	0.89	0.52	1.37	0.77	2.15	0.62	4.62	1.32	5.91	1.25
Hardwood forest Auwald	27.17	4.43	15.48	11.45	24.37	14.35	11.26	6.33	49.90	14.44	12.87	3.69	18.12	3.84
Coniferous forest	113.94	18.59	8.85	6.54	15.99	9.42	50.18	28.21	23.24	6.73	43.48	12.47	22.52	4.77
Fruit-growing intensively	0.91	0.15	0.13	0.10	0.11	0.07	0.18	0.10	0.67	0.19	1.03	0.29	0.56	0.12
Settlement closely	9.78	1.60	7.10	5.25	3.29	1.94	3.89	2.19	8.90	2.57	10.98	3.15	12.05	2.55
Settlement loosely	38.35	6.26	15.78	11.67	7.84	4.62	14.82	8.33	8.94	2.59	28.56	8.19	45.93	9.73
Forest other	66.82	10.90	23.94	17.70	31.32	18.44	23.56	13.25	65.56	18.97	69.14	19.83	88.59	18.77
Water surfaces	0.85	0.14	0.05	0.04	0.18	0.10	0.07	0.04	0.37	0.11	0.26	0.08	2.19	0.46
Viticulture	9.64	1.57	2.51	1.85	3.46	2.04	2.69	1.51	0.59	0.17	2.78	0.80	9.80	2.08
Sum	612.89	100.00	135.22	100.00	169.78	100.00	177.85	100.00	345.57	100.00	348.72	100.00	471.87	100.00

* indicates no area under that land use type

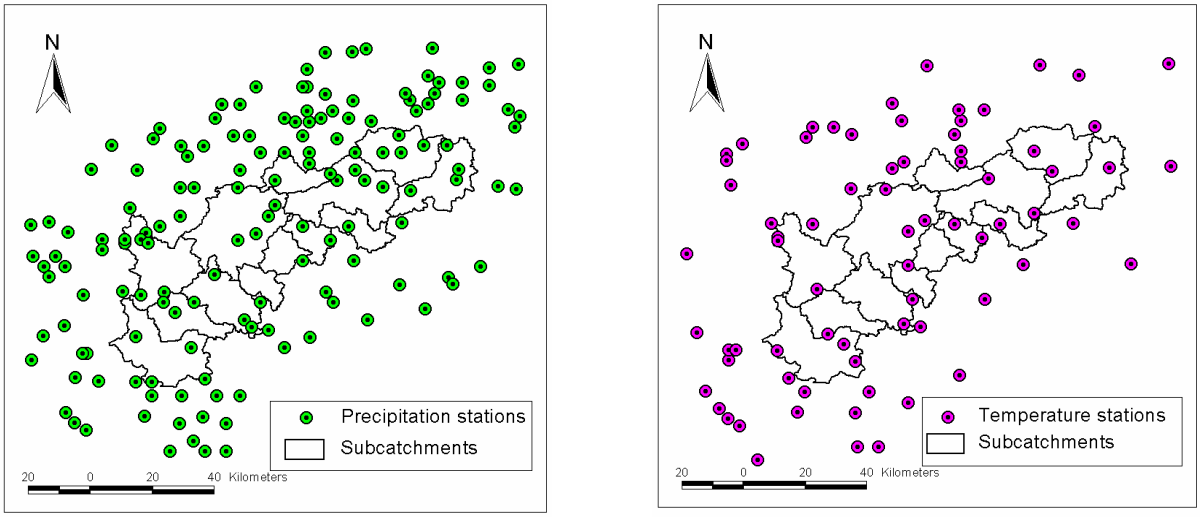

Figure 2.6: Observation network within and around the study catchment: raingauges (left panel) and temperature stations (right panel).

2.4.1 Precipitation and temperature

Precipitation is the main input in a rainfall-runoff model. Temperature is another input to a model that influences the amount of evapotranspiration and snowmelt. Correct assessment of their distribution within a catchment under study is, therefore, a crucial step in rainfall-runoff modeling practice.

The daily amount of precipitation and daily maximum, minimum and mean temperatures from 151 precipitation stations and 74 temperature stations respectively distributed in and around the study catchment were acquired from the DWD for the period from 1961 to 1990 (Figure 2.6). The data obtained from the meteorological stations were point data, and it was necessary to interpolate them in order to calculate areal values for each grid. The External drift kriging method (Ahmed and de Marsily, 1987) was chosen for interpolation allowing the orographic effect to be taken into account by using the topography as an additional variable. This method was used to interpolate precipitation and temperatures on 1 km × 1 km grid resolution. It should be noted that in the study catchment, the rate of increase of precipitation decrease with increasing elevation. The square root of the topographic elevation was assumed as a good approximation to account for this variation and it was used as the drift variable for precipitation (Hundecha, 2005). Since the temperatures show a fairly constant lapse rate, the topographic elevation was used as the drift variable for interpolating the temperature.

The highly variable topography causes highly varying precipitation in the study catchment. The maximum value of mean annual precipitation with 1800 mm is found in the Black Forest at the western border of the catchment, and the minimum annual precipitation with 650 mm in the area of

Stuttgart, close to the outlet. The precipitation data, averaged over the observed time period, exhibit a weak annual cycle, with maximum precipitation in summer for subcatchment, located in the high altitude of the Black Forest (the north-west of the catchment, subcatchment Horb). The average, maximum and minimum of long-term monthly precipitation sum over the catchment is shown in Figure 2.7. Figures 2.8 and 2.9 represent the average, maximum and minimum values of long-term monthly precipitation sum over the Rottweil and Horb subcatchments, respectively.

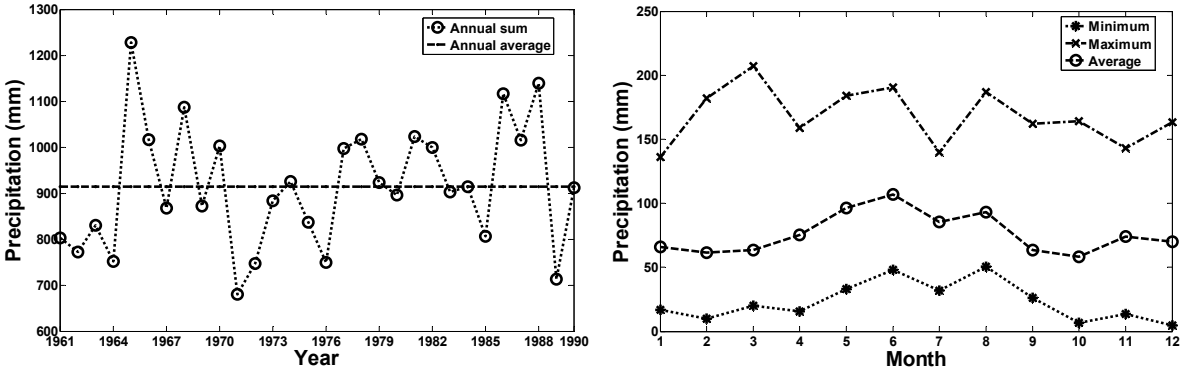

Figure 2.7: Precipitation over the catchment: annual sum (left panel) and monthly sum (right panel).

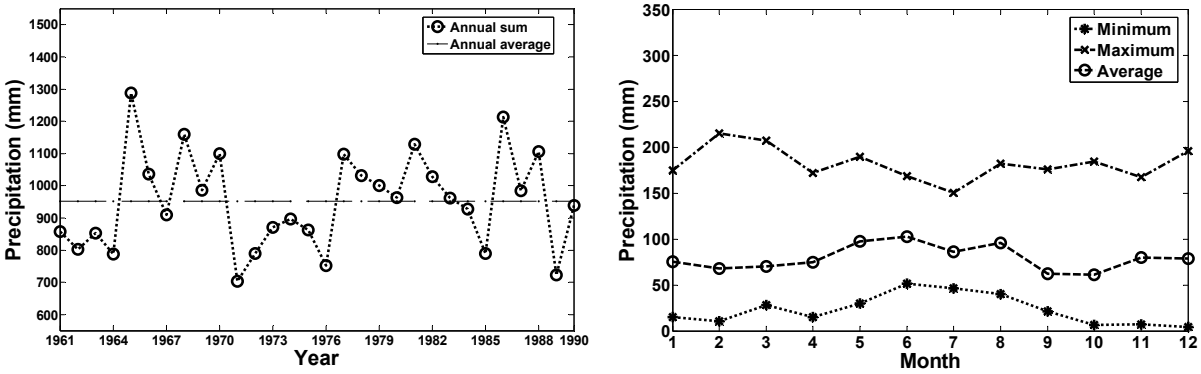

Figure 2.8: Precipitation over the subcatchment Rottweil: annual sum (left panel) and monthly sum (right panel).

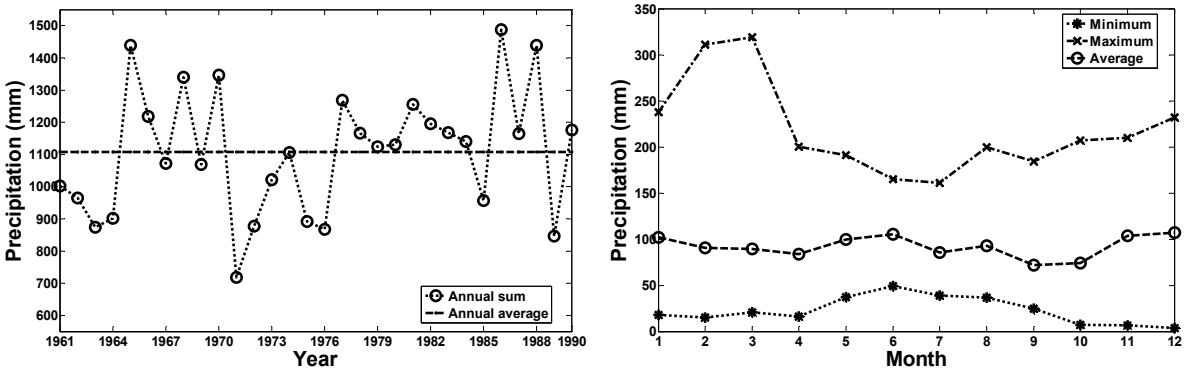

Figure 2.9: Precipitation sum over the subcatchment Horb: annual sum (left panel) and monthly sum (right panel).

The spatial distribution of annual precipitation within the study area for the years 1961, 1970, 1980 and 1990 is depicted in Figure 2.10.

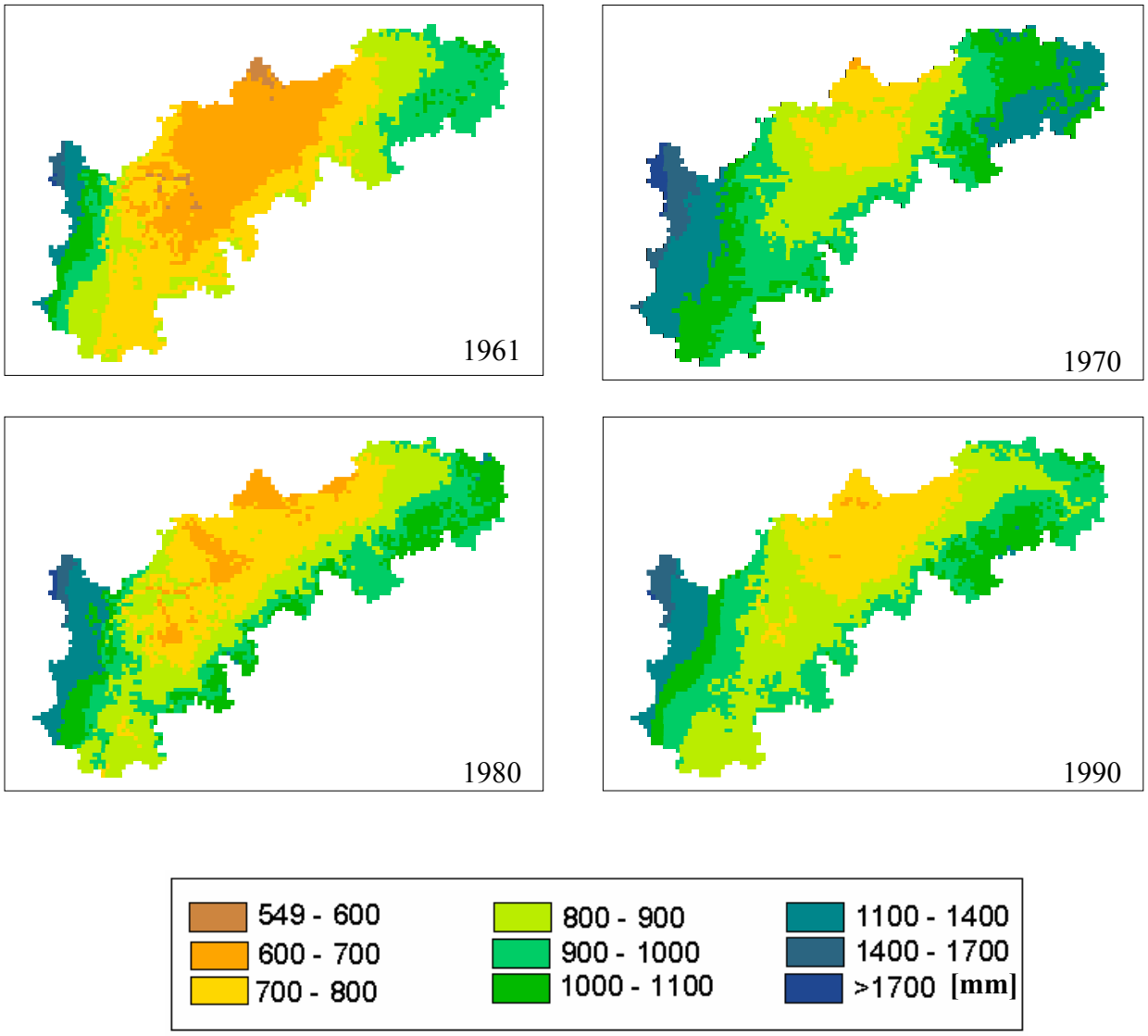

Figure 2.10: Spatial distribution of annual precipitation within the study area for the years 1961, 1970, 1980 and 1990.

Daily mean temperature within the catchment varies between -17.9 °C and 27.3 °C. The annual mean temperature is 8.7 °C. Figure 2.11 shows the mean monthly temperature over the catchment and selected subcatchments, namely Rottweil, Bad Imnau and Plochinegn, Neckar. The minimum, maximum and average values of mean daily temperature and daily amount of precipitation were also calculated for different subcatchments (Table 2.5). The data from 1961 to 1970 was used for calibration and the remaining data was used for validation of the hydrological model latter on. As can be seen in the table, the mean daily temperature in the validation period is slightly higher than that of the calibration period in the majority of the study area. The difference in the mean daily temperature between the validation and calibration periods ranges between 0.4 °C in the Suessen,

Fils subcatchment with no observable changes in the Bad Imnau, Eyach and Rangendingen, Starzel subcathments. A higher difference is observable on the minimum and the maximum mean daily temperature. In contrast, the mean daily precipitation over the validation period in different parts of the study area is between 0 to 11% less than that the corresponding value in the calibration period. The variability of both the daily mean temperature and daily amount of precipitation are more or less similar in the calibration and validation periods.

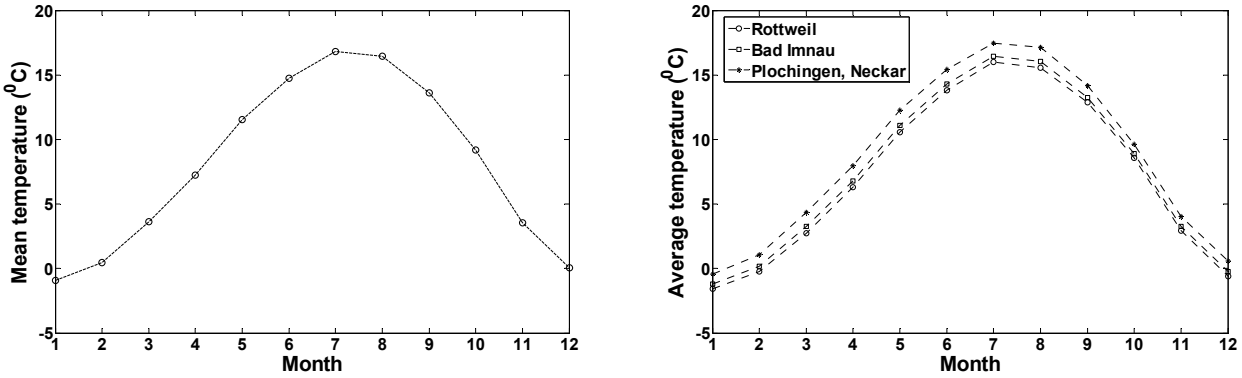

Figure 2.11: Mean monthly temperature over the study catchment (left panel) and over the selected subcatchments (right panel).

2.5 Runoff

The mean runoff for the entire catchment at the outlet in Plochingen is 50.2 m^3/s for the period of 1961 to 1990. The runoff within the catchment is highly variable is illustrated in Table 2.6. The lowest values of 0.5 m^3/s occurred in February for Rottweil gauge, and in September for Oberndorf gauge. Low flow periods for Horb, Plochingen, Fils and Plochingen, Neckar gauges occur mostly in October and at the beginning of November. Flood periods for most of the subcatchments are in February. The highest discharge value of 1031 m^3/s for the observed period of 1961 to 1990 for Plochingen, Neckar gauge took place in May 1978. Since there were some periods of missing data (61% days of the total period) for the discharge gauge at Kirchentellinsfurt, no value is given for this gauge. Figure 2.12 depicts the stream network and discharge gauges of the study catchment.

Table 2.5: Summary of the meteorological variables in the calibration and validation periods in the study area

Subcatchments	**Calibration period**							**Validation period**						
	Mean daily temperature [°C]				Daily amount of precipitation [mm]			Mean daily temperature [°C]				Daily amount of precipitation [mm]		
	Min.	Max.	Mean	St. dev.	Mean	Max.	St. dev.	Min.	Max.	Mean	St. dev.	Mean	Max.	St. dev.
Rottweil	-17.1	23.8	7.1	7.6	2.7	46.4	4.7	-20.2	26.2	7.4	7.2	2.6	67.1	4.9
Oberndorf	-16.2	24.1	7.6	7.6	2.6	45.9	4.6	-20.0	26.5	7.7	7.2	2.5	68.3	4.9
Horb	-16.3	24.1	7.7	7.6	3.1	53.2	5.5	-19.1	26.6	7.9	7.2	3.0	71.6	5.8
Bad Imnau, Eyach	-16.1	24.3	7.7	7.7	2.4	38.1	4.4	-19.9	26.5	7.7	7.2	2.4	63.8	4.6
Rangendingen, Starzel	-16.5	24.4	7.6	7.7	2.4	37.6	4.4	-20.2	26.85	7.6	7.3	2.5	65.0	4.7
Tuebingen, Steinlach	-16.7	24.7	8.0	7.8	2.4	41.9	4.4	-19.9	27.1	8.1	7.3	2.4	62.6	4.7
Kirchentellinsfurt, Neckar	-16.3	24.7	8.4	7.7	2.2	43.6	4.1	-19.3	26.9	8.5	7.3	2.2	49.5	4.3
Wannweil, Echaz	-16.9	24.6	7.9	7.8	2.4	49.6	4.4	-20.5	27.3	8.1	7.3	2.4	66.1	4.8
Riederich, Erms	-19.3	24.5	7.5	7.8	2.5	48.5	4.6	-20.3	27.7	7.7	7.3	2.6	74.9	5.0
Oberensingen, Aich	-15.9	25.5	8.6	7.7	2.1	45.3	4.1	-19.2	27.5	8.8	7.3	2.1	73.5	4.4
Suessen, Fils	-17.0	24.5	7.4	7.8	2.8	52.1	5.1	-19.3	28.2	7.8	7.4	2.8	66.0	5.4
Plochingen, Fils	-15.4	25.2	8.7	7.7	2.6	47.1	4.8	-19.1	28.0	9.0	7.3	2.5	65.5	4.9
Plochingen, Neckar	-16.1	25.3	8.5	7.7	2.4	44.6	4.4	-19.5	27.7	8.8	7.3	2.4	70.5	4.7

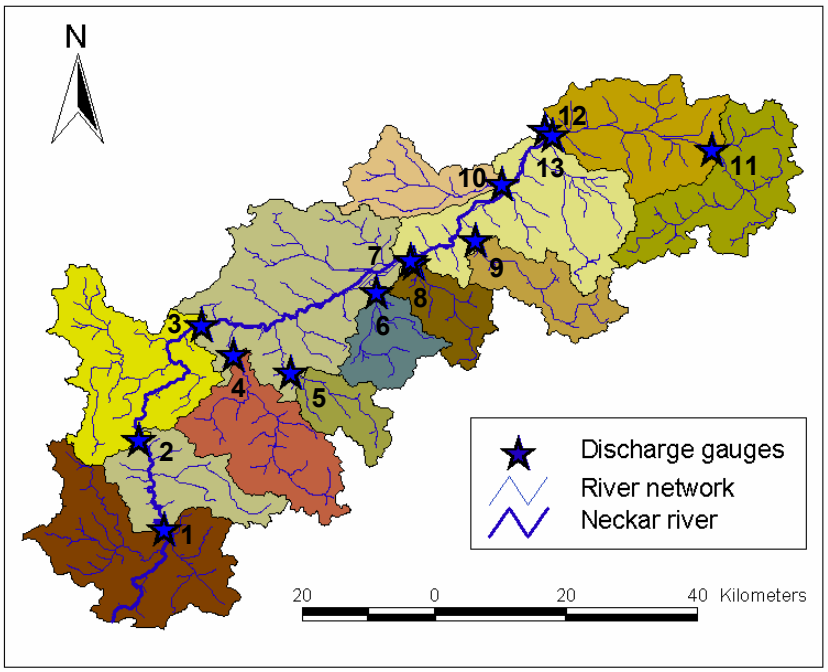

Figure 2.12: Stream network and discharge gauges of the study catchment.

Table 2.6: Characteristics of different discharge gauges in the upper Neckar catchment.

Discharge gauge		Drainage area [km^2]	Discharge measurements [m^3/s]			
			Min.	Max.	Mean	St. dev.
1	Rottweil	456.0	0.5	146.7	5.2	7.1
2	Oberndorf	691.0	0.4	172.7	8.0	9.7
3	Horb	1118.0	1.0	420.3	14.8	18.5
4	Bad Imnau, Eyach	323.0	0.3	85.8	3.5	4.8
5	Rangendingen, Starzel	118.0	0.0	36.2	1.3	1.7
6	Tuebingen, Steinlach	140.0	0.0	46.5	1.8	2.2
7	Kirchentellinsfurt	-	-	-	-	-
8	Wannweil, Echaz	135.0	0.0	34.2	2.8	2.1
9	Riederich, Erms	170.0	0.2	31.7	3.1	2.2
10	Oberensingen, Aich	175.0	0.1	82.2	1.3	2.0
11	Suessen, Fils	340.0	0.6	75.5	6.0	6.2
12	Plochingen, Fils	692.0	0.6	171.2	9.9	11.6
13	Plochingen, Neckar	3962.0	5.3	1031.0	50.2	51.1

2.6 Evapotranspiration

Evapotranspiration (ET) is the process by which water is returned to the atmosphere. It is an important hydrological process that influences the water balance of the catchment. It represents a significant water loss from a catchment. Types of vegetation and land use both considerably affect evapotranspiration, and therefore the amount of water leaving a catchment.

ET is the sum of evaporation and plant transpiration. Evaporation accounts for the movement of water to the air from sources such as the soil, canopy interception, and water bodies. The process of evaporation is influenced by different meteorological variables, the nature of the evaporating surface, and availability of water. The meteorological variables include the energy available from net radiation and ambient air temperature, which is responsible for converting the liquid water into vapour; the humidity gradient at the evaporating surface, which influences the capacity of the water vapour on the evaporating surface to move into the atmosphere; and the wind speed, which removes the water vapour from the adjacent air mass and maintains the humidity gradient. Transpiration accounts for the movement of water within a plant and the subsequent loss of water as vapour through stomata in its leaves. The amount and rate of transpiration depends on the type of vegetation cover and their stage of growth, season of the year, time of the day, availability of water in the root zone, and the same meteorological factors that affect evaporation.

Potential ET is the amount of water that would be evaporated under an optimal set of conditions, among which is an unlimited supply of water. This demand incorporates the energy available for evaporation and the ability of the lower atmosphere to transport evaporated moisture away from the land surface. Actual ET is the amount of water that is actually removed from a surface due to the processes of evaporation and transpiration. Depending on the availability of water, it can be equal or lower than the potential ET. Although it is the actual ET that is used in the water balance calculation, an estimate of the potential ET for a given catchment condition under the prevailing climatic conditions is an important step in rainfall-runoff modeling practice. The actual ET is then estimated based on the potential value and the availability of moisture supply to meet this demand.

There are many methods available for the estimation of potential ET that range from data intensive physical approaches, such as Penman-Monteith equation (Monteith, 1965), to the less data demanding approaches like the Blaney and Criddle (1950); Hargreaves and Samani (1985) method. The Penman-Monteith equation is a predominantly physically-based approach, indicating that the method can be used globally without any additional parameter estimation. A major drawback to application of the Penman-Monteith equation, however, is the relatively high data demand, the method requires air temperature, wind speed, relative humidity, and solar radiation data.

The limitation of reliable data made the Hargreaves and Samani (1985) method the appropriate choice in this study. This method estimates potential ET as a function of extraterrestrial radiation and air temperature.

$$ET_0 = 0.0023 \times 0.408 \times RA \times (T_{avg} + 17.8) \times (T_{\max} - T_{\min})^{0.5} \qquad (2.1)$$

where:

ET_0	[mmd^{-1}]	potential evapotarnspiration
RA	[$MJm^{-2}d^{-1}$]	extraterrestrial radiation
T_{min}	[^oC]	daily minimum temperature
T_{max}	[^oC]	daily maximum temperature
T_{avg}	[^oC]	average daily temperature

The constant 0.408 is used to convert the radiation to evaporation equivalents in mm. Since extraterrestrial radiation can be calculated for a certain day and location (Allen, et al., 1998), only the minimum and maximum temperature requires observation. The Hargreaves method (Hargreaves and Samani, 1985) has been tested using some high quality lysimeter data representing a broad range in climatological conditions (Hargreaves, 1994). The results have indicated that this equation was nearly as accurate as Penman-Monteith on a weekly or longer time step, and was therefore recommended in cases where reliable data were lacking.

The long-term mean monthly potential evapotranspiration for a reference crop (grass) was estimated using the Hargreaves and Samani (1985) method on the same grid used for the interpolation of precipitation and temperature within the study area. Depending on the type of vegetation cover, these values were multiplied by the crop coefficient for the given vegetation type to that of grass to estimate the potential evapotranspiration of other vegetation types.

3 Model structure description

3.1 Model selection for the study

There are numerous criteria which can be used for selecting the appropriate hydrologic model. These criteria are always research study dependent, since every research study has its own specific requirements and needs. Among the various selection criteria, the following had to be considered in selecting the model to be applied in this study:

- The model should not be data intensive. The data requirement should be addressed by the available observations and measurements within the study area.
- The model should not be complex. The model structure should represent the most relevant processes to estimate the desired outputs adequately.
- The model should not have too many parameters.

Based on the above criteria, the HBV model (Bergström and Forsman, 1973) was selected to carry out majority of the study objectives. Originally, the HBV model was developed at the Swedish Hydrological and Meteorological Institute (SMHI) for runoff simulation and hydrological forecasting, but the scope of applications has increased steadily. Based on the original model, a modified version developed at the Institute of Hydraulic Engineering has been used for the study. The following brief introduction to the principal model structure and process representations is based on the description of Bergström, 1995, Lindström et al. (1997), Ehret (2003), Hundecha and Bárdossy (2004) and Das et al. (2006).

3.2 The HBV model

Figure 3.1 shows the principal processes covered by the modified HBV model. The model consists of three main components:

- Snow accumulation and melt routine
- Soil moisture accounting routine
- Runoff response routine

The model uses subcatchments as primary hydrological units. Further zoning of the subcatchments into homogeneous units based on elevation, land use, soil type or combinations of them is possible. On the following pages, each model component is explained in detail.

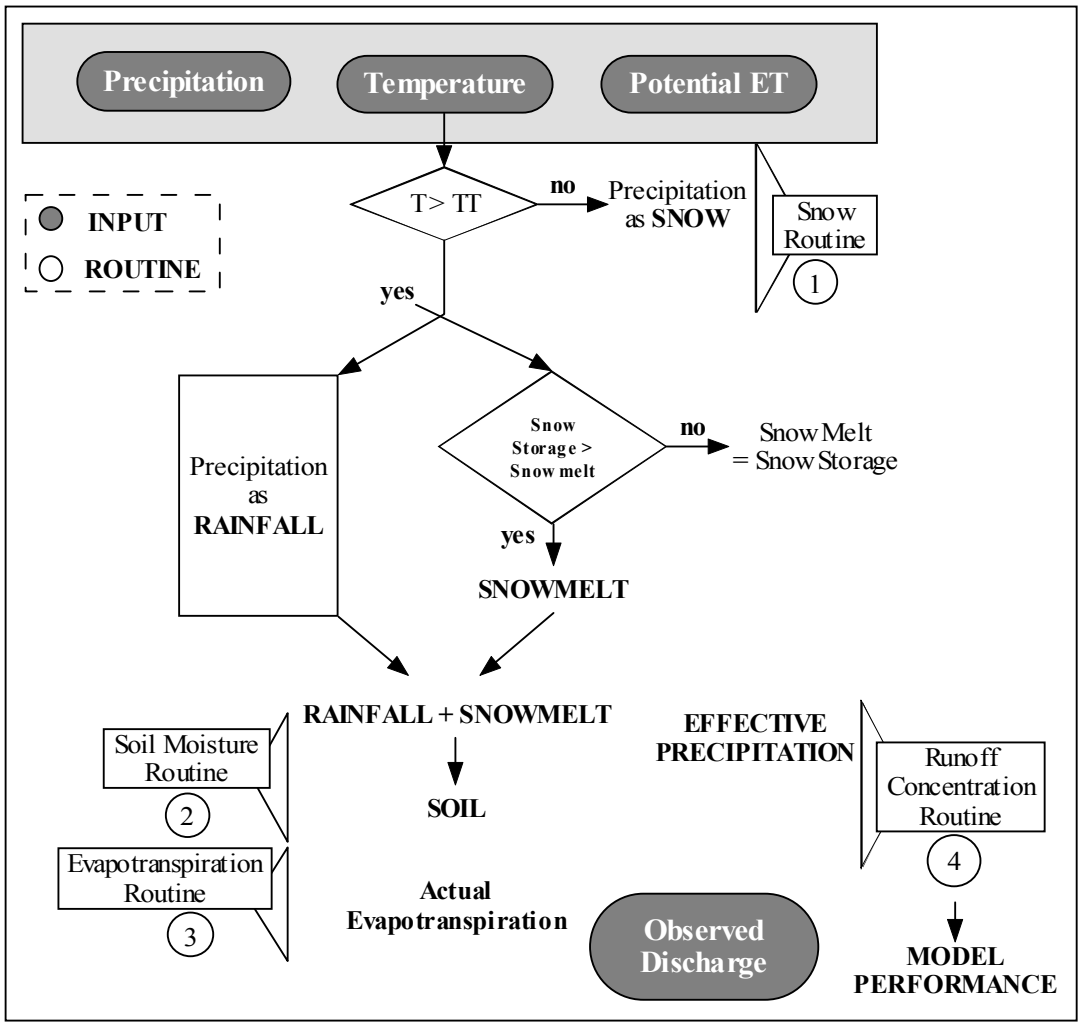

Figure 3.1: Schematic view of the modified HBV model.

3.2.1 Snow accumulation and melt

Snow accumulation and melt is modeled by a degree-day method. In this method, the daily rate of snowmelt in water equivalent is proportional to the increase in daily temperature above a threshold value T_{crit}.

$$MELT = DD \cdot (T - T_{crit}) \tag{3.1}$$

where:

MELT	$[LT^{-1}]$	snowmelt rate as water equivalent
DD	$[L\theta^{-1}T^{-1}]$	degree-day factor
T	$[\theta]$	mean daily air temperature
T_{crit}	$[\theta]$	threshold temperature for snow melt initiation

The precipitation is assumed to accumulate as snow when the air temperature drops below the threshold value T_{crit}. Precipitation input is thus modeled as snow or rain according to the prevailing

temperature. The zoning of subcatchments based on elevation allows the individual consideration of snowfall and snowmelt at different heights.

The snow routine of the HBV model generally has two free parameters, DD and T_{crit}, which have to be estimated by calibration.

In the original HBV model, the degree-day factor, DD, was set as constant. However, it is known that whenever there is rainfall, the energy available in the rainwater with a positive temperature enhances snow melt. In order to include this effect in the rate of snowmelt, the degree-day factor was modified as a linear function of the daily depth of precipitation (Hundecha, 2005).

$$DD = \begin{cases} DD_0 + k.P & if \quad P \le \dfrac{DD_{\max} - DD_0}{k} \\ DD_{\max} & else \end{cases} \tag{3.2}$$

where:

DD_0	$[L\theta^{-1}T^{-1}]$	degree-day factor when there is no rainfall
DD_{max}	$[L\theta^{-1}T^{-1}]$	upper limit to the degree-day factor
P	[L]	daily depth of precipitation
k	[-]	a positive constant

This entails that the degree-day value not only increases with rising temperature but also with higher precipitation amounts. Unrealistically with high snowmelts which might occur with high rainfall intensities are prevented by the degree-day value's upper limit (DD_{max}).

3.2.2 Soil-moisture and effective precipitation

The soil-moisture accounting routine of the HBV model is based on a modification of the bucket theory in that it assumes a statistical distribution of storage capacities in a catchment. The routine computes an index of the wetness of the entire catchment and integrates interception and soil moisture storage. The routine is controlled by two free parameters, FC and β. FC is the maximum soil storage in the basin and β determines the relative contribution to runoff from a millimetre of rain or snowmelt at a given soil-moisture deficit. This is calculated using the following relation.

$$P_{eff} = \left(\frac{SM}{FC}\right)^{\beta} \cdot (P + MELT) \tag{3.3}$$

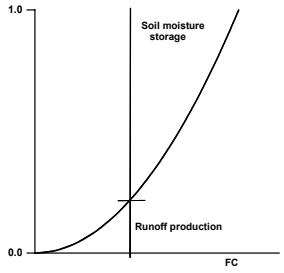

where:

P_{eff}	[L]	effective precipitation
SM	[L]	actual soil-moisture
FC	[L]	maximum soil storage capacity
β	[-]	a model parameter (shape coefficient)
P	[L]	depth of daily precipitation

The remaining part of the rainfall or snow melt is added to the soil moisture until the storage capacity of the soil FC is reached. The effect of the curve determining runoff generation is that the response is gradually increasing with increasing wetness. Thus the routine may be considered to account for small scale properties within the catchment.

3.2.3 Evapotranspiration

The evapotranspiration routine in the HBV model is based on monthly values of potential evapotranspiration as inputs. In order to improve the model performance when either the spring or summer is much colder than normal and when daily changes of the weather inputs need to be taken into account, a correction factor based on mean daily temperatures and long-term averages is included according to the following equation.

$$PE_a = (1 + C \cdot (T - T_m)) \cdot PE_m \qquad (3.4)$$

where:

PE_a	[L]	adjusted potential evapotranspiration
C	$[\theta^{-1}]$	model parameter
T	[θ]	mean daily air temperature
T_m	[θ]	long term mean monthly air temperature
PE_m	[L]	long term mean monthly potential evapotranspiration

The actual soil-moisture has an important influence on the magnitude of the real evapotranspiration. Only in the case of optimum water availability, the actual evapotranspiration occurs at the rate of potential evapotranspiration. In the model, this is accounted for by a soil-moisture limit, PWP, from which the actual evapotranspiration will be linearly reduced according to a lack of water availability.

$$E_a = PE_a \cdot \frac{SM}{PWP} \quad \text{for} \quad SM < PWP$$
$$E_a = PE_a \quad \text{for} \quad SM \geq PWP \qquad (3.5)$$

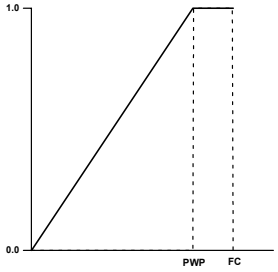

where:

E_a	[L]	actual evapotranspiration
PWP	[L]	soil-moisture limit for evapotranspiration decrease

The actual potential evapotranspiration, E_a, cannot have a negative value.

3.2.4 The response function

The catchment response routine transforms excess water from the soil-moisture routine to discharge at the outlet of each subcatchment. The routine consists of two conceptual reservoirs arranged one over another. The first reservoir simulates the near surface flow and interflow in the sub-surface, while the lower reservoir represents the base flow. Both reservoirs are connected in series by a constant percolation rate and are considered linear with a constant recession coefficient. In addition to the regular outlet, the upper reservoir also features a threshold-dependent runoff component: only if the reservoir level exceeds a certain threshold, will fast runoff from the upper outlet occur. Overall, the response function consists of the following model parameters: three recession coefficients K_0, K_1, K_2, a threshold water level L and a constant percolation rate K_{perc} between upper and lower reservoirs.

$$Q_0 = \begin{cases} \frac{1}{K_0} \cdot (S_i - L) \cdot A_{sc} & \text{for } S > L \\ 0 & \text{for } S \le L \end{cases}$$

$$Q_1 = \frac{1}{K_1} \cdot (S_i) \cdot A_{sc}$$

$$Q_{perc} = \frac{1}{K_{perc}} \cdot (S_i) \cdot A_{sc}$$

$$Q_2 = \frac{1}{K_2} \cdot (S_b) \cdot A_{sc} \qquad (3.6)$$

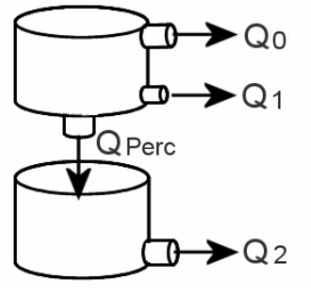

where:

Q_0	[L^3T^{-1}]	near surface flow
Q_1	[L^3T^{-1}]	interflow
Q_{perc}	[L^3T^{-1}]	percolation
Q_2	[L^3T^{-1}]	baseflow
K_0	[T^{-1}]	near surface flow storage constant
K_1	[T^{-1}]	interflow storage constant
K_{perc}	[T^{-1}]	percolation storage constant
K_2	[T^{-1}]	baseflow storage constant
S_i	[L]	upper reservoir water level
S_b	[L]	lower reservoir water level
L	[L]	threshold water level for near surface flow
A_{sc}	[L^2]	subcatchment area

The total runoff is computed as the sum of the outflows from the upper and the lower reservoirs. The total flow is then smoothed using a transformation function, consistsing of a triangular weighing function with one free parameter, MAXBAS.

$$Q = g(t, MAXBAS).(Q_0 + Q_1 + Q_2) \tag{3.7}$$

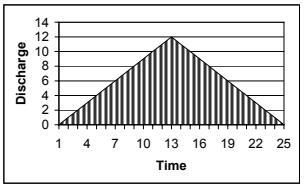

where:

Q	[L^3T^{-1}]	current overall discharge
MAXBAS	[T]	duration of the triangular weighting function (Unit Hydrograph)

3.2.5 River routing

The flow is routed from one node to the other of the river network by the means of Muskingum flood routing method. It represents a river stretch between two sections using a prism and a wedge storage. Following iterative calculation of the two routing parameters, K and x, the flood propagation is calculated according to the formula provided below.

$$Q_{out}(t_i) = C_1' \cdot Q_{in}(t_i) + C_2' \cdot Q_{in}(t_{i-1}) + C_3' \cdot Q_{out}(t_{i-1})$$

$$C_1' = -\frac{K \cdot x - \left(\frac{\Delta t}{2}\right)}{K \cdot (1-x) + \left(\frac{\Delta t}{2}\right)} \;;\; C_2' = \frac{K \cdot x + \left(\frac{\Delta t}{2}\right)}{K \cdot (1-x) + \left(\frac{\Delta t}{2}\right)} \;;\; C_3' = -\frac{K - (K \cdot x) - \left(\frac{\Delta t}{2}\right)}{K \cdot (1-x) + \left(\frac{\Delta t}{2}\right)} \tag{3.8}$$

where:

$Q_{out}(t_i)$	[L^3T^{-1}]	discharge leaving the river stretch at time-step t_i
$Q_{out}(t_{i-1})$	[L^3T^{-1}]	discharge leaving the river stretch at time-step t_{i-1}
$Q_{in}(t_i)$	[L^3T^{-1}]	discharge entering the river stretch at time-step t_i
$Q_{in}(t_{i-1})$	[L^3T^{-1}]	discharge entering the river stretch at time-step t_{i-1}
K	[L]	retention constant of the Muskingum model
x	[-]	weighting factor of the Muskingum model
C_1', C_2', C_3'	[-]	formula parameters

3.3 Development of different model structures

In the existing HBV model structure, the subcatchment is divided into a number of zones according to elevation, land use or soil type or combinations of those characteristics. However, the distribution of each subcatchment into different elevation and land categories is not spatially fixed. It implies that geographical information is taken from actual physical data, and is represented in each subcatchment only as a percentage of the whole area for that subcatchment without keeping track of exactly where that percentage is located in space.

Based on the HBV model concept, four different model structures were developed. The differences and similarities of different structures are summarized below.

3.3.1 Distributed model structure

The modifications were undertaken in the distributed model structure to account for detailed basin characteristics (e.g., soil and land use), processes calculation and highly resolved meteorological variables (e.g., precipitation). The modified model was configured into a raster form. In the modified structure, the catchment can be divided into number of subcatchments, as in the case of existing semi-distributed model structure. However, each subcatchment can be divided into a number of regular grid cells in the modified structure. Thus the advantage of representing the subcatchment as raster form lies in the ability to utilize spatially highly resolved rainfall data, to account for detailed processes calculation and to obtain the detailed configuration of the aforementioned catchment characteristics. The primary difference between the original model structure and the modified distributed structure is the use of grid cells as primary hydrological units in the modified structure (Figure 3.2).

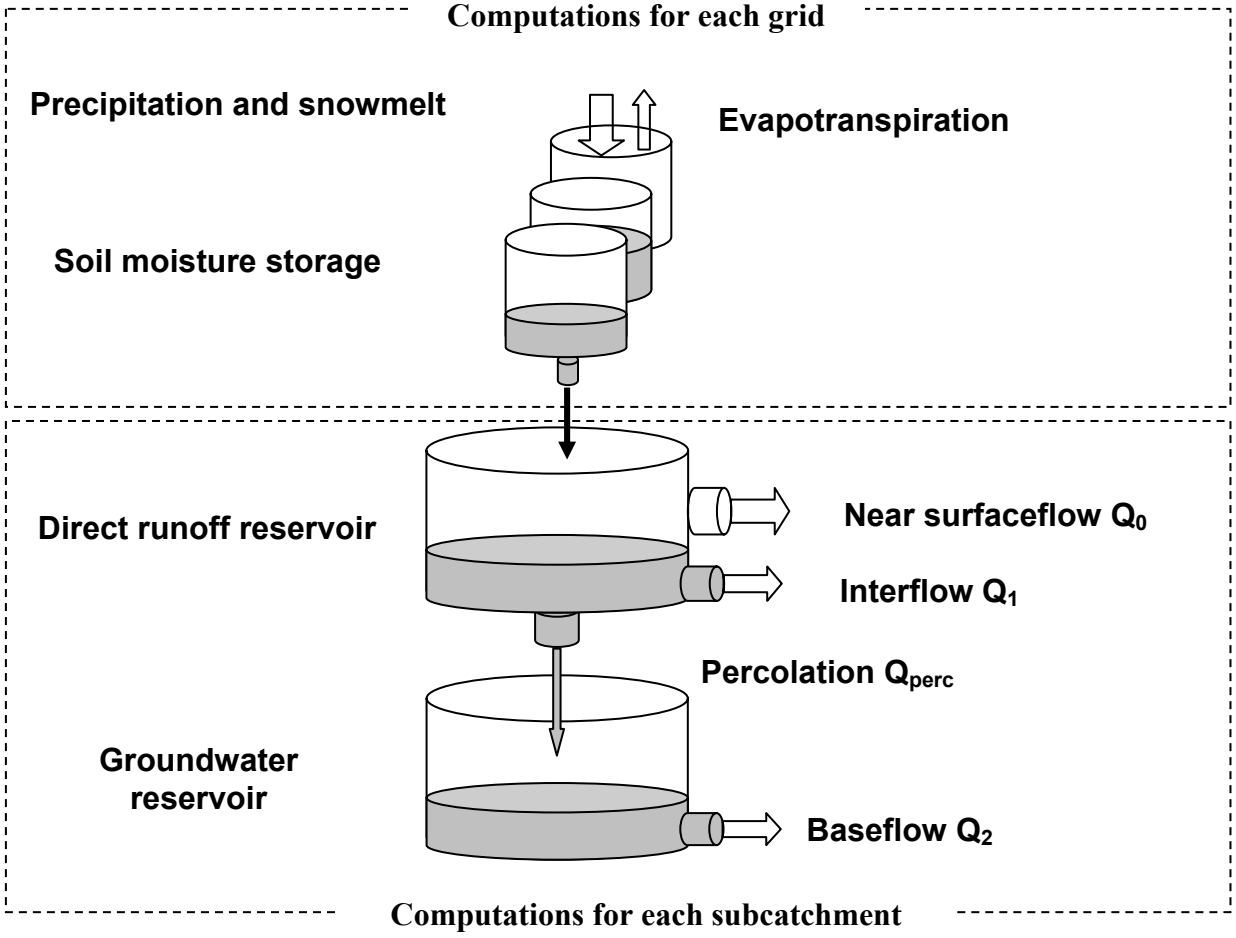

Figure 3.2: Modified distributed model structure and representation of main processes.

Due to this modification in the model structure, the snow accumulation and melt routine, the soil moisture accounting routine and the actual evapotranspiration are computed for each grid cell individually. The runoff response process, which is represented conceptually by reservoirs for direct discharge and base flow, for each subcatchment is kept unchanged as in the original model structure to restrict the numbers of model parameter to be optimized. In principle the model parameters related to snow accumulation and melt and soil moisture accounting routines can be adjusted differently for every grid in the modified model structure. In the present study, the subcatchments were divided into a number of regular grids having an area of 1 km^2. For the modeling of the processes in each grid, the interpolated daily precipitation amount and mean daily temperature on a regular grid of 1 km × 1 km was assigned to every computational grid. The evapotranspiration calculated on 1 km × 1 km grid was used as an input to the model grid.

3.3.2 Semi-distributed model structure

In the semi-distributed model structure sub-division of the subcatchments into a number of different homogenous zones can be accomplished based on the catchment characteristics that have an influence on the runoff generation processes. Topographic elevation, soil type, and land use may be considered in defining zones. The meteorological variables are then assigned for each zone. In principle, the model parameters related to the snow accumulation and melt and the soil moisture accounting routine can be different for each zone.

As elevation affects the distribution of the basic meteorological variables such as precipitation and temperature as well as the rate of evaporation and snow melt and accumulation, it represents an important catchment characteristic that was considered in defining zones in this study. Elevation zones were defined using a contour interval of 75 m. Areas between successive contour intervals were considered homogenous with respect to elevation. The elevation of the study area varies from about 250 m to around 1000 m and therefore, a maximum of 10 elevation zones were defined in each subcatchment. In order to model the processes in each zone, the values of mean daily precipitation amount and the mean daily temperature were assigned in each zone. The meteorological variables for each zone were estimated as the mean of the interpolated values on the regular grids of 1 km × 1 km located within a given zone. The potential evapotranspiration was also averaged over each zone from the calculated evapotranspiration on 1 km × 1 km grids located within a given zone.

3.3.3 Semi-lumped model structure

The meteorological variables and potential evapotranspiration are assigned to each zone similar to the semi-distributed model structure. The only difference between the semi-distributed and semi-

lumped structures lies in the fact that the model parameters for the snow accumulation and melt and soil moisture accounting routines are assigned same values for every zone within each subcatchment. However, those can be different for different subcatchments.

3.3.4 Fully-lumped model structure

The meteorological variables and actual evapotranspiration are assigned to each subcatchment. All the processes namely, snow melt and accumulation, soil moisture accounting and runoff response are calculated for each subcatchment. The model parameters related to snow accumulation and melt and soil moisture accounting routines are maintained for each subcatchment.

For each subcatchment the meteorological variables were estimated as the mean of the interpolated values on the regular grids of 1 km × 1 km located within a given subcatchment. The potential evapotranspiration was also averaged over each subcatchment from the calculated evapotranspiration on 1 km × 1 km grids located within a given subcatchment.

Table 3.1 demonstrates the features of the different model structures.

3.4 Automatic parameter estimation procedure for the HBV model

Conceptual models describe all of the component hydrological processes perceived to be of importance as simplified conceptualization (Kokkonen and Jakeman, 2001). Contrary to more complex, physically-based distributed models such as the MIKE SHE model (Abbott et al., 1986a,b), or the SHETRAN model (Ewen et al., 2000), the required input data are readily available for most applications. In addition to their modest data requirement, conceptual models are usually simple and relatively easy to apply. However, for partly or fully conceptual models, some parameters cannot be considered as physically measured quantities and thus have to be estimated on the basis of the available data and information. Thus, the final parameter estimation must be performed by calibration against observed data. Traditionally, calibration has been performed manually using a trial and error parameter adjustment procedure. The process of manual calibration, however, may be a very tedious and time consuming task, depending on the number of free model parameters and parameter interaction. Furthermore, because of the subjectivity involved, it is difficult to explicitly assess the confidence of the model simulations. Due to this, a great deal of research has been directed to the development of more effective and efficient automatic calibration procedures (Madsen et al., 2002). Effective and efficient state-of-the-art procedures include combinatorial algorithm simulated annealing (Hartmann and Bárdossy, 2005), population-evolution based optimization algorithms such as genetic algorithms (Seibert, 2002) and the shuffled complex evolution method (Duan et al., 1993a,b). The model calibration procedure adopted in this work followed the automatic parameter estimation technique based on the combinatorial optimization

algorithm simulated annealing (Aarts and Korst, 1989). Simulated annealing (Aarts and Korst, 1989) is a Monte Carlo optimization technique (Metropolis et. al., 1953) proposed by Kirkpatrick et al., (1983). A simulated annealing optimization starts with a Metropolis Monte Carlo simulation at high temperature. This means that a relatively large percentage of the random steps that result in an increase in the energy will be accepted. After a sufficient number of Monte Carlo steps, or attempts, the temperature is decreased. The metropolis Monte Carlo simulation is then continued. This process is repeated until the final temperature is reached.

Table 3.1: General features of different model structures.

Model structure	Scale of meteorological variables		Processes calculation scale			Scale of parameterization		Discharge comparison
	Preci. & Temp.	Pot. ET	Eff. Preci.	Actual ET	Runoff Concent.	Soil parameters	Snow parameters	
Fully-lumped	sub catch	sub catch	sub catch	sub catch	sub catch	sub catch	sub catch	sub catch
Semi-lumped	zone	zone	zone	zone	Sub catch	sub catch	sub catch	sub catch
Semi-distributed	zone	zone	zone	zone	sub catch	zone	zone	sub catch
Distributed	grid	grid	grid	grid	sub catch	geoclass A (SC & LC)	geoclass B (LC)	sub catch

Total number of subcatchments (sub catch):	13
Total number of grids in the catchment :	3962
Total number of zones in the catchment:	82
Total number of geoclasses A (based on Soil Class-SC and Landuse Class -LC):	28
Total number of geoclasses B (based on Landuse Class-LC):	4

Optimization by simulated annealing mimics the physical process of annealing, which is the process of growing a crystal in a fluid by melting the fluid at higher temperature and cooling slowly to a lower temperature in a way that minimizes the energy of the system. At the end of this process, the crystal attains at its lowest energy state. In statistical mechanics, experiments that determine the low-temperature state of a material spend a long time at the vicinity of the freezing point. If this is not done, then either the resulting crystal may have many defects or the substance may form a glass, with no crystalline order (Kirkpatrick et. al., 1983). Thus, finding the low temperature state of a system, when a description for calculating its energy is given, is an optimization problem like those in combinatorial optimization. The temperature of a physical system has no obvious equivalent in the optimized systems. In simulated annealing, temperature is the control parameter.

The implementation of an automatic model calibration procedure requires the selection of the followings (Yapo et al., 1996):

- a calibration data set
- a 'goodness-of-fit' measure i.e., objective function
- an automatic parameter estimation procedure i.e., optimization algorithm
- a region of the parameter space to be searched i.e., a feasible parameter space
- a validation procedure to determine the degree of uncertainty in the model

The most important part of this procedure is the selection of an appropriate objective function.

3.4.1 Objective function

For the determination of an appropriate set of parameters, the performance of a model must be measured, i.e., the objective criteria to measure the quality of the results must be defined. A typical objective function is the Nash Sutcliffe coefficient (R_m^2) (Nash and Sutcliffe, 1970) was used. The model was calibrated with the dual objective of simulating the observed daily discharge and preserving the mean runoff over longer periods based on the procedure described by Hartmann and Bárdossy, 2005. This was achieved by a simultaneous calibration of the model for the daily and longer time scales. The different aggregation times are calculated as follows. Assuming $Q_o(t_i)$ is the observed discharge series and $Q_s(\theta,t_i)$ is the simulated discharge with model parameter θ for the time step t_i. According to the selected time period P and whether extremes are considered or not, the weight for time t_i is defined as $w(t_i,P,x)$. Considering the time step of the model is t_i-t_{i-1}= t; I is the total number of time steps and l is the summation index. Thus R_m^2 can be defined for time steps $j\Delta t$ as:

$$R_m^2(j,P,\theta,x) = 1 - \frac{\sum_{l=1}^{\frac{I}{j}} \left(\sum_{i=1}^{j} Q_0(t_{(l-1).j+i}).w(t_{(l-1).j+i},P,x) - \sum_{i=1}^{j} Q_s(t_{(l-1).j+i}).w(t_{(l-1).j+i},P,x) \right)^2}{\sum_{l=1}^{\frac{I}{j}} \left(\sum_{i=1}^{j} Q_0(t_{(l-1).j+i}).w(t_{(l-1).j+i},P,x) - \sum_{i=1}^{j} \overline{Q_o}.w(t_{(l-1).j+i},P,x) \right)^2} \quad (3.9)$$

where, in case extremes are not emphasized (x=1):

$$w(t_i,P,1) = \begin{cases} 0 & if \quad i \notin P \\ 1 & else \end{cases} \quad (3.10)$$

or, in case extremes are emphasized (x=2):

$$w(t_i,P,2) = \begin{cases} 0 & if \quad i \notin P \\ \sqrt{Q_0(t_i) + Q_s(t_i)} & else \end{cases} \quad (3.11)$$

The calibration of the model was performed for different time intervals. Thus, multiple objectives were considered when calibrating the model. The overall objective function to be optimized is therefore the arithmetic sum of the Nash-Sutcliffe coefficients corresponding to the discharges at the different time scales defined as:

$$S(P,\theta) = \alpha_1 R_m^2(1,P,\theta,1) + \alpha_2 R_m^2(1,P,\theta,2) + \alpha_3 R_m^2(365,P,\theta,1) \quad (3.12)$$

The weights α_1, α_2 & α_3 are defined by the user depending on the application purposes. For this study, the main objective is the estimation of the daily and the peak discharges, while preserving the annual water balance. The values of α_1, α_2 & α_3 were assigned as 1, 2 and 1 respectively.

3.4.2 Automatic optimization algorithm Simulated Annealing

The algorithm of the simulated annealing method applied for maximizing the objective function to optimize the HBV model parameters is as follows:

1. Select a starting annealing temperature and a number of iterations N_s to be tried before decreasing the temperature. Select a reduction factor in which the temperature decreases.
2. Compute the initial value of an objective function (O_0) using the initial value of the model parameters. These parameters for the HBV model are, for example, parameters for the snow module, soil module, runoff concentration module and river routing module. Assign at the first time $O_{old}=O_0$.

3. Change the randomly selected parameter value slightly and calculate the objective function (O_{new}) using the new value. If $O_{new}>O_{old}$ the change is accepted (positive change). Else calculate the probability of acceptance pa defined as:

$$p_a = \exp\left(\frac{O_{old} - O_{new}}{T_a}\right) \tag{3.13}$$

where:

O_{old}	old objective function
O_{new}	new objective function
T_a	annealing temperature

Accept the change with probability p_a (negative change) and undo it with probability ($1-p_a$).

This Step ensures that the optimization does not stop at any local minima but will converge toward a global minimum. The annealing temperature T_a regulates the probability of negative changes. The lower T_a indicates less likely the acceptance of a negative change.

4. Repeat the previous step N_s times.

5. Reduce the annealing temperature slightly at a rate defined at step 1. Repeat steps 3 and 4.

6. Repeat the previous step until the termination criteria is reached.

With this optimization algorithm, it is possible to include all kind of known preconditions on the model parameters. Appropriate constraints were assigned for the ranges of the parameters based on the previous studies (Hundecha, 2005). Table 3.2 depicts the model parameters selected to be optimized by the automatic calibration procedure. The interval is broadly defined such that it can include almost all feasible parameter values. Alongside these, other physically meaningful constraints were applied on some model parameters. Here for example, close constraints on soil properties were applied according to the soil types, e.g., the conceptual parameter FC was always kept higher than PWP. Two hundred iteration steps were used, each having a number of repetition steps. To consider non-uniqueness of the optimal parameter set, the same objective functions was used for at least three times with different set of random numbers each time.

Table 3.2**:** Model parameters selected to be optimized by the automatic calibration procedure.

Parameter	Unit	Minimum	Maximum
Snow accumulation and melt module			
T_{crit}	[°C]	-2.0	+2.0
DD_0	[$mm°C^{-1}day^{-1}$]	0.5	5.0
DD_{max}	[$mm°C^{-1}day^{-1}$]	10	
k	[-]	0.0	0.5
Runoff generation module			
FC	[mm]	100.0	400.0
PWP	[mm]	10.0	FC-10.0
β	[-]	1.0	5.0
Runoff concentration module			
L	[mm]	1.0	30.0
K_0	[h]	0.5	20
K_1	[h]	5.0	50.0
K_{perc}	[h]	20.0	100.0
K_2	[h]	10.0	1000.0
River routing module			
K	[h]	0.8	10.0
x	[-]	0.1	0.4

3.4.3 Automatic calibration for different model structures

In the distributed model structure, the model parameters were calibrated based on the concept of hydrological response units (geoclasses) in order to reduce the problem of over-parameterization. A geoclass is defined on the basis of soil type and land use information. The soil type and land use type were re-classified into a smaller number of classes; 7 classes for soil types and 4 classes for land use types. The mentioned catchment characteristics were then categorized into 28 geoclasses. The parameters involved in the soil module (e.g., FC, PWP and β) were optimized based on the geoclasses. Here, for each parameter of each geoclass, a range of maximum and minimum was calculated based on the soil type. Optimized parameters corresponding to the 28 geoclasses were assigned to the grids. Grids (irrespective of location) with similar geoclasses will receive the same value. Thus the calibration procedure based on the hypothesis that the model elements with identical landscape characteristics have similar hydrological behaviour, and should consequently be assigned the same parameter values. During calibration, parameters related to the snow module were optimized and assigned the same value for all the subcatchments.

In the semi-distributed model structure the optimized model parameters related to the soil moisture accounting and snow accumulation and melt routines were different for different zones within a given subcatchment. On the other hand, the optimised parameters were kept constant for every zone within a given subcatchment for the semi-lumped model structure. In the fully-lumped model structure, the parameters were optimized individually for each subcatchment.

3.5 Modeling time step

In order to properly model the magnitude and the time distribution of flood flows from a catchment, rainfall series of higher time resolution is required, since high rainfall intensities over shorter periods have a significant effect on the peak of a flood. However, daily records of meteorological data were used in the present study. Disaggregation of the daily amount by uniformly distributing it through out the day was implemented and the model was run at a time step of 6 hours for the study (Hundecha, 2005).

3.6 The SHETRAN model

To carry out one of the objectives of the research the physically-based spatially-distributed modeling system SHETRAN was also applied. The SHETRAN modeling system was developed at the Water Resource Systems Research Laboratory (WRSRL), University of Newcastle upon Tyne, and is based on the SHE (Systeme Hydrologique Europeen) (Abbott et al., 1986a,b) which was developed by international collaboration among groups in the United Kingdom, Denmark and France.

The following brief introduction to the principal model structure and process representations in the SHETRAN model is mainly based on the description of Ewen et al. (2000), Parkin et al., 2000 and Bathurst et al., 2005.

SHETRAN is a three-dimensional, coupled surface/subsurface, physically-based, spatially-distributed, finite-difference model for coupled water flow, multifraction sediment transport and multiple reactive solute transport in catchments (Figure 3.3). SHETRAN simulates hydrological, sediment transport and landslide response of a catchment. It incorporates a detailed description in time and space of the flow and transport in the catchment. SHETRAN represents processes using physical laws applied on a three-dimensional finite-difference mesh. The mesh follows the topography of the catchment and the parameters of the physical laws vary from point to point on the mesh thus allowing the representation of the spatial heterogeneity of the physical properties of the rocks, soils, vegetation cover, etc.

The main advantage of SHETRAN over existing physically based, spatially-distributed, catchment modeling systems lies in its comprehensive nature and its capabilities for modeling subsurface flow and transport. The subsurface is treated as a variably saturated heterogeneous porous medium and fully three-dimensional flow and transport can be simulated for combinations of confined, unconfined and perched systems. The “unsaturated zone” is modeled as an integral part of the subsurface, and subsurface flow and transport are coupled directly to surface flow and transport. Unlike SHE, SHETRAN has not followed the “layered” approach (i.e., ground surface,

unsaturated zone, and saturated zone) for computation. The main computational structures in SHETRAN are “stream links” and “columns” (Figure 3.3). River networks are modeled as networks of stream links, and the rest of the basin is modeled as a set of columns, each containing its own part of the ground surface and vegetation. Each column comprises of many finite-difference cells, stacked one above the other, and there may be a different soil or rock associated with each cell. There is lateral flow between cells in neighboring columns, as well as vertical flow in each column, thus giving flow in three dimensions. Three main components lie at the core of SHETRAN, one each for water flow, sediment transport and solute transport. Flow is assumed not to be affected by sediment transport and sediment transport not to be affected by solute transport. The three components lie in a natural hierarchy.

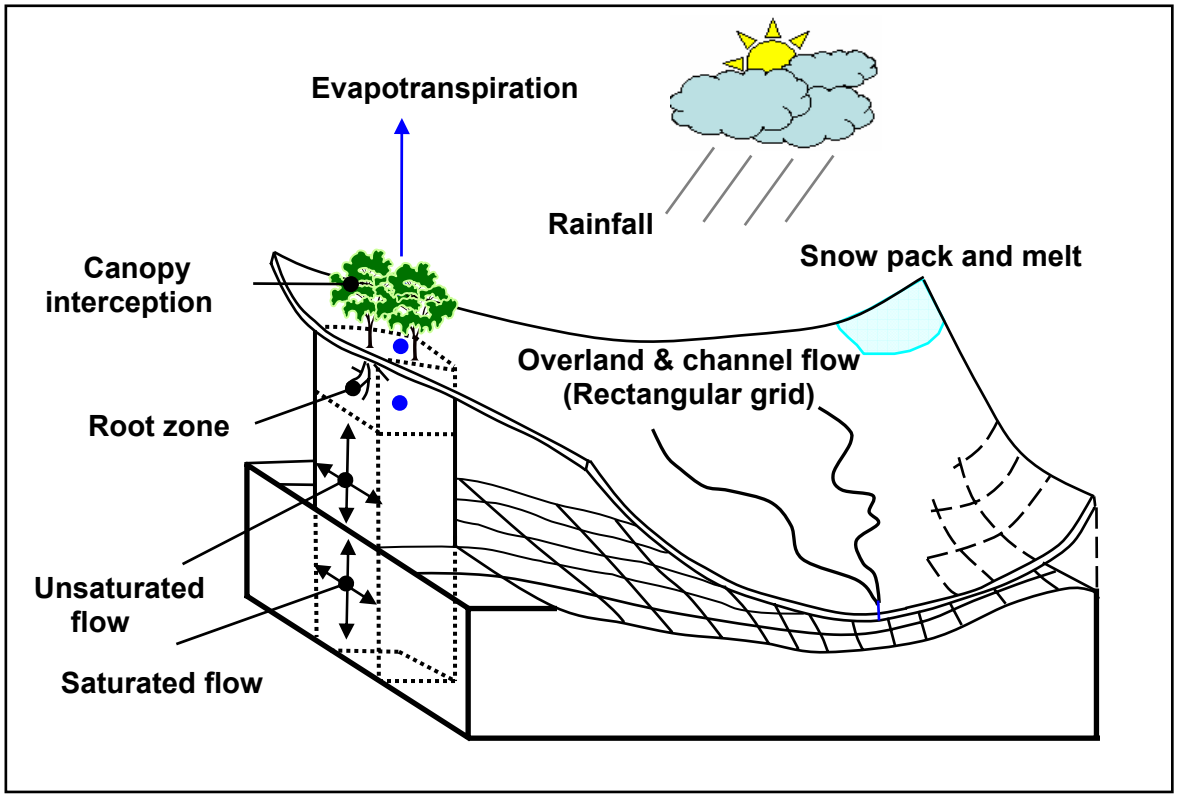

Figure 3.3**:** Schematic diagram of the SHETRAN model.

The water flow model component of the SHETRAN modeling system (version 4.3), used for the present study, was obtained from the WRSRL. Necessary modifications were undertaken with the collaboration of WRSRL to work with highly spatially resolved meteorological forcing variables. Table 3.3 shows Flow equations used in the SHETRAN model.

Table 3.3: Flow equations in SHETRAN

Process	Equation
Subsurface flow	Variably saturated flow equation (3D)
Overland flow	Saint-Venant equations, diffusion approximation (2D)
Channel flow	Saint-Venant equations, diffusion approximation (flow in a network of 1D channels)
Canopy interception and drip	Rutter equation
Evaporation[1]	Penman-Monteith equation (PME) (or as fraction of potential evaporation rate)
Snowpack and melt[2]	Accumulation equation and energy budget melt equation (or degree-day melt equation)

[1] To represent Evaporation process the option as fraction of potential evaporation rate is applied in the present study.

[2] To represent snow pack and melt process degree-day melt equation is applied in the present study.

Table 3.4 depicts main processes represented in the water flow component of the SHETRAN model.

Table 3.4: Main processes represented in the water flow component of the SHETRAN model.

Processes
• Canopy interception of rainfall • Evaporation and transpiration • Infiltration to subsurface • Surface runoff (overland, overbank, and channels) • Snow pack development and snowmelt • Storage and 3D flow in variably saturated subsurface • Combinations of confined, unconfined, perched aquifers • Transfers between subsurface water and water • Ground-water seepage discharge • Well abstraction • River augmentation and abstraction • Irrigation

Table 3.5 presents main data requirement for physical properties and initial and boundary conditions in SHETRAN.

Table 3.5: Main data for physical properties and initial and boundary conditions in SHETRAN.

Data requirement
• Precipitation and meteorological data for each station
• Station numbers for each column and river link
• Size and location of columns, river links, and finite-difference cells
• Soil/rock types and depths for each column
• Land-use/vegetation for each column
• Man-controlled channel flow diversions and discharges
• Rates of borehole pumping, artificial recharge, flow diversions, and so forth
• Initial hydraulic potentials for subsurface
• Initial overland and channel flow depths
• Initial snow pack thicknesses and temperatures
• Boundary hydraulic potentials (or flow rates)
• Boundary stream inflow rates
• Canopy drainage parameters and storage capacities
• Ground cover fractions
• Canopy resistances and aerodynamic resistances (for PME)
• Vegetation root density distribution over depth
• Porosity and specific storage of soils/rocks
• Metric potential functions for soils/rocks
• Unsaturated hydraulic conductivity functions for soils/rocks
• Saturated hydraulic conductivity of soils/rocks
• Snow density, zero-plane displacement, and roughness height

3.7 The SHETRAN model calibration

In principle, the parameters of a physically based spatially distributed model should not require calibration. They are supposedly based on measurements and are truly representative of that part of the catchment for which they were evaluated. However, within the model there are approximations in the representation of physical processes and potential inconsistencies among the model grid scale, the scale at which property measurements are made and the scale relevant to each particular hydrological process. A degree of calibration or adjustment of parameter values is, therefore, likely to be needed to minimize the differences between observed and simulated responses. Such calibration, however, should be constrained by physical plausibility so that the parameter values either lie in a physically realistic range or can otherwise be explained by physical reasoning. Furthermore, given the large number of parameters, it is not realistic to obtain an accurate calibration by gradually varying all the parameters individually or in combination. Typically with SHETRAN, calibration is, therefore, limited to only the few parameters to which the simulation is most sensitive. These are the Strickler resistance coefficient for the overland flow, ratio of actual to potential evapotranspiration at soil field capacity, the Van Genuchten exponent n for soil moisture/tension curve and the soil saturated zone hydraulic conductivity (Ewen et al., 2000; Lukey et al., 2000).

3.8 Goodness-of-fit criteria in simulations

The standard split sampling model calibration procedure was followed. The model calibration period runs from 1961 to 1970 using the observed daily discharges. The subsequent period until 1990 was used to validate the calibrated model. In order to minimize the effect of the initial states of the subcatchments on the model performance, the first 12 months were used as a warm up period and the model simulation results during this period were not used to compute the model performance.

3.8.1 Overall model simulations performance

The simulation results were compared using different statistical criteria, namely, the Nash-Sutcliffe coefficient, the relative accumulated difference, the peak error, the index of Agreement and Root mean squared difference.

The Nash-Sutcliffe coefficient (R_m^2) (Nash and Sutcliffe, 1970) is defined as:

$$R_m^{\ 2} = 1 - \frac{\sum_{i=i}^{N} (Q_o(t_i) - Q_s(t_i))^2}{\sum_{i=1}^{N} (Q_o(t_i) - \overline{Q_o})^2} \qquad (3.14)$$

where:

$Q_o(t_i)$	[m^3/s]	observed daily discharge
$Q_s(t_i)$	[m^3/s]	simulated daily discharge
$\overline{Q}_o$	[m^3/s]	mean observed daily discharge
N	[-]	number of time steps

The range of R_m^2 lies between 1.0 (perfect fit) and -∞. An efficiency of lower than zero indicates that the mean value of the observed times series would have been a better predictor than the model.

The relative accumulated difference and the *peak error* were computed to judge the performance of the model with regard to its ability to maintain the water balance and its estimation capacity of the peak flow.

The relative accumulated difference (*rel. accdif.*) is defined as:

$$rel.accdif. = \frac{\sum_{i=1}^{N} (Q_s(t_i) - Q_o(t_i))}{\sum_{i=1}^{N} Q_o(t_i)} \qquad (3.15)$$

where:

$Q_o(t_i)$	[m^3/s]	observed daily discharge
$Q_s(t_i)$	[m^3/s]	simulated daily discharge
N	[-]	number of time steps

Accordingly, the *peak error* is defined based on the relative difference of the mean annual simulated and observed peak discharges:

$$peak\ error = \frac{\overline{Q}_{s(\max)} - \overline{Q}_{o(\max)}}{\overline{Q}_{o(\max)}} \tag{3.16}$$

where:

$\overline{Q}_{o(\max)}$	[m^3/s]	mean annual maximum observed discharge
$\overline{Q}_{s(\max)}$	[m^3/s]	mean annual maximum simulated discharge

The index of agreement, a measure of differences between the observed and model simulated means and variances, was also calculated. The index of agreement varies from 0.0 to 1.0, with higher values indicating better agreement between the model and observations.

The index of agreement (*AI*) is defined as:

$$AI = 1 - \frac{\sum_{i=i}^{N} \left(Q_o(t_i) - Q_s(t_i)\right)^2}{\sum_{i=1}^{N} \left(\left|Q_s(t_i) - \overline{Q}_o\right| + \left|Q_o(t_i) - \overline{Q}_o\right|\right)^2} \tag{3.17}$$

where:

$Q_o(t_i)$	[m^3/s]	observed daily discharge
$Q_s(t_i)$	[m^3/s]	simulated daily discharge
$\overline{Q}_o$	[m^3/s]	mean observed daily discharge
N	[-]	number of time steps

The potential error in the denominator represents the largest value that the squared difference of each pair can attain. Because the mean squared error is in the numerator, *AI* is very sensitive to peak flows and insensitive for low flow conditions.

Additionally, the root mean squared error (*RMSE*) between the observed and simulated discharges was computed. *RMSE* is defined as:

$$RMSE = \left(\frac{1}{N} \left(\sum_{i=1}^{N} \left(Q_s(t_i) - Q_o(t_i)\right)^2 \right) \right)^{0.5} \tag{3.18}$$

where:

$Q_o(t_i)$	[m^3/s]	observed daily discharge
$Q_s(t_i)$	[m^3/s]	simulated daily discharge
N	[-]	number of time steps

The mean model performance (R^2_{mm}) is calculated using the model performances obtained at the measured discharge gauges. The model performances obtained at the Kirchentellinsfurt, Neckar, Wannweil, Echaz and Riederich, Erms gauges were not considered for the calculation of the mean model performance. Kirchentellinsfurt, Neckar was not considered due to its large number of missing measurements. The performances at the Wannweil, Echaz and Riederich, Erms gauges were not considered because the drainage area of those gauges is located at the karstic formation. R^2_{mm} is calculated using the Nash-Sutcliffe coefficient values obtained during the calibration and validation periods, defined as:

$$R^2_{mm} = \frac{1}{L}\sum_{i=1}^{L}\frac{[R^2_m(calibration)_i + R^2_m(validation)_i]}{2} \tag{3.19}$$

where:

$R^2_m(calibration)_i$	[-]	Nash-Sutcliffe coefficient during calibration period
$R^2_m(validation)_i$	[-]	Nash-Sutcliffe coefficient during validation period
L	[-]	number of subcatchments

Higher values of R^2_{mm} indicate better mean model performance.

The value of model parameters' transferability (T_m) is also computed to evaluate their transferability during the simulation period when the model parameters were not allowed to change. The model parameters' transferability is calculated using the following equation.

$$T_m = \max\left(R^2_m(calibration)_i - R^2_m(validation)_i\right)_{i=1,\ldots,L} \tag{3.20}$$

where:

$R^2_m(calibration)_i$	[-]	Nash-Sutcliffe coefficient during calibration period
$R^2_m(validation)_i$	[-]	Nash-Sutcliffe coefficient during validation period
L	[-]	number of subcatchments

As we are more concerned about deterioration of model performance in the validation period, therefore, the maximum positive difference of the model performance was considered in the above equation as an index of model parameters' transferability.

Lower values of T_m indicate better model parameters' transferability.

3.8.2 Event statistics

The event statistics were also calculated for different gauges using the simulated and observed discharges. The average absolute error (*AE*) and root mean squared error (see eq. 3.18) were calculated for each annual maximum flood event. The average absolute error (*AE*) is defined as:

$$AE = \frac{1}{N_p} \sum_{i=1}^{N_p} \left| \left(Q_{sp}(t_i) - Q_{op}(t_i) \right) \right| \tag{3.21}$$

where:

$Q_{op}(t_i)$	[m^3/s]	observed daily discharge within each annual event
$Q_{sp}(t_i)$	[m^3/s]	simulated daily discharge within each annual event
N_p	[-]	number of time step in a particular peak event

4 Influence of spatial variability of precipitation in a hydrological model

4.1 Introduction

In this chapter attempts have been made to elaborate the following two aspects: (a) the impacts of spatial variability of precipitation on the hydrological modeling results and (b) the reliability of model parameters, calibrated from a certain level of input information, to use for simulations with different level of input precipitation information. The distributed and semi-distributed structures of the HBV model were applied. Interpolated precipitation by external drift kriging (Ahmed and de Marsily, 1987) from the available point raingauge measurements were used to represent the spatial variation of rainfall. In the first section of the chapter, the averaged precipitation over different spatial resolutions obtained from interpolated precipitation was used as a main forcing input in the model. In the second section, a discussion on the question (b) is made. The model performance was assessed through the analysis of the simulated hydrographs and the computation of goodness-of-fit indexes.

4.2 Data preparation and model simulations

The daily precipitation and the daily average temperature were interpolated on a 1 km × 1 km grid. In order to investigate the impact of the spatial variability of precipitation, the interpolated precipitation was averaged over different spatial scales. The spatial scales range from 4 km^2 to 25 km^2 (Table 4.1).

The original interpolated precipitation and averaged precipitation over different spatial resolutions were used as a main forcing input in the models. The distributed and semi-distributed model structures of the HBV model were applied in accordance to the study objectives. The simulated hydrographs obtained using original and averaged precipitation were analyzed by comparison of their Nash-Sutcliffe coefficients and other goodness-of-fit indices. The areal averaged precipitation and their corresponding spatial resolution are shown in Table 4.1.

Table 4.1: Areal averaged precipitation and corresponding spatial resolution.

Spatial resolution of precipitation [km^2]	Simulation abbreviation
1	1×1
4	2×2
9	3×3
16	4×4
25	5×5

4.2.1 Simulations using the distributed HBV model structure

The distributed structure of the HBV model was calibrated using the interpolated precipitation on 1 km × 1 km grid. The other input variables required to setup the model were assigned at the same model grid. Table 4.2 summarizes the model performance for the calibration and validation periods at different discharge gauges.

Table 4.2: Model performances using the distributed HBV model for the calibration and validation periods.

Gauge	Simulation period	R_m^2	Rel. accdif.	Peak error	RMSE
Rottweil	calibration	0.69	0.13	-0.42	3.91
	validation	0.71	0.17	-0.38	3.88
Oberndorf	calibration	0.73	0.03	-0.42	5.10
	validation	0.72	0.07	-0.34	5.19
Horb	calibration	0.82	0.05	-0.27	7.66
	validation	0.77	0.15	-0.30	9.15
Bad Imnau, Eyach	calibration	0.71	-0.07	-0.43	2.47
	validation	0.74	-0.02	-0.45	2.49
Rangendingen, Starzel	calibration	0.59	0.03	-0.55	1.18
	validation	0.59	0.29	-0.45	1.10
Riederich, Erms	calibration	0.72	-0.01	-0.12	1.20
	validation	0.67	0.04	-0.08	1.21
Oberensingen, Aich	calibration	0.71	0.11	-0.11	1.10
	validation	0.70	0.18	0.02	1.32
Suessen, Fils	calibration	0.77	-0.17	-0.17	3.03
	validation	0.80	-0.09	-0.25	2.78
Plochingen, Fils	calibration	0.79	-0.12	-0.33	5.30
	validation	0.77	-0.01	-0.40	5.62
Plochingen, Neckar	calibration	0.84	-0.05	-0.23	20.39
	validation	0.83	0.02	-0.28	21.47

As shown in Table 4.2, the Nash-Sutcliffe coefficient for the simulation of the daily discharge in the subcatchments during the calibration period has values ranging between 0.59 and 0.84 with a mean value of 0.74 and the Nash-Sutcliffe coefficient for the validation period ranging between 0.59 and 0.83 with a mean value of 0.73. It can be observed that the model performances increased with the increase of drainage area. The relatively low value of Nash-Sutcliffe coefficient was noticed for small subcatchments due to higher uncertainty in the precipitation estimation for small subcatchments. The highest Nash-Sutcliffe coefficient value was observed during both calibration and validation period at the catchment outlet Plochingen, Neckar. The lowest value was observed at the gauge Rangendingen, Starzel, which is, in part, located in a karstic geological formation.

The calibrated model was then run for the validation period using the averaged precipitation over different spatial resolutions mentioned earlier. In this simulation experiment, the model resolution was also 1 km × 1 km. Table 4.3 summarizes the model performance at selected two gauges, Horb and Plochingen, Neckar.

Table 4.3: Model performances obtained using spatially averaged precipitation through the application of the distributed HBV model at selected two gauges Horb and Plochingen, Neckar.

Resolution of precipitation [km^2]	Horb				Plochingen, Neckar			
	R_m^2	Rel. accdif.	Peak error	RMSE	R_m^2	Rel. accdif.	Peak error	RMSE
1	0.77	0.15	-0.30	9.15	0.83	0.02	-0.28	21.47
4	0.77	0.13	-0.32	9.01	0.83	0.02	-0.28	21.33
9	0.75	0.13	-0.33	9.55	0.81	0.02	-0.28	22.78
16	0.77	0.13	-0.32	9.02	0.83	0.02	-0.28	21.32
25	0.77	0.13	-0.32	9.01	0.83	0.03	-0.28	21.32

No significant differences were observed in the model performances when the calibrated model using 1 km × 1 km grid precipitation was run for the validation period using averaged precipitation over different spatial scales. No distinguishable differences were also observed in terms of relative accumulative difference and peak error (Table 4.3).

Figures 4.1 and 4.2 show the scatter plots of observed discharges and simulated discharges obtained using the spatially averaged precipitation for Rottweil and Riederich, Erms gauges, respectively.

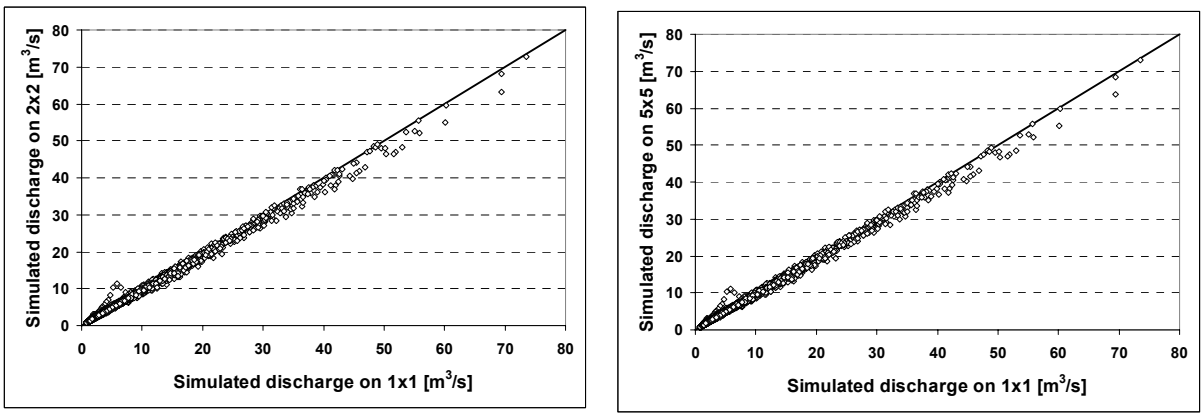

Figure 4.1: Scatter plots of simulated discharges using spatially averaged precipitation through the application of the distributed HBV model for the gauge at Rottweil: 1 km^2 vs 4 km^2 (left panel) and 1 km^2 vs 25 km^2(right panel).

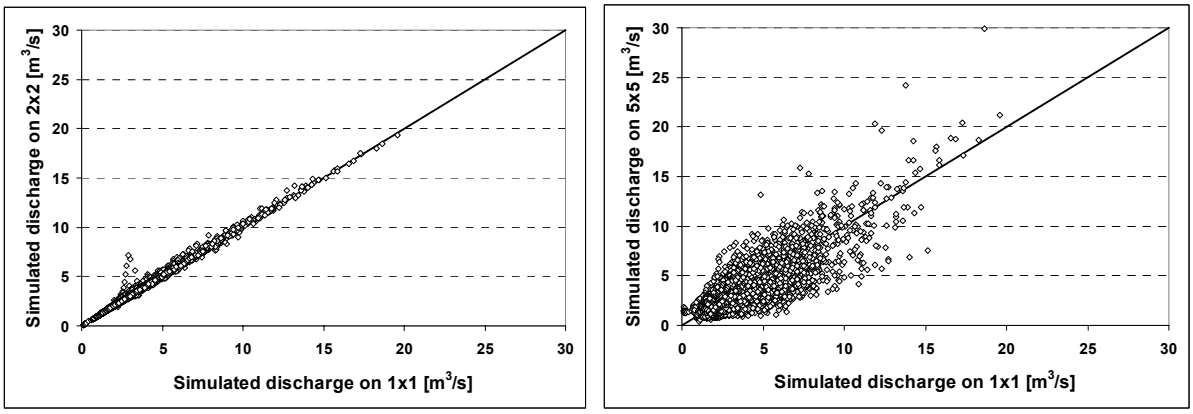

Figure 4.2: Scatter plots of simulated discharges using spatially averaged precipitation through the application of the distributed HBV model for the gauge at Riederich, Erms: 1 km^2 vs 4 km^2 (left panel) and 1 km^2 vs 25 km^2(right panel).

The mean difference (*meandiff*) and mean squared difference (*meansqdiff*) between the model simulated discharges using spatially averaged precipitation for different gauges were also calculated.

$$meandiff = \frac{1}{N}\left(\sum_{i=1}^{N}\left(Q_{ss}(t_i) - Q_{so}(t_i)\right)\right) \tag{4.1}$$

$Q_{ss}(t_i)$	[m^3/s]	daily simulated discharges using averaged precipitation over one resolution
$Q_{so}(t_i)$	[m^3/s]	daily simulated discharges using averaged precipitation over different resolution
N	[-]	number of time steps

The *meansqdiff* is defined as:

$$meansqdiff = \frac{1}{N}\left(\sum_{i=1}^{N}\left(Q_{ss}(t_i) - Q_{so}(t_i)\right)^2\right) \tag{4.2}$$

$Q_{ss}(t_i)$	[m^3/s]	daily simulated discharges using averaged precipitation over one resolution
$Q_{so}(t_i)$	[m^3/s]	daily simulated discharges using averaged precipitation over different resolution
N	[-]	number of time steps

Tables 4.4 and 4.5 represent the *meandiff* and *meansqdiff* for the gauge at Horb. These were calculated using the simulated discharges produced using spatially averaged precipitation.

Table 4.4: Mean difference between the simulated discharges obtained using spatially averaged precipitation through the application of the distributed HBV model for the gauge at Horb.

spatial resolution	1×1	2×2	3×3	4×4	5×5
1×1	0.00	0.26	0.25	0.23	0.22
2×2	-0.26	0.00	-0.01	-0.03	-0.03
3×3	-0.25	0.01	0.00	-0.02	-0.02
4×4	-0.23	0.03	0.02	0.00	0.00
5×5	-0.22	0.03	0.02	0.00	0.00

Table 4.5: Mean squared difference between the simulated discharges obtained using spatially averaged precipitation through the application of the distributed HBV model for the gauge at Horb.

spatial resolution	1×1	2×2	3×3	4×4	5×5
1×1	0.00	0.63	0.96	0.59	0.58
2×2	0.63	0.00	0.83	0.00	0.01
3×3	0.96	0.83	0.00	0.85	0.81
4×4	0.59	0.00	0.85	0.00	0.00
5×5	0.58	0.01	0.81	0.00	0.00

Relatively higher differences were observed between the simulated discharges obtained using precipitation at 1 km^2 resolution and the simulated discharges resulting from the precipitation averaged over the remaining spatial scales (Tables 4.4 and 4.5).

The Nash-Sutcliffe coefficient was computed for different years during the validation period at the different discharge gauges. Figure 4.3 shows the yearly model performance for the gauges at Horb and Suessen, Fils.

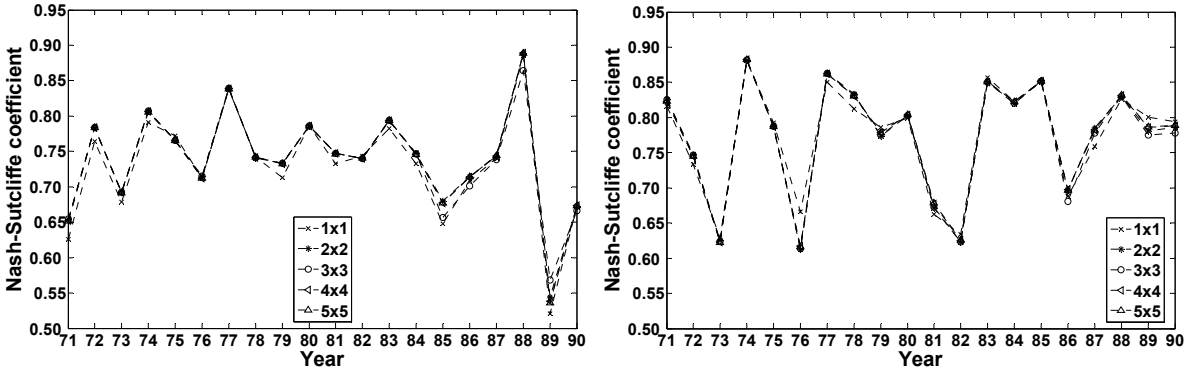

Figure 4.3: Nash-Sutcliffe coefficient calculated using spatially averaged precipitation through the application of the distributed HBV model for the gauges at Horb (left panel) and Suessen, Fils (right panel).

It can be observed that there is no significant difference resulting from the different spatially averaged precipitation for the majority of the years.

To investigate the influence of spatially averaged precipitation during different seasons, the Nash-Sutcliffe coefficient was also computed on seasonal basis for the validation period. This was calculated using the simulated discharges resulting from spatially averaged precipitation.

Figure 4.4 (left panel) shows the seasonal model performance for the gauge at Horb. The overall mean value of the seasonal Nash-Sutcliffe coefficient is shown in Figure 4.4 (right panel). The overall mean value was calculated using the Nash-Sutcliffe coefficients obtained at all gauges used for the evaluation.

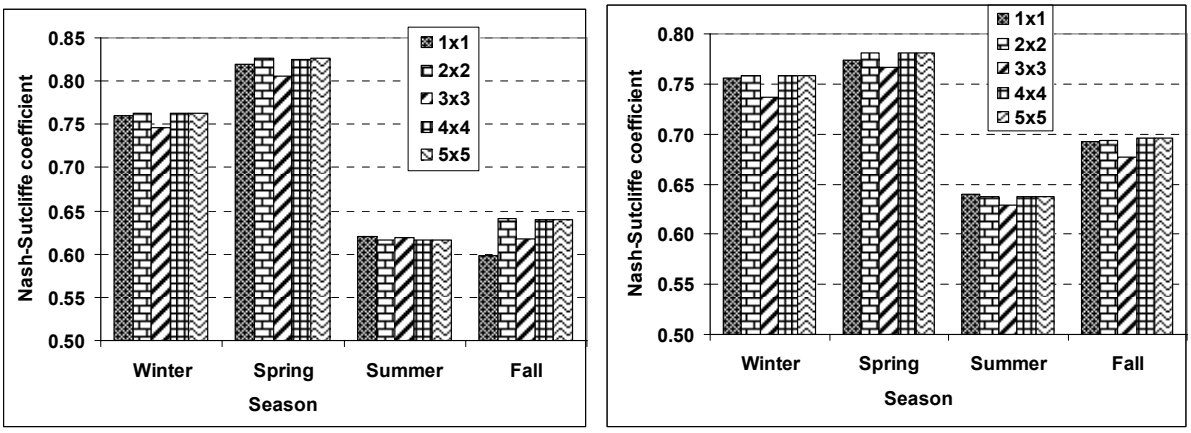

Figure 4.4: Seasonal Nash-Sutcliffe coefficients using spatially averaged precipitation through the application of the distributed HBV model for the gauge at Horb (left panel). Mean seasonal Nash-Sutcliffe coefficient over the catchment using spatially averaged precipitation through the application of the distributed HBV model (right panel).

The figures show that there are significant differences in the model performance during the different seasons; there is a remarkable deterioration in the model performance during the summer season. This is due to the presence of convective precipitation events that were not well captured by the coarse raingauge networks. However, no significant differences were observed for a season using the spatially averaged precipitation.

The event statistics were calculated for each flood event in order to investigate the differences to simulate peak discharges, resulting from different spatially averaged precipitation. The average absolute error and root mean squared error were calculated for each annual maximum flood event for this purpose.

The average absolute error and root mean squared error for the gauge at Rottweil are shown in Figure 4.5. Figure 4.6 shows the average absolute error and root mean squared error for the gauge at Horb.

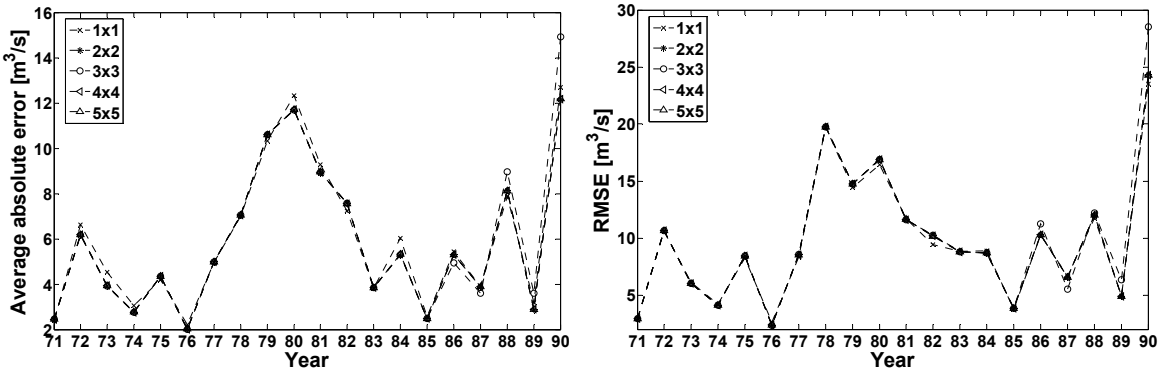

Figure 4.5: Event statistics at each annual maximum flood event for the gauge at Rottweil using spatially averaged precipitation through the application of the distributed HBV model: average absolute error (left panel) and root mean squared error (right panel).

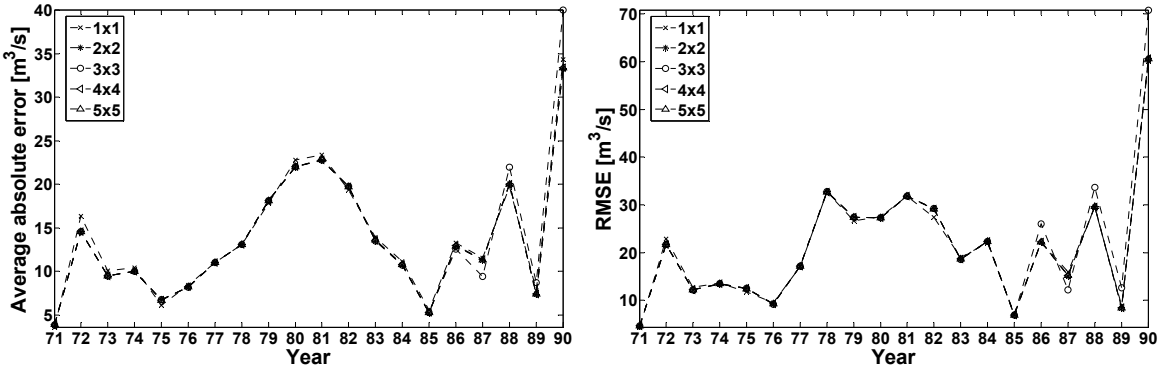

Figure 4.6: Event statistics at each annual maximum flood event for the gauge at Horb using spatially averaged precipitation through the application of the distributed HBV model: average absolute error (left panel) and root mean squared error (right panel).

On average, the absolute error with respect to the annual maximum discharges for the gauge at Rottweil ranges between 9.0% and 9.3% using the spatially averaged precipitation. The same value for the gauge at Horb ranges between 9.2% to 9.4%.

Figure 4.7 shows the scatter plots of the root mean squared error of the annual maximum flood events resulting using different spatially averaged precipitation for the Suessen, Fils gauge.

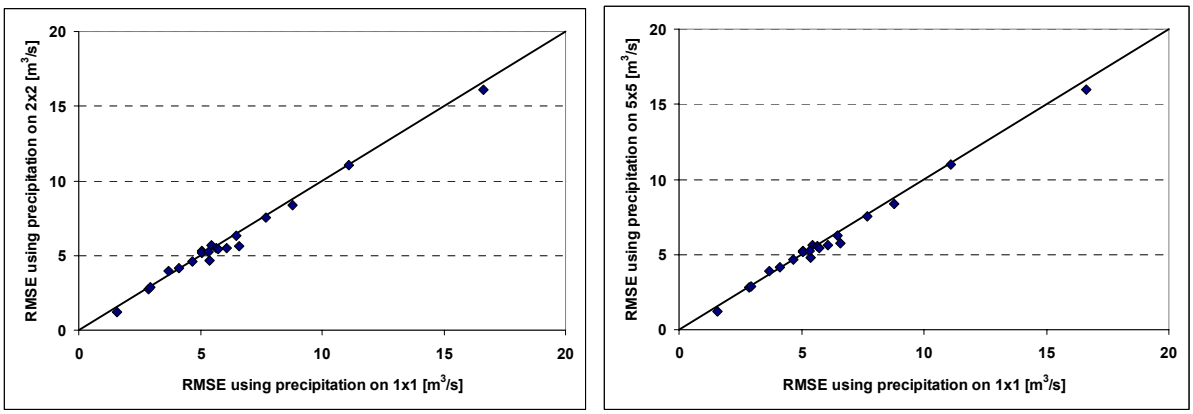

Figure 4.7: Scatter plots of root mean squared error of the annual maximum flood events using spatially averaged precipitation through the application of the distributed HBV model for the gauge at Suessen, Fils.

From the event statistics as presented in figures above, it can be observed that there is no significant difference when using different spatially averaged precipitation for the annual maximum flood events.

4.2.2 Simulations using the semi-distributed HBV model structure

A similar simulation experiment was carried out using the semi-distributed structure of the HBV model. The meteorological variables for each zone were estimated as the mean of the interpolated values on the regular grids of 1 km × 1 km. The potential evapotranspiration was also averaged over each zone from the calculated evapotranspiration on 1 km × 1 km grids. The model was calibrated using the input data on the above mentioned spatial scale. Table 4.6 shows the model performance using the semi-distributed model structure for the calibration and validation periods.

Table 4.6: Model performance obtained using the semi-distributed HBV model for the calibration and validation periods.

Gauge	Simulation period	R_m^2	Rel. accdif.	Peak error	RMSE
Rottweil	calibration	0.78	0.00	-0.22	3.30
	validation	0.79	0.03	-0.08	3.35
Oberndorf	calibration	0.80	0.01	-0.17	4.37
	validation	0.76	0.05	0.01	4.81
Horb	calibration	0.84	0.02	-0.08	7.13
	validation	0.82	0.10	-0.07	8.05
Bad Imnau, Eyach	calibration	0.79	0.00	-0.21	2.12
	validation	0.80	0.05	-0.20	2.20
Rangendingen, Starzel	calibration	0.67	-0.01	-0.16	1.05
	validation	0.59	0.22	-0.04	1.09
Riederich, Erms	calibration	0.79	-0.02	-0.18	1.03
	validation	0.77	0.02	-0.06	1.02
Oberensingen, Aich	calibration	0.77	0.01	-0.12	0.97
	validation	0.66	0.05	-0.08	1.21
Suessen, Fils	calibration	0.78	0.00	-0.10	2.96
	validation	0.79	0.09	-0.16	2.82
Plochingen, Fils	calibration	0.81	0.01	-0.12	5.06
	validation	0.81	0.13	-0.21	5.10
Plochingen, Neckar	calibration	0.86	-0.01	-0.07	19.12
	validation	0.86	0.05	-0.08	19.18

As shown in Table 4.6, the Nash-Sutcliffe coefficient for the simulation of the daily discharge during the calibration period has values ranging between 0.67 and 0.86 with a mean value of 0.79.

The Nash-Sutcliffe coefficients for the validation period are ranging between 0.59 and 0.86 with a mean value of 0.77. As observed in the distributed model structure, the highest Nash-Sutcliffe coefficient value was observed at the catchment outlet Plochingen, Neckar during both the calibration and validation periods. The lowest value was observed at the gauge Rangendingen, Starzel.

Comparing the performances using the distributed and semi-distributed model structures, the semi-distributed model, in general, performs better than the distributed model. Relatively higher differences in the model performances are observed in the smaller subcatchments.

Further, the precipitation for each zone was calculated using the averaged precipitation over different spatial scales, mentioned earlier. The calibrated model was then run using the spatially averaged precipitation for the validation period. The other input data, namely mean daily temperature and daily potential evapotranspiration, were assigned at the same spatial scale that was used for the calibration.

Table 4.7 presents the model performance resulting from spatially averaged precipitation at selected two gauges, namely Horb and Plochingen, Neckar.

Table 4.7: Model performance obtained using spatially averaged precipitation through the application of the semi-distributed HBV model for selected gauges.

Resolution of precipitation [km^2]	Horb				Plochingen, Neckar			
	R_m^2	Rel. accdif.	Peak error	RMSE	R_m^2	Rel. accdif.	Peak error	RMSE
1	0.82	0.10	-0.07	8.05	0.86	0.05	-0.08	19.18
4	0.83	0.06	-0.13	7.74	0.87	0.04	-0.10	18.89
9	0.83	0.06	-0.13	7.74	0.87	0.03	-0.10	18.87
16	0.83	0.06	-0.12	7.74	0.87	0.03	-0.10	18.86
25	0.83	0.06	-0.12	7.73	0.87	0.03	-0.10	18.85

No significant differences were observed in the model performance when the model was run using averaged precipitation at different spatial scales, as observed with the distributed model described earlier. Figures 4.8 and 4.9 show the scatter plots of the simulated discharges obtained using the spatially averaged precipitation for Rottweil and Riederich, Erms gauges, respectively.

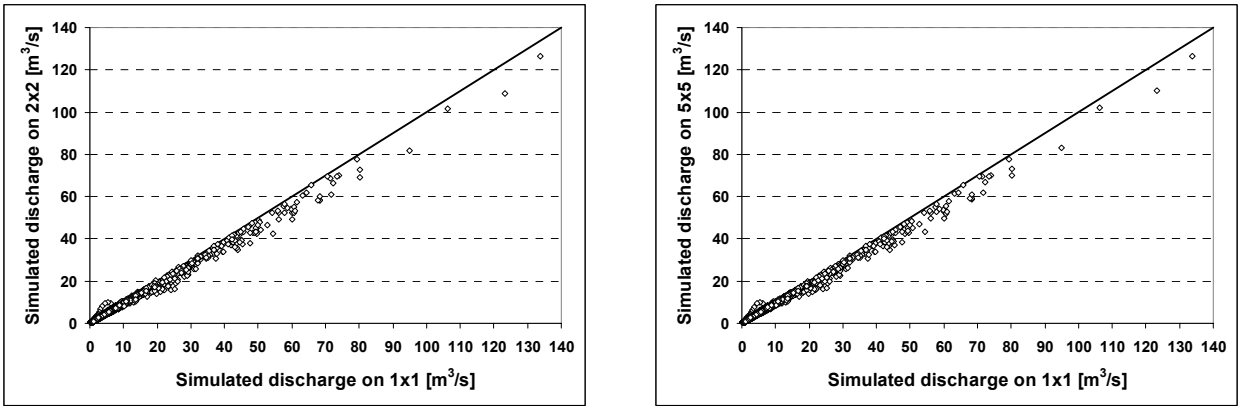

Figure 4.8: Scatter plots of the simulated discharges resulting using spatially averaged precipitation through application of the semi-distributed HBV model at the Rottweil gauge: 1 km^2 vs 4 km^2 (left panel) and 1 km^2 vs 25 km^2 (right panel).

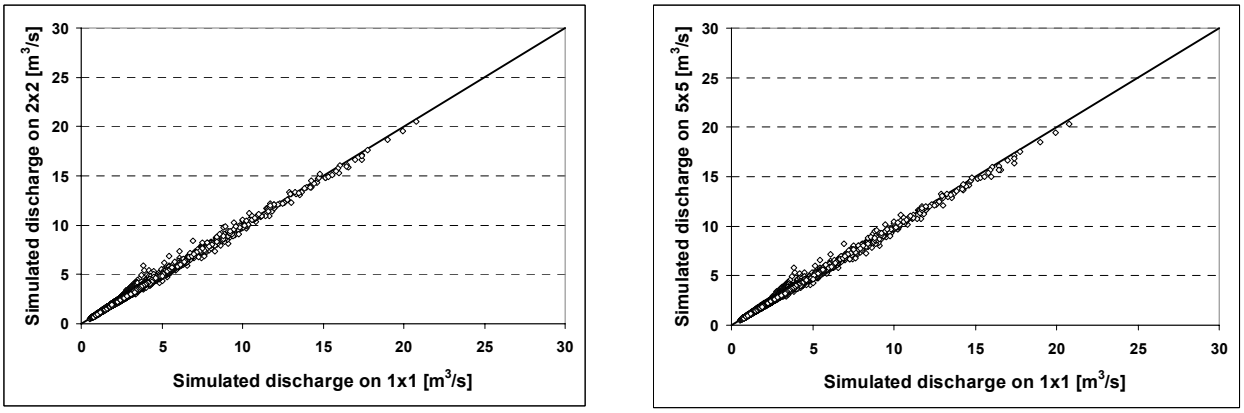

Figure 4.9: Scatter plots of the simulated discharges resulting using spatially averaged precipitation through the application of the semi-distributed HBV model for the Riederich, Erms gauge: 1 km^2 vs 4 km^2 (left panel) and 1 km^2 vs 25 km^2 (right panel).

Tables 4.8 and 4.9 show the mean differences and mean squared differences between the simulated discharges obtained using spatially averaged precipitation for the Horb gauge.

Table 4.8: Mean differences between the simulated discharges resulted using spatially averaged precipitation through the application of the semi-distributed HBV model for the gauge at Horb.

spatial resolution	1×1	2×2	3×3	4×4	5×5
1×1	0.00	0.55	0.56	0.54	0.55
2×2	-0.55	0.00	0.01	-0.01	0.00
3×3	-0.56	-0.01	0.00	-0.02	-0.01
4×4	-0.54	0.01	0.02	0.00	0.01
5×5	-0.55	0.00	0.01	-0.01	0.00

Table 4.9: Mean squared differences between the simulated discharges resulted using spatially averaged precipitation through the application of the semi-distributed HBV model for the gauge at Horb.

spatial resolution	1×1	2×2	3×3	4×4	5×5
1×1	0.00	2.06	2.02	1.91	1.91
2×2	2.06	0.00	0.00	0.01	0.01
3×3	2.02	0.00	0.00	0.00	0.01
4×4	1.91	0.01	0.00	0.00	0.00
5×5	1.91	0.01	0.01	0.00	0.00

As obverted with the distributed model structure, relatively higher differences were observed between the simulated discharges obtained using precipitation at 1 km^2 resolution and the simulated discharges resulting from the precipitation averaged over the remaining spatial scales (Tables 4.8 and 4.9).

The Nash-Sutcliffe coefficient was also computed for different years during the validation period for the different gauges. Figure 4.10 shows the yearly model performance at the Horb and Suessen, Fils, gauges.

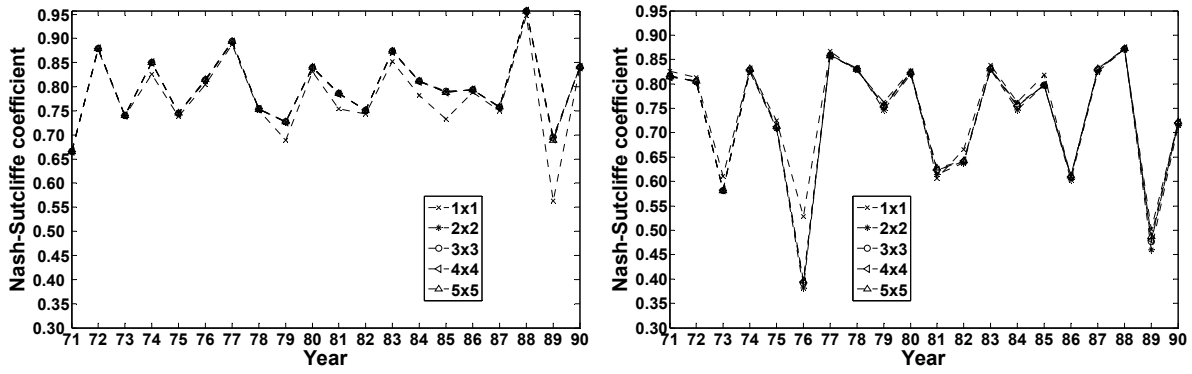

Figure 4.10: Annual Nash-Sutcliffe coefficient obtained using spatially averaged precipitation through the application of the semi-distributed HBV model for the gauges at Horb (left panel) and Suessen, Fils (right panel).

The semi-distributed structure also shows no distinct difference in the use of different spatially averaged precipitation for most of the year in the validation period, as observed with the distributed model structure.

Further, the Nash-Sutcliffe coefficient was computed on a seasonal basis for the simulated discharges. Figure 4.11 (left panel) shows the seasonal model performance for the Horb gauge and Figure 4.11 (right panel) shows the overall mean Nash-Sutcliffe coefficient.

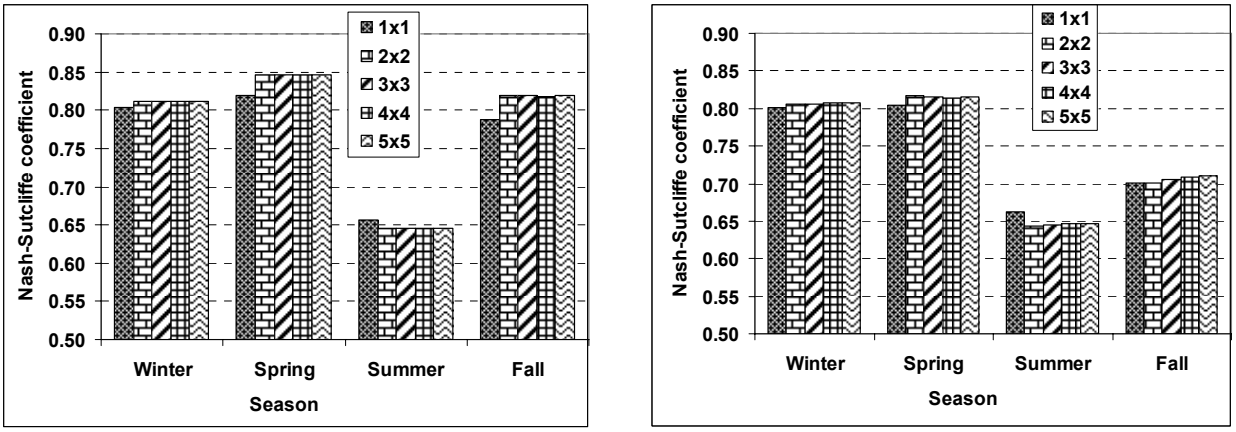

Figure 4.11: Seasonal Nash-Sutcliffe coefficients using spatially averaged precipitation through the application of the semi-distributed HBV model at the Horb gauge (left panel). Mean seasonal Nash-Sutcliffe coefficient over the catchment using spatially averaged precipitation through application of the semi-distributed HBV model (right panel).

The average absolute error and root mean squared error were also calculated for each maximum annual flood event for different discharges. No considerable differences were observed using different spatially averaged precipitation, as observed with the distributed model structure.

The analysis using the distributed and semi-distributed model structures of HBV indicate that there in generally no distinguishable differences are observed in the model performances when using spatially averaged precipitation. The insensitivity of the model performances to the use of spatially averaged precipitation is, however, strongly dependent on the case study. It should be noted that obtaining the same values of goodness-of-fit indices does not indicate that the simulation was insensitive to the precipitation field. Indeed, the different spatial representations of the precipitation field did not provide the same simulated discharges as might be reflected in Tables 4.5 and 4.9, rather they show similar performances because none of the types is a perfect representation of reality. It should also be mentioned that the precipitation fields used for the analysis were interpolated from the point raingauge measurements.

4.3 Reliability of model parameters, calibrated from a certain level of input information, to use for simulations with different level of precipitation information

This section reports the work carried out to identify the reliability of the parameters obtained from the calibration with a set of precipitation input, for using in model simulations with a different set of precipitation input. The work by Obled et al., (1994); Chauby et al., (1999) and Arnaud et al., (2002) explicitly deals with the calibration issue. They carried out different parameterisations through varying the spatial representation of precipitation in order to use the parameter set most consistent with the input in validation. Brath et al., (2004) performed calibrations over different

input precipitation types and the simulations results compared with those derived when using a fixed parameter set, calibrated by most dense raingauge network available. They concluded that the parameterization resulting from historical data with a relatively poor spatial resolution may be considered reliable for more detailed rainfall fields. This is because it is reasonable to assume that the calibration procedure partly compensates for the input error (Brath et al., 2004). Zehe et al., (2005) showed that the usage of biased (spatially homogenized precipitation) input during parameter estimation yields a biased model structure, which provides poor simulation results when used with highly distributed precipitation input.

Consequently, the aim of the simulation experiment in the following section is to investigate whether the model parameters obtained using a given rainfall input type may also be considered reliable for a different spatial resolution of precipitation input data. The semi-distributed model structure of HBV was used for this investigation. Thus the model calibrated, using precipitation input with one level of information, was run for the validation period using precipitation with another level of information. In real-world applications, it is indeed frequently the case that the spatial variability of precipitation data may vary because of the addition or subtraction of raingauge measuring stations or developments of new measuring technologies (e.g., weather radar rainfall data, Collier, 1989; Ehret, 2002).

In order to investigate the mentioned phenomena, the following 3 cases were considered:

Case I: the model calibrated using the precipitation for each zone (Pzone) was run for the validation period with (a) the precipitation for each zone (Pzone), (b) the uniform precipitation obtained from each subcatchment (Psubcatch) and (c) the uniform precipitation obtained for the catchment (Pcatch).

Case II: the model calibrated with the uniform precipitation obtained from each subcatchment (Psubcatch) was run with (a) the uniform precipitation obtained from each subcatchment (Psubcatch), (b) the precipitation for each zone (Pzone) and (c) the uniform precipitation obtained for the catchment (Pcatch).

Case III: the model calibrated with the uniform precipitation obtained for the catchment (Pcatch) was run with (a) the uniform precipitation obtained for the catchment (Pcatch), (b) the precipitation for each zone (Pzone) and (c) the uniform precipitation obtained from each subcatchment (Psubcatch).

The value of Psubcatch was obtained using the interpolated precipitation on the grids located within a given subcatchment. The model grid located within each subcatchment was assigned the same uniform averaged precipitation obtained for an individual subcatchment. The value of Pcatch

was obtained using the interpolated precipitation on the grids located within the complete catchment. Similarly, the model grid located within the catchment was assigned the uniform averaged precipitation over the catchment. Finally, the precipitation for zones, for the semi distributed HBV model, was calculated using these two types of uniform precipitation and the interpolated precipitation on 1 km × 1 km grid. The HBV model was then calibrated using each of the input precipitation and run using the other two types of precipitation and also the same type of precipitation, used for calibration, for the validation period.

4.3.1 Simulation results of Case I:

In the first simulation experiment, the model calibrated using Pzone was run using Psubcatch and Pcatch for the validation period Table 4.10 presents the model performances.

Table 4.10: Model performances obtained using Psubcatch and Pcatch for the validation period. The model was calibrated using Pzone.

Gauge	Type of precipitation	R_m^2	Rel. accdif.	Peak error	RMSE
Rottweil	using Pzone	0.79	0.03	-0.08	3.35
	using Psubcatch	0.79	0.03	-0.10	3.31
	using Pcatch	0.76	-0.10	-0.31	3.57
Oberndorf	using Pzone	0.76	0.05	0.01	4.81
	using Psubcatch	0.77	0.05	0.00	4.78
	using Pcatch	0.77	-0.06	-0.21	4.73
Horb	using Pzone	0.82	0.10	-0.07	8.05
	using Psubcatch	0.82	0.10	-0.07	7.99
	using Pcatch	0.76	-0.14	-0.37	9.39
Bad Imnau, Eyach	using Pzone	0.80	0.05	-0.20	2.20
	using Psubcatch	0.79	0.05	-0.20	2.23
	using Pcatch	0.70	0.13	-0.13	2.69
Rangendingen, Starzel	using Pzone	0.59	0.22	-0.04	1.09
	using Psubcatch	0.59	0.22	-0.04	1.09
	using Pcatch	0.45	0.28	0.07	1.27
Oberensingen, Aich	using Pzone	0.66	0.05	-0.08	1.21
	using Psubcatch	0.66	0.05	-0.08	1.20
	using Pcatch	0.49	0.58	0.30	2.36
Suessen, Fils	using Pzone	0.79	0.09	-0.16	2.82
	using Psubcatch	0.79	0.09	-0.17	2.80
	using Pcatch	0.71	-0.06	-0.27	3.30
Plochingen, Fils	using Pzone	0.81	0.13	-0.21	5.10
	using Psubcatch	0.81	0.13	-0.21	5.08
	using Pcatch	0.72	0.04	-0.29	6.16
Plochingen, Neckar	using Pzone	0.86	0.05	-0.08	19.18
	using Psubcatch	0.87	0.04	-0.08	19.06
	using Pcatch	0.86	0.03	-0.07	19.72

As shown in Table 4.10, it can be observed that the model performances are different depending on whether the input precipitation type during calibration was changed or kept the same. It also indicates that the model performance deteriorated when the applied precipitation input was less detailed than that used for the calibration of the model. However, when the level of precipitation input was not changed too much, the model performance did not show significant differences. Also, the difference in the model performance was found to be more significant in the smaller subcatchments as compared to the larger ones.

Figure 4.12 shows the seasonal model performance for the Horb and Riederich, Erms, gauges, respectively.

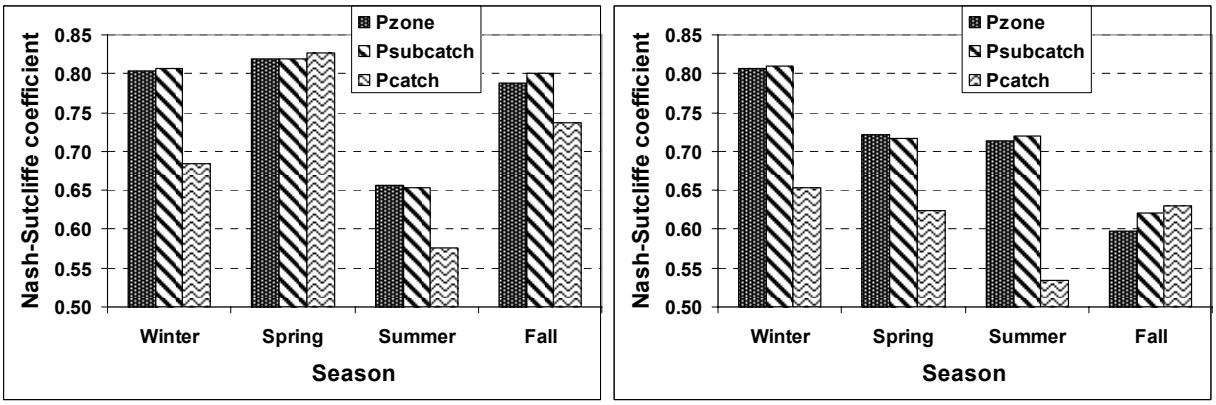

Figure 4.12: Seasonal Nash-Sutcliffe coefficients for the gauges at Horb (left panel) and Riederich, Erms (right panel). The model calibrated using Pzone was run using Psubcatch and Pcatch for the validation period.

Figures 4.13 and 4.14 show the event statistics for the gauges at Horb and Suessen, respectively.

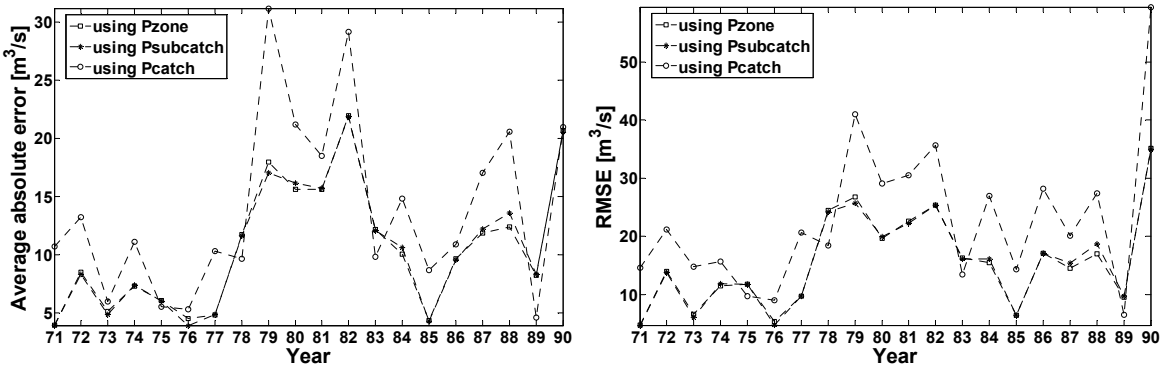

Figure 4.13: Event statistics at each annual maximum flood event for the gauge at Horb: average absolute error (left panel) and root mean squared error (right panel). The model calibrated using Pzone was run using Psubcatch and Pcatch for the validation period.

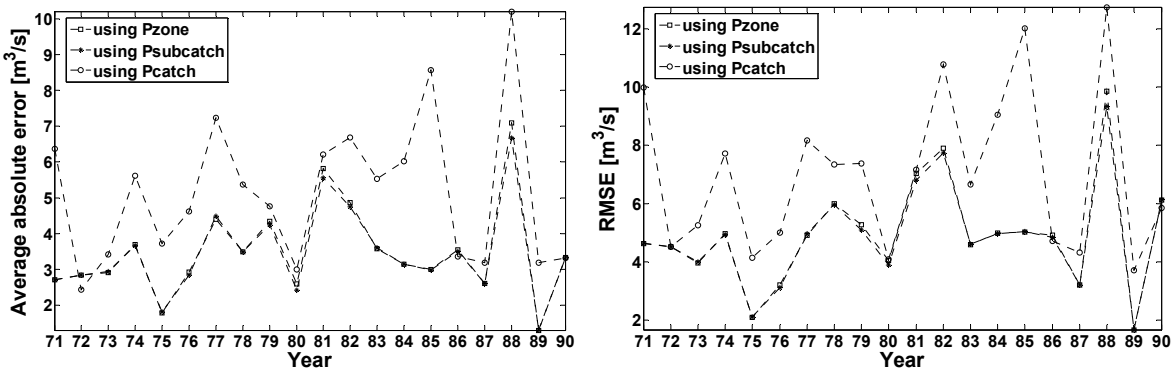

Figure 4.14: Event statistics at each annual maximum flood event for the gauge at Suessen, Fils: average absolute error (left panel) and root mean squared error (right panel). The model calibrated using Pzone was run using Psubcatch and Pcatch for the validation period.

Figures 4.12, 4.13 and 4.14 indicate that there is significant reduction in the model performance when the calibrated model using Pzone was run using Pcatch, whereas there is no distinct difference when the calibrated model was run using Psubcatch. On average, the absolute error with respect to the annual maximum discharges for the gauge at Horb ranges between 7.3 % and 10.2%. The highest error was observed when the calibrated model using Pzone was run using Pcatch. The same value for the gauge at Suessen, Fils ranges between 8.1% to 12.3% and the highest error was observed when the calibrated model using Pzone was run using Pcatch.

4.3.2 Simulation results using Case II:

The model calibrated using Psubcatch was run using Pzone and Pcatch for the validation period in this experiment. The model performance for the validation period is shown in Table 4.11.

Table 4.11: Model performances obtained using Pzone and Pcatch for the validation period. The model was calibrated using Psubcatch.

Gauge	Type of precipitation	R_m^2	Rel. accdif.	Peak error	RMSE
Rottweil	using Psubcatch	0.80	0.03	-0.13	3.26
	using Pzone	0.80	0.03	-0.13	3.27
	using Pcatch	0.75	-0.10	-0.34	3.59
Oberndorf	using Psubcatch	0.77	0.03	0.00	4.78
	using Pzone	0.77	0.03	0.00	4.79
	using Pcatch	0.77	-0.08	-0.22	4.69
Horb	using Psubcatch	0.82	0.11	-0.08	7.95
	using Pzone	0.82	0.11	-0.08	7.95
	using Pcatch	0.76	-0.13	-0.37	9.32
Bad Imnau, Eyach	using Psubcatch	0.79	0.07	-0.19	2.24
	using Pzone	0.79	0.08	-0.19	2.23
	using Pcatch	0.69	0.16	-0.11	2.71

Table 4.11 (continued): Model performances obtained using Pzone and Pcatch for the validation period. The model was calibrated using Psubcatch.

Gauge	Type of precipitation	R_m^2	Rel. accdif.	Peak error	RMSE
Rangendingen, Starzel	using Psubcatch	0.59	0.23	-0.03	1.09
	using Pzone	0.59	0.23	-0.02	1.10
	using Pcatch	0.44	0.28	0.05	1.28
Oberensingen, Aich	using Psubcatch	0.66	0.06	-0.07	1.22
	using Pzone	0.65	0.05	-0.07	1.22
	using Pcatch	0.39	0.58	0.33	2.36
Suessen, Fils	using Psubcatch	0.79	0.09	-0.17	2.82
	using Pzone	0.79	0.09	-0.17	2.83
	using Pcatch	0.70	-0.05	-0.29	3.36
Plochingen, Fils	using Psubcatch	0.82	0.14	-0.17	5.00
	using Pzone	0.82	0.14	-0.17	5.01
	using Pcatch	0.72	0.05	-0.25	6.13
Plochingen, Neckar	using Psubcatch	0.87	0.02	-0.10	18.70
	using Pzone	0.87	0.03	-0.10	18.73
	using Pcatch	0.86	0.01	-0.08	19.27

Table 4.11 indicates that the model performance diminished when the calibrated model was run using Pcatch. A similar trend was observed on the seasonal basis and also in terms of event statistics for the annual maximum flood events.

Figure 4.15 shows the seasonal model performance for the gauges at Horb and Suessen, Fils , respectively.

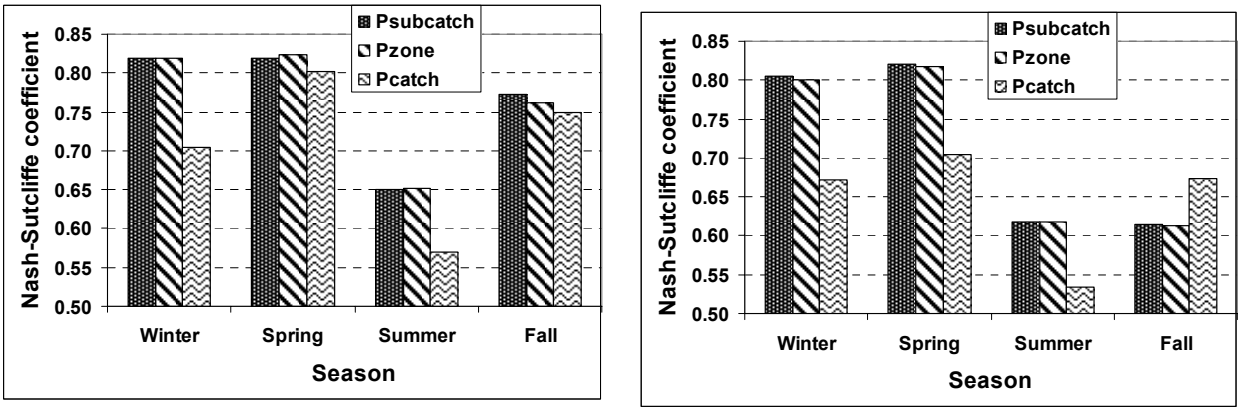

Figure 4.15: Seasonal Nash-Sutcliffe coefficients for the gauges at Horb (left panel) and Suessen, Fils (right panel). The model calibrated using Psubcatch was run using Pzone and Pcatch for the validation period.

Figures 4.16 and 4.17 represent the event statistics for the gauges at Horb and Suessen, Fils, respectively.

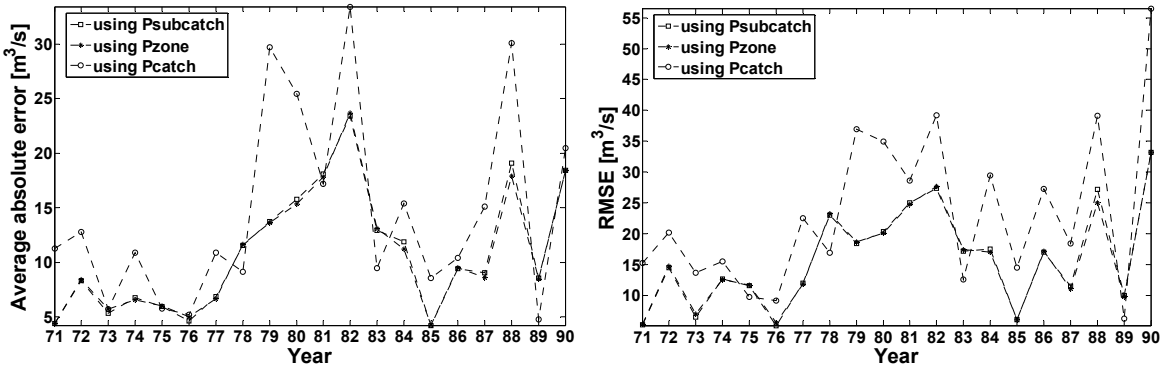

Figure 4.16: Event statistics at each annual maximum flood event for the gauge at Horb: average absolute error (left panel) and root mean squared error (right panel). The model calibrated using Psubcatch was run using Pzone and Pcatch for the validation period.

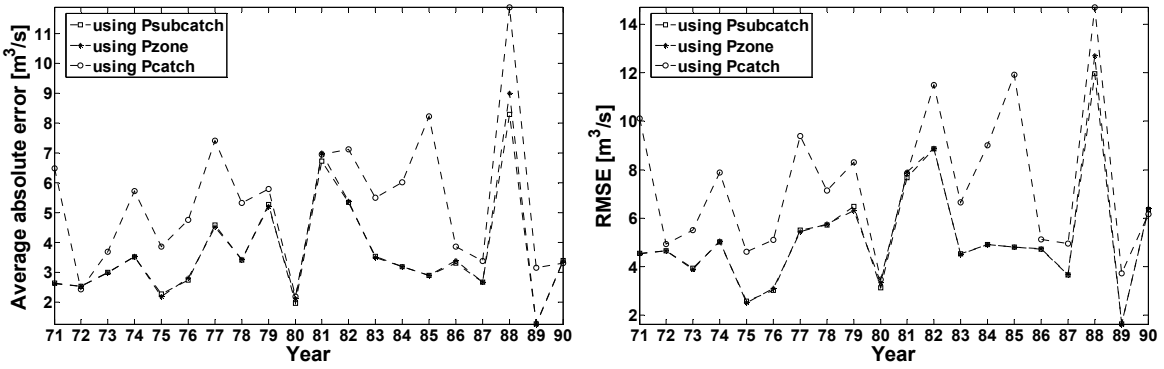

Figure 4.17: Event statistics at each annual maximum flood event for the gauge at Suessen, Fils: average absolute error (left panel) and root mean squared error (right panel). The model calibrated using Psubcatch was run using Pzone and Pcatch for the validation period.

On average, the absolute error with respect to the annual maximum discharges for the gauge at Horb ranges between 7.5% and 10.4%. The highest error was observed when the calibrated model using Psubcatch was run using Pcatch. The same value for the gauge at Suessen, Fils ranges between 8.4% to 12.7% and the highest error was observed when the calibrated model using Psubcatch was run using Pcatch.

4.3.3 Simulation results using Case III:

In the third simulation experiment, the model calibrated using Pcatch was run using Pzone and Psubcatch for the validation period. Table 4.12 shows the model performance for the validation period.

Table 4.12: Model performances obtained using Pzone and Psubcatch for the validation period. The model was calibrated using Pcatch.

Gauge	Type of precipitation	R_m^2	Rel. accdif.	Peak error	RMSE
Rottweil	using Pcatch	0.74	0.12	-0.13	3.69
	using Pzone	0.62	0.25	0.10	4.45
	using Psubcatch	0.63	0.25	0.10	4.39
Oberndorf	using Pcatch	0.75	0.07	-0.05	4.94
	using Pzone	0.63	0.18	0.17	5.98
	using Psubcatch	0.64	0.18	0.17	5.93
Horb	using Pcatch	0.79	-0.04	-0.28	8.65
	using Pzone	0.77	0.20	0.03	9.06
	using Psubcatch	0.78	0.20	0.02	9.00
Bad Imnau, Eyach	using Pcatch	0.72	0.12	-0.27	2.60
	using Pzone	0.78	0.04	-0.33	2.28
	using Psubcatch	0.78	0.04	-0.33	2.30
Rangendingen, Starzel	using Pcatch	0.58	0.18	-0.20	1.11
	using Pzone	0.66	0.14	-0.26	0.99
	using Psubcatch	0.67	0.13	-0.26	0.99
Oberensingen, Aich	using Pcatch	0.49	0.07	-0.31	1.48
	using Pzone	0.47	-0.35	-0.63	1.52
	using Psubcatch	0.46	-0.35	-0.63	1.52
Suessen, Fils	using Pcatch	0.67	0.02	-0.16	3.55
	using Pzone	0.70	0.17	-0.02	3.36
	using Psubcatch	0.70	0.17	-0.02	3.35
Plochingen, Fils	using Pcatch	0.69	0.13	-0.23	6.46
	using Pzone	0.76	0.22	-0.14	5.67
	using Psubcatch	0.76	0.22	-0.14	5.67
Plochingen, Neckar	using Pcatch	0.86	0.03	-0.11	19.65
	using Pzone	0.85	0.05	-0.11	19.90
	using Psubcatch	0.85	0.05	-0.12	19.81

As shown in Table 4.12, the model performance deteriorated for some of the subcatchments when the calibrated model was run using Psubcatch and Pcatch. However, model performance improved for some of the subcatchments when the calibrated model was utilizing relatively more detailed precipitation information.

Figure 4.18 shows the seasonal model performance for the Horb and Suessen, Fils, gauges respectively.

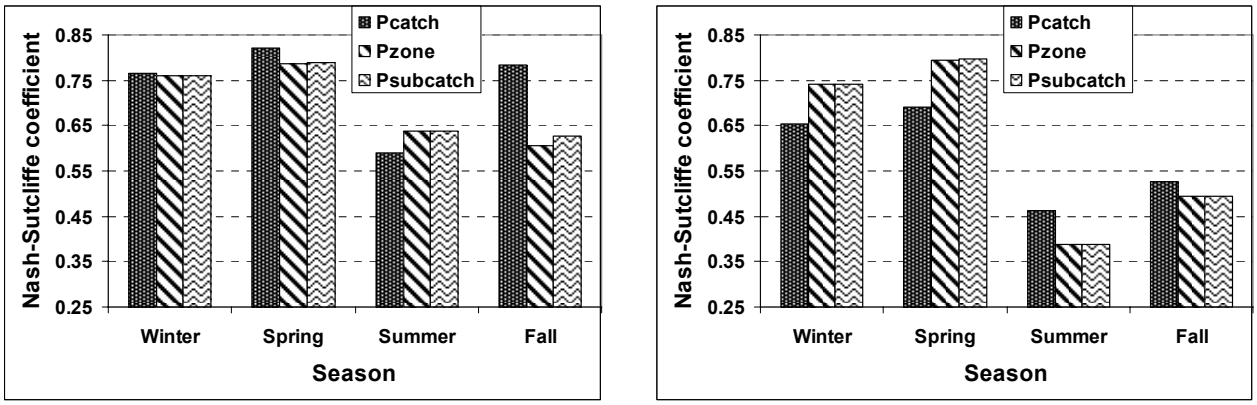

Figure 4.18: Seasonal Nash-Sutcliffe coefficients for the gauges at Horb (left panel) and Suessen, Fils (right panel). The model calibrated using Pcatch was run using Pzone and Psubcatch for the validation period.

Figures 4.19 and 4.20 represent the event statistics for the Horb and Suessen, Fils, gauges, respectively.

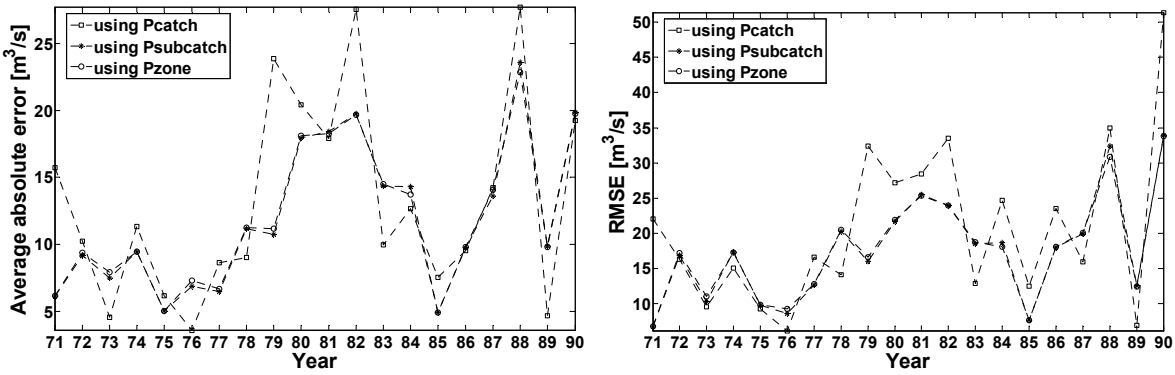

Figure 4.19: Event statistics at each annual maximum flood event for the gauge at Horb: average absolute error (left panel) and root mean squared error (right panel). The model calibrated using Pcatch was run using Pzone and Psubcatch for the validation period.

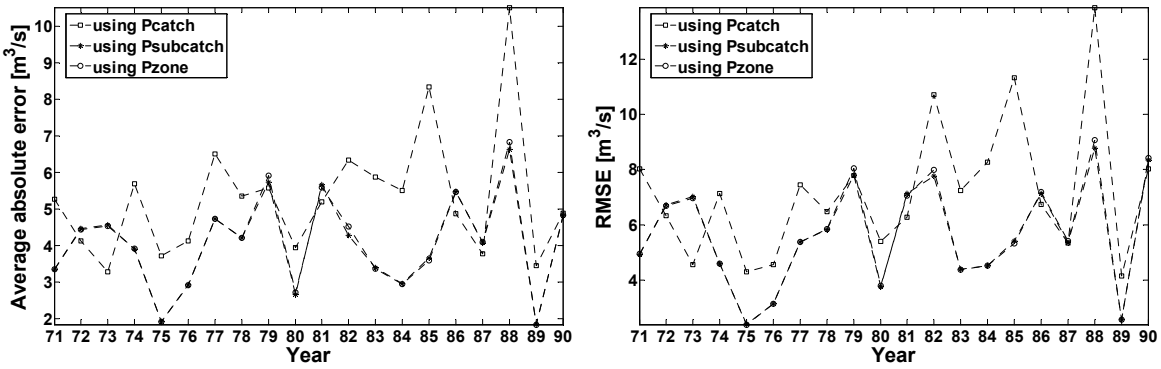

Figure 4.20: Event statistics at each annual maximum flood event for the gauge at Suessen, Fils: average absolute error (left panel) and root mean squared error (right panel). The model calibrated using Pcatch was run using Pzone and Psubcatch for the validation period.

Figures 4.19 and 4.20 indicate that there was improvement in the event statistics when the calibrated model using Pcatch was run using Pzone and Psubcatch.

On average, the absolute error with respect to the annual maximum discharges for the gauge at Horb ranges between 8.5% and 10.1%. The lower error was observed when the calibrated model using Pcatch was run using either Psubcatch or Pzone. The same value for the gauge at Suessen, Fils ranges between 9.6% to 12.7%. The lower error was observed when the calibrated model using Pcatch was run using either Psubcatch or Pzone.

Comparing the results of the three cases, it can be observed that the model performance deteriorated when the model calibrated with either Pzone or Psubcatch was run with the precipitation averaged over the catchment (Pcatch). Also, it is observed that a considerable equivalent model performances can be obtained when the model calibrated using Pzone was run using Psubcatch or vice versa.

The simulation experiments show that there is dependency of the model's parameters on the data used for its calibration. In fact, there is compensation among the model parameters when it is calibrated using Pzone or Psubcatch, as the level of input (precipitation) details is almost the same in both the cases. The results support the findings of Brath et al., (2004). They suggested that the parameterization resulting from historical data with a relatively poor spatial resolution may be considered reliable for more detailed rainfall fields. However, such compensation cannot be achieved when the level of input precipitation is reduced substantially, as in the case of Pcatch. Moreover, parameterization yields biased model structure, which provides poor simulation results when used with relatively spatially detailed precipitation input.

4.4 Concluding remarks

This study demonstrates number of simulation experiments to investigate the influence of the spatial variability of precipitation on the predictive uncertainty using a conceptual rainfall-runoff model in a meso-scale catchment.

In the first part of the study the interpolated precipitation from point raingauge measurements and averaged precipitation over different spatial resolutions were used as a main forcing input into the distributed and semi-distributed structures of the HBV model. The results demonstrate that there is no significant difference in the model performance calibrated using 1 km × 1 km grid precipitation and run using averaged precipitation on different spatial scales. This may be due to the fact that the averaged precipitation was obtained from the interpolated precipitation values (external drift kriging) which are already smoothed, and due to the coarse raingauge network.

Comparing the performances using the distributed and semi-distributed model structures of the HBV model, the semi-distributed model, in general, performs better than the distributed model.

Relatively higher differences in the model performances are observed for the smaller subcatchments.

The second part of the study was related to the model calibrated using precipitation with one level of information and run using precipitation with another level of information. The results indicate that there could be a significant deterioration in the model performance when the model calibrated using detailed precipitation was run using relatively less detailed precipitation (for expamle model calibrated using radar rainfall data and run using coarse raingauge data). When the level of main forcing precipitation input is different for the model simulation than that used for calibration, one should be cautious.

5 Comparison of modeling performance using different representations of spatial variability

5.1 Introduction

The objective of this section is to explore a solution to the question: Will a higher spatial resolution of model input data necessarily, as most people assume, lead to a better model performance? An attempt is made to modify the conceptual rainfall-runoff model HBV to incorporate a spatially-distributed structure. Its predictive performance was then assessed and compared with other model structures, namely semi-distributed, semi-lumped and fully-lumped, of the HBV model in accordance with the study objective. To reproduce the spatial variation of the meteorological input at the catchment scale, external drift kriging (Ahmed and de Marsily, 1987) was applied to enable interpolation from the available point measurements over the investigated area. The simulated hydrographs obtained using different model structures were analyzed through the comparisons of the computed Nash-Sutcliffe coefficient and other goodness-of-fit indices.

5.2 Simulations using different model structures

The different model structures were setup and calibrated using the automatic calibration procedure based on the simulated annealing optimization algorithm. The same calibration period and calibration objectives were used for each model structure. The details on the data preparation to setup the different model structures and model calibration are described in the Chapter III.

A summary of the performances of different model structures in the calibration period are shown in Table 5.1. It can be observed that the Nash-Sutcliffe coefficient for the simulation of the daily discharge in the subcatchments during the calibration period has values ranging between 0.61 and 0.84, with a mean value of 0.73 for the distributed structure. The minimum, maximum and mean values of Nash-Sutcliffe coefficients obtained using the semi-distributed model structure are 0.68, 0.86 and 0.78 respectively. The values of the Nash-Sutcliffe coefficients obtained using the semi-lumped model structure range between 0.65 and 0.87, with a mean value of 0.78.

Table 5.1: Performances of different model structures for different gauges during the calibration period.

Gauge	Model structure	R_m^2	Rel. accdif.	Peak error	AI	RMSE
Rottweil	Distributed	0.69	0.16	-0.43	0.74	3.97
	Semi-distributed	0.78	0.00	-0.20	0.80	3.34
	Semi-lumped	0.73	0.01	-0.21	0.77	3.67
	Fully-lumped	0.74	0.01	-0.22	0.77	3.64
Oberndorf	Distributed	0.72	0.07	-0.43	0.77	5.18
	Semi-distributed	0.79	-0.01	-0.15	0.80	4.44
	Semi-lumped	0.78	0.02	-0.18	0.78	4.52
	Fully-lumped	0.77	0.02	-0.19	0.77	4.68
Horb	Distributed	0.82	0.08	-0.28	0.81	7.72
	Semi-distributed	0.84	0.02	-0.06	0.81	7.19
	Semi-lumped	0.84	0.02	-0.10	0.80	7.23
	Fully-lumped	0.83	0.02	-0.13	0.80	7.42
Bad Imnau, Eyach	Distributed	0.75	0.00	-0.25	0.76	2.30
	Semi-distributed	0.78	0.01	-0.20	0.77	2.18
	Semi-lumped	0.74	0.08	-0.22	0.72	2.34
	Fully-lumped	0.72	0.06	-0.25	0.72	2.46
Rangendingen, Starzel	Distributed	0.61	0.02	-0.48	0.68	1.14
	Semi-distributed	0.68	0.00	-0.12	0.69	1.04
	Semi-lumped	0.65	0.00	-0.17	0.67	1.08
	Fully-lumped	0.64	0.00	-0.17	0.66	1.10
Riederich, Erms	Distributed	0.64	-0.08	-0.56	0.70	1.27
	Semi-distributed	0.75	0.02	-0.08	0.71	1.05
	Semi-lumped	0.74	0.03	-0.16	0.69	1.08
	Fully-lumped	0.73	0.02	-0.13	0.69	1.10
Oberensingen, Aich	Distributed	0.72	0.08	-0.07	0.71	1.09
	Semi-distributed	0.79	0.01	-0.10	0.73	0.95
	Semi-lumped	0.78	0.01	-0.14	0.73	0.96
	Fully-lumped	0.77	0.01	-0.13	0.70	0.99
Suessen, Fils	Distributed	0.76	-0.11	-0.18	0.77	3.12
	Semi-distributed	0.78	0.01	-0.13	0.74	2.99
	Semi-lumped	0.81	-0.01	-0.16	0.78	2.74
	Fully-lumped	0.78	0.00	-0.13	0.74	3.00
Plochingen, Fils	Distributed	0.79	-0.05	-0.32	0.77	5.30
	Semi-distributed	0.79	0.02	-0.07	0.75	5.22
	Semi-lumped	0.83	0.01	-0.09	0.79	4.70
	Fully-lumped	0.82	0.01	-0.07	0.78	4.83
Plochingen, Neckar	Distributed	0.84	0.01	-0.22	0.80	20.34
	Semi-distributed	0.86	-0.03	-0.09	0.80	19.23
	Semi-lumped	0.87	0.02	-0.06	0.80	18.68
	Fully-lumped	0.86	0.02	-0.09	0.79	18.87

The Nash-Sutcliffe coefficient obtained using the fully-lumped model structure ranges between 0.64 and 0.86, with a mean value of 0.76. The table also indicates that the highest Nash-Sutcliffe coefficient value was observed at the catchment outlet Plochingen, Neckar using all four model structures. Among the different model structures, the semi-distributed and semi-lumped models show relatively higher mean values of the Nash-Sutcliffe coefficients. There is clear underestimation to simulate the mean annual maximum discharges over the calibration period.

A Summary of the performance of the different model structures in the validation period is shown in Table 5.2. The Nash-Sutcliffe coefficient for the simulation of the daily discharge in the subcatchments during the validation period has values ranging between 0.59 and 0.82, with a mean value of 0.72 for distributed model, as observed in Table 5.2. The minimum, maximum and mean values of the Nash-Sutcliffe coefficient obtained using the semi-distributed model are 0.55, 0.87 and respectively 0.75. In the semi-lumped model structure, the values of the Nash-Sutcliffe coefficient range between 0.58 and 0.86, with a mean value of 0.75. The Nash-Sutcliffe coefficient obtained using the fully-lumped model structure ranges between 0.55 and 0.87, with a mean value of 0.74. As observed in the calibration period, the highest Nash-Sutcliffe coefficient value was observed at the catchment outlet Plochingen, Neckar using all model structures. The lowest value of the Nash-Sutcliffe coefficient was observed at the gauge Rangendingen, Starzel, which is partly located in a karstic geological formation. Among the four different model structures, the semi-distributed and semi-lumped structures show relatively higher mean values of the Nash-Sutcliffe coefficient, as also observed in the calibration period. Among the distributed and semi-distributed model structures, relatively higher differences are observed for smaller subcatchements.

There is clear pattern in the underestimation of mean annual maximum discharges, as observed in the calibration period. The maximum underestimation of about 60% was observed using the distributed model structure at the gauge Riederich, Erms, where the water balance is partly affected by the karstic geological formations.

Table 5.2: Model performances of the different model structures during the validation period.

Gauge	Model structure	R_m^2	Rel. accdif.	Peak error	AI	RMSE
Rottweil	Distributed	0.70	0.19	-0.41	0.72	4.07
	Semi-distributed	0.79	0.03	-0.06	0.80	3.42
	Semi-lumped	0.72	0.03	-0.12	0.76	3.93
	Fully-lumped	0.76	0.03	-0.16	0.77	3.61
Oberndorf	Distributed	0.72	0.12	-0.36	0.76	5.37
	Semi-distributed	0.75	0.03	0.05	0.79	5.04
	Semi-lumped	0.76	0.06	-0.02	0.77	4.91
	Fully-lumped	0.76	0.06	0.03	0.77	4.95
Horb	Distributed	0.76	0.18	-0.31	0.77	9.43
	Semi-distributed	0.82	0.11	-0.05	0.80	8.11
	Semi-lumped	0.82	0.10	-0.10	0.79	8.22
	Fully-lumped	0.82	0.10	-0.08	0.79	8.28
Bad Imnau, Eyach	Distributed	0.76	0.07	-0.31	0.76	2.42
	Semi-distributed	0.80	0.06	-0.20	0.76	2.21
	Semi-lumped	0.77	0.13	-0.22	0.72	2.40
	Fully-lumped	0.77	0.10	-0.24	0.72	2.37
Rangendingen, Starzel	Distributed	0.59	0.29	-0.37	0.64	1.08
	Semi-distributed	0.55	0.24	0.07	0.67	1.13
	Semi-lumped	0.58	0.23	0.03	0.66	1.09
	Fully-lumped	0.55	0.24	0.04	0.64	1.14
Riederich, Erms	Distributed	0.62	-0.03	-0.59	0.70	1.37
	Semi-distributed	0.70	0.07	-0.15	0.70	1.21
	Semi-lumped	0.71	0.07	-0.23	0.68	1.19
	Fully-lumped	0.69	0.06	-0.19	0.68	1.24
Oberensingen, Aich	Distributed	0.62	0.14	-0.01	0.56	1.24
	Semi-distributed	0.66	0.06	-0.06	0.63	1.17
	Semi-lumped	0.65	0.05	-0.09	0.62	1.19
	Fully-lumped	0.62	0.06	-0.08	0.61	1.24
Suessen, Fils	Distributed	0.81	-0.03	-0.27	0.75	2.72
	Semi-distributed	0.79	0.10	-0.18	0.61	2.79
	Semi-lumped	0.81	0.08	-0.23	0.74	2.66
	Fully-lumped	0.77	0.09	-0.21	0.64	2.96
Plochingen, Fils	Distributed	0.77	0.08	-0.40	0.65	5.60
	Semi-distributed	0.81	0.15	-0.18	0.56	5.15
	Semi-lumped	0.83	0.14	-0.21	0.66	4.88
	Fully-lumped	0.82	0.13	-0.20	0.63	4.97
Plochingen, Neckar	Distributed	0.82	0.08	-0.26	0.78	22.03
	Semi-distributed	0.87	0.02	-0.09	0.82	18.78
	Semi-lumped	0.86	0.07	-0.07	0.78	19.27
	Fully-lumped	0.87	0.07	-0.11	0.78	19.08

Figure 5.1 shows the scatter plots of the simulated and observed daily discharges obtained using different model structures at the gauge Horb. It can be observed that low flows and medium peak

flows were estimated well by different model structures, while higher peak flows were underestimated. The peak flows generally occurred during the winter period in the study catchment. This underestimation of the peak flows may be due to an improper representation of the snow accumulation and snow melting phenomena or the simplification adopted in the model to simulate water redistribution in the soil.

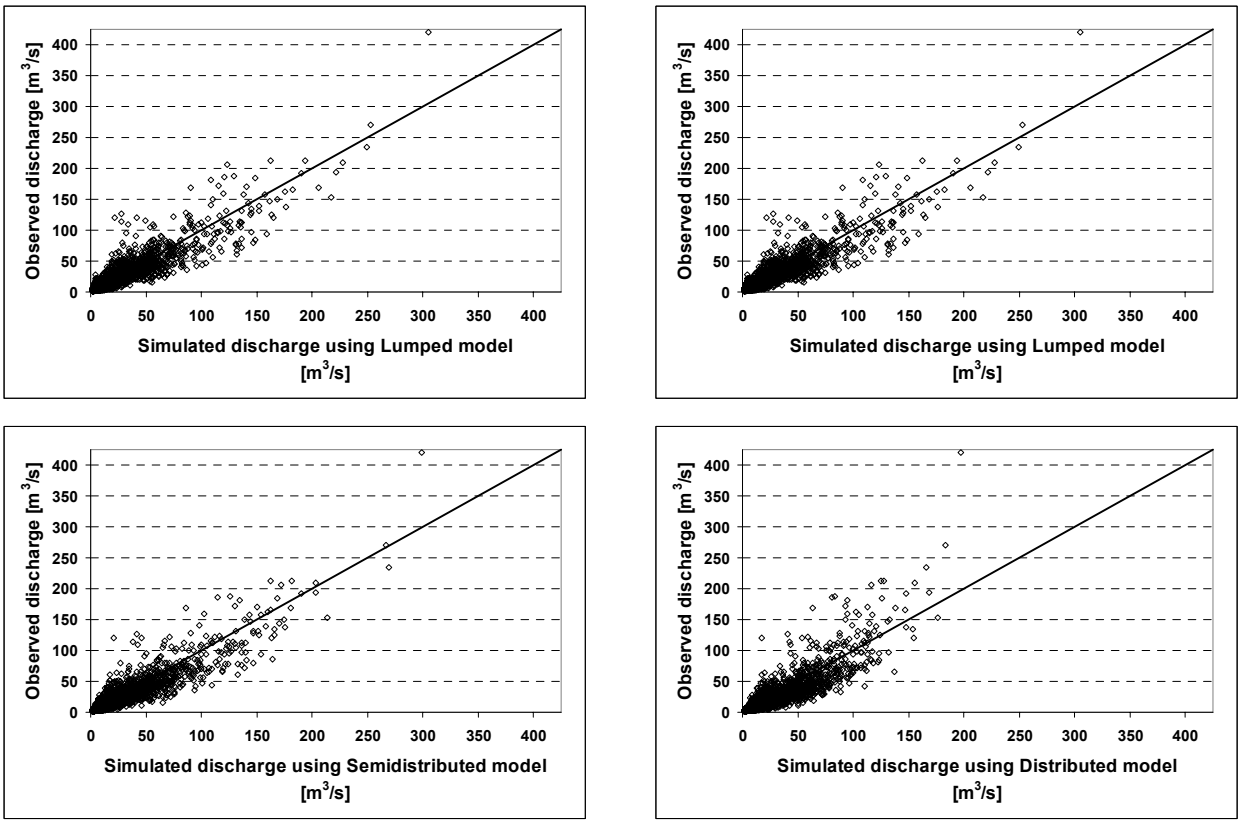

Figre 5.1: Scatter plots of the model simulated and the observed daily discharges using different model structures at the Horb gauge for the validation period.

The RMSE as a function of correlation coefficient in the calibration and validation periods are shown in Figures 5.2 and 5.3 for the gauges at Horb and Plochingen, Neckar, respectively.

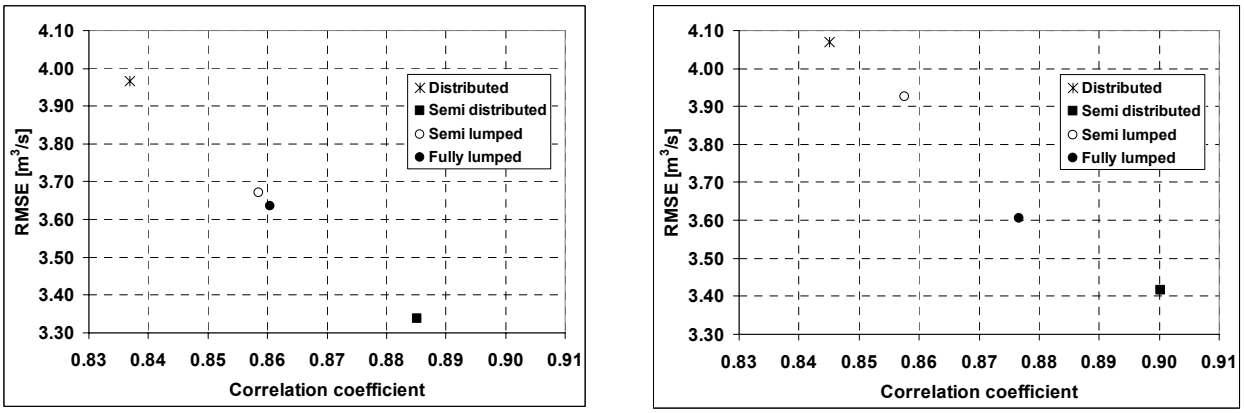

Figure 5.2: RMSE versus correlation coefficients using different model structures for the gauging station at Horb during calibration period (left panel) and during validation period (right panel).

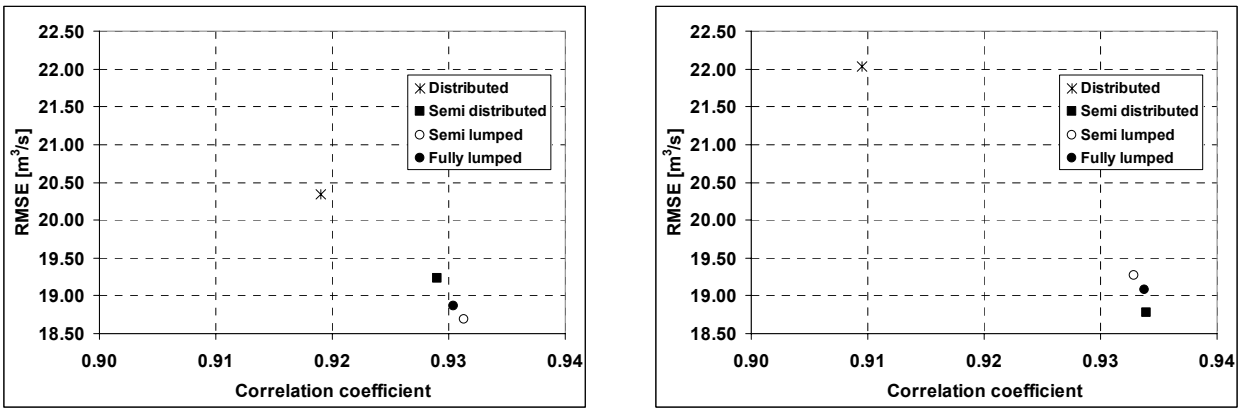

Figure 5.3: RMSE versus correlation coefficients using different model structures for the gauging station at Plochingen, Neckar during calibration period (left panel) and validation period (right panel).

As shown in Figures, the highest correlation coefficients with the lowest RMSE values are observed using the semi-distributed model structure. Among the semi-distributed, semi-lumped and fully-lumped model structures, less difference in the values of correlation coefficients and RMSE are observed for the outlet gauge at Plochingen, Neckar.

Regarding modeling of runoff at higher time scales, the performance of the models in terms of the Nash-Sutcliffe coefficient shows a similar trend, as observed at the daily time scale. However, the model performance improves with increasing time scale using the all model structures. A Summary of the Nash-Sutcliffe coefficient at 7 days and 30 days time scale obtained using the different model structures in the validation period is shown in Table 5.3. These Nash-Sutcliffe coefficients show the model performance in simulating the 7 days and 30 days mean discharges of a moving window.

Table 5.3: Nash-Sutcliffe coefficients at 7 days and 30 days time scale obtained using the different model structures in the validation period.

Gauge	Model structure	Nash-Sutcliffe coefficient	
		7 days time scale	30 days time scale
Rottweil	Distributed	0.82	0.86
	Semi-distributed	0.86	0.90
	Semi-lumped	0.82	0.89
	Fully-lumped	0.82	0.89
Oberndorf	Distributed	0.81	0.87
	Semi-distributed	0.82	0.87
	Semi-lumped	0.80	0.88
	Fully-lumped	0.80	0.88
Horb	Distributed	0.84	0.87
	Semi-distributed	0.86	0.89
	Semi-lumped	0.86	0.88
	Fully-lumped	0.86	0.88
Bad Imnau, Eyach	Distributed	0.84	0.87
	Semi-distributed	0.86	0.86
	Semi-lumped	0.82	0.82
	Fully-lumped	0.82	0.82
Riederich, Erms	Distributed	0.69	0.69
	Semi-distributed	0.80	0.80
	Semi-lumped	0.79	0.80
	Fully-lumped	0.79	0.80
Oberensingen, Aich	Distributed	0.69	0.67
	Semi-distributed	0.78	0.81
	Semi-lumped	0.78	0.80
	Fully-lumped	0.78	0.80
Suessen, Fils	Distributed	0.82	0.82
	Semi-distributed	0.82	0.81
	Semi-lumped	0.80	0.81
	Fully-lumped	0.80	0.81
Plochingen, Fils	Distributed	0.84	0.85
	Semi-distributed	0.84	0.82
	Semi-lumped	0.86	0.85
	Fully-lumped	0.86	0.85
Plochingen, Neckar	Distributed	0.88	0.90
	Semi-distributed	0.89	0.91
	Semi-lumped	0.89	0.91
	Fully-lumped	0.89	0.91

Figure 5.4 shows the model performance obtained using different model structures at different gauges in the validation period. The model performance obtained using the semi-distributed and semi-lumped model structures are relatively better, in general, as compared to the other model structures. It can be observed that model performances are better for larger subcatchments using all

the model structures. This is a general trend for the conceptual model. It can also be noticed that there are higher differences in the model performances for the smaller and medium-sized subcatchments, while the differences are negligible for the gauge at outlet of the catchment.

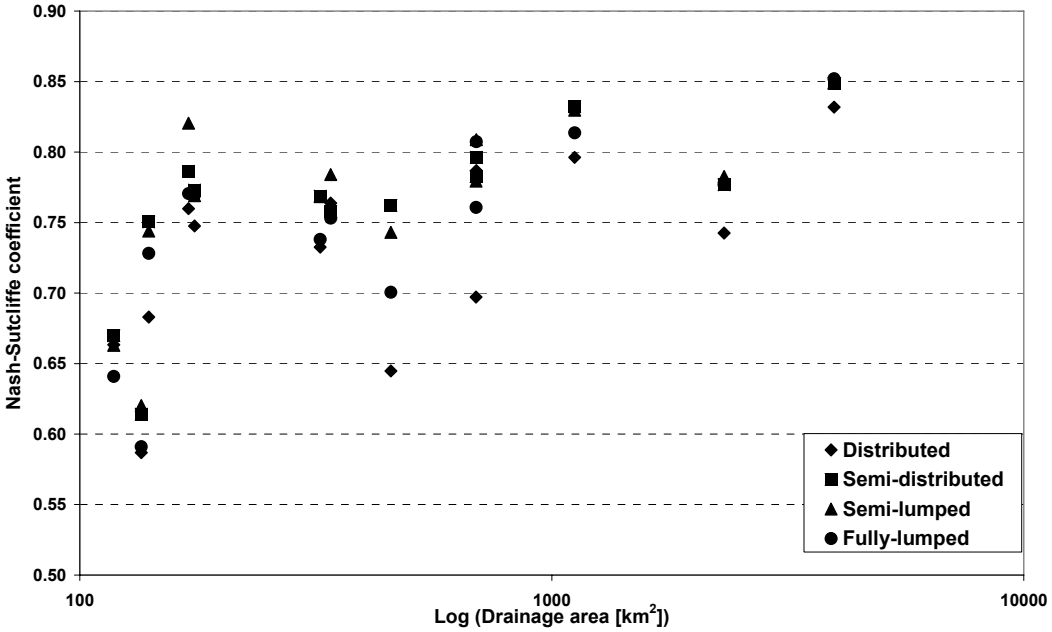

Figure 5.4: Nash-Sutcliffe coefficient using different model structures for different subcatchments.

The flow duration curves obtained using different model structures for the Horb gauge in the validation period is shown in Figure 5.5.

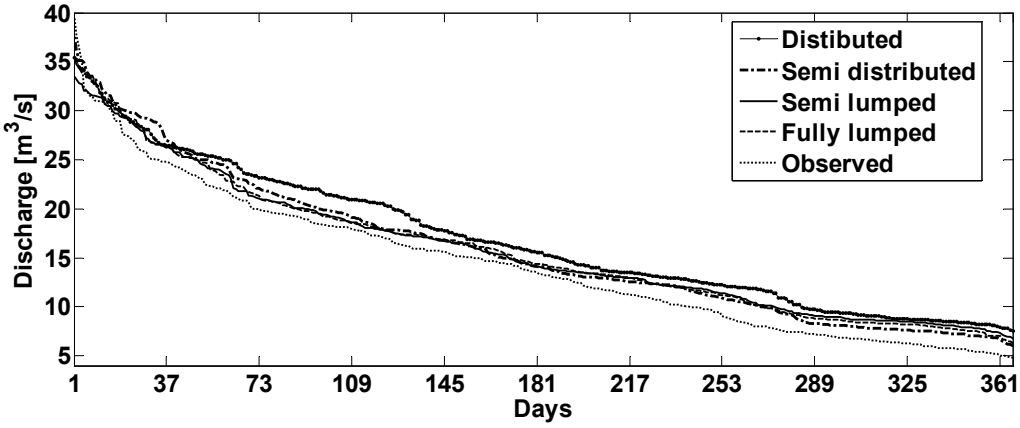

Figure 5.5: Flow duration curves obtained using different model structures at the Horb gauge for the validation period.

There is a trend of overestimation to simulate the mean values of low and medium discharges using the different model structures. However there is underestimation to simulate the mean values of high discharges (Figure 5.5).

The computed mean model performance and parameters' transferability are shown in Table 5.4. The mean model performance and parameters' transferability were calculated using the Nash-Sutcliffe coefficient values obtained during the calibration and validation periods.

Table 5.4: Mean model performance and parameters' transferability obtained using different model structures.

Model structure	Mean model performance	Model parameters' transferability
Distributed	0.75	0.06
Semi-distributed	0.80	0.05
Semi-lumped	0.80	0.04
Fully-lumped	0.79	0.04

The highest value of mean model performance was observed using the semi-distributed and semi-lumped model structures, as shown in the above table. The worst model parameters' transferability was observed for the distributed model structure.

The Nash-Sutcliffe coefficient was also computed on a seasonal basis in order to investigate the model performances during different seasons in the calibration and validation periods. Figure 5.6 shows seasonal model performance in the validation period for the gauges at Horb and Plocingen, Neckar. As shown in Figure 5.6, the seasonal model performances are observed better, in general, for the semi-distributed model structure. However, the performance is comparatively poor in the summer season using all the model structures. This is because of the convective precipitation events, which are more localized and are not well captured by the coarse raingauge networks.

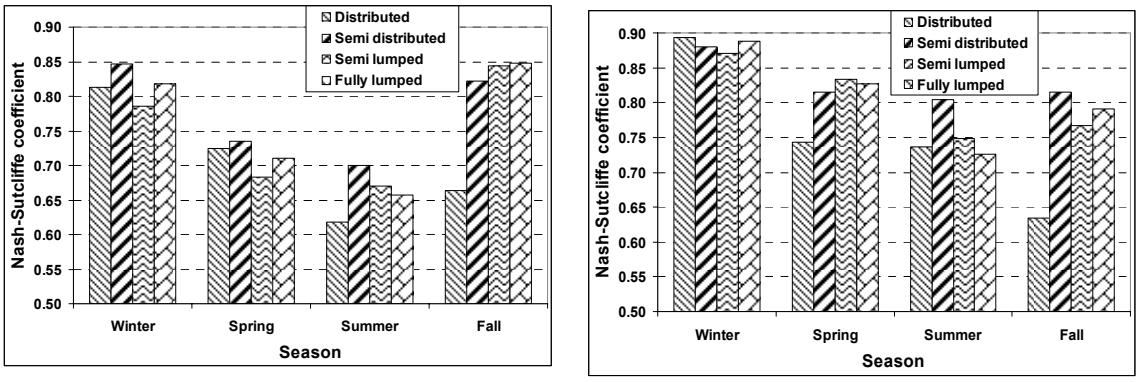

Figure 5.6: Seasonal Nash-Sutcliffe coefficients obtained using different model structures for the validation period for the gauges at Horb (left panel) and Plochingen, Neckar (right panel).

Further, the Nash-Sutcliffe coefficient was computed for different years during the calibration and validation periods for different gauges to investigate the variation of the model performance from year to year. Figure 5.7 shows the annual model performance during the validation period for

the gauges at Rottweil and Horb. It can be observed that the distributed model does not outperform when compared to other model structures for most of the year in the validation period.

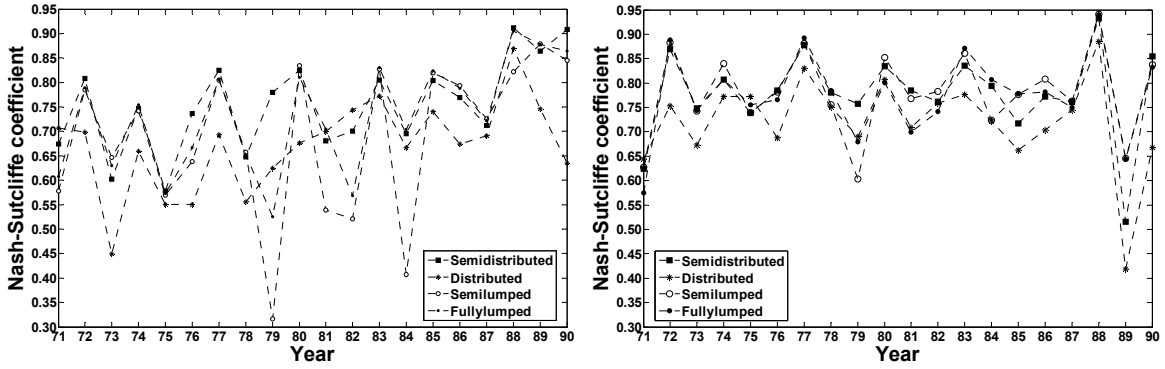

Figure 5.7: Annual Nash-Sutcliffe coefficient during the validation period for the gauges at Rottweil (left panel) and Horb (right panel).

On average, the standard deviation of the yearly Nash-Sutcliffe coefficients is relatively higher using the distributed model structure as compared to the same obtained using the other model structures. This implies that the model performance using the distributed structure is not consistent.

The average absolute error and root mean squared error were also calculated for each annual maximum flood event to investigate the peak discharge estimation performance using the different model structures. Figures 5.8 and 5.9 show the average absolute error and root mean squared error obtained using different model structures for the gauges at Rottweil and Horb, respectively.

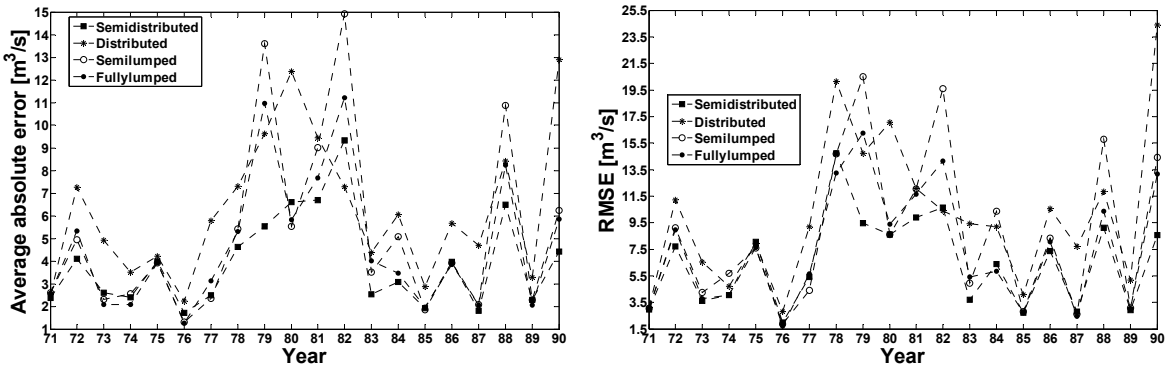

Figure 5.8: Event statistics for different years during the validation period obtained using different model structures for the gauge at Rottweil: average absolute error (left panel) and root mean squared error (right panel).

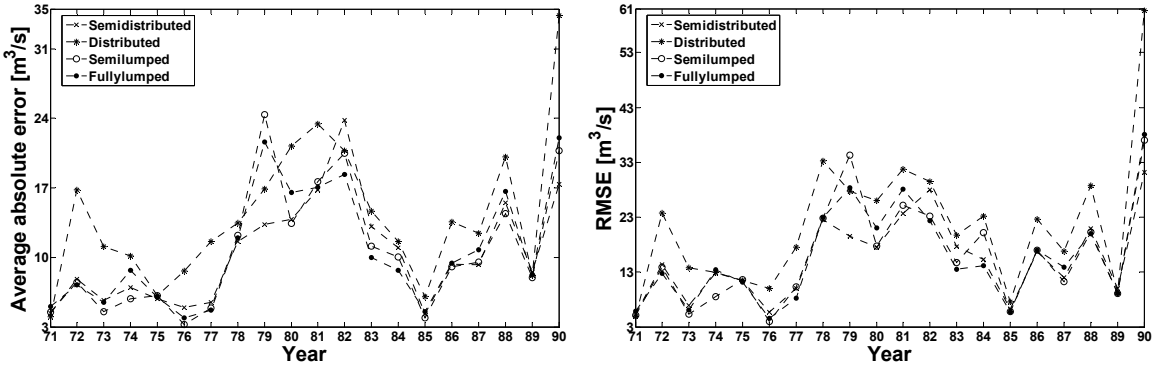

Figure 5.9: Event statistics for different years during the validation period using different model structures for the gauge at Horb: average absolute error (left panel) and root mean squared error (right panel).

The higher errors were observed for the distributed model structure, as shown in Figures 5.8 and 5.9. On average, the absolute error with respect to the annual maximum discharges for the gauge at Rottweil ranges between 6.6% and 9.8% using the four different model structures. The highest error was observed using the distributed model structure. The same value for the gauge at Horb ranges between 7.2% to 9.6% and the highest error was observed using the distributed model structure, as observed for the gauge at Rottweil.

It is worth mentioning that the model comparisons in this study were made based on stream flow, an integrated measure of hydrological response, at different subcatchments' outlets. The results showed that interpolated precipitation values on finer resolution did not improve the simulation accuracy in either the calibration or validation periods. It appeared that the additional information about the spatial variability of the precipitation did not provide any additional benefit. However, the main difficulty with the spatially-distributed calculation arises from the enormous spatial variability of hydrological processes which complicates the up scaling of point measurements. The main inputs to the model, precipitation and temperature, were interpolated from the coarse observation network. The estimation of precipitation input from the point measurements to the grid cells in the distributed model is more difficult. Additionally, a conceptual model always needs a degree of calibration based on hydrological response data. Due to the high degree of model parameter interaction and dependency, the calibration task for a distributed model is even more difficult.

Figure 5.10 compares the model performance using different model structures obtained without optimized model parameters and the performance with optimized parameters, for the calibration and validation periods.

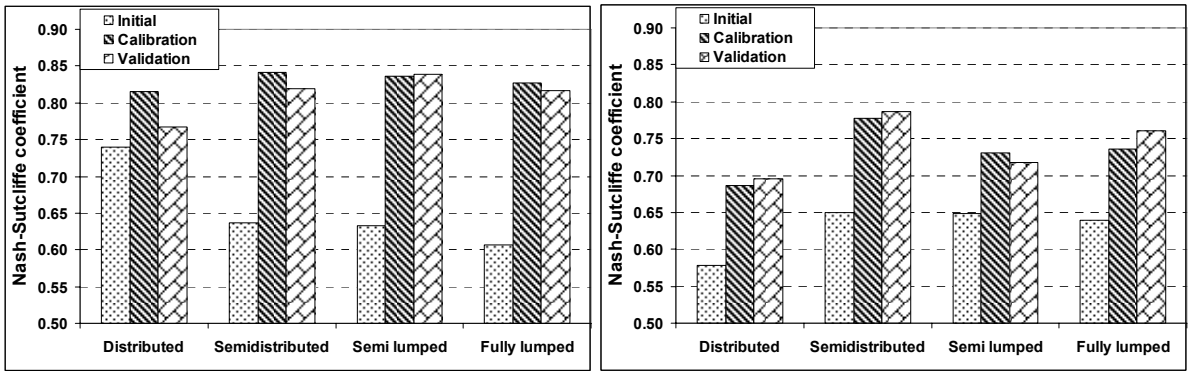

Figure 5.10: Nash-Sutcliffe coefficients obtained using different model structures with and without optimization of the model parameters for the gauges at Rottweil (left panel) and Horb (right panel).

It can be noticed that the calibrated models have improved model performance on the average over uncalibrated models since uncalibrated models do not have the benefit of accounting for the bias in the rainfall input over the calibration period. It may also be observed that the rate of improvement is relatively low for the distributed model structure. This may be due to the huge number of parameters to be optimized and their underlying dependency and the problems to estimate the areal precipitation on finer grids used for the distributed HBV model. Table 5.5 compares the model performance using two different attempts for the calibration of the model parameters of the distributed model structure. For the second attempt, the number of repetitions was doubled compared to the first attempt in the automatic optimization algorithm. Table 5.5 indicates that there was an improvement in the model performance as a result of doubling the number of repetitions in the optimization scheme. However, the model performance still did not improve significantly compared to the other structures. Perhaps there was a higher compensation for the bias in the rainfall input over the calibration period for the simpler model structures.

Table 5.5: Nash-Sutcliffe coefficients for different gauges obtained through the application of the distributed HBV model using different optimization trails.

	Rottweil	Oberndorf	Horb	Bad Imnau, Eyach	Suessen, Fils	Plochingen, Fils	Plochingen, Neckar
Calibration(I)	0.69	0.72	0.82	0.75	0.76	0.79	0.84
Calibration(II)	0.72	0.77	0.83	0.76	0.77	0.78	0.84
Validation(I)	0.70	0.72	0.76	0.76	0.81	0.77	0.82
Validation(II)	0.70	0.74	0.77	0.76	0.80	0.77	0.82

5.3 Concluding remarks

A solution to the query ‘Will a higher spatial resolution of model input data necessarily lead to a better model performance?’ is explored in this chapter. Four different model structures based on the

HBV model was developed for simulating hydrological processes in a meso-scale catchment. The spatial variation of the meteorological input at the catchment scale was produced using the external drift kriging method from the available point measurements. The performance was assessed using different model performance evaluation criteria. For the present study catchment, the semi-distributed and semi-lumped model structures outperformed the distributed and lumped model structures for the given level of observation. Among the model performances obtained using the distributed and semi-distributed structures, relatively higher differences are observed for smaller subcatchements. However, the differences in the model performances are less for the larger subcatchments.

The results highlighted that using interpolated precipitation values on finer resolution did not improve the simulation accuracy in either the calibration or validation periods. The additional information about the spatial variability of the precipitation data did not provide any additional benefit to simulate the discharge at the subcatchments' outlets. The results suggested that finer input is not necessarily always better and the selection of the model structure should be guided by the principal of parsimony, purpose and the availability of observations.

The findings of this study may be due to the following reasons:

(1) More detailed information about topography, vegetation and other relevant landscape characteristics may assist in the determination of model parameters; and this may improve the predictions of runoff. However, the major problem in this study was determination of areal precipitation for the model grid cells. The precipitation used in the present study was interpolated from the available point raingauges, which does not account enough for the spatial variability of the precipitation. In fact, the parameter values in principle may compensate for an incomplete representation of the precipitation field. Perhaps there was a higher compensation for the bias in the rainfall input over the calibration period for the relatively simple model structures. Thus in the semi-distributed and semi-lumped model structures, the error representing the spatial variability of precipitation was possibly compensated by the model parameterization. However the error in representing spatial variability of precipitation in finer resolution is more and perhaps dominated the bias compensation in the rainfall input by the calibration procedure for the distributed model structure. Additionally, the model parameterization for the distributed structure is more challenging due to the parameters' large number of degrees of freedom and their underlying interactions.

(2) The HBV model, used for the present study, is a conceptually lumped model. This fact may perhaps constraint its performance in accounting for the spatially resolved input data.

(3) Moreover, there can be a trade-off between model complexity and the available observations, i.e., the resolution of input data and the model structure itself interact when generating model uncertainty.

However, considering the practical difficulties in applying a physically-based distributed hydrological model, lumped models and lumped modeling experience can be fully exploited in a distributed modeling framework, with necessary modifications in the process representation.

The use of fully, spatially resolved radar rainfall data or combination of radar-raingauge rainfall data may be used to re-examine the outcomes of the comparison of different model structures carried out in this study.

6 Assessing the impacts of raingauge density on the simulation results of a hydrological model

6.1 Introduction

The question, 'What is the impact on the simulated hydrographs of interpolated precipitation at different spatial resolutions through varying raingauge networks?' is explored in this chapter. First, a method based on combinatorial optimization algorithm simulated annealing (Aarts and Korst, 1989) was used to identify the optimal locations of particular number of raingauges. Secondly, distributed and semi-distributed model structures of the HBV model were used to investigate the effect of the number of raingauges and their locations on the predictive uncertainty of hydrological models. The performance of the HBV model was analyzed as a function of the raingauge density through the comparisons of Nash-Sutcliffe coefficient and other goodness-of-fit indices. In the second section the influence of the rainfall observation network on model calibration and application was examined. This study seeks to determine whether the parameters calibrated using the rainfall coming from one type of network have the ability to represent the phenomena governing the rainfall-runoff process with the input provided by a different configuration of the raingauge network. The semi-distributed model structure was calibrated using precipitation produced from different raingauges network. The calibrated model was then run for the validation period using the precipitation obtained from the raingauges network which was not used for the calibration. Other experiments were carried out to analyze the reliability of supplementing missing precipitation measurements used for the calibration with data estimated using a multiple linear regression technique, and running the model using that precipitation combined with available observed precipitation. At the end a set of experiments carried out to investigate the influence of temperature gauges on the model simulation results.

6.2 Raingauge selection method and data preparation

The raingauges that have no missing measurements for the period between 1961 - 1990 and are located within or up to 30 km from the study catchment were used as a basis of complete raingauge network. The raingauge networks were selected from the complete network using the combinatorial optimization algorithm simulated annealing (Aarts and Korst, 1989). The main idea behind the raingauge selection algorithm was to identify a uniform set of locations for a particular number of raingauges.

The algorithm was applied repeatedly to obtain optimal locations of different number of raingauges. Seven networks consisting of different number of raingauges ranging from 5 to 51 were obtained. Figure 6.1 shows the spatial distribution of the selected raingauges.

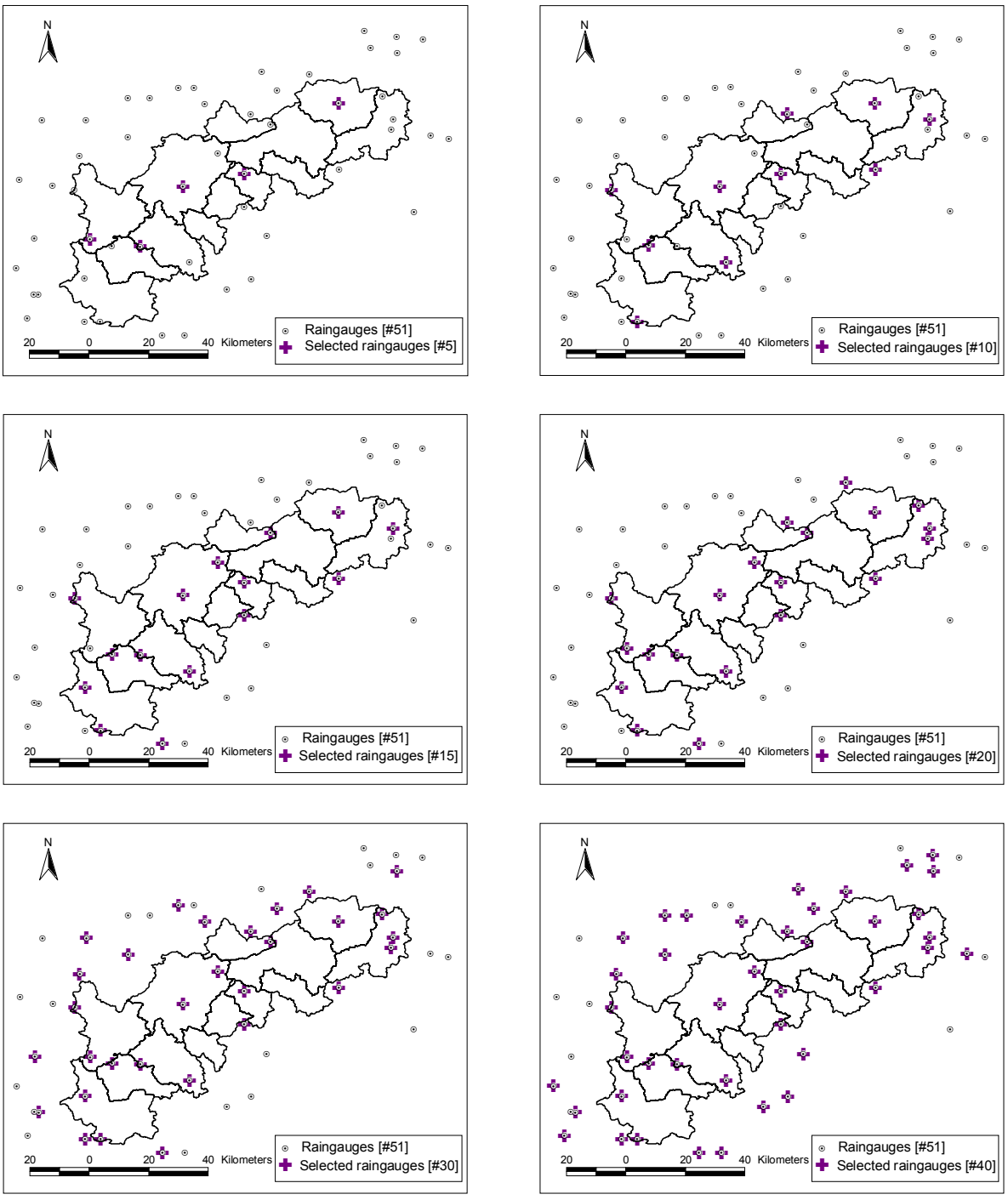

Figure 6.1: Geographical locations of selected raingauge networks.

The point measurements obtained from the selected raingauge networks were interpolated on a 1 km × 1 km grid using the external drift kriging method (Ahmed and de Marsily, 1987). Figure 6.2 depicts the standard deviation of the interpolated precipitation over the catchment. It can be

observed that the variability of the interpolated precipitation decreases with an increasing number of raingauges, but there is no change in the variability beyond a certain number of raingauges.

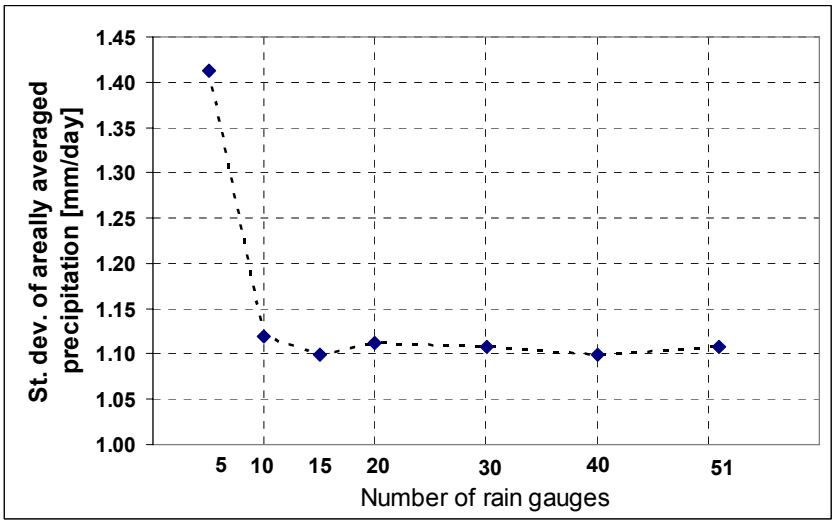

Figure 6.2: Standard deviation of areally averaged precipitation vs. number of raingauges.

6.3 Model simulations

The interpolated precipitation from the different raingauge networks was used to simulate hydrographs using the distributed and semi-distributed structures of the HBV model. The models were calibrated using the interpolated precipitation obtained from the different networks. The other input data, namely daily mean temperature and daily potential evapotranspiration, were kept unchanged in each calibration. Thus the input precipitation was different in each calibration. The automatic calibration method based on the combinatorial algorithm simulated annealing (Aarts and Korst, 1989) was used to optimize the model parameters.

6.3.1 Simulations using the distributed HBV model structure

A summary of the model performance for the calibration period using the distributed model structure for selected three gauges is shown in Table 6.1. Table 6.2 shows the model performance for the validation period. The model performances are shown for the gauges at Horb and Suessen, Fils because there were major variations in the number of raingauges within each network for the drainage area of these two gauges.

Table 6.1: Model performance through the application of the distributed HBV model using different number of raingauges for the calibration period.

Number of raingauges	Horb				Suessen, Fils				Plochingen,Neckar			
	R_m^2	Rel. accdif.	Peak error	RMSE	R_m^2	Rel. accdif.	Peak error	RMSE	R_m^2	Rel. accdif.	Peak error	RMSE
10	0.77	0.15	-0.21	8.59	0.72	-0.20	-0.26	3.36	0.83	-0.01	-0.20	21.20
20	0.83	0.05	-0.23	7.47	0.76	-0.15	-0.18	3.09	0.85	-0.02	-0.20	19.99
30	0.82	0.05	-0.22	7.72	0.74	-0.24	-0.27	3.25	0.83	-0.08	-0.26	21.06
40	0.82	0.07	-0.25	7.68	0.74	-0.19	-0.23	3.24	0.83	-0.05	-0.25	21.00
51	0.82	0.08	-0.24	7.72	0.74	-0.20	-0.16	3.25	0.83	-0.08	-0.25	21.07

Table 6.2: Model performance through the application of the distributed HBV model using different number of raingauges for the validation period.

Number of raingauges	Horb				Suessen, Fils				Plochingen,Neckar			
	R_m^2	Rel. accdif.	Peak error	RMSE	R_m^2	Rel. accdif.	Peak error	RMSE	R_m^2	Rel. accdif.	Peak error	RMSE
10	0.73	0.19	-0.28	10.09	0.81	-0.10	-0.32	2.67	0.81	0.04	-0.24	22.89
20	0.78	0.13	-0.25	9.12	0.82	-0.03	-0.24	2.61	0.83	0.05	-0.21	21.81
30	0.78	0.14	-0.26	9.12	0.80	-0.14	-0.30	2.75	0.82	-0.01	-0.27	21.94
40	0.75	0.15	-0.29	9.60	0.81	-0.08	-0.29	2.71	0.82	0.02	-0.26	22.18
51	0.76	0.16	-0.28	9.51	0.78	-0.10	-0.20	2.91	0.82	-0.01	-0.27	22.26

As shown in Table 6.2, the values of Nash-Sutcliffe coefficient for the validation period for the gauge at Horb range between 0.73 and 0.78. The values of Nash-Sutcliffe coefficient for the validation period for the gauge at Suessen, Fils range between 0.78 and 0.81. Also, the values of Nash-Sutcliffe coefficient for the gauge at Plochingen, Neckar range between 0.81 and 0.83. The network consisting of 10 raingauges yields the lowest model performance, whereas the highest model performance was observed using the 20 raingauge network. The model simulation bias is considerably higher using the precipitation resulting from 10 raingauge network. Interestingly, increase of raingauge stations above 20 did not improve the model performance; on the contrary the model performance was reduced slightly. As observed in the validation period, the highest values of Nash-Sutcliffe coefficient were also observed in the calibration period using the 20 raingauge network (Table 6.1).

Regarding modeling of runoff at higher time scales, the model performance in terms of the Nash-Sutcliffe coefficient shows a similar trend, as observed at the daily time scale. The worst performance is observed using the 10 raingauges network. However the performance improves with increasing time scale for all the raingauge networks. A summary of the Nash-Sutcliffe coefficients at a 7 day and 30 day time scale in the validation period is shown in Table 6.3. The Nash-Sutcliffe coefficients show the model performance in simulating the 7 days and 30 days mean discharges of a moving window.

Table 6.3: Nash-Sutcliffe coefficient at 7 days and 30 days time scale through the application of the distributed HBV model for the validation period for selected three gauges.

Gauge	Number of raingauges	Nash-Sutcliffe coefficient	
		7 days time scale	30 days time scale
Horb	10	0.79	0.81
	20	0.85	0.87
	30	0.85	0.88
	40	0.82	0.86
	51	0.83	0.86
Suessen, Fils	10	0.84	0.86
	20	0.85	0.87
	30	0.83	0.84
	40	0.84	0.84
	51	0.81	0.81
Plochingen,Neckar	10	0.86	0.88
	20	0.88	0.90
	30	0.88	0.90
	40	0.87	0.89
	51	0.87	0.90

The mean model performance and model parameters' transferability obtained using precipitation from different raingauges are shown in Table 6.4. The mean model performance and model parameters' transferability was calculated using the Nash-Sutcliffe coefficients obtained at the different gauges during the calibration and validation periods.

Table 6.4: Mean model performance and model parameters' transferability obtained using different raingauge networks through the application of the distributed HBV model.

Number of raingauges	Mean model performance	Model parameters' transferability
10	0.72	0.04
20	0.76	0.04
30	0.75	0.03
40	0.74	0.06
51	0.74	0.05

The highest value of mean model performance was observed using the 20 raingauges network, as shown in the above table. The worst model parameters' transferability was observed for the 40 raingauges network.

Figure 6.3 shows the seasonal Nash-Sutcliffe coefficient obtained using the precipitation produced from different raingauge networks.

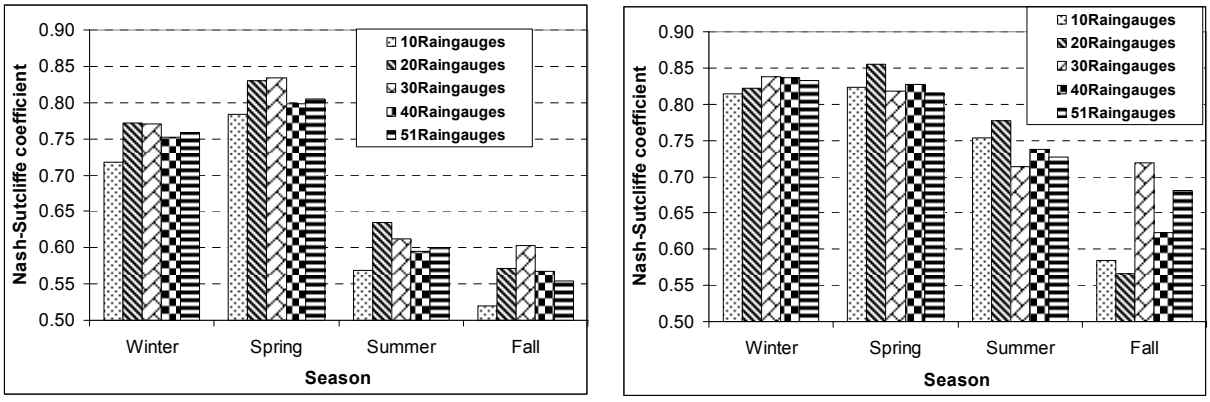

Figure 6.3: Seasonal Nash-Sutcliffe coefficients using precipitation produced from different raingauge networks through the application of the distributed HBV model during the validation period for the gauges at Horb (left panel) and Plochingen, Neckar (right panel).

The above figure indicates that the poorest model performance was observed using the 10 raingauge network for all seasons. Among the seasons, the poorest performance was observed during the summer season for all the considered raingauge networks. This is due to the fact that

there are convective precipitation events during the summer season, which are more localized and are not well captured by any of the raingauge networks.

Comparing the model performance for the gauges at Horb and Plochingen, Neckar, better model performance are observed for the gauge at Plochingen, Neckar for all seasons.

The event statistics were calculated for each annual maximum flood event for the validation period. Figure 6.4 depicts the average absolute error and root mean squared error for the gauge at Horb.

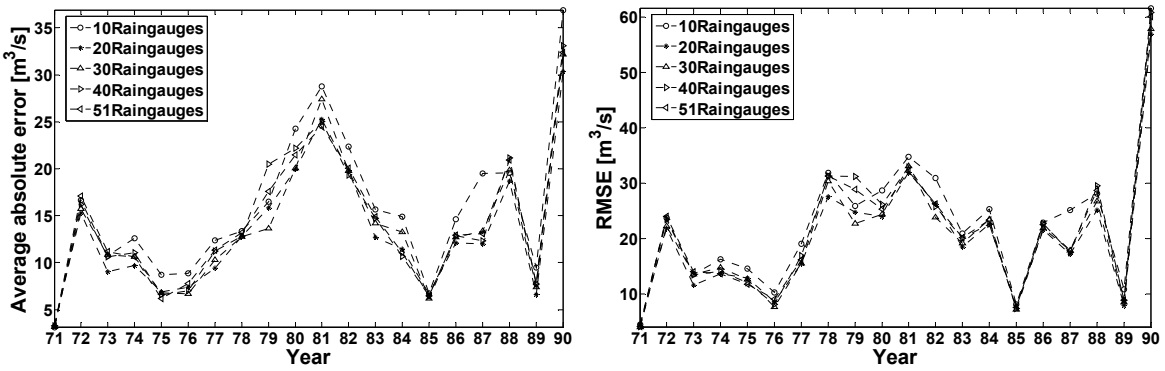

Figure 6.4: Event statistics for each annual maximum flood event through the application of the distributed HBV model using varying raingauge networks during the validation period for the gauge at Horb: average absolute error (left panel) and root mean squared error (right panel).

Figure 6.5 shows the average absolute error and root mean squared error for the gauge at Suessen, Fils.

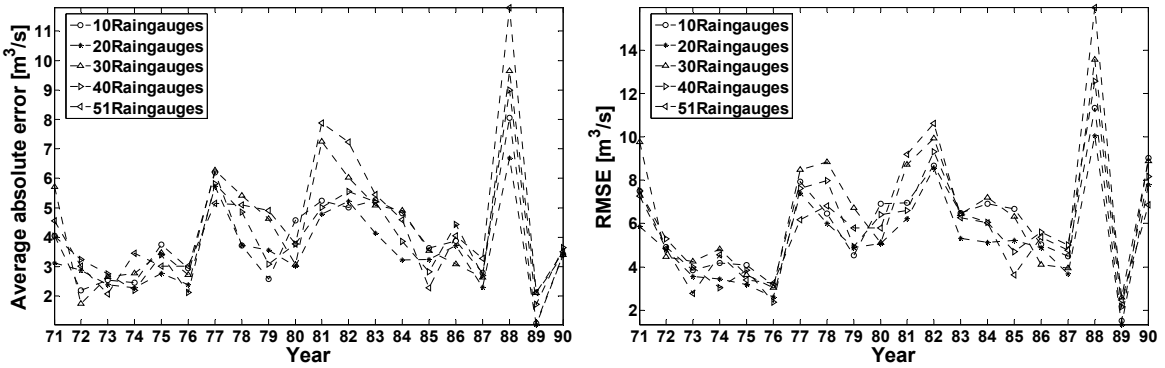

Figure 6.5: Event statistics for each annual maximum flood event through the application of the distributed HBV model using varying raingauge networks during the validation period for the gauge at Suessen, Fils: average absolute error (left panel) and root mean squared error (right panel).

On average, the absolute error with respect to the annual maximum discharges for the gauge at Horb ranges between 8.9% and 10.6% using the precipitation produced from varying raingauge

networks. The same value for the gauge at Suessen, Fils ranges between 8.1% to 10.4%. The highest errors were observed using the network consisting of 10 raingauges. However, the errors were not significantly reduced by increasing the number of raingauges more than 20 raingauges.

6.3.2 Simulations using the semi-distributed HBV model structure

A similar simulation experiment was carried out using the semi-distributed model structure. For the semi-distributed structure, networks consisting of 5 and 15 raingauges were used in addition to the networks used for the distributed model structure. Table 6.5 show the model performance for selected three gauges using the precipitation produced from different raingauges network for the calibration period. The model performance for the validation period is shown in Table 6.6. The network consisting of 5 raingauges yields the minimum model performance, whereby the highest model performance was observed using the 20 raingauge network. As observed in the distributed model, interestingly, increasing the raingauge numbers above 20 did not improve the model performance; in fact the Nash-Sutcliffe coefficient was reduced slightly in some cases. The best model performance for Suessen, Fils was observed using the 15 raingauge network. On the other hand, the best model performance for the Plochingen, Neckar was observed using the 30 raingauge network. This shows the influence of the spatial distribution of raingauges within each subcatchment. The number of raingauges is different for different subcatchments within each selected network (Figure 6.1). The difference in number of raingauges within and close to each subcatchment influences the interpolated precipitation.

Table 6.5: Model performance through the application of the semi-distributed HBV model using precipitation interpolated from different raingauge networks for the calibration period.

Number of raingauges	Horb				Suessen, Fils				Plochingen,Neckar			
	R_m^2	Rel. accdif.	Peak error	RMSE	R_m^2	Rel. accdif.	Peak error	RMSE	R_m^2	Rel. accdif.	Peak error	RMSE
5	0.82	-0.05	-0.17	7.70	0.72	0.00	-0.14	3.33	0.84	-0.03	-0.06	20.54
10	0.83	0.04	-0.10	7.37	0.77	-0.02	-0.12	3.08	0.86	0.00	-0.10	18.80
15	0.86	0.01	-0.13	6.76	0.75	-0.02	-0.12	3.18	0.87	0.01	-0.10	18.53
20	0.86	0.02	-0.11	6.80	0.77	0.01	-0.10	3.03	0.87	0.00	-0.08	18.42
30	0.85	0.02	-0.08	6.86	0.77	-0.01	-0.11	3.02	0.88	-0.01	-0.12	18.59
40	0.85	0.02	-0.08	7.04	0.77	-0.03	-0.10	3.05	0.86	0.00	-0.07	18.97
51	0.84	0.04	-0.05	7.24	0.76	0.00	-0.12	3.11	0.86	-0.02	-0.08	19.13

Table 6.6: Model performance through the application of the semi-distributed HBV model using precipitation interpolated from different raingauge networks for the validation period.

Number of raingauges	Horb				Suessen, Fils				Plochingen,Neckar			
	R_m^2	Rel. accdif.	Peak error	RMSE	R_m^2	Rel. accdif.	Peak error	RMSE	R_m^2	Rel. accdif.	Peak error	RMSE
5	0.81	0.06	-0.12	8.47	0.76	0.08	-0.19	3.03	0.84	0.05	-0.01	20.85
10	0.81	0.05	-0.11	8.61	0.79	0.09	-0.14	2.82	0.87	0.04	-0.09	19.20
15	0.83	0.09	-0.12	8.05	0.80	0.09	-0.19	2.76	0.87	0.07	-0.06	18.96
20	0.84	0.09	-0.12	7.99	0.79	0.13	-0.15	2.86	0.87	0.06	-0.06	18.99
30	0.84	0.09	-0.09	7.80	0.80	0.10	-0.17	2.78	0.89	0.05	-0.10	18.65
40	0.83	0.10	-0.09	7.99	0.79	0.09	-0.15	2.81	0.86	0.06	-0.06	19.35
51	0.82	0.11	-0.07	8.16	0.77	0.12	-0.16	2.93	0.87	0.04	-0.06	19.10

Table 6.7 represents the mean model performance and model parameters' transferability obtained through the application of the semi-distributed model structure using the precipitation produced from different raingauge networks.

Table 6.7: Mean model performance and parameters' transferability obtained through the application of the semi-distributed HBV model using the precipitation produced from different raingauge networks.

Number of raingauges	Mean model performance	Model parameters' transferability
5	0.74	0.12
10	0.78	0.03
15	0.80	0.04
20	0.80	0.04
30	0.82	0.04
40	0.80	0.05
51	0.80	0.05

It can be observed that the lowest mean model performance was observed using the 5 raingauge network. The highest value was observed using the 30 raingauge network. However, there was not remarkable change in the mean model performance when the number of raingauges was increased to more than 15. The worst model parameters' transferability was observed using the 5 raingauge network.

The inability of the 5 raingauge network to adequately represent the precipitation field seems to negatively influence the estimation of parameters, further increasing the remarkable simulation errors. Moreover, the unsatisfactory results obtained using the 5 raingauge network certainly indicate a definite lack in its ability to represent the precipitation fields. On the other hand, the model performance was not significantly improved when using more than 15 raingauges. In fact, there was a slight deterioration in the overall model performance. This is because there are only 20 raingauges within and close to the catchment. Estimating the precipitation fields using raingauges located considerably at far distance from the boundary of the catchment, perhaps, brings more error in the model simulation.

Figure 6.6 shows the seasonal model performance for the Suesen, Fils and Plochingen, Neckar, gauges.

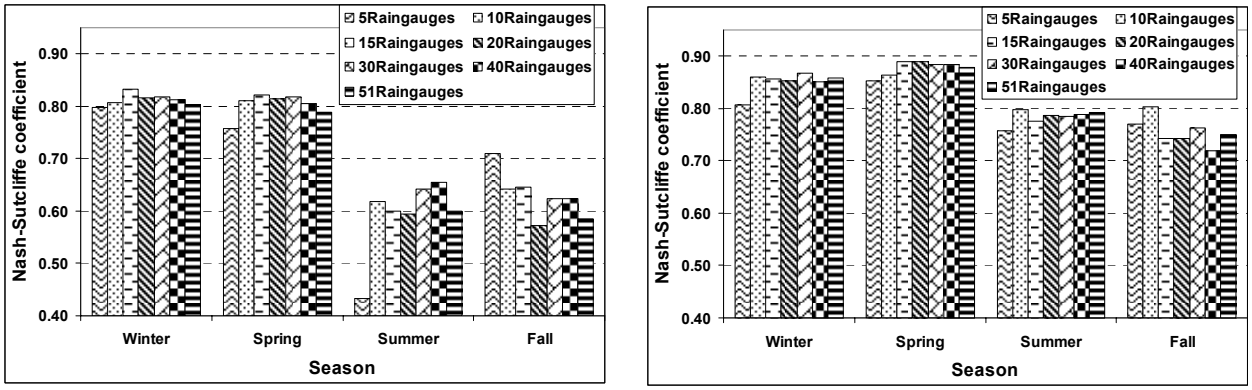

Figure 6.6: Seasonal Nash-Sutcliffe coefficients using the precipitation produced from different number of raingauges through the application of the semi-distributed HBV model during the validation period for the gauges at Suessen, Fils (left panel) and Plochingen, Neckar (right panel).

A significant inability to represent the spatial precipitation fields using 5 raingauges network in the smaller subcatchment for the summer season can be observed (Figure 6.6).

Further, the event statistics were calculated for each annual maximum flood event. Figures 6.7 & 6.8 show the average absolute error and root mean squared error for the gauges at Horb and Suessen, Fils, respectively.

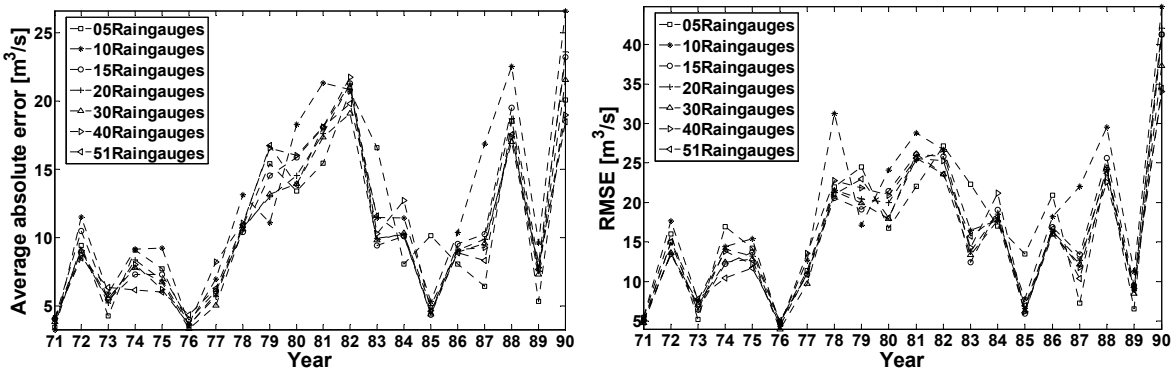

Figure 6.7: Event statistics for each annual maximum flood event through the application of the semi-distributed HBV model using different raingauges networks during the validation period for the gauge at Horb: average absolute error (left panel) and root mean squared error (right panel).

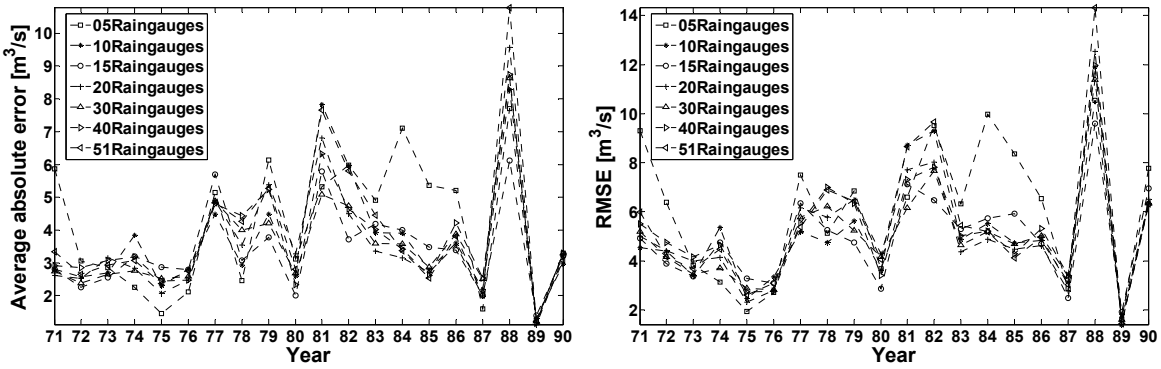

Figure 6.8: Event statistics for each annual maximum flood event through the application of the semi-distributed HBV model using different raingauges networks during the validation period for the gauge at Suessen, Fils: average absolute error (left panel) and root mean squared error (right panel).

On average, the absolute error with respect to the annual maximum discharges for the gauge at Horb ranges between 6.9% and 8.4% using the precipitation produced from varying raingauge networks. The same value for the gauge at Suessen, Fils ranges between 8.2% to 9.2%. The highest errors yielded using the network consisting of 5 raingauges. On the other hand, the errors were not significantly reduced by increasing the number of raingauges to more than 20, as observed for the distributed model structure.

Comparing the performances using the distributed and semi-distributed model structures, the semi-distributed model, in general, performs better than the distributed model using the different raingauge networks.

It may be noted that obtaining similar goodness-of-fit indices does not mean that the simulation was insensitive to the spatial variability of the precipitation fields obtained using different number of raingauges. In fact, the two models using different precipitation fields did not give the same hydrograph. Because there are differences in the average absolute error and root mean squared error obtained using precipitation produced from varying raingauge networks. In general, it can be noted that using too coarse a raingauge network for estimating the rainfall fields can give rise to remarkable errors, for the both the distributed and semi-distributed model structures. However, the network formed by the threshold number of raingauges (20-30 in the present study) provides an acceptable estimate of the precipitation fields, while other modeling errors will dominate in that case.

6.4 Influence of the rainfall observation network on model calibration and application

It may be of interest to investigate the results of the simulations obtained with the rainfall input when the model is parameterized according to a different type of input data. It is, in fact, frequently

the case that a raingauge network changes due to an addition or subtraction of raingauges. The raingauge network can be strengthened by the addition of new instruments, so that a more detailed representation of rainfall is allowed, but, for calibration purposes, past observations are available only over the original, less numerous measuring points. On the other hand, in the case of an operational flood forecasting system, the opposite situation may occur. In the flood forecasting system, the rainfall-runoff model is usually calibrated using all the available flood events. However, during the operational forecasting time, the precipitation data from all past observation stations may not be available due to a malfunctioning of a few of the observations in the network or the observation data may not be available in time.

In such cases, it is crucial to understand if the parameters calibrated using the rainfall coming from one type of network have the ability to represent the phenomena governing the rainfall-runoff process with the input provided by the different configuration of the raingauge network.

In the following section, the aim of the simulation experiment was, thus, to investigate the influence of the spatial resolution of the rainfall input on the calibration of the semi-distributed model structure. First, the semi-distributed structure of the HBV model was calibrated with the precipitation interpolated from the available observed rainfall of varying raingauge networks. The calibrated model was then run using the same precipitation used for the calibration as well as interpolated precipitation based on networks of reduced and increased raingauge density.

As for example, the model was first calibrated using precipitation interpolated from 10 and 20 raingauges. The calibrated model using 10 raingauges was then run using precipitation obtained from 20 raingauges for the validation period and vice versa. This experiment is indicated in tables and figures, latter on, as follows: **10/10:** calibrated with 10 raingauges and validated with 10 raingauges; **20/20:** calibrated with 20 raingauges and validated with 20 raingauges; **10/20:** calibrated with 10 raingauges and validated with 20 raingauges and **20/10:** calibrated with 20 raingauges and validated with 10 raingauges.

It can be noticed that the model calibrated using less detailed precipitation (precipitation from 10 raingauges) often slightly improves when it was run using relatively more detailed precipitation (precipitation from 20 raingauges) (Table 6.8). On the other hand, the model performance obtained using precipitation from 20 raingauges deteriorated when the same model was run using precipitation obtained from 10 raingauges.

In fact, the parameter values in principle may compensate for an incomplete representation of the precipitation field, provided they were updated by performing a new calibration, for which the input precipitation was estimated from the reduced raingauges network. However, there was no such type of compensation for the second case when the calibrated model using 20 raingauges was run using

precipitation obtained from the 10 raingauge network. This demonstrates the inability of the 10 raingauges to adequately represent the precipitation field for the catchment.

Table 6.8: Model performances using the input precipitation information obtained from different number of raingauges.

		Rottweil	Horb	Riederich, Erms	Suessen, Fils	Plochingen, Fils	Plochingen ,Neckar
10/10	R_m^2	0.74	0.80	0.75	0.79	0.82	0.87
	Rel. accdif.	-0.05	0.07	-0.01	0.09	0.12	0.04
	Peak error	-0.23	-0.14	-0.06	-0.14	-0.16	-0.09
	RMSE	3.74	8.61	1.05	2.82	5.03	19.20
20/20	R_m^2	0.78	0.83	0.76	0.79	0.81	0.87
	Rel. accdif.	0.00	0.09	0.02	0.13	0.17	0.06
	Peak error	-0.07	-0.12	-0.03	-0.15	-0.16	-0.06
	RMSE	3.49	7.99	1.03	2.86	5.07	18.99
10/20	R_m^2	0.74	0.82	0.77	0.78	0.80	0.88
	Rel. acc dif.	-0.18	-0.03	0.00	0.13	0.19	0.01
	Peak error	-0.36	-0.25	-0.06	-0.13	-0.12	-0.13
	RMSE	3.75	8.10	1.02	2.91	5.22	18.06
20/10	R_m^2	0.66	0.77	0.75	0.79	0.82	0.84
	Rel. accdif.	0.13	0.19	0.00	0.09	0.10	0.08
	Peak error	0.08	0.00	-0.04	-0.16	-0.20	-0.01
	RMSE	4.28	9.32	1.06	2.79	4.95	20.84

The following simulation experiment was carried out in order to investigate whether the estimated precipitation at the missing raingauges, together with the precipitation data from the remaining stations that were used during the model calibration, has any benefit over the model operated by precipitation from the reduced raingauges. A new spatial representation of the rainfall input was considered: the precipitation was estimated using a multiple linear regression technique (Montgomery and Peck, 1982) at specific locations (the precipitation data for the 10 raingauges network are treated as missing measurements for the model validation period in the present example) of a selected raingauge network (20 raingauges network in the present example). The observed precipitation was considered at the remaining 10 locations of the 20 raingauges network. The model, calibrated with the precipitation data obtained from 20 raingauges, was then run in the validation period using the precipitation field above described.

Thus, in this experiment, the precipitation of the 10 raingauges (the location of these stations are same of the 10 raingauges network) within the 20 raingauges network was considered missing for the validation period. The multiple linear coefficients at the locations of the above 10 raingauges were derived using the precipitation measurements of the neighboring stations and the available precipitation measurements at those 10 raingauges.

Regression analysis is a statistical technique generally used for investigating and modeling the relationship between variables. A regression model that involves more than one regressor variable is called a multiple regression model. The general purpose of multiple regressions is to learn more about the relationship between several independent or predictor variables and a dependent or criterion variable.

Consider that the precipitation for a particular station is missing for some time period. The missing measurements then can be estimated using the measurements of the neighboring stations through the application of the multiple linear regression coefficients. A multiple regression model that can describe this relationship is as follows:

$$R(u_s) = \beta_0 + \beta_1 R(u_1) + \beta_2 R(u_2) + ... + \beta_k R(u_k) + \varepsilon \qquad (6.1)$$

where $R(u_s)$ denotes the missing precipitation measurements of a particular station at a location u_s; $u_1, u_2, \ldots, u_k$ denotes the precipitation measurement locations of the remaining stations and ε is a statistical error. The parameters β_j, j = 0, 1,…, k are called the regression coefficients (Montgomery and Peck, 1982). Coefficients are calculated using all available observations.

Thus, the missing measurements at the mentioned 10 raingauges were estimated using the derived multiple linear regression coefficient. The precipitation was then interpolated using the estimated precipitation at the 10 raingauges and also the remaining 10 raingauges within the 20 raingauge network. As a result, the interpolated precipitation field consisted of 20 raingauges once again, however, with 10 raingauges of precipitation data estimated using the multiple linear regression and the remaining 10 from the observed data.

Figure 6.9 shows the model performance for selected six gauges during the validation period using the different level of input precipitation information. The data shown in Table 6.7 is partly used to prepare the Figure 6.9. In the following tables and figures **20/20MLR** indicates model calibrated with 20 raingauges and validated with 20 raingauges (rainfall estimated at 10 locations considered as missing measurements).

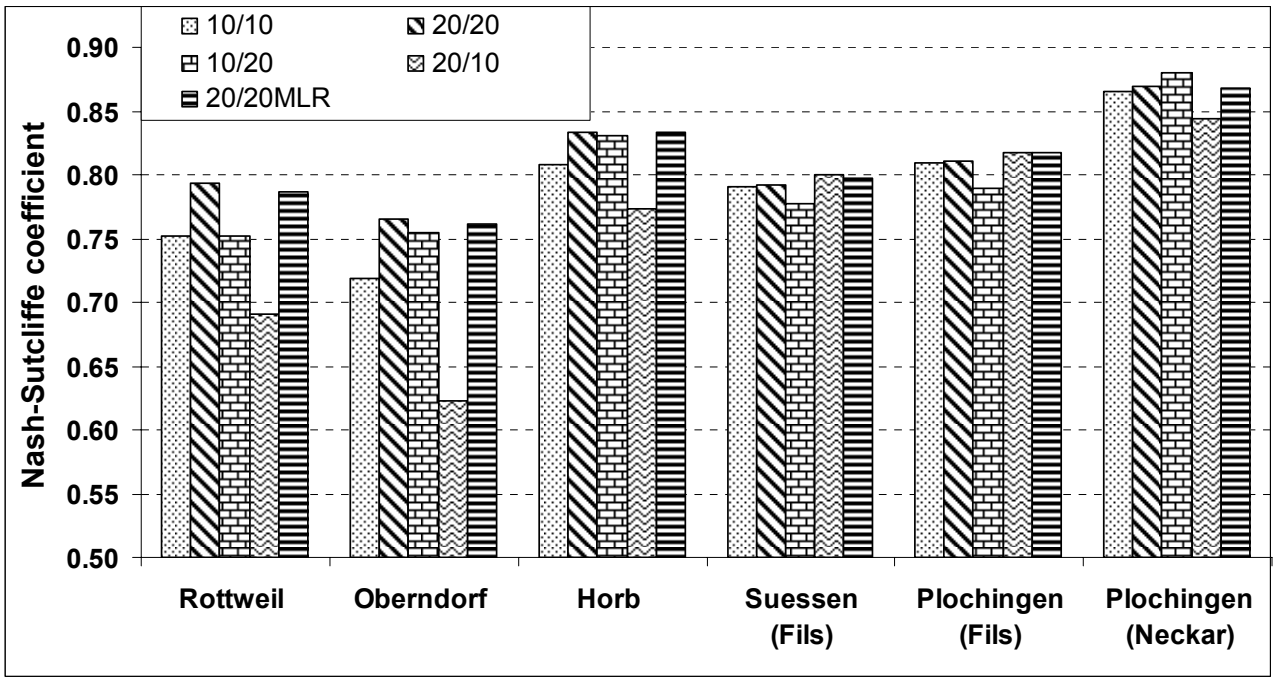

Figure 6.9: Nash-Sutcliffe coefficient obtained using different level of precipitation input information for the validation period for selected six gauges.

It can be observed that the model performed well when it was calibrated using precipitation from 20 raingauges and was run with an incomplete observed data set combined with data generated using the multiple linear regression technique at the locations of the remaining 10 raingauges.

A summary of the Nash-Sutcliffe coefficients at a 7 day and 30 day time scale in the validation period are shown in Table 6.9.

Table 6.9: Nash-Sutcliffe coefficients at 7 days and 30 days time scale obtained using different level of precipitation input information for selected six gauges for the validation period.

Gauge	Number of raingauges	Nash-Sutcliffe coefficient	
		7 days time scale	30 days time scale
Rottweil	20/10	0.76	0.82
	20/20MLR	0.86	0.90
Oberndorf	20/10	0.69	0.77
	20/20MLR	0.83	0.88
Horb	20/10	0.80	0.82
	20/20MLR	0.89	0.91
Suessen, Fils	20/10	0.82	0.80
	20/20MLR	0.82	0.80
Plochingen, Fils	20/10	0.85	0.83
	20/20MLR	0.85	0.82
Plochingen, Neckar	20/10	0.88	0.90
	20/20MLR	0.90	0.92

Regarding modeling of runoff at higher time scales, the model performance in terms of the Nash-Sutcliffe coefficient shows a similar trend as that observed earlier at the daily time scale. The table indicate that the model performance improves at the higher time scales.

Figure 6.10 depicts the average absolute error and root mean squared error for the gauge at Rottweil.

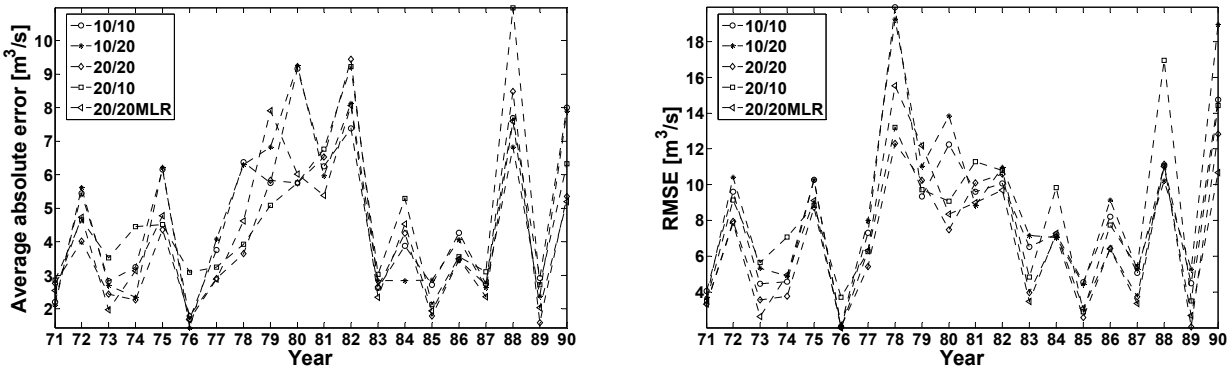

Figure 6.10: Event statistics for each annual maximum flood event during the validation period using precipitation obtained from different raingauge networks and estimated precipitation for the gauge at Rottweil: average absolute error (left panel) and root mean squared error (right panel).

On average, the absolute error with respect to the annual maximum discharges for the gauge at Rottweil ranges between 6.8% and 8.2%. The highest error was observed when the calibrated model using 20 raingauges was run using 10 raingauges. The error reduced to 6.9% when the calibrated model using 20 raingauges was run using 20 raingauges, however, with 10 raingauges of precipitation data estimated using the multiple linear regression technique and the remaining 10 from the observed data.

This analysis indicates that model performance reduces when the model calibrated using more detailed input precipitation information is run using precipitation obtained from a reduced raingauge networks. The analysis also highlights that the missing measurements can be supplemented using a simple multiple linear regression technique or another appropriate data filling technique.

6.5 Influence of temperature stations on the model simulation results

To investigate the influence of the temperature gauges on the predictive uncertainty, the following simulation experiment was carried out. The eighteen temperature gauges were selected from the network, having no missing measurements and within and around 20 km from the catchment. Then, three different networks, consisting of 18, 11 and 6 temperature gauges (Figure 6.11), were used to interpolate the daily mean temperature over the grid used before. The

interpolated temperature was averaged over the zone and used in the semi-distributed HBV model. The model was calibrated using the temperature data obtained from the different temperature networks. The other input data, namely daily precipitation amount and daily potential evapotranspiration, were kept unchanged in each calibration. The raingauge network consisting of 30 raingauges was used to prepare the input precipitation.

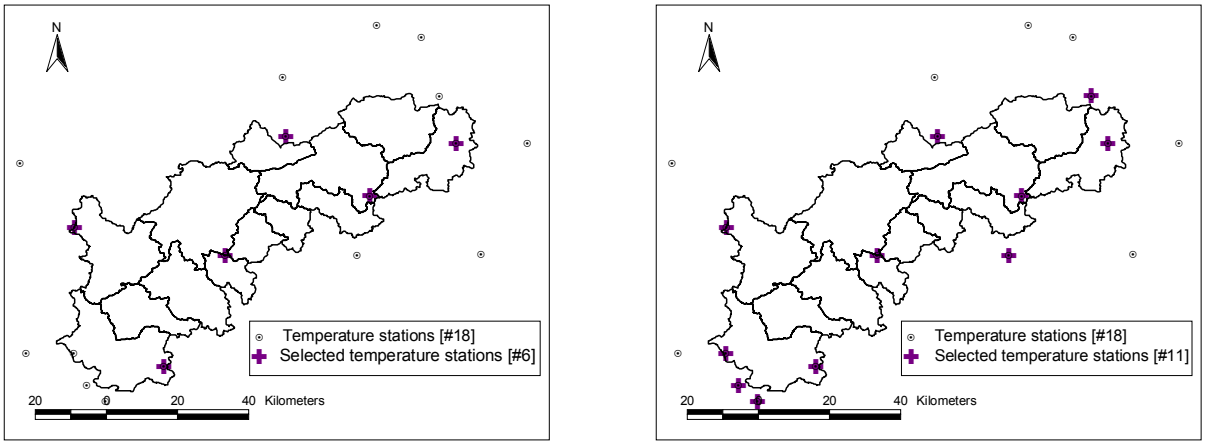

Figure 6.11: Geographical locations of temperature gauges in selected networks.

Tables 6.9 and 6.10 show the model performance using the varying temperature gauges for the calibration and validation periods, respectively. As shown in Table 6.11, the minimum and maximum values of the overall Nash-Sutcliffe coefficient during the validation period for the simulation of the daily discharge for the gauge Rottweil are 0.77 and 0.80, respectively. The network consisting of 6 temperature gauges yields the minimum model performance, whereby the highest model performance was obtained using the 18 temperature gauges network. Interestingly, the highest model performance for the gauge Horb was obtained using 6 temperature gauges. The best model performance for the outlet gauge Plochingen, Neckar was observed using the 11 temperature gauges network. This is due to the difference in spatial locations of the temperature gauges in the selected networks. This shows the influence of the spatial distribution of temperature gauges within each subcatchment.

Table 6.10: Model performance using the different number of temperature gauges for the calibration period.

Number of temperature gauges	Rottweil				Horb				Plochingen,Neckar			
	R_m^2	Rel. accdif.	Peak error	RMSE	R_m^2	Rel. accdif.	Peak error	RMSE	R_m^2	Rel. accdif.	Peak error	RMSE
6	0.80	0.00	-0.17	3.20	0.86	0.02	-0.08	6.66	0.87	-0.01	-0.10	18.40
11	0.78	0.01	-0.15	3.34	0.85	0.02	-0.08	6.87	0.87	-0.01	-0.11	18.49
18	0.78	0.00	-0.16	3.34	0.84	0.04	-0.05	7.25	0.86	-0.03	-0.09	18.95

Table 6.11: Model performance using the different number of temperature gauges for the validation period.

Number of temperature gauges	Rottweil				Horb				Plochingen,Neckar			
	R_m^2	Rel. accdif.	Peak error	RMSE	R_m^2	Rel. accdif.	Peak error	RMSE	R_m^2	Rel. accdif.	Peak error	RMSE
6	0.77	0.01	-0.05	3.54	0.84	0.09	-0.09	7.75	0.87	0.04	-0.08	18.55
11	0.78	0.02	-0.07	3.47	0.84	0.09	-0.09	7.79	0.88	0.05	-0.09	18.17
18	0.80	0.01	-0.09	3.34	0.83	0.11	-0.07	8.07	0.88	0.03	-0.07	18.48

Figure 6.12 shows the seasonal Nash-Sutcliffe coefficient obtained using different temperature gauges.

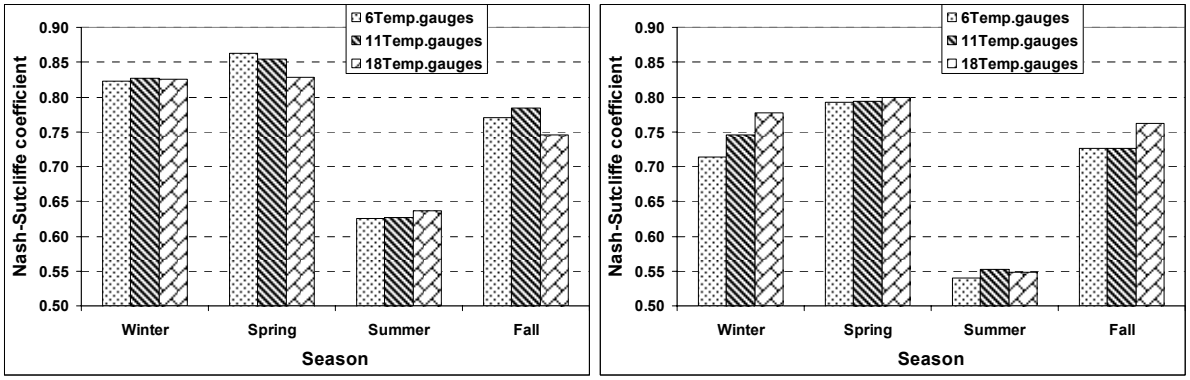

Figure 6.12: Seasonal Nash-Sutcliffe coefficient obtained using different temperature stations during the validation period for the gauges at Rottweil (left panel) and Horb (right panel).

It can be observed that the selected temperature stations still do influence in the model performance and this is more evident during the winter season, as could be expected. This is because there is more fluctuation in the winter temperature and that affects the snow melt and accumulation procedure.

6.6 Concluding remarks

In this chapter attempts have been made to describe several experiments investigating the influence of the spatial representation of the precipitation input, with distributed and semi-distributed model structures. A first set of experiments considered the spatial representation of precipitation from varying raingauge networks. It showed that the number and spatial distribution of raingauges affects the simulation results. It was found that the model performances worsen radically with an excessive reduction of raingauges. However, the performances were not significantly improved by increasing the number of raingauges more than a certain threshold number.

Comparing the performances using the distributed and semi-distributed structures of the HBV model, the semi-distributed model, in general, performs better than the distributed model using the precipitation of each raingauge network.

A second set of analysis considered the model calibration using one type of input precipitation and was run using another type of precipitation data. The analysis indicated that models using different raingauge networks might need their parameters recalibrated. Specifically, the HBV model calibrated with dense information fail when run with sparse information. While, the HBV model calibrated with sparse information can perform well when run with dense information.

A third set of experiments analyzed the reliability of supplementing missing precipitation measurements used for the calibration with data estimated using a multiple linear regression technique, and running the model using that precipitation combined with observed precipitation. The results showed that the model performs well when calibrated with a complete set of observed precipitation and when run with an incomplete observed data set combined with estimated data. This result offers an encouraging perspective for the implementation of such a procedure for an operational flood forecasting system. Further research is needed in this direction to prove the practical applicability.

At the end a set of experiments showed the influence of temperature gauges on the model simulation results. The influence is relatively low compared to that introduced by the raingauges. The influence is more evident during the winter season, as could be expected.

7 Conditionally-simulated precipitation and hydrological modeling

7.1 Introduction

One of the most important hydrological model inputs is precipitation. Because the precipitation varies in space and time within a catchment, it is usually interpolated from the measurements of an available raingauge network for model computational units using interpolation techniques like kriging, Thiessen polygon, and inverse distance method. However, hydrologists have long recognized the problems of interpolating point raingauge measurements to estimate spatial rainfall fields. Kriging as mostly used interpolation techniques provides idealized smooth rainfall fields and does not possess the same fluctuation pattern (Haberlandt and Gattke, 2004). However the variability of rainfall has a considerable impact in hydrological model's predictive uncertainty (Zehe et al., 2005). Simulations usually conditional on the observations preserve typical fluctuation patterns (Mantoglou and Wilson, 1982).

The aim of this chapter is, thus, to investigate the uncertainty incurred in the HBV model simulations due to spatial uncertainty of precipitation. The first section of this chapter describes two different spatial rainfall simulation procedures employed to generate conditionally-simulated precipitation. In the second section, the benefits of using conditionally-simulated precipitation in hydrological modeling are described using the semi-distributed HBV model.

7.2 Data preparation and spatial rainfall simulation

The spatial distribution of the daily precipitation and the daily average temperature were produced on a 500 m × 500 m grid using the external drift kriging method (Ahmed and de Marsily, 1987) from the available point measurements. The semi-distributed HBV model was setup and then calibrated using the automatic calibration procedure based on simulated annealing (Aarts and Korst, 1989). The calibrated model was validated using the interpolated precipitation. Further, conditionally-simulated precipitation was also used as an input to the model for the validation period. The conditionally-simulated precipitation was generated using turning bands simulation (Bárdossy, 2003; Mantoglou and Wilson, 1982) and copula-based simulation methods. The modeling performance was assessed at the three discharge gauges namely, Rottweil, Oberndorf and Horb. Figure 7.1 depicts the discharge gauges and elevation zones used for the semi-distributed HBV model structure.

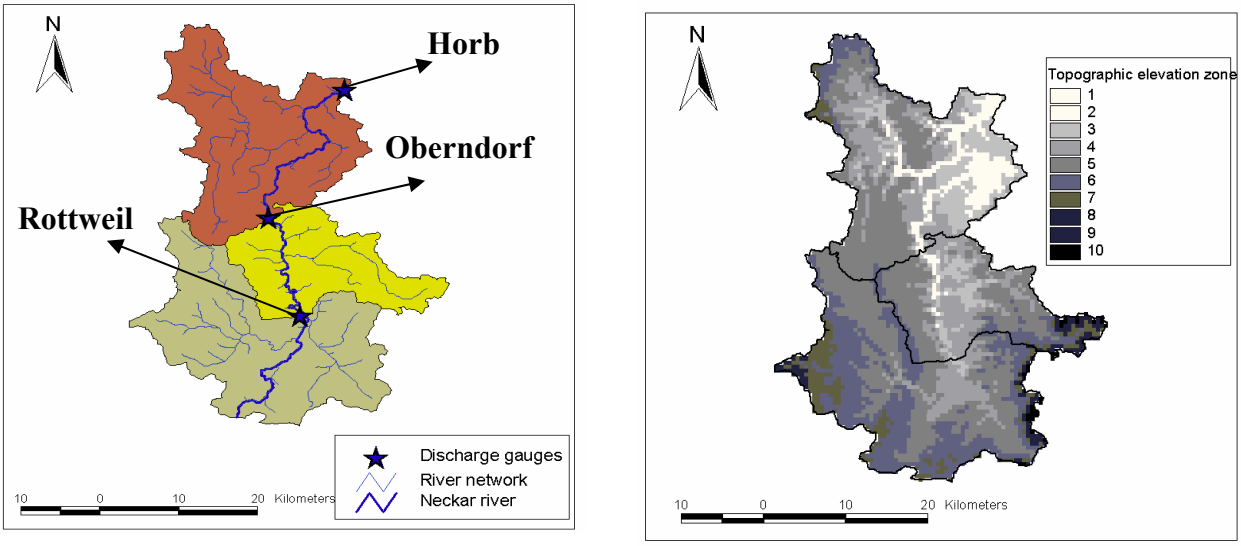

Figure 7.1: Stream network and discharge gauges (left panel) and elevation zone for different subcatchments (right panel).

7.2.1 Conditional spatial rainfall simulation

It is well recognized that kriging provides a smooth mapping of the variable under consideration. This is because the minimum estimation variance as the optimization criterion necessarily yields less variable estimators. (Bárdossy, 2003). The disadvantage is the loss of variability, for example, small values may be over- and large values may be under-estimated. This may lead to simulation errors, particularly if the data are used for modeling floods. In that case the high non-linearity between input and output as well as extreme values determine the modeling response. One means of preserving this variability is the conditional spatial simulation of precipitation providing several equally probable realizations. Subsequent runs of a hydrological model using these different realizations of precipitation would then allow an assessment of uncertainty from the precipitation input and provide a less biased model result (Haberlandt and Gattke, 2004). There are different methods available for spatial stochastic simulation of a random variable, such as Gaussian sequential simulation, turning bands simulation, simulated annealing, etc. (Deutsch and Journel, 1992; Goovaerts, 1997; Bárdossy , 2003).

In this study, conditionally-simulated rainfall was generated using two approaches: (1) conditionally-simulated precipitation using turning bands simulation (hereafter referred as turning bands simulation) and (2) turning bands simulation using copula (hereafter referred as copula-based simulation).

The following brief introduction to the turning bands simulation is mainly based on the description of Mantoglou and Wilson (1982), Kottegoda and Kassim (1991) and Bárdossy (2003).

The turning bands method was originally introduced by Matheron (1973), and has seen extensive application in multi-dimensional spatial simulation (Mantoglou and Wilson, 1982). This method is based on the theory of the random fields. The main principle of this approach is that sets of one dimensional simulation are merged to one multi-dimensional set, while preserving the statistical properties of the random field. One dimensional simulation is performed for different possible directions "turning" around a center point. Depending on the variogram, different covariance structures have to be used for the one dimensional simulations (Bárdossy, 2003).

Hence, by applying the covariance structure to the rain field, which is indeed a two dimensional space process, each uni-directional process is generated by a spectral method (Kottegoda and Kassim, 1991; Bárdossy, 2003). It is assumed that the field to be simulated is second-order stationary and isotropic. It is also assumed that the covariance *C(r)* of the simulated field is known. Instead of simulating the two dimensional field directly, one thus carries out simulations along several lines using a uni-dimensional covariance function that corresponds to the two-dimensional one. Then at each point of the two-dimensional field a weighted sum of the corresponding values of the line processes is assigned.

Considering that for a set of lines $l = 1,\ldots,L_n$, all going through the origin of the coordinate system, random functions with zero mean and covariance functions *C(r)* are simulated independently. Let $R_l(u)$ for $l = 1,\ldots,L_n$ be these functions. Then for a point u the random function *R(u)* can be defined as:

$$R(u) = \frac{1}{\sqrt{L_n}} \sum_{l=1}^{L_n} R_l\left(\langle u, v_l \rangle\right) \tag{7.1}$$

where $\langle .,. \rangle$ denotes the scalar product of the vectors, and v_l is the unit vector on line l.

The advantage of the method is that it is nearly independent of the number of points. Moreover, it preserves the statistics of the real random field. However, the method has the disadvantage that one-dimensional covariance structure corresponding to the variogram must be calculated or given analytically (Bárdossy, 2003).

The measurement data are not used directly in the unconditional simulation. It is only through the variogram that they influence simulation results (Bárdossy, 2003). The knowledge of the value of a selected parameter at a given point restricts the possible values in a neighborhood. Those realizations are especially interesting where the simulated values equal the measured values at the observation points. Thus, unconditional simulations are conditioned with the help of a simple transformation, as defined below (Bárdossy, 2003):

$$R_c(u) = R^*(u) + \left(R_s(u) - R_s^*(u)\right) \tag{7.2}$$

where:

$R_s(u)$ is the simulated value at point u
$R_s^*(u)$ is the kriging estimator of Z_s based on the simulated values at the measurement points
$R_c(u)$ is the conditionally-simulated value at a point u
$R^*(u)$ is the kriging estimator of Z based on the measurement data

Because of the exactness property of kriging, for measurement points at u_i

$$\begin{aligned} R^*(u_i) &= R(u_i) \\ R_S^*(u_i) &= R_S(u_i) \end{aligned} \tag{7.3}$$

Thus by definition:

$$R_C(u_i) = R(u_i) \tag{7.4}$$

This means that the above modification of the unconditional simulation reproduces the measured values at the observation points. The conditioning of the unconditional simulation does not influence the variability; $R_c(u)$ and $R_s(u)$ have the same variogram.

Figure 7.2 shows the principal steps for conditionally-simulated precipitation using turning bands simulation. The principal steps for conditionally-simulated precipitation using copula-based simulation are depicted in Figure 7.3.

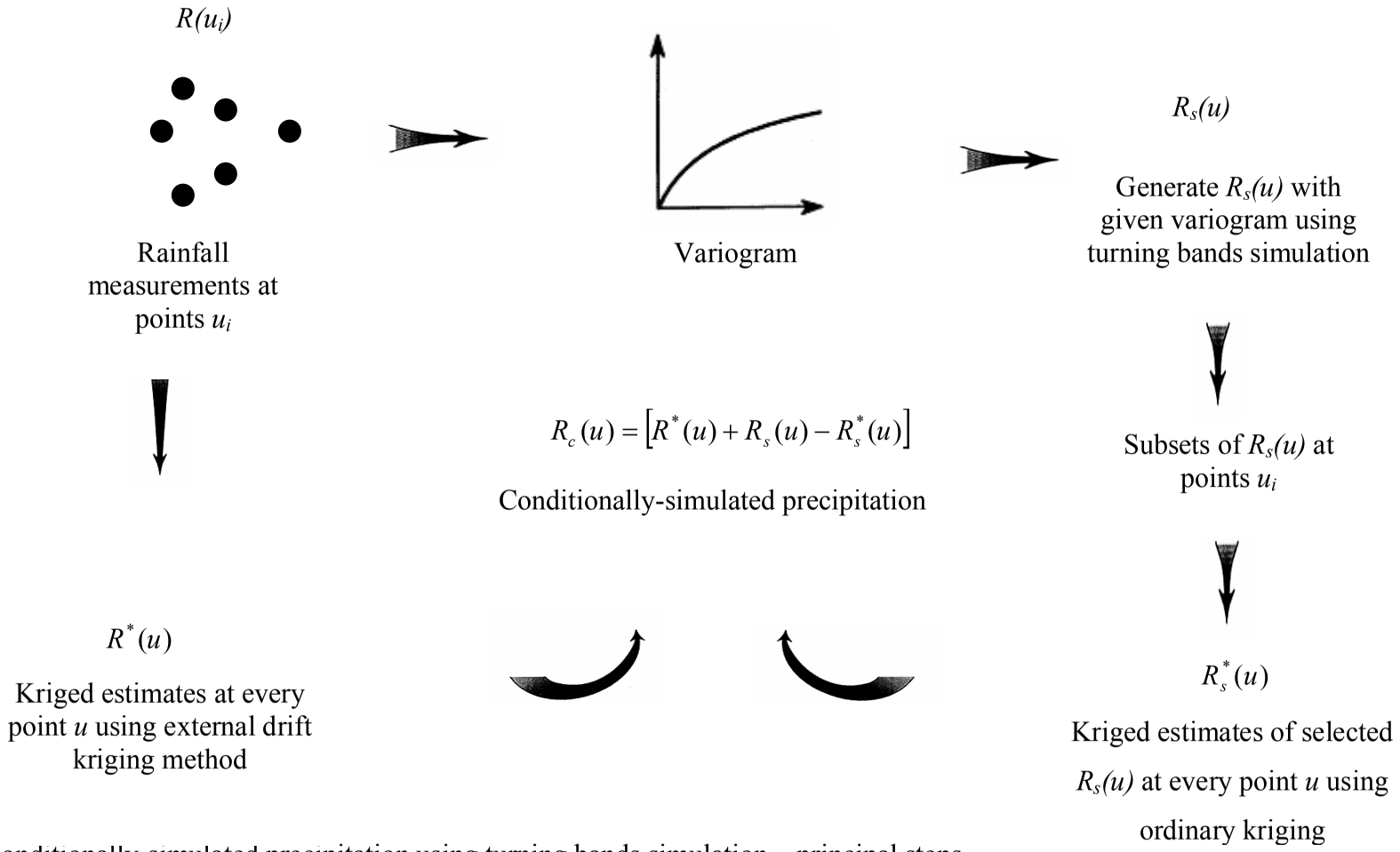

Figure 7.2: Conditionally-simulated precipitation using turning bands simulation – principal steps.

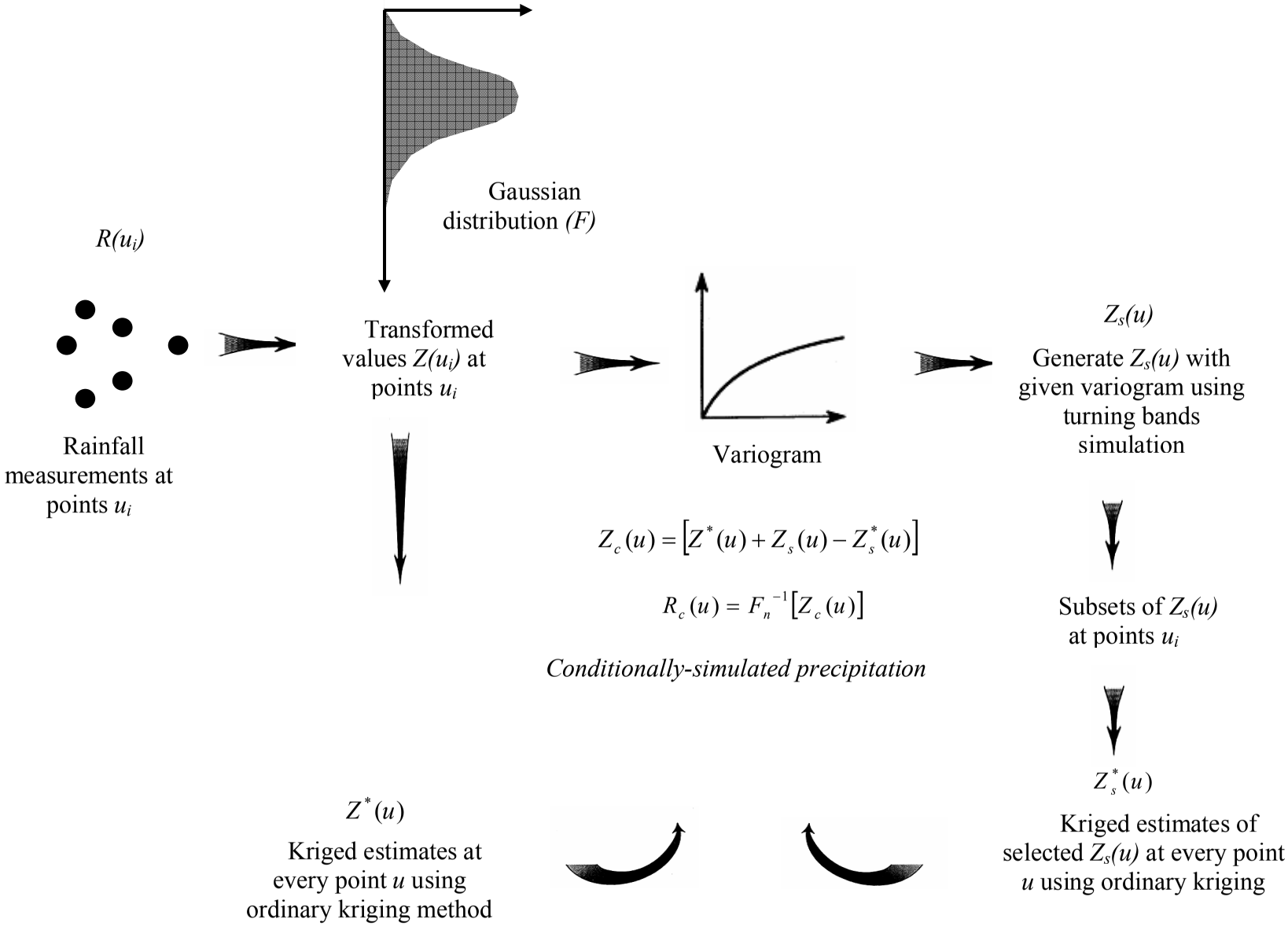

Figure 7.3: Conditionally-simulated precipitation using copula-based simulation – principal steps.

The rainfall simulation procedure using turning bands simulation follows the steps mentioned below:

a. The rainfall is observed at discrete points from raingauges.
b. The raingauge observations are used to obtain the best linear unbiased estimate of rainfall on a specified regular grid using the kriging method.
c. The random rainfall field is simulated on the specified regular grid using the turning bands simulation with the variogram constructed using the observed data.
d. Only the simulated rainfall values at the raingauge positions are used to estimate the interpolated values of the simulated rainfall at each grid point.
e. At each grid point, the deviation of the simulated and interpolated values of the simulated rainfall field is calculated as follows.

$$deviation(u) = \left[R_s(u) - R_s^*(u)\right] \tag{7.5}$$

Thus, at the raingauge locations, this deviation is always equal to zero.

f. The field of deviation, obtained in step e, is added to the rain field from raingauge interpolation.

$$R_c(u) = R^*(u) + \left[R_s(u) - R_s^*(u)\right] \tag{7.6}$$

g. A rainfall field that follows the mean field of the raingauge interpolation while preserving the mean field deviations from the simulated field is obtained.

For copula-based simulation, the steps are more or less similar (Figure 7.3). Copulas are no more than multivariate distributions on the unit hypercube with uniform marginal distribution. They describe the dependence of multivariate distributions with any kind of marginal distribution. They are also invariant to monotonic transformations of the variables. The main advantage of using copulas is that marginal distributions of individual variables can be of any form. Thus copula is insensitive to the problems arising due to highly skewed distributions (for example, extreme values resulting from measurement error) (see for more details Bárdossy, 2006).

The main difference between two spatial rainfall simulation approaches lies in the fact that the rainfall from the raingauge observations is first transformed to Gaussian distribution function for the copula-based simulation. This is done because in the turning bands simulation method, it is assumed that the values of the field to be simulated at each point are normally distributed (Mantoglou and Wilson, 1982), and kriging is also done assuming the fields are normally distributed. The variogram is thus constructed using the normally distributed transformed values of

the raingauge measurements. The kriging and simulation of the rainfall fields are then carried out using the transformed values. After conditioning the simulated field using the observations, which are normally distributed values, the conditionally-simulated values are transformed back. This transformation is done using the empirical distribution function calculated based on the observations. Thus the conditionally-simulated values followed the original distribution function of the observations.

The principal steps of the copula-based simulation are described below:

Step1: Calculate the empirical distribution function $F_n(R)$ according to observations $R(u_i)$. This is done by calculating the ranks of the observed data set.

Step 2: Calculate the normally distributed values $Z(u_i)$ from the probability of the measurement values using the inverse normal distribution function.

$$\Phi^{-1}\left(F_n(R(u_i))\right) = Z(u_i) \tag{7.7}$$

where Φ being the distribution function of the standard normal distribution.

Step 3: Simulate the values $Z_s(u)$ by turning bands simulation method using these normally distributed transformed values and conditioning the simulated values using these transformed values at the observations. Thus the conditionally-simulated values $Z_c(u)$ follow the normal distribution function.

Step 4: Calculate the probability $\Phi\left(Z_c(u)\right)$ from the conditionally-simulated values $Z_c(u)$ using the normal distribution function.

Step 5: Back transformation of the probability $\Phi\left(Z_c(u)\right)$ obtained at step 4, using the inverse of the empirical distribution function, already calculated at step 1, to obtain the target value. Thus the target value again follows the same distribution obtained using the measurements.

$$F_n^{-1}\left(\Phi(Z_c(u))\right) = R_s(u) \tag{7.8}$$

7.2.2 Interpolated and simulated precipitation fields

Twenty one realizations of conditionally-simulated rainfall were generated using the mentioned two approaches namely, turning bands simulation and copula-based simulation. This number of realization attempted in this study is less; however, the high computational demand imposed this constraint.

Figure 7.4 shows the frequency diagram for the precipitation from different sources for the selected date 08.12.1978.

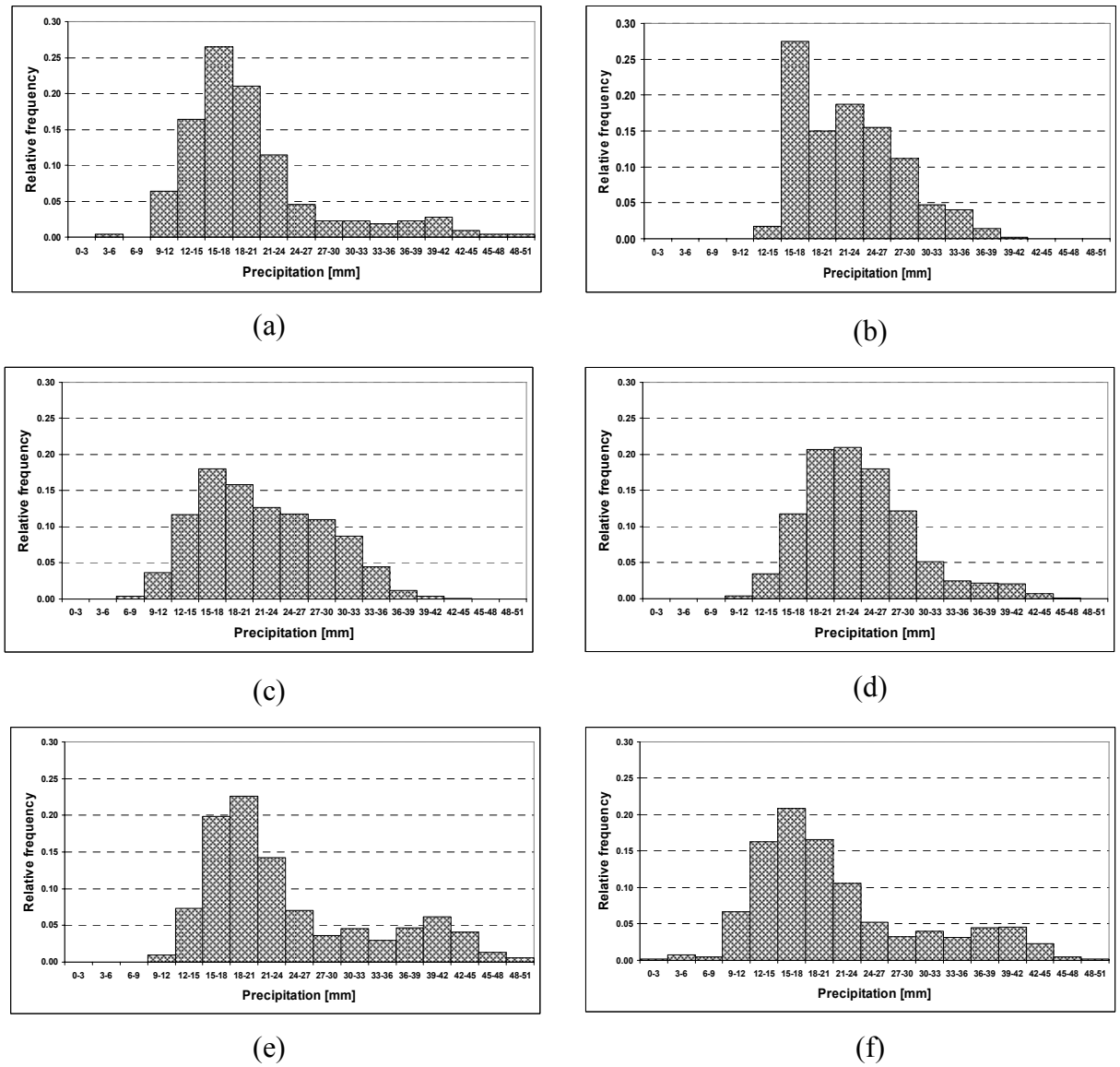

Figure 7.4: Histogram of precipitation for the date 08.12.1978 (a) observed station data (b) interpolated precipitation (c) & (d) turning bands simulation (e) & (f) copula-based simulation.

It can be observed that the distribution of copula-based simulation closely follows the distribution of the observed station data (Figure 7.4). Figure 7.5 depicts a comparison between spatial distribution of interpolated and simulated precipitation for the selected date 08.12.1978. Each map contains mean and standard deviation (std. dev.) of the simulated and interpolated precipitation for that date. As can be seen, the smooth interpolation map is clearly different from the two simulation maps. The simulation maps indicate significantly more spatial variability but still conserve the major pattern.

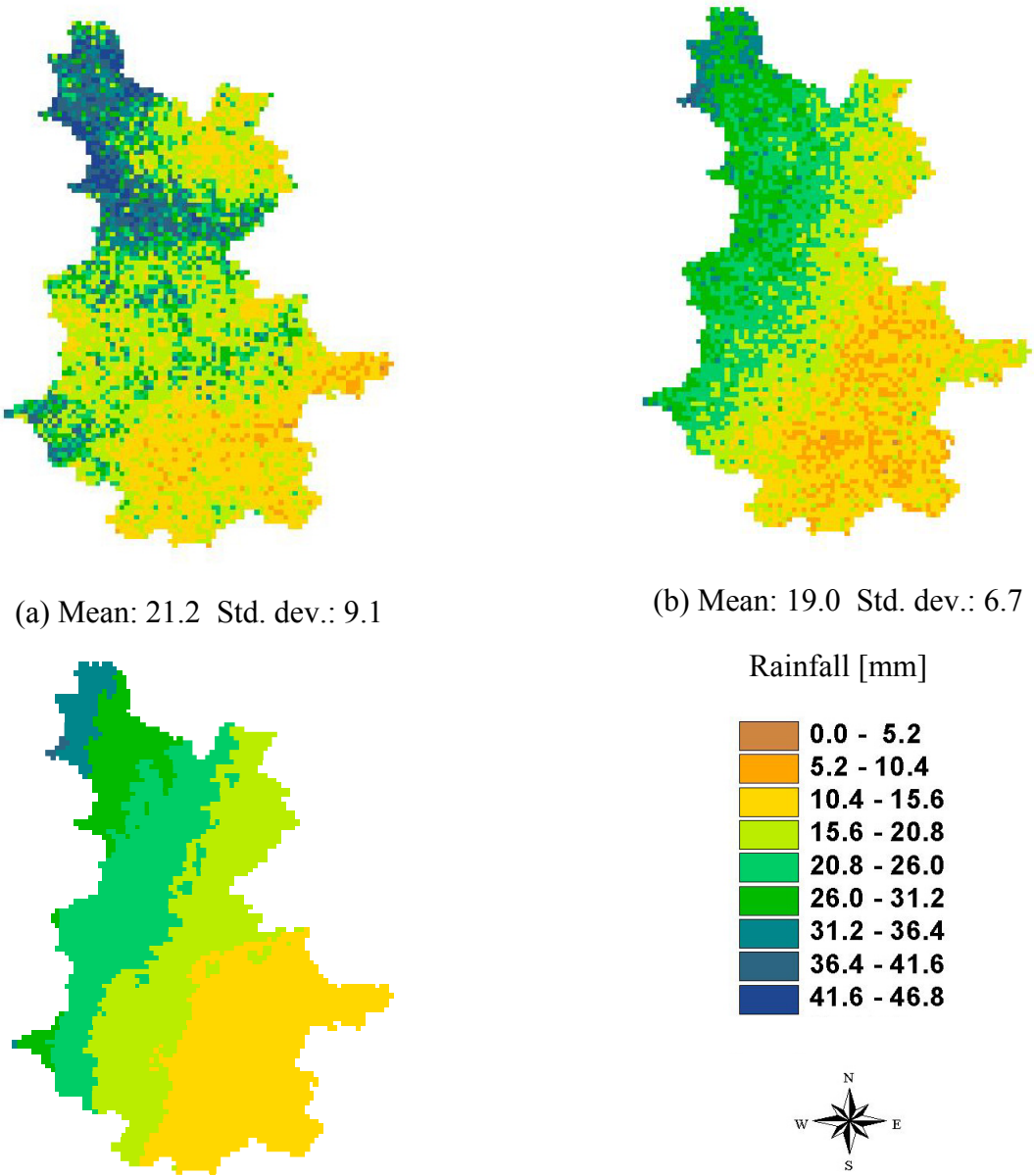

(a) Mean: 21.2 Std. dev.: 9.1

(b) Mean: 19.0 Std. dev.: 6.7

(c) Mean: 19.5 Std. dev.: 5.6

Figure 7.5: Spatial distribution of rainfall for 08.12.1978 (a) copula-based simulation (b) turning bands simulation (c) interpolated rainfall using external drift krging.

Comparing the two simulation maps, the map obtained using turning bands simulation shows a more structured pattern. It is worth mentioning that the external drift kriging method was used for the turning bands simulation. However, for the copula-based simulation the ordinary kriging method was used. Thus the difference of the spatial variability in the conditionally-simulated precipitation is also influenced by this consideration. The application of external drift kriging method, which is capable to consider additional information like elevation for rainfall interpolation, can be incorporated as an alternative of ordinary kriging method in the copula-based simulation.

The descriptive statistics and total number of dry grids over the catchment (here dry grids are defined as the mean precipitation less than 8 mm over the catchment) were computed using the interpolated precipitation. The values were calculated from the days having a total rainfall amount greater than 8 mm (Table 7.1).

Table 7.1: The descriptive statistics calculated from the interpolated precipitation.

Mean	Std. dev.	Skewness	Max.	Dry grid no.
14.3	4.1	0.6	28.8	3.0

The above statistics were also calculated from each realization of the conditionally-simulated precipitation obtained using the copula-based and turning bands simulation. Table 7.2 shows the overall mean values of the statistics calculated from the realizations.

Table 7.2: The overall mean values of the descriptive statistics of the conditionally-simulated precipitation.

	Mean	Std. dev.	Skewness	Max.	Dry grid no.
Copula-based simulation	14.0	5.6	0.8	36.7	20.0
Turning bands simulation	14.3	5.8	0.3	35.3	88.0

Comparing the Tables 7.1 and 7.2, it can be observed that the mean value of standard deviation is higher for the conditionally-simulated precipitation compared to the same of the interpolated precipitation. Among the two spatial rainfall simulation methods, the turning bands simulation shows slightly higher variability; however, the mean value of skewness is higher for the rainfall simulated using copula-based simulation. The total number of dry grids is higher for the rainfall simulated using turning bands simulation.

7.3 Conditionally-simulated rainfall and the semi-distributed HBV model

The semi-distributed HBV model was setup, calibrated and validated using the interpolated precipitation. Table 7.3 shows the model performance for the calibration and validation periods.

Table 7.3: Model performances for different gauges using the interpolated precipitation for the calibration and validation periods.

Gauge	Simulation period	R_m^2	Rel. accdif.	Peak error	RMSE
Rottweil	calibration	0.78	0.01	-0.22	3.29
	validation	0.79	0.04	-0.13	3.40
Oberndorf	calibration	0.81	0.01	-0.18	4.24
	validation	0.78	0.06	-0.01	4.70
Horb	calibration	0.86	0.01	-0.13	6.73
	validation	0.84	0.10	-0.12	7.74

It can be observed that the Nash-Sutcliffe coefficient for the simulation of the daily discharge in the subcatchments during the calibration period has values ranging between 0.78 and 0.86, with a mean value of 0.82. The Nash-Sutcliffe coefficient for the validation period has values ranging between 0.78 and 0.84, with a mean value of 0.80. The highest Nash-Sutcliffe coefficient value is observed for the gauge at Horb, both for the calibration and validation periods.

Further, the conditionally-simulated precipitation of each realization, obtained using the turning bands and copula-based simulation, was used to calculate the mean value over each elevation zone used for the semi-distributed HBV model. The averaged precipitation over the elevation zone was then used as an input precipitation to the calibrated HBV model. Table 7.4 shows the model performances obtained using the conditionally-simulated precipitation for the validation period. The value of each model performance criteria shown in Table 7.4 is the overall mean value calculated from the model performances obtained using the twenty one realizations.

As shown in Table 7.4, the mean values of Nash-Sutcliffe coefficient for the gauge at Horb when using the precipitation based on copula simulation and the turning bands simulation are 0.85 and 0.82, respectively. The mean error to estimate the annual peaks using the precipitation by the copula-based simulation is slightly higher than that obtained using the interpolated precipitation. However, this error is lower when the model is running with the precipitation obtained using the turning bands simulation than the same obtained using the interpolated precipitation. It can also be observed that the model simulation bias is higher using the precipitation obtained by the turning bands simulation as compared to the same obtained using the precipitation produced by the copula-based method.

Table 7.4: Mean model performances using the simulated precipitation for different gauges during the validation period.

		Rottweil	Oberndorf	Horb
Copula-based simulation	R_m^2	0.79	0.79	0.85
	Rel. accdif.	0.00	0.01	0.04
	Peak error	-0.16	-0.03	-0.16
	RMSE	3.38	4.65	7.58
Turning bands simulation	R_m^2	0.76	0.74	0.82
	Rel. accdif.	0.12	0.13	0.17
	Peak error	-0.09	0.05	-0.09
	RMSE	3.64	5.09	8.21

The average simulated discharge time series were calculated using the simulated discharges obtained using the conditionally-simulated precipitation. The model performances were then calculated using the average simulated discharges and the observed discharges (Table 7.5). The average values of the simulated discharges are used to compute the model performances, because it is reasonable to consider that a large number of realizations of conditionally-simulated precipitation somehow capture the non-linearity of the complicated precipitation process and each of them is one of the probable realizations. It can be observed that the Nash-Sutcliffe coefficient, calculated using the average simulated discharges obtained using different realizations of precipitation based on copula-based simulation, is higher than that obtained using the interpolated precipitation. On the contrary, the Nash-Sutcliffe coefficient, calculated from the average simulated discharges obtained using different realizations of precipitation based on turning bands simulation, is lower than that obtained using the interpolated precipitation. The time series of maximum simulated discharges were also calculated using the simulated discharges obtained using the conditionally-simulated precipitation. Thus this discharge series consists of maximum value of simulated discharges from all the realizations of the simulated discharges. Also the Nash-Sutcliffe coefficient was computed using the maximum simulated discharge series and the observed discharge series to investigate the model performance to estimate the peak discharges. It can be observed that the Nash-Sutcliffe coefficient, calculated using the maximum values of the simulated discharges obtained from different realizations of the both conditionally-simulated precipitation, is low compared to the same obtained using the interpolated precipitation. However, the peak estimation is better when using the maximum values of the simulated discharges obtained from the realizations of the conditionally-simulated precipitation as compared to the same obtained using the interpolated precipitation.

Table 7.5: Model performance using the average and maximum values of the simulated discharges obtained using simulated precipitation for the different gauges.

	Rottweil				Oberndorf				Horb			
	R_m^2	Rel. accdif.	Peak error	RMSE	R_m^2	Rel. accdif.	Peak error	RMSE	R_m^2	Rel. accdif.	Peak error	RMSE
Using interpolated precipitation	0.79	0.04	-0.13	3.40	0.78	0.06	-0.01	4.70	0.84	0.10	-0.12	7.74
Using mean of turning bands simulation	0.77	0.12	-0.10	3.55	0.76	0.13	0.04	4.96	0.82	0.17	-0.09	8.10
Using maximum of turning bands simulation	0.65	0.28	0.01	4.36	0.61	0.27	0.19	6.26	0.77	0.27	0.00	9.37
Using mean of copula-based simulation	0.80	-0.01	-0.16	3.31	0.80	0.01	-0.04	4.55	0.85	0.04	-0.16	7.49
Using maximum of copula-based simulation	0.73	0.13	-0.04	3.81	0.72	0.12	0.09	5.30	0.83	0.13	-0.08	8.07

It can also be observed that the model simulation bias, using the maximum values of the simulated discharges obtained from the conditionally-simulated precipitation, is higher than the same obtained using the interpolated precipitation. Among the two spatial rainfall simulation methods, the model simulation bias is double for the turning bands simulation as compared to the same obtained using the copula-based simulation.

The standard deviation obtained using the conditionally-simulated precipitation and the daily observed discharge for the Horb gauge is shown in Figure 7.6.

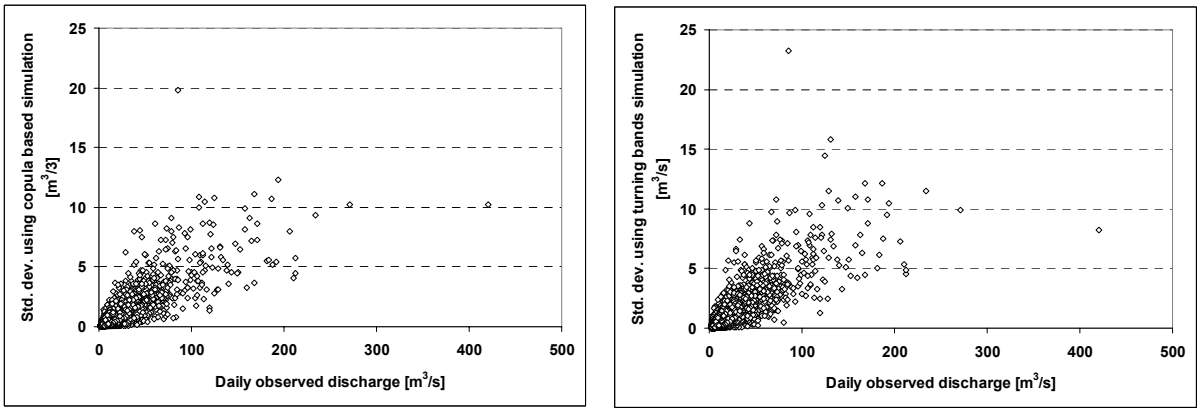

Figure 7.6: Observed discharge vs. Standard deviation of the simulated discharges using copula-based simulation (left panel) and turning bands simulation (right panel).

It can be noticed that there is high variability in the simulated discharges for high observed discharge values. This indicates an involvement of the higher uncertainty to simulate the high discharges.

Figure 7.7 shows seasonal Nash-Sutcliffe coefficient for the gauges at Rottweil and Horb. The seasonal Nash-Sutcliffe coefficient was calculated using the average values of the simulated discharges obtained using different realizations of the conditionally-simulated precipitation. It can be observed that the model performance is comparatively poor in the summer season even with the use of the conditionally-simulated precipitation. This is because there are convective precipitation events in the summer season which are more localized.

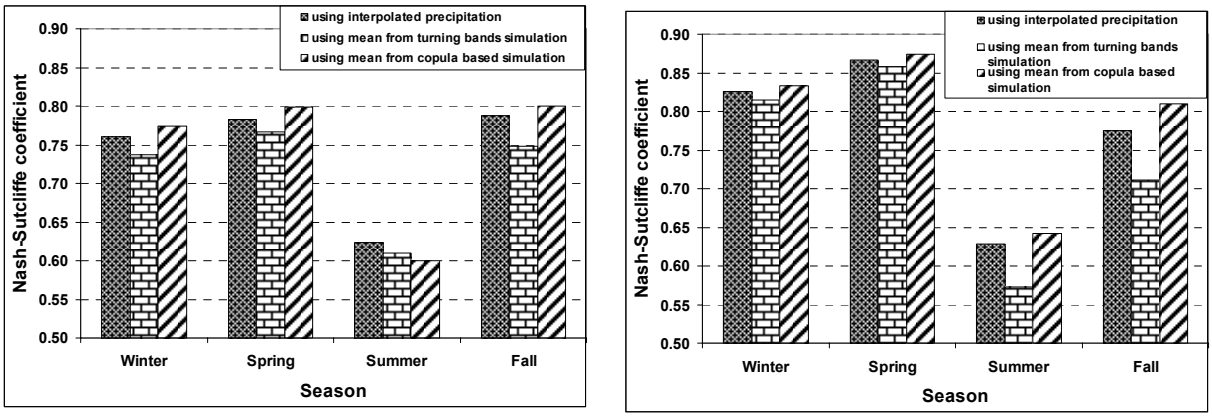

Figure 7.7: Seasonal Nash-Sutcliffe coefficient using simulated and interpolated precipitation for the gauges at Rottweil (left panel) and Horb (right panel).

The hydrographs corresponding to the maximum, minimum and mean of the simulated discharges obtained using different realizations of the simulated precipitation through the application of the turning bands simulation and copula-based simulation are shown in Figures 7.8 and 7.9, respectively. The figures are shown for a selected flood peak in the validation period for the gauge at Horb.

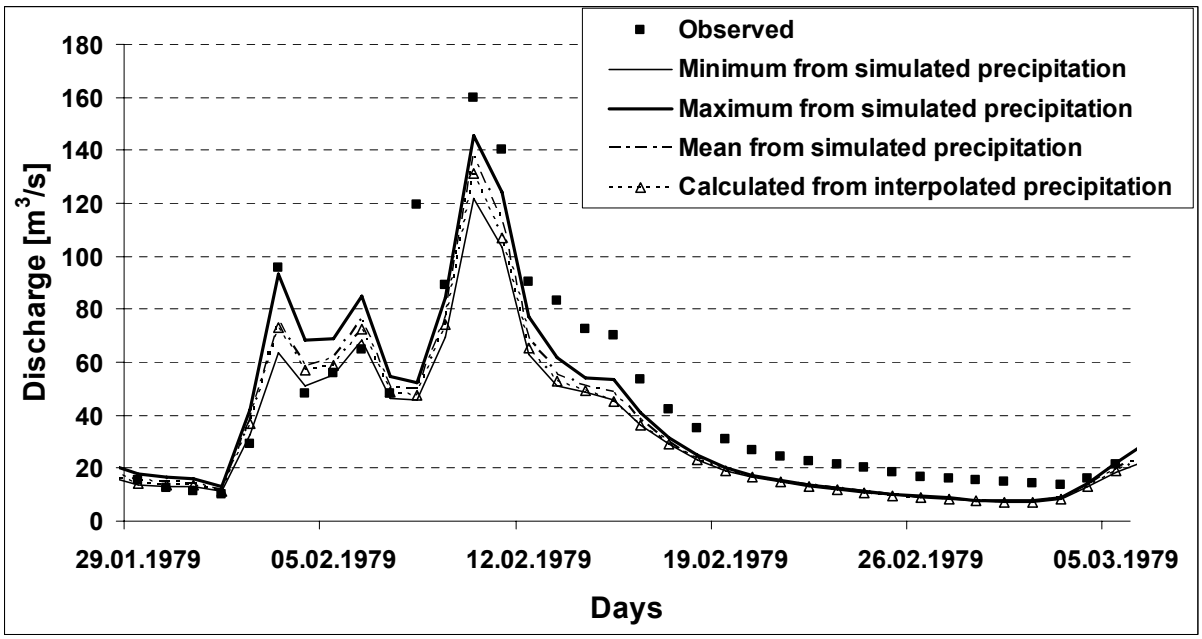

Figure 7.8: Comparisons between calculated discharges from interpolated precipitation and conditionally-simulated precipitation using turning bands simulation with observed discharge for the gauge at Horb in the validation period.

It can be observed that the flood event is better estimated using the conditionally-simulated precipitation (Figures 7.8 and 7.9). It can also be noticed that there is higher uncertainty in the simulated discharges obtained using the conditionally-simulated precipitation for high discharge, however, such uncertainty is less for low discharge.

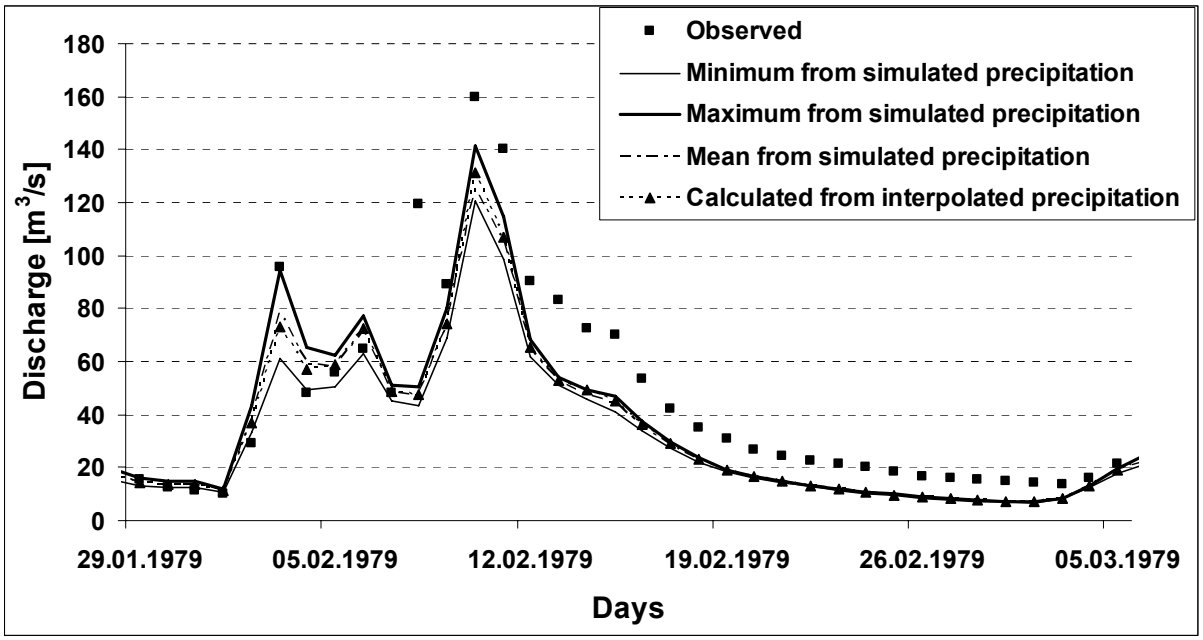

Figure 7.9: Comparisons between calculated discharges from interpolated precipitation and conditionally-simulated precipitation using copula-based simulation with observed discharge for the gauge at Horb in the validation period.

Figure 7.10 shows the standard deviation of the simulated discharges obtained using the conditionally simulated precipitation for the selected flood peak in the validation period for the gauge at Horb.

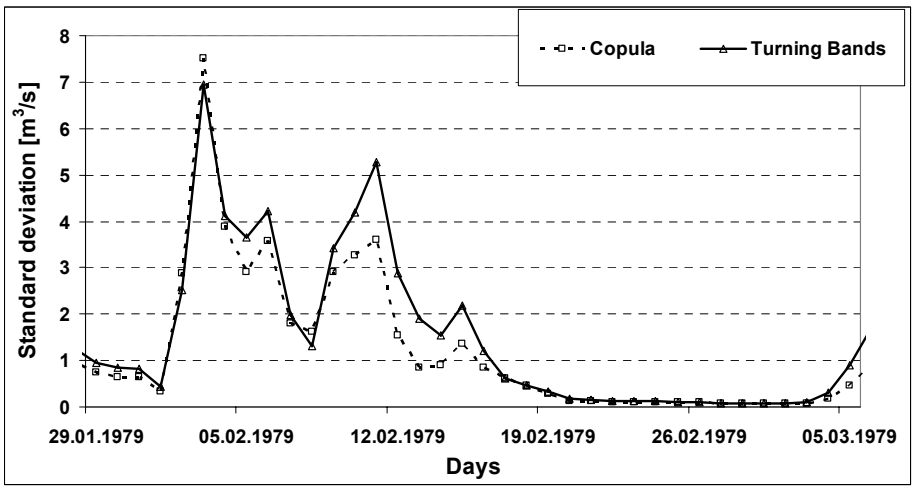

Figure 7.10: Standard deviation of the simulated discharges for the selected flood peaks in the validation period at the gauge Horb obtained using the conditionally-simulated precipitation.

Figure 7.10 indicates that the standard deviation of the simulated discharges obtained using the turning bands simulation is relatively higher than that obtained using the copula-based simulation.

7.4 Concluding remarks

In this chapter attempts have been made to investigate the benefit using the simulated precipitation for the hydrological modeling. Two different spatial rainfall simulation methods were applied for conditional rainfall simulation. The precipitation was simulated using turning bands simulation and copula-based simulation. The comparison of the conditionally-simulated precipitation and interpolated precipitation highlights that conditional spatial rainfall simulation indicates significantly more variability in the simulated rainfall.

The conditionally-simulated precipitation was then used to simulate discharges for a meso-scale catchment using the semi-distributed rainfall-runoff model HBV. The study showed that the modeling performance using the mean of the simulated discharges obtained using conditionally-simulated precipitation based on turning bands simulation was worser than that obtained using interpolated precipitation. While, the model performance using the mean of the simulated discharges obtained using conditionally-simulated precipitation through the application of copula-based simulation was better than that obtained using the interpolated precipitation. The analysis also highlighted that the modeling performance was better using both types of conditionally-simulated precipitation than that obtained using the interpolated precipitation if only floods are considered. Thus conditional spatial precipitation simulation is reasonable for flood modeling.

Application of the Gaussian copulas for spatial precipitation simulation was very encouraging. The application of non-Gaussian copula can also be aimed as an alternative of the Gaussian copula as further research efforts.

8 Uncertainty investigation in model simulation and in identifying the model parameters of a conceptual model due to uncertain precipitation

8.1 Introduction

Uncertainty is an unavoidable element in any hydrologic modeling study (Beven, 2001). This uncertainty stems from the parameters, the model structure and measurements of input and output data. Precipitation is one of the most important hydrological model inputs. Precipitation is governed by complicated physical processes, which are inherently nonlinear and extremely sensitive (Bárdossy and Plate, 1992). Nevertheless, inadequate representation of spatial variability of precipitation in modeling can be partly responsible for modelling errors. This may also lead to the problem in parameter estimation of a conceptual model. Because for partly or fully conceptual models, some parameters cannot be considered as physically measured quantities and have to be estimated on the basis of the available data and information. Thus the performance of a conceptual model tends to depend on parameter optimization. The interpolated precipitation can be used as an input precipitation to a conceptual model and the model parameters can then be estimated by calibration. It is already seen that interpolation provides idealized smooth precipitation fields and does not possess the same fluctuation pattern. The uncertainty in spatial variability of precipitation may thus introduce significant uncertainty in the optimized parameters of a model.

The research objective of this study is therefore two fold:

1. To study the uncertainty in the model's simulations due to spatial uncertainty in precipitation input.

This study was carried out using the physically-based spatially-distributed modeling system SHETRAN and the conceptual semi-distributed rainfall-runoff model HBV. The similar simulation experiment was documented in the previous chapter using the HBV model. Conditionally-simulated precipitation using copula-based simulation was used as an input precipitation to the SHETRAN and the HBV models. The simulated discharges by means of different realizations of the conditionally-simulated precipitation were then analyzed to assess and quantify the uncertainty in the simulated discharges.

2. To investigate the uncertainty incurred in the model parameters of a conceptual rainfall-runoff model arising from uncertain precipitation.

A dual rainfall-runoff modeling strategy was employed for this investigation. Figure 8.1 explains the applied modeling strategy schematically.

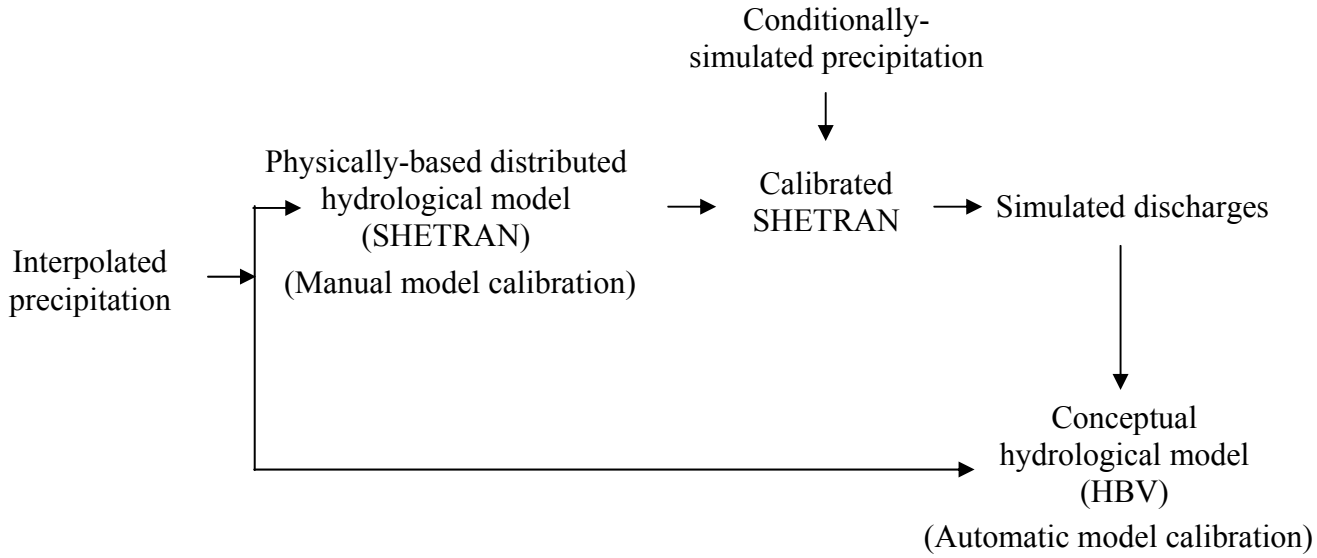

Figure 8.1: Schematic flow chart of the dual modeling procedure.

The following steps were followed in accordance to the mentioned investigation.

Step 1: Set up of the physically-based hydrological model SHETRAN and HBV model using the interpolated precipitation obtained using the external drift Kriging method (Ahmed and de Marsily, 1987).

Step 2: The conditionally-simulated precipitation was then used as an input precipitation to the calibrated SHETRAN model to simulate the discharges. A number of realizations of the conditionally-simulated precipitation were used.

Step 3: The simulated discharges from the previous step, produced using the different realizations of simulated precipitation, were used to identify the model parameters of the conceptual rainfall-runoff model HBV.

The SHETRAN model was assumed, in this experiment, to represent the true copy of the prevailing hydrological system of the study catchment. It was considered that SHETRAN acts as a virtual catchment. It is well recognized that it is not possible to represent the actual spatial variability of precipitation through interpolation of the point measurements. The conditionally-simulated precipitation is one of the probable realizations of the natural condition and was attemped to capture the non-linearity of complicated precipitation process. A large number of realizations of conditionally-simulated precipitation were used as an input precipitation into the SHETRATN model to obtain the reaction as what may happen in the real catchments. Thus the simulated discharges are the results due to one of the probable realizations. The simulated discharges were then used as a basis to calibrate the HBV model to investigate the impact of spatially variability of precipitation on the identification of the model parameters. The calibration of the HBV model was carried out automatically by means of the combinatorial optimization algorithm simulated annealing

(Aarts and Korst, 1989). Finally, different sets of optimized parameters of the HBV model were investigated to assess and quantify the uncertainty associated with the optimized model parameters.

In the present study, the models were applied to a portion of the Upper Neckar catchment (up to gauge Horb; approximately 1200 km^2) (Figure 8.2).

8.2 Models and simulations

8.2.1 The SHETRAN model

The SHETRAN model was configured to the catchment property data and then calibrated and validated against the available precipitation and discharge data for the study catchment. The catchment was subdivided into 500 m × 500 m grid squares, with river channel elements running along the edges of the grid squares. Figure 8.2 presents the SHETRAN grid for the study catchment together with tops of SHETRAN columns, river network, and ground surface elevations. Four vegetation types were chosen for the catchment: forest, urban area, agricultural and water body. Standard vegetation parameters were used for each type, taken from literature. Strickler roughness coefficients for overland flow were specified for each vegetation type, with values ranging from 1.2 $m^{1/3}s^{-1}$ for forest to 25 $m^{1/3}s^{-1}$ for water body. Each SHETRAN grid square was split vertically into 25 horizontal layers, and two soil/geology categories were chosen for the grid squares based on geology and soil maps.

The required input meteorological values for every SHETRAN model grid were obtained through interpolation. The potential evapotranspiration was calculated using the Hargreaves and Samani method (Hargreaves and Samani, 1985). The interpolated daily precipitation amount, mean daily temperature and potential evpotranspiration were used as inputs to all of the SHETRAN model grid squares. Thus each of the SHETRAN grid squares has a different daily precipitation, evapotranspiratin and temperature. It was recognized that this was not a satisfactory representation of spatial variability, particularly for precipitation, but this constraint was imposed by the nature of the available data. The model was calibrated and validated using continuous simulation within the period 1961-1980. A split sample approach was followed, using the period 1961-1970 for calibration, and the period 1971-1980 for validation. The maximum time step of 4 hours was used for the SHETRAN model simulation. However, this time step can be further reduced internally during rainfall events.

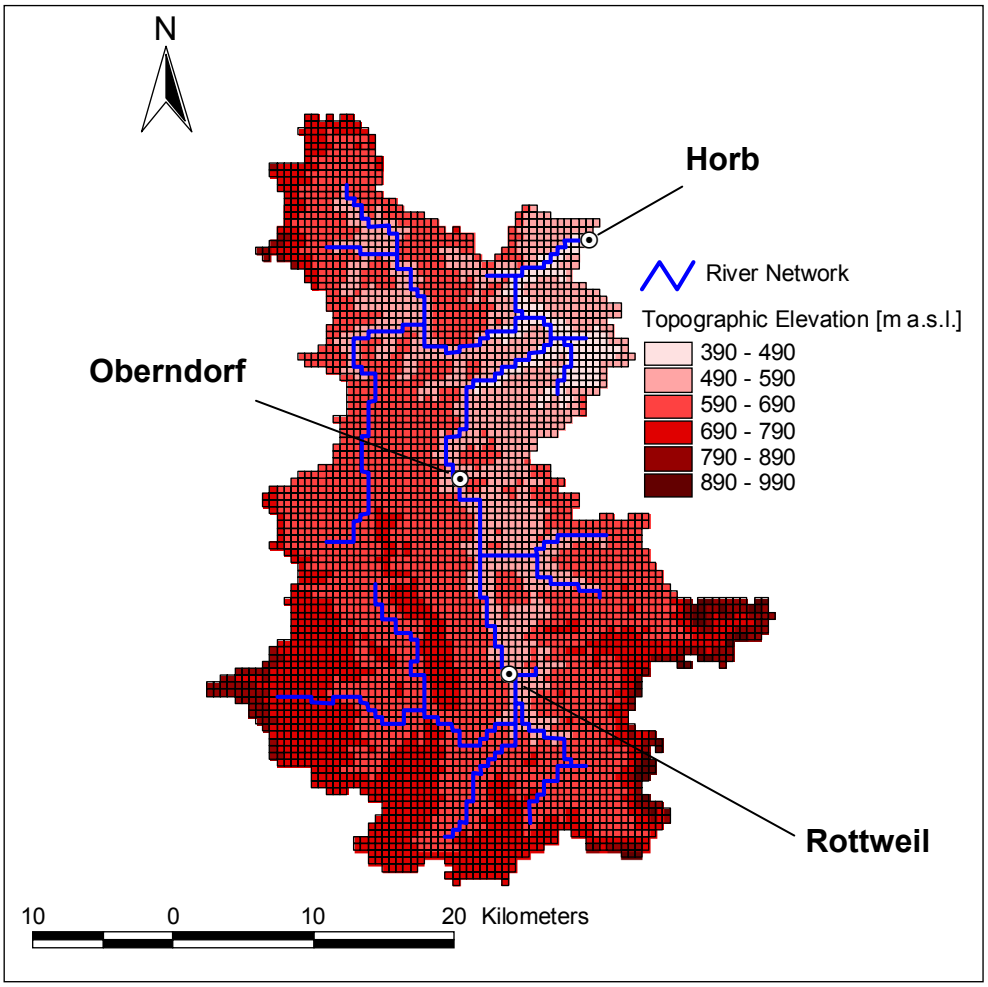

Figure 8.2: SHETRAN grid showing tops of SHETRAN columns, river network, and ground surface elevations.

During the calibration, adjustments were made to some of the parameters to which the results are most sensitive. These were the Strickler resistance coefficient for the overland flow, ratio of actual to potential evapotranspiration at soil field capacity, the Van Genuchten exponent *n* for soil moisture/tension curve and the soil saturated zone hydraulic conductivity. The thick gravel deposits on which the main river channel runs, had also an important effect on the simulation by reducing the peak flow and increasing flows during the recession. Satisfactory agreement was obtained between the measured and simulated discharge for the gauge at Horb with Nash-Sutcliffe coefficient of 0.62 for the calibration and 0.55 for the validation period.

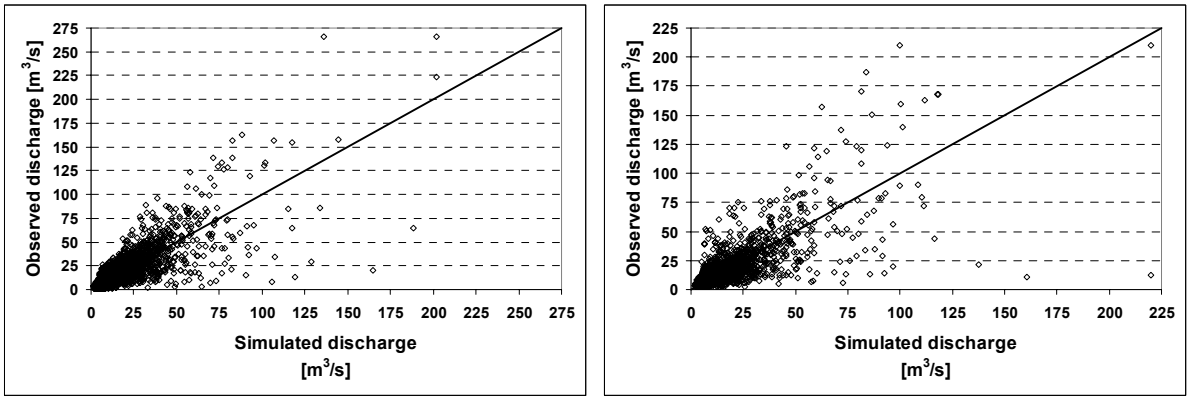

Figure 8.3: Scatter plots of the observed and simulated discharges for the gauge at Horb during the calibration period (left panel) and validation period (right panel).

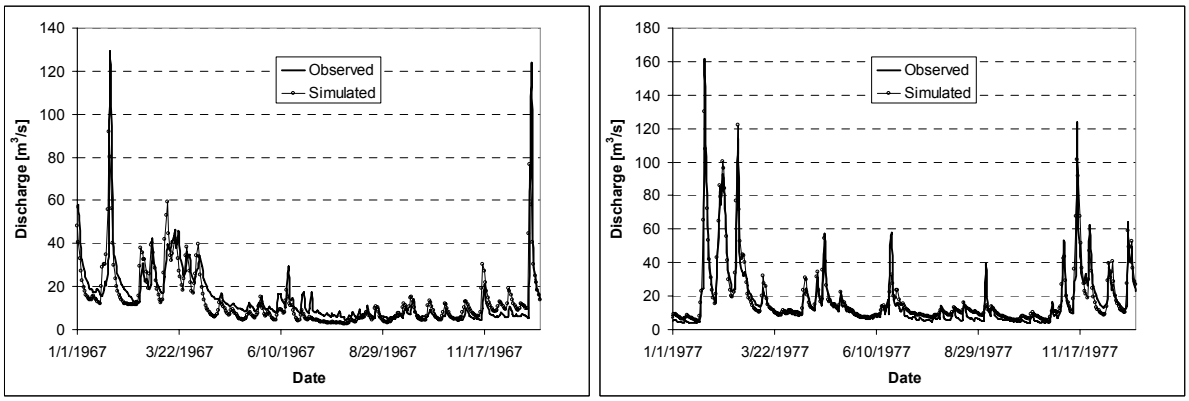

Figure 8.4: Comparison between observed and simulated discharges for the gauge at Horb for selected time period during the calibration period (left panel) and validation period (right panel).

It can be observed that there is underestimation of peak events both for the calibration and validation periods (Figures 8.3 and 8.4). The underestimation is perhaps due to the use of the daily precipitation data. The daily precipitation is uniformly disaggregated over a 24 hour period when it was applied to the model. So the model receives uniform rainfall for 24 hours whereas in fact there may be very heavy rainfall for couple of hours or so. The heavy rainfall may produce infiltration excess runoff, however, the uniformly disaggregated precipitation would not produce this sort of response. This problem can be overcome possibly by disaggregating the daily precipitation into hourly data using disaggregation algorithm (Gyasi-Agyei, 2002). However, this was not attempted due to mainly constraints of time.

Figure 8.5 depicts the water content in the upper soil column at the end of the validation period.

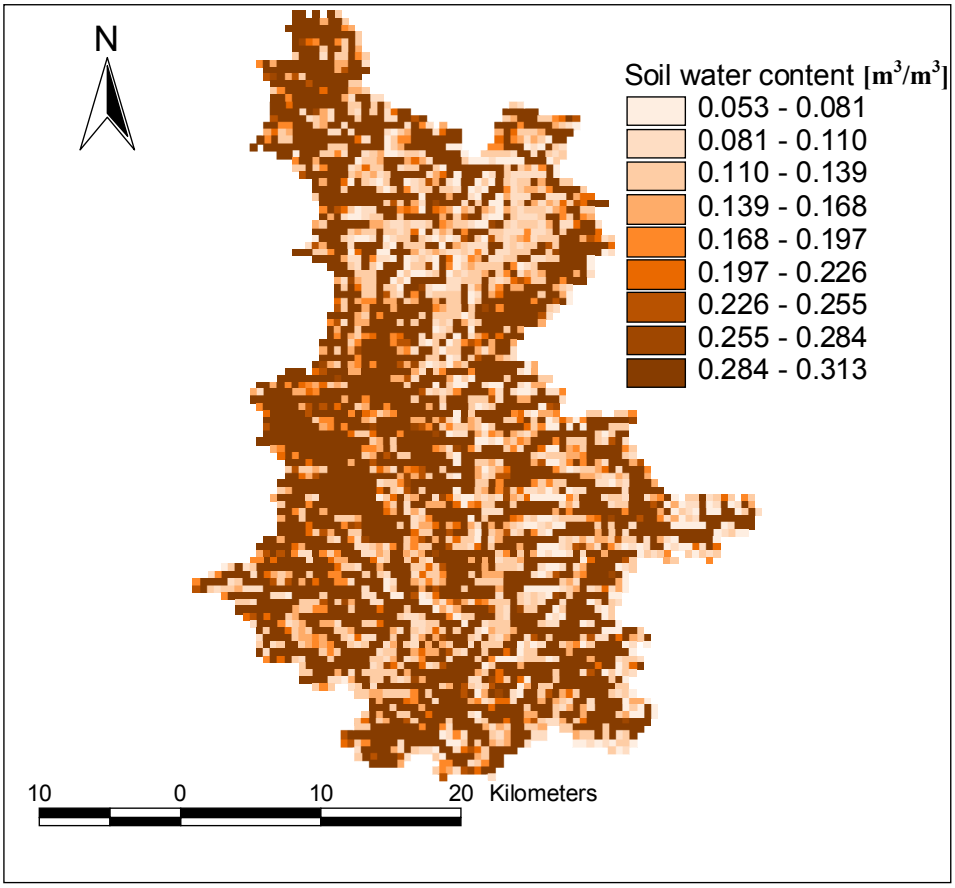

Figure 8.5: Soil water content in the upper soil column at the end of the validation period.

8.2.2 The HBV model

The spatial distribution of the daily precipitation and the daily average temperature were produced on the same 500 m × 500 m grid, as used in the SHETRAN model, by the external drift kriging method (Ahmed and de Marsily, 1987) from the available point measurements. The interpolated meteorological variables were then averaged over each elevation zone to set up the semi-distributed HBV model. The model was calibrated using an automatic calibration procedure based on simulated annealing optimization algorithm (Aarts and Korst, 1989). The same calibration and validation period, as used in SHETRAN, was used for the HBV model. The model time step of 6 hours was used for the simulation. Excellent agreement was obtained between the measured and simulated discharge for the gauge at Horb with Nash-Sutcliffe coefficient of 0.86 for the calibration and 0.83 for the validation period.

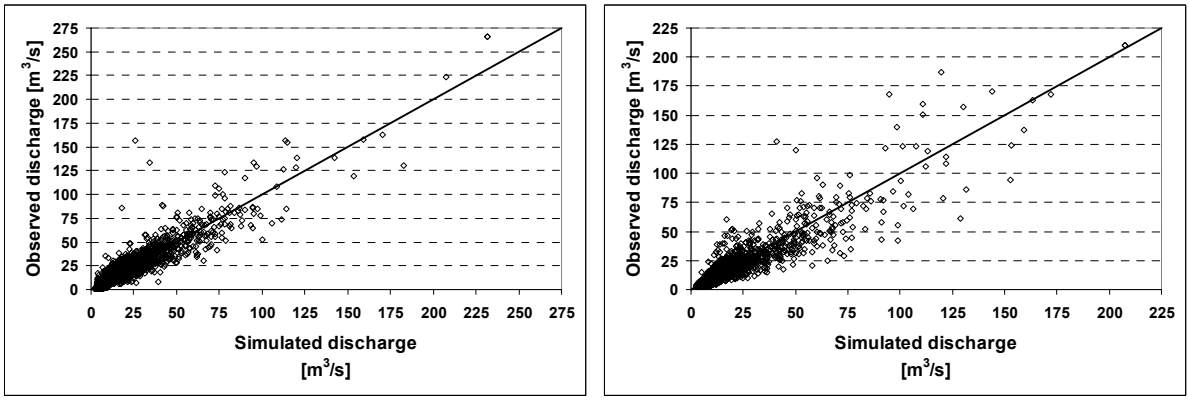

Figure 8.6: Scatter plots of observed and simulated discharges for the gauge at Horb during the calibration period (left panel) and validation period (right panel).

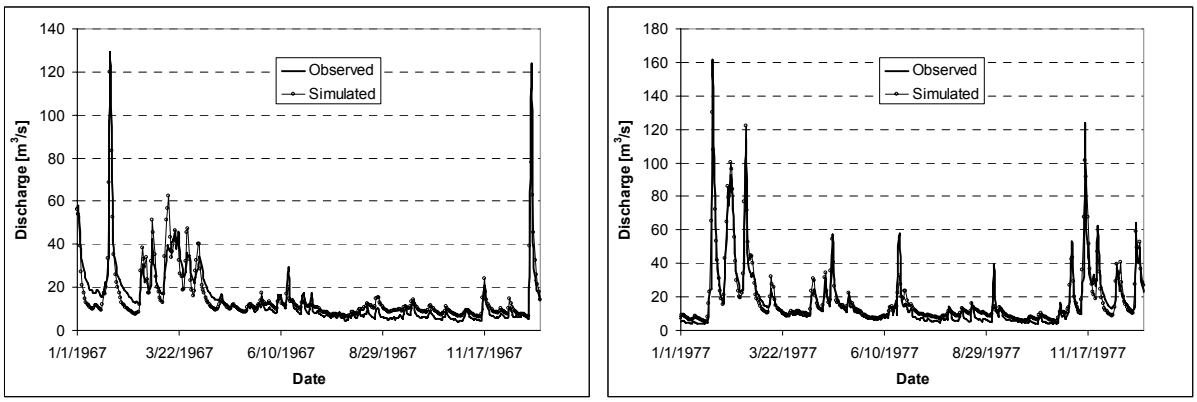

Figure 8.7: Comparison between observed and simulated discharges for the gauge at Horb for selected time period during the calibration period (left panel) and validation period (right panel).

Comparing the performances of the SHETRAN and HBV model, it is clear that the HBV model performs better to simulate the discharge at the catchment outlet. It is worth mentioning that estimation of areal precipitation for the SHETRAN model grid cells from the point measurements are very difficult. This is because the error in representing spatial variability of precipitation in finer resolution is more. It should also be mentioned that an automatic calibration procedure was used to optimize the model parameters for the HBV model. Hundreds of simulation trails was attempted within the automatic calibration procedure to optimize the model parameters of HBV. On the other hand, in SHETRAN, only few simulation trails were attempted to adjust some of the parameters to which the results are most sensitive due to mainly long simulation time requirement. Another potential reason for lower performance of SHETRAN could be due to the use of daily precipitation data and simplification of the basin characteristics, for example, use of only two soil/geology classes. The grid resolution used for the SHETRAN model is 500 m × 500 m which is coarse resolution. Perhaps by using a higher resolution grid cells the better model performances can be

obtained. However, the problem to determine of areal precipitation for finer SHETRAN model grid cells from the point measurements should also be considered.

8.3 Uncertainty in the models' simulations due to spatial variability of precipitation

Fifty realizations of conditionally-simulated rainfall were generated on the same 500 m × 500 m model grid using the copula based simulation. This spatial rainfall simulation procedure was adopted due to better overall performance (described in the chapter VIII). Conditionally-simulated precipitation was used as input to the SHETRAN model to simulate discharges for the validation period. For each elevation zone, mean values from each realization of conditionally-simulated precipitation was also calculated. The averaged precipitation was then used to the calibrated HBV model as input precipitation in the validation period.

Table 8.1 shows the statistics of Nash-Sutcliffe coefficient obtained using the different realizations of conditionally-simulated precipitation for different gauges. The table indicates that there is variation in the models' performance that result from the uncertainty in the spatial variability of precipitation. Figures 8.8 and 8.9 present the uncertainty in the simulated discharges due to spatial variability of precipitation. The standard deviation was calculated from the simulated discharges obtained using the different realizations of conditionally-simulated precipitation.

Table 8.1: Statistics of Nash-Sutcliffe coefficient obtained using the different realizations of conditionally-simulated precipitation using the SHETRAN and HBV model for different gauges.

Gauge	Simulation period	Minimum	First quartile	Median	Third quartile	Maximum
Rottweil	SHETRAN	0.47	0.48	0.49	0.50	0.51
	HBV	0.72	0.73	0.74	0.74	0.76
Oberndorf	SHETRAN	0.49	0.50	0.51	0.52	0.53
	HBV	0.74	0.76	0.77	0.77	0.79
Horb	SHETRAN	0.55	0.56	0.56	0.56	0.57
	HBV	0.82	0.83	0.84	0.85	0.87

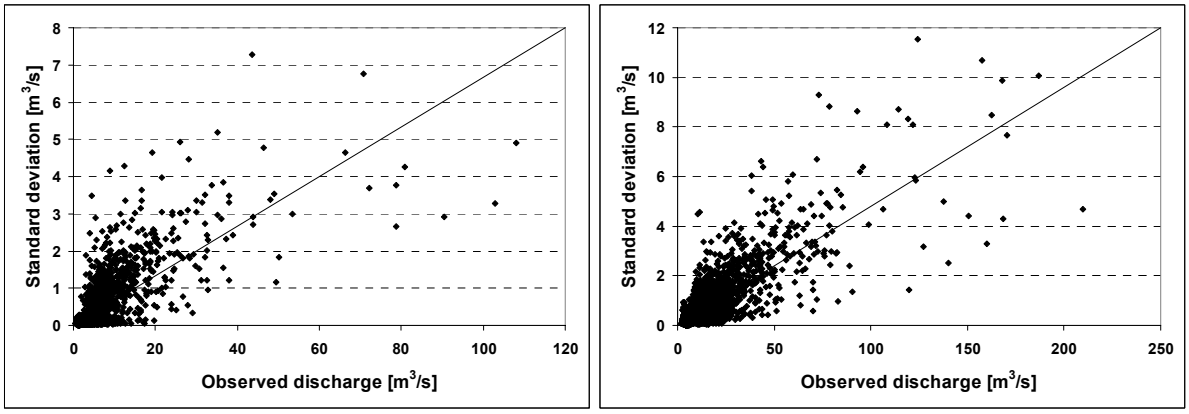

Figure 8.8: Daily discharges vs. standard deviation using the HBV model for the gauges at Rottweil (left panel) and Horb (right panel).

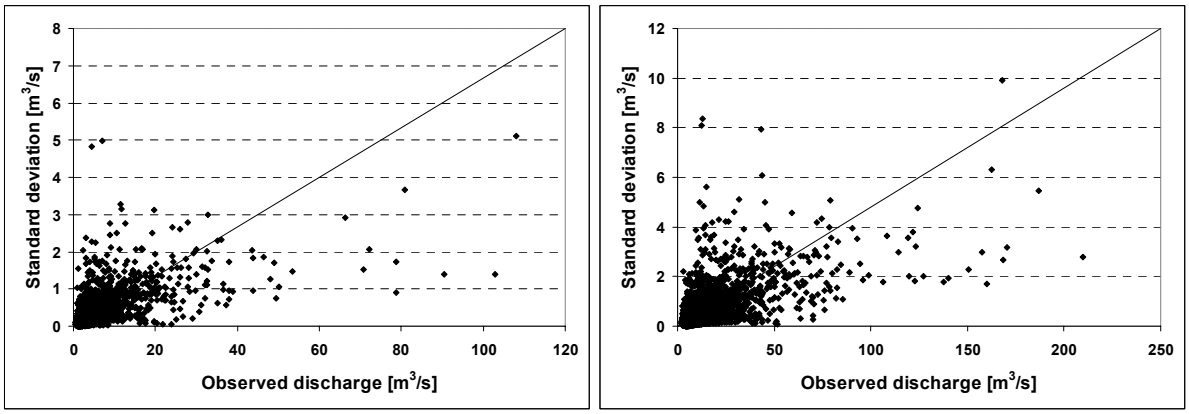

Figure 8.9: Daily discharges vs. standard deviation using the SHETRAN model for the gauges at Rottweil (left panel) and Horb (right panel).

It can be observed that there is high variability in the simulated discharge obtained using the both models for high discharge values (Figures 8.8 and 8.9). This indicates an involvement of the higher uncertainty to simulate the high discharge.

The simulated discharges using different realizations of simulated precipitation for selected flood event in the validation period for the gauge at Horb is shown in Figure 8.10. In the figure dashed line indicates observed discharges and the simulated discharges are indicated by the continuous lines.

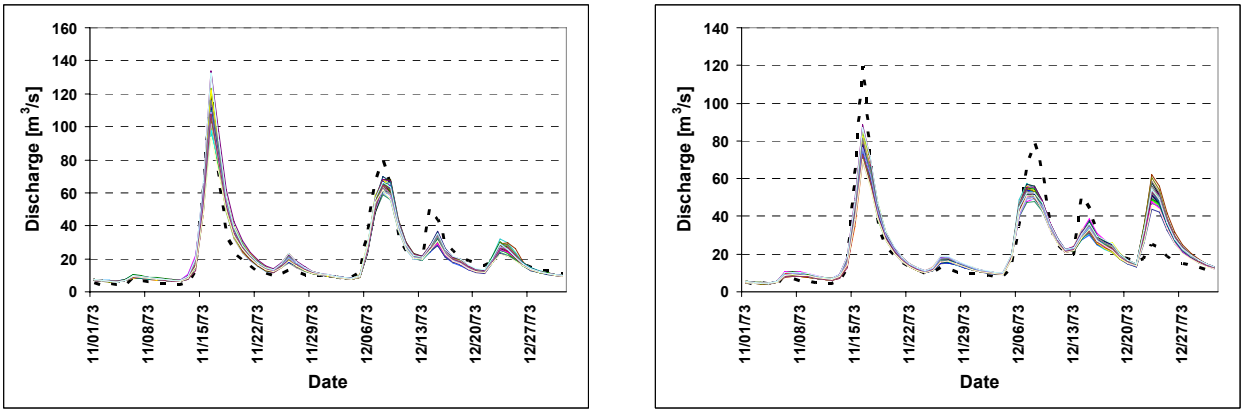

Figure 8.10: Comparison between observed and simulated discharges for selected flood event in the validation period for the gauge at Horb using the HBV model (left panel) and the SHETRAN model (right panel).

As expected, better hydrographs can not be obtained by the SHETRAN model even using the simulated precipitation. Nevertheless, focusing on the precipitation forcing, it can be observed that the variability of the simulated hydrographs is high for the both models, in particular for the peak events. The simulated peak discharges exhibit a big range which implies that the predictive uncertainty is considerable.

8.4 Effect of rainfall spatial variability on the HBV model parameters uncertainty

The simulated discharges obtained using the SHETRAN model was used as basis for calibrating the HBV model using the interpolated precipitation as input in this simulation experiment. The HBV model was automatically calibrated by means of the combinatorial optimization algorithm simulated annealing (Aarts and Korst, 1989). There were fifty independent optimization runs for the HBV model. These runs were done using the automatic calibration procedure, each using the simulated discharges obtained from the SHETRAN model as basis for the calibration. Two parameters for the snow module (DD_0 and T_{crit}) for each elevation class, three parameters for the runoff generation module (FC, PWP and β) for each elevation class and five parameters for the runoff concentration module (L, K_0, K_1, K_2 and K_{perc}) for each subcatchment were optimized. No explicit dependence between the parameters was considered. As a result, fifty parameter vectors were generated. Following this, the HBV model was applied using those calibrated parameter vectors and the model performance was assessed. Table 8.2 represents the statistics of Nash-Sutcliffe coefficient, showing the lower to upper quartile fractions of the Nash-Sutcliffe coefficients resulting from different optimized parameter vectors for different gauges. The values of R_m^2 were computed based on the simulated discharges by the HBV model and the simulated discharges by the

SHETRAN model which was assumed as original discharges produced due to the forcing precipitation.

Table 8.2: Statistics of Nash-Sutcliffe coefficient obtained from different optimized parameter vectors.

Gauge	Minimum	First quartile	Median	Third quartile	Maximum
Rottweil	0.69	0.70	0.71	0.71	0.73
Oberndorf	0.68	0.70	0.70	0.71	0.72
Horb	0.70	0.72	0.74	0.76	0.77

Figure 8.11 depicts the flow duration curves for the gauges at Rottweil and Horb. The flow duration curves were calculated using the simulated discharges resulting from different optimized model parameter vectors.

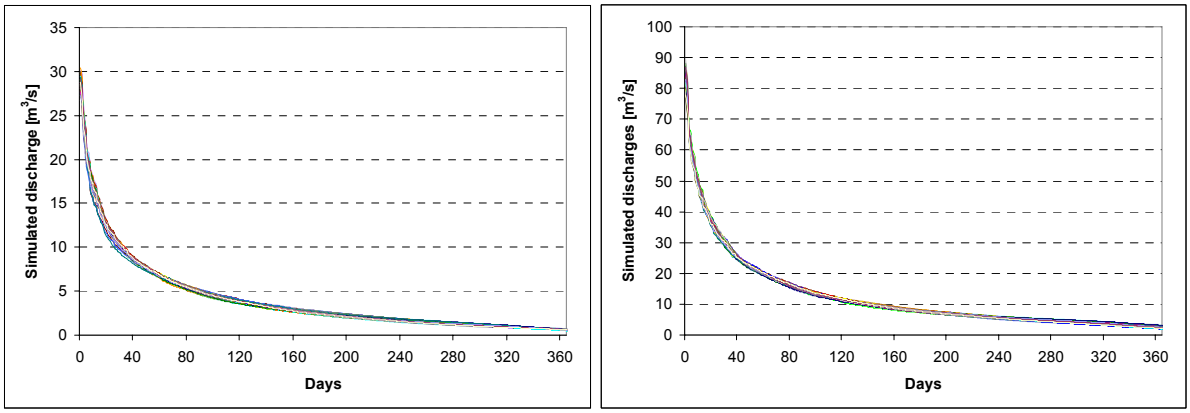

Figure 8.11: Mean flow duration curves obtained using the simulated discharges resulting from different optimized parameter vectors for the gauges at Rottweil (left panel) and Horb (right panel).

Figure 8.12 shows the scatter plots of the selected model parameters together with the corresponding model performance (Nash-Sutcliffe coefficient) for the Horb subcatchment. The values of the parameters FC, β, DD_0 and T_{crit} are shown for one elevation class for the Horb subcatchment. The values for other elevation classes showed a similar behavior, however, varying in magnitude (not shown here).

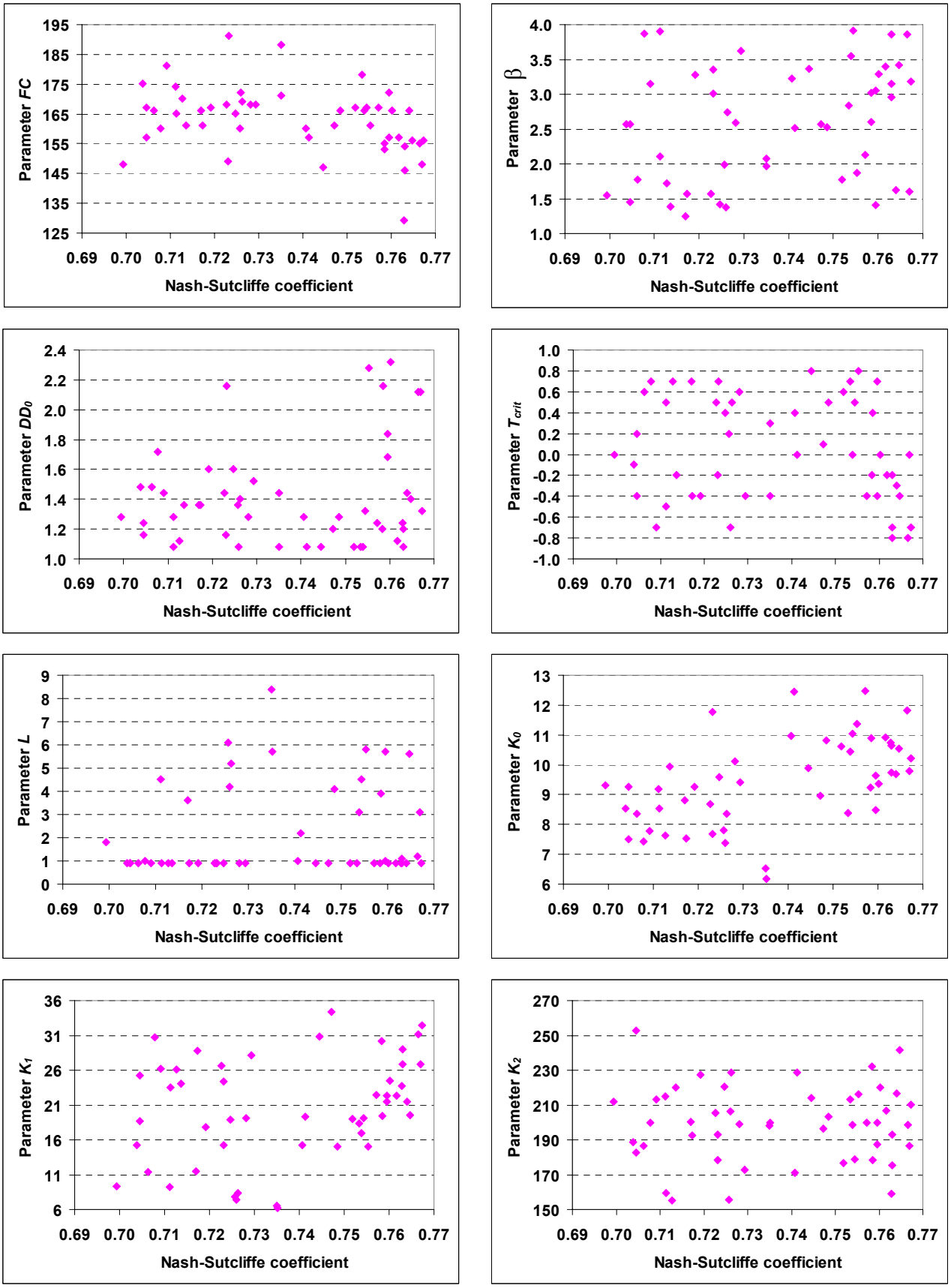

Figure 8.12: Scatter plots of the optimized model parameters for the Horb subcatchment.

Figure 8.12 indicates a large uncertainty in the estimated model parameters due to the spatial variability of the precipitation. The similar behaviors were observed for the other parameters and also for other subcatchments (not shown here).

The variability in the optimized model parameters induced by the spatial variability of rainfall can quantitatively be described using standard deviation (σ_θ) and coefficient of variation (CV_θ). These statistics are defined as:

$$\sigma_\theta = \left(\frac{1}{N_\theta} \sum_{i=1}^{N_\theta} \left(\theta_i - \bar{\theta} \right)^2 \right)^{0.5} \tag{8.1}$$

$$CV_\theta = \frac{\sigma_\theta}{\bar{\theta}} \tag{8.2}$$

where:

θ_i optimized parameter value
$\bar{\theta}$ mean of the optimized parameter
N_θ number of calibration trails (50 in the present study)

Parameter variability induced by spatial variability of rainfall for the Horb subcatchment is shown in Table 8.3. Coefficient of variation and standard deviation are numerical representations of the variability in the data. The results indicate that there is a high variation in the optimized parameters due to spatial variability of rainfall. The variations are more for some parameters than the others.

Table 8.3: Parameter variability induced by spatial variability of rainfall for the Horb subcatchment.

Parameters	Minimum	Maximum	Mean	σ_θ	CV_θ
FC	129.2	191.2	163.2	12.1	0.1
PWP	63.5	107.5	91.1	11.5	0.1
β	1.2	3.9	2.6	0.9	0.3
DD_0	1.1	2.3	1.4	0.4	0.3
T_{crit}	-0.8	0.8	0.1	0.5	9.8
L	0.9	8.4	2.2	2.1	1.0
K_0	6.2	12.5	9.4	1.6	0.2
K_1	6.2	34.4	20.5	7.7	0.4
K_2	155.1	252.9	199.3	23.3	0.1
K_{perc}	20.4	22.8	21.4	0.6	0.0

The study indicates that there can be a large uncertainty in the parameter estimation due to inadequate representation of spatial variability of precipitation (Figure 8.12).

It may be also interesting to investigate the optimized parameters as a vector. Figure 8.13 depicts ten selected parameter vectors resulted the similar model performance for the Horb subcatchment. Each parameter value was standardized with respect to its mean and standard deviation, defined as:

$$S_{\theta,i} = \left.\frac{\left(\theta_i - \overline{\theta}\right)}{\sigma_\theta}\right|_{i=1,\ldots,T_\theta} \tag{8.3}$$

where:

$S_{\theta,i}$	standardized value of a parameter
θ_i	parameter value
$\overline{\theta}$	mean of the parameter value
σ_θ	standard deviation of the parameter
T_θ	number of selected trails

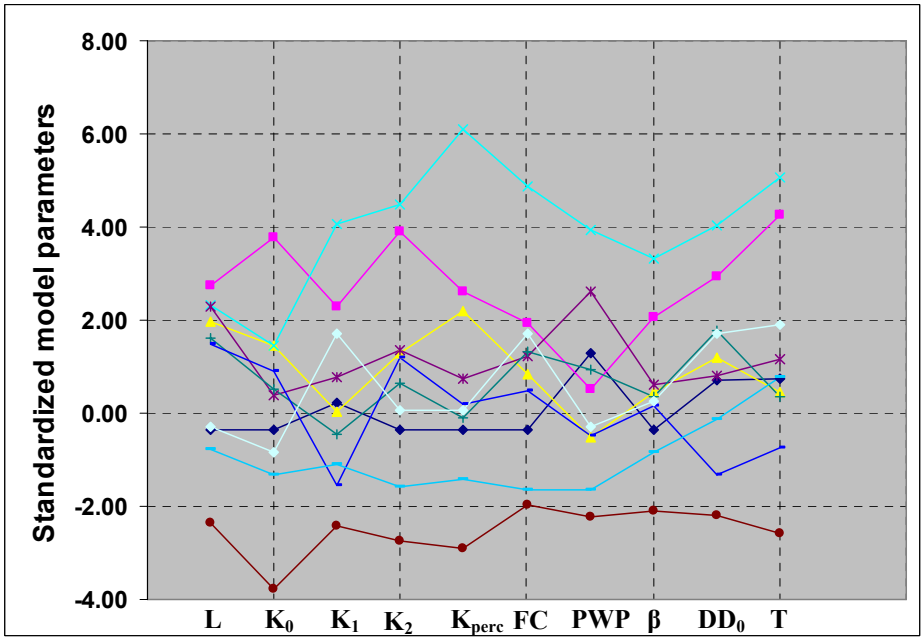

Figure 8.13: Standardized values of the optimized model parameters for the Horb subcatchment. Each line indicates each parameter vector.

The figure shows an interesting internal compensation among the model parameters. It can be noticed that for a particular parameter vector, one parameter can be low while the remaining parameters in that vector are compensating it resulting in a similar model performance.

8.5 Concluding remarks

In this chapter attempts was made to investigate the influence of the spatial representation of the precipitation input to the model simulation results and the uncertainty to identify the conceptual model parameters. This study was carried out using the physically-based spatially-distributed modeling system SHETRAN and the conceptual semi-distributed rainfall-runoff model HBV.

The results obtained by the SHETRAN and HBV models, using the conditionally-simulated precipitation, demonstrated that inadequate spatial variability of precipitation is partly responsible for modeling errors. The simulated discharges, using different realizations of simulated precipitation, exhibit a larger variability among the different realizations, particularly at the peak events. The study also indicated that inadequate representation of spatial variability of precipitation is partly responsible for the problems of parameter estimation. There can be a great uncertainty in the estimation of the model parameters due to the spatial variability of the precipitation. Thus spatial variability must be captured and used as an input to the hydrological model in order to eliminate the errors due to input rainfall data.

Parameter uncertainty comes into play when developing and validating a model. The results of this simulation experiment indicate that even in the case of physically-based distributed parameter models, uncertainty in the parameter estimates would be observed. This is because the input error may come from the spatial variability of rainfall.

The study also shows that it was not possible to achieve a better model performance at the catchment outlet when applying a complex physically-based spatially-distributed model instead of a conceptual simple model. Higher complexity did not provide better model performance. However, the major problem in this study was determination of areal precipitation for the SHETRAN model grid cells. Additionally, it is worth mentioning that parameter estimation method that was applied successfully for the conceptual model can not be applied for the physically based model. Because this automatic optimization algorithm requires a large number of model simulations to obtain the optimum solution. Nevertheless, the quality of the performance of the SHETRAN model was enough good to allow for further investigation.

9 Summary and Recommendations

9.1 Summary

The estimation and representation of the input precipitation in rainfall-runoff modeling are crucial. The importance of the spatial variability of precipitation in hydrological applications has been addressed to this dissertation. The research questions, posed in Chapter 1 and reiterated below, have motivated and guided the research.

a. How does the spatial variability of precipitation influence the hydrological simulation results?

b. Will a higher spatial resolution of model input data necessarily lead to a better model performance?

c. What is the impact on the simulated discharges of interpolated precipitation at different spatial resolutions through varying raingauge networks?

d. Is there any benefit of using conditionally-simulated precipitation in hydrological modeling?

The main objective of this study was to answer the above research questions. Supplementary objectives were: (1) to investigate the reliability of the parameters obtained from calibration over input data different from those used in model simulations and (2) to study the uncertainty in identifying the model parameters of a conceptual model due to uncertain precipitation.

Attempts made towards answering the above research queries are summarized in this chapter.

The theme of Chapter 4 was dedicated to investigate the influence of the spatial variability of precipitation on the predictive uncertainty of a conceptual rainfall-runoff model. The interpolated precipitation from point raingauge measurements and averaged precipitation over different spatial resolutions were used as a main forcing input into the model. The spatial scale ranges from 1 km^2 to 25 km^2. The distributed and semi-distributed structures of the conceptual rainfall-runoff model HBV were applied. The simulated hydrographs obtained using original interpolated precipitation and averaged precipitation were analyzed by comparison of their Nash-Sutcliffe coefficients and other goodness-of-fit indices. No significant differences were observed in the calibrated model performance using 1 km × 1 km grid precipitation and averaged precipitation at different spatial scales for either the distributed or semi-distributed model structure. However, minor differences were observed for peak discharge estimation. The study was then extended to identify the reliability of the parameters obtained from the calibration with a set of precipitation input for using in model simulations with a different set of precipitation input. In order to investigate this phenomenon, the semi-distributed model structure was calibrated using (a) the uniform precipitation obtained from

each subcatchment (Psubcatch) (b) the uniform precipitation obtained for the catchment (Pcatch) and (c) the precipitation for each zone (Pzone). The results indicate that there is significant deterioration in the model performance when the model calibrated using detailed precipitation (either Pzone or Psubcatch) is run using relatively less detailed precipitation (Pcatch). In contrast, minimal improvements of model performance are observed when the model calibrated using less detailed precipitation (Pcatch) is run with comparatively detailed precipitation data (either Pzone or Psubcatch).

An answer to the question 'Will a higher spatial resolution of model input data necessarily lead to a better model performance?' was explored in Chapter 5. Four different structures, namely fully lumped, semi-lumped, semi-distributed and distributed, of the HBV model were used to explore the solution to this question. The external drift kriging method (Ahmed and de Marsily, 1987) was applied to interpolate the meteorological varaiables from the available point measurements. The calibrations of the different model structures were carried out by means of the simulated annealing optimization algorithm. The simulated hydrographs obtained at the subcatchments' outlets using different model structures were analyzed through comparison of the computed Nash-Sutcliffe coefficients and other goodness-of-fit indices. The results indicate that for the study catchment, semi-distributed and semi-lumped model structures outperform the distributed and fully-lumped model structures under the given level of observations. The study indicates that using interpolated precipitation on finer resolution does not improve the simulation accuracy in either the calibration or validation periods. The results suggest that finer input data is not necessarily always better and the selection of the model structure should be guided by the principal of parsimony, purpose and nature of the available observation.

In Chapter 6, the impact on the simulated hydrographs of interpolated precipitation at different spatial resolutions through varying raingauge networks was studied. The optimal locations of a particular number of raingauges within a netwrok were determined by means of combinatorial algorithm simulated annealing (Aarts and Korst, 1989). The spatial representations of precipitation were estimated from the selected raingauge networks. The distributed and semi-distributed structures of the HBV model were then used to investigate the effect of the number of raingauges and their locations on the predictive uncertainty of the hydrological models. The analysis indicates that the number and spatial distribution of raingauges affect the simulation results. It has been found that the model performances worsen radically with an excessive reduction of raingauges. However, the performances were not significantly improved by increasing the number of raingauges more than a certain threshold number. The influence of the rainfall observation network on model calibration and application was also examined. The study seeks to determine whether the

parameters calibrated using the rainfall coming from one type of network have the ability to represent the phenomena governing the rainfall-runoff process with the input provided by a different configuration of the raingauge network. The semi-distributed structure of the HBV model was calibrated using interpolated precipitation produced from different raingauges network. The calibrated model was then run for the validation period using the precipitation obtained from the raingauges network which was not used for the calibration. The analysis indicates that models using different raingauge networks may need their parameters recalibrated. Specifically, models calibrated with dense precipitation information fail when run with sparse information. While, models calibrated with sparse information can perform well when run with dense information. Other experiments were carried out to analyze the reliability of supplementing missing precipitation measurements used for the calibration with data estimated using a multiple linear regression technique and running the model using that precipitation combined with observed precipitation. The results suggest that the model performs well both when calibrated with a complete set of observed precipitation and when run with an incomplete data set combined with estimated data. This finding offers an encouraging perspective for the implementation of such a procedure for an operational flood forecasting system. A last set of experiments was carried out to investigate the influence of temperature gauges on the model simulation results while keeping the number of raingauges constant. The results indicate that the temperature gauges influence the model simulation results, for the study catchment particularly in winter. However, this influence is relatively low compared to that introduced by the raingauges.

The benefits of using conditionally-simulated precipitation in hydrological modeling were described in chapter 7. The semi-distributed model structure of the HBV was calibrated using the interpolated precipitation. The calibrated model was then run using interpolated and conditionally-simulated precipitation in the validation period. Conditionally-simulated precipitation was generated using turning bands simulation and a Gaussian copula method. The comparison of the conditionally simulated precipitation and interpolated precipitation highlights that conditional spatial rainfall simulation indicates significantly more variability in the simulated rainfall. Moreover, the modeling performance using the mean of the conditional simulations was worse than that when using interpolated rainfall in the case of turning bands simulation and better in the case of simulation based on a Gaussian copula, if the whole period is considered. However, if only floods are considered, the model performance is found to be better using either type of simulated rainfall than the model using interpolated rainfall.

Attempts have been made to investigate the influence of the spatial representation of the precipitation input to the model simulation results and the uncertainty to identify the conceptual

model parameters in Chapter 8. This study was carried out using the physically-based hydrological model SHETRAN and the conceptual rainfall-runoff model HBV. Conditionally-simulated precipitation based on copula-based simulation was used as input precipitation to the SHETRAN and the HBV models. The simulated discharges by means of different realizations of the conditionally-simulated precipitation were analyzed to assess and quantify the uncertainty in the simulated discharges. The study was then extended to investigate the uncertainty to identify the parameters of the HBV model. The simulated discharges from SHETRAN were used as basis for calibrating the HBV model using the interpolated precipitation. The SHETRAN model was assumed, in this experiment, to represent the true copy of the prevailing hydrological system of the study catchment. It was considered that SHETRAN acts as a virtual catchment. The study indicated that inadequate representation of spatial variability of precipitation in modeling is partly responsible for modeling errors and also this leads to the problems in parameter estimation of a conceptual hydrological model.

9.2 Concluding remarks

A number of simulation experiments were carried out to investigate the impact of spatial variability of precipitation on the predictive uncertainty of hydrological models. The main findings are:

(1) No significant differences in the model performance are observed when the model is run using averaged precipitation at different spatial scales. However, there is clear deterioration in the model performance during the summer season. The results also indicate that there can be a significant deterioration in the model performance when the model calibrated using detailed precipitation is run using relatively less detailed precipitation. When the level of main forcing precipitation input is different for the model simulation than that used for calibration, one should be cautious.

(2) The study on the comparison of modeling performance using different representations of spatial variability indicates that for the present study catchment semi-distributed and semi-lumped model structures out-performs the distributed and lumped model structures for the given level of information. The study highlights that using interpolated rainfall on finer resolution does not improve the simulation accuracy in either the calibration or validation periods at the subcatchments' outlet. Perhaps there is a higher compensation for the bias in the rainfall input over the calibration period for the relatively simple model structures. Also, the error in representing spatial variability of precipitation in finer resolution is more and, perhaps, dominating the bias compensation in the rainfall input by

the calibration procedure for distributed model structure, even with the scope of large number of parameters to be adjusted.

(3) The study related to assess the impacts of raingauge density on the simulation results shows that the number and spatial distribution of raingauges affects the simulation results. It is found that the model performances worsen radically with an excessive reduction of raingauges. However, the performances are not significantly improved by increasing the number of raingauges more than a certain threshold number. The analysis also indicates that models using different raingauge networks might need their parameters recalibrated. Specifically, models calibrated with dense information fail when run with sparse information. However, the models calibrated with sparse information can perform well when run with dense information. Also, the model calibrated with complete set of observed precipitation and being run with incomplete observed data in associated with the data estimated using multiple linear regression technique at the locations treated as missing measurements, performed well. This result offers an encouraging perspective for the implementation of such a procedure for an operational flood forecasting system. Further research is needed in this direction to find the practical applicability.

(4) Conditional spatial rainfall simulation indicates significant more variability in the rainfall. The analysis also indicates that the model performs better for modeling the peak discharges using conditionally-simulated rainfall than the model using interpolated rainfall. Thus conditional rainfall simulation is reasonable for flood modeling. Application of Gaussian copulas for spatial rainfall simulation is very encouraging. The analysis also highlights that inadequate representation of spatial variability of precipitation is partly responsible for modeling errors and also this leads to the problems in parameter estimation of a conceptual hydrological model.

The study suggested that even in the case of physically-based distributed models, uncertainty in the model simulations would be observed. This is because the input error may come from the spatial variability of rainfall.

9.3 Recommendations for future works

Based on the investigations carried out during the different modeling experiments and the scope of the work presented in this dissertation, the following outlooks towards the direction of future work are suggested:

(1) Interpolated precipitation from the point raingauge measurements is used in this study. Further research can be directed to obtain a better perspective of the precipitation

integration on the predictive uncertainty of a rainfall-runoff model using radar rainfall data in addition to raingauge data.

(2) Considering the practical difficulties in applying a physically-based distributed hydrological model lumped models and lumped modeling experience can be fully exploited in a distributed modeling framework. The use of fully, spatially resolved radar rainfall data or a combination of radar-raingauge rainfall data may be used to re-examine the outcomes of the comparison of different model structures carried out in this study.

(3) Application of copulas for rainfall simulation was very encouraging. Non-Gaussian copulas can be used to generate conditionally-simulated rainfall as a future attempts.

(4) The research questions addressed in this study were analysed mainly through the application of the modified HBV model. The uncertainty in identifying the model parameters of a conceptual model due to uncertain precipitation was investigated using a dual rainfall-runoff modeling strategy through the application of the physically-based spatially-distributed modeling system SHETRAN and the conceptual rainfall-runoff model HBV. However, other models having different runoff generation mechanism may also be dealt with.

10 References

Aarts, E. and Korst, J. 1989. Simulated Annealing and Boltzmann Machines A Stochastic Approach to Combinatorial Optimization and Neural Computing. John Wiley & Sons, Inc., Chichester.

Abbott, M. B., Bathurst, J. C., Cunge, J. A., O'Connell, P. E., and Rasmussen, J. 1986a. An introduction to the European Hydrologic System-Systeme Hydrologique Europeen, SHE, 1: History and philosophy of a physically-based, distributed modelling system. *Journal of Hydrology*. 87, 45-59.

Abbott, M. B., Bathurst, J. C., Cunge, J. A., O'Connell, P. E., and Rasmussen, J. 1986b. An introduction to the European Hydrological System-Systeme Hydrologique Europeen, SHE, 2: Structure of a physically-based, distributed modelling system. *Journal of Hydrology*. 87, 61-77.

Ahmed, S. and de Marsily, G. 1987. Comparison of geostatistical methods for estimating transmissivity using data on transmissivity and specific capacity. *Water Resources Research*. 23(9), 1717-1737.

Allen, R.G., Pereira, L.S., Raes, D. and Smith, M. 1998. Crop Evapotranspiration-Guidelines for computing Crop Water Requirements. FAO Irrigation and Drainage Paper 56.

Arnaud, P., Bouvier, C., Cisneros, L. and Dominguez, R. 2002. Influence of rainfall spatial variability on flood prediction. *Journal of Hydrology*. 260, 216-230.

Atkinson, S., R. A. Woods and M. Sivapalan. 2002. Climate and landscape controls on water balance model complexity over changing time scales. *Water Resources Research*. 38(12), 1314, 50.1-50.17.

Atkinson, S., M. Sivapalan, R. A. Woods and N. R. Viney. 2003. Dominant physical controls of hourly streamflow predictions and an examination of the role of spatial variability: Mahurangi catchment, New Zealand. *Advances in Water Resources*. 26(2), 219-235.

Bathurst, J. C., Moretti, G., El-Hames, A., Moaven-Hashemi, A. and Burton, A. 2005. Scenario modelling of basin-scale, shallow landslide sediment yield, Valsassina, Italian Southern Alps. *Natural Hazards and Earth System Sciences*. 5: 189–202.

Bárdossy, A. and Plate, E. 1992. Space-Time Model for Daily Rainfall using Atmospheric Circulation Patterns. *Water Resources Research*. 28(5), 1247 - 1259.

Bárdossy, A., Hartmann and Giese, H. 1999. Impact of climate change on river basin hydrology under different climatic conditions. Final report CC-HYDRO.

Bárdossy, A. 2003. Concepts of geostatistics and stochastic modelling. Lecture notes, University of Stuttgart, Germany

Bárdossy, A. 2006. Copula based geostatistical models for groundwater quality parameters. *Water Resources Research*, accepted.

Bergström, S. and Forsman, A. 1973. Development of a conceptual deterministic rainfall-runoff model. *Nordic Hydrology*. 4: 174-170.

Bergström, S., 1995. The HBV model. In: Singh, V. (Ed.), Computer Models of Watershed Hydrology. Water Resources Pub., 443–476.

Beven, K.J. and Hornberger, G.M. 1982. Assessing the effect of spatial pattern of precipitation in modeling streamflow hydrographs. *Water Resources Bulletin*. 18, 823-829.

Beven, K.J. 1989. Changing ideas in Hydrology: the case of Physically-based models. *Journal of Hydrology*. 105: 157-172.

Beven, K.J. 2001. Rainfall-Runoff Modelling: The Primer. John Wiley and Sons, Chichester.

Blaney, H.F. and Criddle, W.D. 1950. Determining water requirements in irrigation areas from climatological and irrigation data. USDA, SCS-TP 96.

Brath, A., Montanari, A. and Toth E. 2004. Analysis of the effects of different scenarios of historical data availability on the calibration of a spatially-distributed hydrological model. *Journal of Hydrology*. 291, 232-253.

Butts, M.B., Jeffrey T. Paynea, Michael Kristensen and Henrik Madsen. 2004. An evaluation of the impact of model structure on hydrological modelling uncertainty for streamflow simulation. *Journal of Hydrology*. 298, 242-266.

Chaubey, I., Hann, C.T., Grunwald, S. and Salisbury, J.M. 1999. Uncertainty in the models parameters due to spatial variability of rainfall. *Journal of Hydrology*. 220, 46-61.

Collier, C. 1989. Applications of Weather Radar Systems. Ellis Horwood Limited, Chichester.

Das, T., Bárdossy, A. and Zehe, E. 2006. Influence of spatial variability of precipitation on distributed rainfall-runoff modeling. PUB: Promise and Progress, M. Sivapalan, T. Wagener, S. Uhlenbrook, E. Zehe, V. Lakshmi, X. Liang, Y. Tachikawa & P. Kumar (Editors), IAHS Publication 303.

Deutsch, C.V. and Journel, A.G. 1992. GSLIB: Geostatistical Software Library and User's Guide. Oxford University Press, Oxford, New York.

Dibike, Y. B. and Coulibaly, P. 2005. Hydrologic Impact of Climate Change in the Saguenay Watershed: Comparison of Downscaling Methods and Hydrologic Models. *Journal of Hydrology*. 307, 145-163.

Dong, X., Dohmen-Janssen C. M., and Booij M.J. 2005. Appropriate Spatial Sampling of Rainfall or Flow Simulation. *Hydrological Sciences Journal*. 50(2), 279-297.

Duan, Q.Y., Gupta, V.K. and Sorooshian, S. 1993a. Shuffled complex evolution approach for effective and efficient optimization. *Journal of Optimization Theory and Applications*. 76(3), 501-521.

Duan, Q.Y., Sorooshian, S. and Gupta, V.K. 1993b. Optimal use of the SCE-UA global optimization method for calibrating watershed models. *Journal of Hydrology*. 158, 265-284.

Duncan, M.R., Austin, B., Fabry, F. and Austin, G.L. 1993. The effect of gauge sampling density on the accuracy of stream flow prediction for rural catchments. *Journal of Hydrology*. 142, 445-476.

Ehret, U. 2002. Rainfall and Flood Nowcasting in Small Catchments using Weather Radar. Doctoral Thesis, submitted to University of Stuttgart, Germany.

Ewen J., Parkin G. and O'Connell P.E. 2000. SHETRAN: distributed river basin flow and transport modeling system. *Journal of Hydrologic Engineering*. 5: 250-258.

Farmer D, Sivapalan, M. and Jothityangkoon, C. 2003. Climate, soil, and vegetation controls upon the variability of water balance in temperate and semiarid landscapes: Downward approach to water balance analysis. *Water Resources Research*. 39(2): 1035.

Finnerty, B. D., Smith, M. B., Seo, D .J., Koren, V. and Moglen, G. E. 1997. Space-time scale sensitivity of the Sacramento model to radar-gage precipitation inputs. *Journal of Hydrology*. 203, 21-38.

Freeze, R.A. and Harlan, R.L. 1969. Blueprint for a physically-based digitally-simulated hydrological response model. *Journal of Hydrology*. 9, 237-258.

Goovaerts, P. 1997.Geostatistics for Natural Resources Evalution. Oxford University Press, New York, Oxford.

Goovaerts, P. 2000. Geostatistical approaches for incorporating elevation into spatial interpolation of rainfall. *Journal of Hydrology*. 228, 113-129.

Götzinger, J. and Bárdossy, A. 2005. Integration and calibration of a conceptual rainfall-runoff model in the framework of a decision support system for river basin management. *Advances in Geosciences*. 5, 31–35.

Grayson, R.B. and Blöschl, G. (Eds.), 2000. Spatial Patterns in Catchment Hydrology: Observations and Modeling. Cambridge University Press, Cambridge, UK.

Gyasi-Agyei, Y. 2005. Stochastic disaggregation of daily rainfall into one-hour time scale. *Journal of Hydrology*. 309, 178-190.

Haberlandt, U. and Gattke, C. 2004. Spatial interpolation v. Simulation of precipitation for rainfall-runoff modelling – a case study in the Lippe river basin. Hydrology: Science & Practice for the 21st Century (Vol. 1).

Hartmann, G. and Bárdossy, A. 2005. Investigation of the uncertainty of hydrological modeling for climate change impact assessment. Regional Hydrological Impacts of Climatic Change - Impact Assessment and Decision Making, Editor: Wagener, Thorsten & Stewart Franks, IAHS Redbook, Publ. 295.

Hargreaves, G.H. and Samani Z. A. 1985. Reference crop evapotranspiration from temperature. *Applied Engr. Agric.* 1:96-99.

Hargreaves, G., H. 1994. Defining and using reference evapotranspiration. *Journal of Irrigation and Drainage Engineering, ASCE*. 120(6): 1132-1139.

Hundecha, Y., 2005. Regionalization of parameters of a conceptual rainfall runoff model. Doctoral Thesis, submitted to University of Stuttgart, Germany

Hundecha, Y. and Bárdossy, A. 2004. Modeling of the effect of land use changes on the runoff generation of a river basin through parameter regionalization of a watershed model. *Journal of Hydrology*. 292, 281–295.

Kirkpatrick, S., C.D.Gelatt, and M.P.Vecchi. 1983. Optimization by simulated annealing. *Science*. 220, 671-680.

Kokkonen T. S. and Jakeman A. J. 2001. A comparison of metric and conceptual approaches in rainfall-runoff modeling and its implications. *Water Resources Research*. 37(9), 2345-2352.

Koren, V.I., B.D. Finnerty, J.C. Schaake, M.B.Smith, D.-J.Seo, and Q.-Y. Duan. 1999. Scale dependencies of hydrologic models to spatial variability of precipitation. *Journal of Hydrology*. 217(3-4), 285-302.

Kottegoda, N.T. and Kassim, A.H.M. 1991. The turning bands method with the fats-Fourier transform as an aid to the determination of storm movement. *Journal of Hydrology*. 127, 55-69.

Krajewski, W.F., Lakshimi, V., Georgakakos, K.P. and Jain, S.C. 1991. A monte carlo study of rainfall sampling effect on a distributed catchment model. *Water Resources Research*. 27 (1), 119-128.

Kuczera, G. and Williams, B.J. 1992. Effect of rainfall errors on accuracy of design flood estimates. *Water Resources Research*. 28(4), 1145-1153.

Lee, H., McIntyre, N., Wheater, H. and Young, A. 2005. Selection of conceptual models for regionalisation of the rainfall-runoff relationship. *Journal of Hydrology*. 312, 109–124.

Liang, X., Guo, J. and Leung L.R. 2004. Assessment of the effects of spatial resolutions on daily water flux simulations. *Journal of Hydrology*. 298, 287-310.

Lindström, G., Johansson, B., Persson, M., Gardelin, M. and Bergström, S. 1997. Development and test of the distributed HBV-96 hydrological model. *Journal of Hydrology*. 201, 272 - 288.

Lukey, B. T., Sheffield, J., Bathurst, J. C., Hiley, R. A. and Mathys, M. 2000. Test of the SHETRAN technology for modelling the impact of reforestation on badlands runoff and sediment yield at Draix, France. *Journal of Hydrology.* 235, 44-62.

Madsen, H. 2000. Automatic calibration of a conceptual rainfall-runoff model using multiple objectives. *Journal of Hydrology*. 235, 276-288.

Mantoglou, A. and Wilson, J.L. 1982. The Turning Bands Method for Simulation of Random Fields Using Line Generation by a Spectral Method. *Water Resources Research*. 18(5), 1379-1394.

Matheron G. 1973. The intrinsic random functions and their applications. *Advances in Applied Probability*. 5, 439-468.

Merritt, W.S., Younes, A., Mark, B., Bill, T., Stewart C. and Denise N. 2006. Hydrologic response to scenarios of climate change in subwatersheds of the Okanagan basin, British Columbia. *Journal of Hydrology*. 326, 79-108.

Metropolis, N., A. Rosenbluth, M. Rosenbluth, A. Teller and E. Teller. 1953. Equation of State Calculations by Fast Computing Machines. *Journal of Chemical Physics*. 21(6), 1087-1092.

Monteith, J.L. 1965. Evaporation and environment. In: The state and movement of water in living organisms. G. T. Fogy (Editor), Proceedings of the 19th Symposium, Society of Experimental Biology, Cambridge University Press, London, 205-234.

Montgomery, D. C. and E. A. Peck. 1982. Introduction to linear regression analysis. John Wiley and Sons, New York, New York, USA.

Mutzner, H. 1991. The significance of areal rainfall distribution for flows from a very small urban drainage catchment. *Atmospheric Research*. 27, 99-107.

Nash, J. E. and Sutcliffe, J. V. 1970. River flow forecasting through conceptual models. Part I. A discussion of principles. *Journal of Hydrology*. 10, 282-290.

Niemczynowicz, J. 1991. On the storm movement and its implications. *Atmospheric Research*. 27, 109-127.

Obled, C.H., Wendling, J. and Beven, K. 1994. The sensitivity of hydrological models to spatial rainfall patterns: an evaluation using observed data. *Journal of Hydrology*. 159, 305-333.

Ogden, F.A. and Julien, P.Y. 1994. Runoff model sensitivity to radar rainfall resolution. *Journal of Hydrology*. 158, 1-18.

O'Loughlin, G., Huber, W., and Chocat, B. 1996. Rainfall-runoff processes and modelling. *Journal of Hydraulic Research*. 34, 6, 733–751.

Parkin, G., Ewen, J. and O'Connell, P. E. 2000. SHETRAN: a coupled surface/subsurface modelling system for 3D water flow and sediment and solute transport in river basins. ASCE *Journal of Hydrologic Engineering*. 5, 250-258.

Reed S., Koren V., Smith M., Zhang Z., Moreda F., Seo D.-J. and DMIP participants. 2004. Overall distributed model intercomparison project results. *Journal of Hydrology*. 298 (1-4): 27-60.

Refsgaard, J.C., and J. Knudsen. 1996. Operational validation and intercomparisons of different types of hydrological models. *Water Resources Research*. 32(7), 2189-2202.

Samaniego, L. 2003. Hydrological consequences of landuse/land cover and climatic changes in mesoscale catchments. Doctoral Thesis, submitted to University of Stuttgart, Germany.

Schilling, W. and Fuchs, L. 1986. Errors in stormwater modeling – a quantitative assessment. *ASCE Journal of Hydraulic Engineering*. 102 (2), 111-123.

Seibert, J. 1997. Estimation of Parameter Uncertainty in the HBV Model. *Nordic Hydrology*. 28(4/5): 247-262.

Seibert, J. 2000. Multi-criteria calibration of a conceptual runoff model using a genetic algorithm. *Hydrology and Earth system Sciences*. 4(2), 215-224.

Sieber, A., and Uhlenbrook, S. 2005. Sensitivity analyses of a distributed catchment model to verify the model structure. *Journal of Hydrology*. 310, 216-235.

Shah, S.M.S., O'Donnell, P.E. and Hosking, J.R.M. 1996. Modeling the effects of spatial variability in rainfall on catchment response 2: experiments with distributed and lumped models. *Journal of Hydrology*. 175, 89-111.

Smith M.B., Victor I. Koren, Ziya Zhang, Seann M. Reed, Jeng-J. Pan and Fekadu Moreda. 2004a. Runoff response to spatial variability in precipitation: an analysis of observed data. *Journal of Hydrology*. 298, 267-286.

Smith, M. B., D.-J. Seo, V. I. Koren, S. M. Reed, Z. Zhang, Q. Duan, F. Moreda, and S. Cong. 2004b. The distributed model intercomparison project (DMIP): motivation and experiment design. *Journal of Hydrology*. 298, 4-26.

St-Hilarie, A., Ouarda, T.B.M.J., Lachance, M., Bobée, B., Gaudet, J. and Gibnac, C. 2003. Assessment of the impact of meteorological network density on the estimation of basin precipitation and runoff: a case study. *Hydrological Processes.* 17(18), 3561-3580.

Stehlik, J. and Bárdossy, A. 2002. Multivariate stochastic downscaling model for generating daily Rainfall series based on atmospheric circulation. *Journal of Hydrology*. 256, 120–141.

Syed, K. H., Goodrich, D. C., Myers, D. E., and Sorooshian, S. 2003. Spatial characteristics of thunderstorm rainfall fields and their relation to runoff. *Journal of Hydrology*. 271, 1–21.

Toth, E. and Brath, A. 2003. Use of spatially-distributed or lumped precipitation inputs in conceptual and black-box models for runoff forecasting. Proceedings of the ESF LESC exploratory workshop held at Bologna, Italy, October 24-25 2003, 197-211.

Uhlenbrook, S., Roser, S. and Tilch, N. 2004. Hydrological process representation at the meso-scale: the potential of a distributed, conceptual catchment model. *Journal of Hydrology*. 291, 278-296.

Vieux, B.E. 2001. Distributed Hydrologic Modeling using GIS. Water Science and Technology Library, Volume 38.

Winchell, M., Gupta, V.H. and Sorooshian, S. 1998. On the simulation of infiltration and saturation excess runoff using radar-based rainfall estimates: effects of algorithm uncertainty and pixel aggregation. *Water Resources Research*. 34(19), 2655-2670.

Wood, E.F. 1976. An analysis of the effects of parameter uncertainty in deterministic hydrologic models. *Water Resources Research*. 12 (5), 925-932.

Yapo P. O., H. V. Gupta, and S. Sorooshian. 1996. Automatic Calibration of Conceptual Rainfall-Runoff models: Sensitivity to Calibration Data. *Journal of Hydrology*. 181:23-48.

Zehe, E., Becker, R., Bárdossy, A. and Plate, E. 2005. Uncertainty of simulated catchment runoff response in the presence of threshold processes: role of initial soil moisture and precipitation. *Journal of Hydrology*. 315 (1-4):183-202.

Institut für Wasserbau
Universität Stuttgart

Pfaffenwaldring 61
70569 Stuttgart (Vaihingen)
Telefon (0711) 685 - 64717/64741/64752/64679
Telefax (0711) 685 - 67020 o. 64746 o. 64681
E-Mail: iws@iws.uni-stuttgart.de
http://www.iws.uni-stuttgart.de

Direktoren
Prof. Dr. rer. nat. Dr.-Ing. András Bárdossy
Prof. Dr.-Ing. Rainer Helmig
Prof. Dr.-Ing. Silke Wieprecht

Vorstand *(Stand 31.10.2006)*
Prof. Dr. rer. nat. Dr.-Ing. A. Bárdossy
Prof. Dr.-Ing. R. Helmig
Prof. Dr.-Ing. S. Wieprecht
Prof. Dr.-Ing. habil. B. Westrich
Jürgen Braun, PhD
Dr.-Ing. H. Class
Dr.-Ing. A. Färber
Dr.-Ing. H.-P. Koschitzky
PD Dr.-Ing. W. Marx

Emeriti
Prof. Dr.-Ing. Dr.-Ing. E.h. Jürgen Giesecke
Prof. Dr.h.c. Dr.-Ing. E.h. Helmut Kobus, Ph.D.

Lehrstuhl für Wasserbau und Wassermengenwirtschaft
Leiter: Prof. Dr.-Ing. Silke Wieprecht
Stellv.: PD Dr.-Ing. Walter Marx, AOR

Lehrstuhl für Hydrologie und Geohydrologie
Leiter: Prof. Dr. rer. nat. Dr.-Ing. András Bárdossy
Stellv.: Dr.-Ing. Arne Färber

Lehrstuhl für Hydromechanik und Hydrosystemmodellierung
Leiter: Prof. Dr.-Ing. Rainer Helmig
Stellv.: Dr.-Ing. Holger Class, AOR

***VEGAS,* Versuchseinrichtung zur Grundwasser- und Altlastensanierung**
Leitung: Jürgen Braun, PhD
Dr.-Ing. Hans-Peter Koschitzky, AD

Versuchsanstalt für Wasserbau
Leiter: apl. Prof. Dr.-Ing. Bernhard Westrich

Verzeichnis der Mitteilungshefte

5 Plate, Erich: *Beitrag zur Bestimmung der Windgeschwindigkeitsverteilung in der durch eine Wand gestörten bodennahen Luftschicht*,
und
Röhnisch, Arthur; Marotz, Günter: *Neue Baustoffe und Bauausführungen für den Schutz der Böschungen und der Sohle von Kanälen, Flüssen und Häfen; Gestehungskosten und jeweilige Vorteile*, sowie Unny, T.E.: *Schwingungsuntersuchungen am Kegelstrahlschieber*, 1967

6 Seiler, Erich: *Die Ermittlung des Anlagenwertes der bundeseigenen Binnenschiffahrtsstraßen und Talsperren und des Anteils der Binnenschiffahrt an diesem Wert*, 1967

7 *Sonderheft anläßlich des 65. Geburtstages von Prof. Arthur Röhnisch mit Beiträgen von* Benk, Dieter; Breitling, J.; Gurr, Siegfried; Haberhauer, Robert; Honekamp, Hermann; Kuz, Klaus Dieter; Marotz, Günter; Mayer-Vorfelder, Hans-Jörg; Miller, Rudolf; Plate, Erich J.; Radomski, Helge; Schwarz, Helmut; Vollmer, Ernst; Wildenhahn, Eberhard; 1967

8 Jumikis, Alfred: *Beitrag zur experimentellen Untersuchung des Wassernachschubs in einem gefrierenden Boden und die Beurteilung der Ergebnisse*, 1968

9 Marotz, Günter: *Technische Grundlagen einer Wasserspeicherung im natürlichen Untergrund*, 1968

10 Radomski, Helge: *Untersuchungen über den Einfluß der Querschnittsform wellenförmiger Spundwände auf die statischen und rammtechnischen Eigenschaften*, 1968

11 Schwarz, Helmut: *Die Grenztragfähigkeit des Baugrundes bei Einwirkung vertikal gezogener Ankerplatten als zweidimensionales Bruchproblem*, 1969

12 Erbel, Klaus: *Ein Beitrag zur Untersuchung der Metamorphose von Mittelgebirgsschneedecken unter besonderer Berücksichtigung eines Verfahrens zur Bestimmung der thermischen Schneequalität*, 1969

13 Westhaus, Karl-Heinz: *Der Strukturwandel in der Binnenschiffahrt und sein Einfluß auf den Ausbau der Binnenschiffskanäle*, 1969

14 Mayer-Vorfelder, Hans-Jörg: *Ein Beitrag zur Berechnung des Erdwiderstandes unter Ansatz der logarithmischen Spirale als Gleitflächenfunktion*, 1970

15 Schulz, Manfred: *Berechnung des räumlichen Erddruckes auf die Wandung kreiszylindrischer Körper*, 1970

16 Mobasseri, Manoutschehr: *Die Rippenstützmauer. Konstruktion und Grenzen ihrer Standsicherheit*, 1970

17 Benk, Dieter: *Ein Beitrag zum Betrieb und zur Bemessung von Hochwasserrückhaltebecken*, 1970

18 Gàl, Attila: *Bestimmung der mitschwingenden Wassermasse bei überströmten Fischbauchklappen mit kreiszylindrischem Staublech*, 1971, vergriffen

19 Kuz, Klaus Dieter: *Ein Beitrag zur Frage des Einsetzens von Kavitationserscheinungen in einer Düsenströmung bei Berücksichtigung der im Wasser gelösten Gase*, 1971, vergriffen

20 Schaak, Hartmut: *Verteilleitungen von Wasserkraftanlagen*, 1971

21 *Sonderheft zur Eröffnung der neuen Versuchsanstalt des Instituts für Wasserbau der Universität Stuttgart mit Beiträgen von*
Brombach, Hansjörg; Dirksen, Wolfram; Gàl, Attila; Gerlach, Reinhard; Giesecke, Jürgen; Holthoff, Franz-Josef; Kuz, Klaus Dieter; Marotz, Günter; Minor, Hans-Erwin; Petrikat, Kurt; Röhnisch, Arthur; Rueff, Helge; Schwarz, Helmut; Vollmer, Ernst; Wildenhahn, Eberhard; 1972

22 Wang, Chung-su: *Ein Beitrag zur Berechnung der Schwingungen an Kegelstrahlschiebern*, 1972

23 Mayer-Vorfelder, Hans-Jörg: *Erdwiderstandsbeiwerte nach dem Ohde-Variationsverfahren*, 1972

24 Minor, Hans-Erwin: *Beitrag zur Bestimmung der Schwingungsanfachungsfunktionen überströmter Stauklappen*, 1972, vergriffen

25 Brombach, Hansjörg: *Untersuchung strömungsmechanischer Elemente (Fluidik) und die Möglichkeit der Anwendung von Wirbelkammerelementen im Wasserbau*, 1972, vergriffen

26 Wildenhahn, Eberhard: *Beitrag zur Berechnung von Horizontalfilterbrunnen*, 1972

27 Steinlein, Helmut: *Die Eliminierung der Schwebstoffe aus Flußwasser zum Zweck der unterirdischen Wasserspeicherung, gezeigt am Beispiel der Iller*, 1972

28 Holthoff, Franz Josef: *Die Überwindung großer Hubhöhen in der Binnenschiffahrt durch Schwimmerhebewerke*, 1973

29 Röder, Karl: *Einwirkungen aus Baugrundbewegungen auf trog- und kastenförmige Konstruktionen des Wasser- und Tunnelbaues*, 1973

30 Kretschmer, Heinz: *Die Bemessung von Bogenstaumauern in Abhängigkeit von der Talform*, 1973

31 Honekamp, Hermann: *Beitrag zur Berechnung der Montage von Unterwasserpipelines*, 1973

32 Giesecke, Jürgen: *Die Wirbelkammertriode als neuartiges Steuerorgan im Wasserbau*, und Brombach, Hansjörg: *Entwicklung, Bauformen, Wirkungsweise und Steuereigenschaften von Wirbelkammerverstärkern*, 1974

33 Rueff, Helge: *Untersuchung der schwingungserregenden Kräfte an zwei hintereinander angeordneten Tiefschützen unter besonderer Berücksichtigung von Kavitation*, 1974

34 Röhnisch, Arthur: *Einpreßversuche mit Zementmörtel für Spannbeton - Vergleich der Ergebnisse von Modellversuchen mit Ausführungen in Hüllwellrohren*, 1975

35 *Sonderheft anläßlich des 65. Geburtstages von Prof. Dr.-Ing. Kurt Petrikat mit Beiträgen von*: Brombach, Hansjörg; Erbel, Klaus; Flinspach, Dieter; Fischer jr., Richard; Gàl, Attila; Gerlach, Reinhard; Giesecke, Jürgen; Haberhauer, Robert; Hafner Edzard; Hausenblas, Bernhard; Horlacher, Hans-Burkhard; Hutarew, Andreas; Knoll, Manfred; Krummet, Ralph; Marotz, Günter; Merkle, Theodor; Miller, Christoph; Minor, Hans-Erwin; Neumayer, Hans; Rao, Syamala; Rath, Paul; Rueff, Helge; Ruppert, Jürgen; Schwarz, Wolfgang; Topal-Gökceli, Mehmet; Vollmer, Ernst; Wang, Chung-su; Weber, Hans-Georg; 1975

36 Berger, Jochum: *Beitrag zur Berechnung des Spannungszustandes in rotationssymmetrisch belasteten Kugelschalen veränderlicher Wandstärke unter Gas- und Flüssigkeitsdruck durch Integration schwach singulärer Differentialgleichungen*, 1975

37 Dirksen, Wolfram: *Berechnung instationärer Abflußvorgänge in gestauten Gerinnen mittels Differenzenverfahren und die Anwendung auf Hochwasserrückhaltebecken*, 1976

38 Horlacher, Hans-Burkhard: *Berechnung instationärer Temperatur- und Wärmespannungsfelder in langen mehrschichtigen Hohlzylindern*, 1976

39 Hafner, Edzard: *Untersuchung der hydrodynamischen Kräfte auf Baukörper im Tiefwasserbereich des Meeres*, 1977, ISBN 3-921694-39-6

40 Ruppert, Jürgen: *Über den Axialwirbelkammerverstärker für den Einsatz im Wasserbau*, 1977, ISBN 3-921694-40-X

41 Hutarew, Andreas: *Beitrag zur Beeinflußbarkeit des Sauerstoffgehalts in Fließgewässern an Abstürzen und Wehren*, 1977, ISBN 3-921694-41-8, vergriffen

42 Miller, Christoph: *Ein Beitrag zur Bestimmung der schwingungserregenden Kräfte an unterströmten Wehren*, 1977, ISBN 3-921694-42-6

43 Schwarz, Wolfgang: *Druckstoßberechnung unter Berücksichtigung der Radial- und Längsverschiebungen der Rohrwandung*, 1978, ISBN 3-921694-43-4

44 Kinzelbach, Wolfgang: *Numerische Untersuchungen über den optimalen Einsatz variabler Kühlsysteme einer Kraftwerkskette am Beispiel Oberrhein*, 1978, ISBN 3-921694-44-2

45 Barczewski, Baldur: *Neue Meßmethoden für Wasser-Luftgemische und deren Anwendung auf zweiphasige Auftriebsstrahlen*, 1979, ISBN 3-921694-45-0

46 Neumayer, Hans: *Untersuchung der Strömungsvorgänge in radialen Wirbelkammerverstärkern*, 1979, ISBN 3-921694-46-9

47 Elalfy, Youssef-Elhassan: *Untersuchung der Strömungsvorgänge in Wirbelkammerdioden und -drosseln*, 1979, ISBN 3-921694-47-7

48 Brombach, Hansjörg: *Automatisierung der Bewirtschaftung von Wasserspeichern*, 1981, ISBN 3-921694-48-5

49 Geldner, Peter: *Deterministische und stochastische Methoden zur Bestimmung der Selbstdichtung von Gewässern*, 1981, ISBN 3-921694-49-3, vergriffen

50 Mehlhorn, Hans: *Temperaturveränderungen im Grundwasser durch Brauchwassereinleitungen*, 1982, ISBN 3-921694-50-7, vergriffen

51 Hafner, Edzard: *Rohrleitungen und Behälter im Meer*, 1983, ISBN 3-921694-51-5

52 Rinnert, Bernd: *Hydrodynamische Dispersion in porösen Medien: Einfluß von Dichteunterschieden auf die Vertikalvermischung in horizontaler Strömung*, 1983, ISBN 3-921694-52-3, vergriffen

53 Lindner, Wulf: *Steuerung von Grundwasserentnahmen unter Einhaltung ökologischer Kriterien*, 1983, ISBN 3-921694-53-1, vergriffen

54 Herr, Michael; Herzer, Jörg; Kinzelbach, Wolfgang; Kobus, Helmut; Rinnert, Bernd: *Methoden zur rechnerischen Erfassung und hydraulischen Sanierung von Grundwasserkontaminationen*, 1983, ISBN 3-921694-54-X

55 Schmitt, Paul: *Wege zur Automatisierung der Niederschlagsermittlung*, 1984, ISBN 3-921694-55-8, vergriffen

56 Müller, Peter: *Transport und selektive Sedimentation von Schwebstoffen bei gestau tem Abfluß*, 1985, ISBN 3-921694-56-6

57 El-Qawasmeh, Fuad: *Möglichkeiten und Grenzen der Tropfbewässerung unter besonderer Berücksichtigung der Verstopfungsanfälligkeit der Tropfelemente*, 1985, ISBN 3-921694-57-4, vergriffen

58 Kirchenbaur, Klaus: *Mikroprozessorgesteuerte Erfassung instationärer Druckfelder am Beispiel seegangsbelasteter Baukörper*, 1985, ISBN 3-921694-58-2

59 Kobus, Helmut (Hrsg.): *Modellierung des großräumigen Wärme- und Schadstofftransports im Grundwasser*, Tätigkeitsbericht 1984/85 (DFG-Forschergruppe an den Universitäten Hohenheim, Karlsruhe und Stuttgart), 1985, ISBN 3-921694-59-0, vergriffen

60 Spitz, Karlheinz: *Dispersion in porösen Medien: Einfluß von Inhomogenitäten und Dichteunterschieden*, 1985, ISBN 3-921694-60-4, vergriffen

61 Kobus, Helmut: *An Introduction to Air-Water Flows in Hydraulics,* 1985, ISBN 3-921694-61-2

62 Kaleris, Vassilios: *Erfassung des Austausches von Oberflächen- und Grundwasser in horizontalebenen Grundwassermodellen,* 1986, ISBN 3-921694-62-0

63 Herr, Michael: *Grundlagen der hydraulischen Sanierung verunreinigter Porengrundwasserleiter,* 1987, ISBN 3-921694-63-9

64 Marx, Walter: *Berechnung von Temperatur und Spannung in Massenbeton infolge Hydratation,* 1987, ISBN 3-921694-64-7

65 Koschitzky, Hans-Peter: *Dimensionierungskonzept für Sohlbelüfter in Schußrinnen zur Vermeidung von Kavitationsschäden,* 1987, ISBN 3-921694-65-5

66 Kobus, Helmut (Hrsg.): *Modellierung des großräumigen Wärme- und Schadstofftransports im Grundwasser,* Tätigkeitsbericht 1986/87 (DFG-Forschergruppe an den Universitäten Hohenheim, Karlsruhe und Stuttgart) 1987, ISBN 3-921694-66-3

67 Söll, Thomas: *Berechnungsverfahren zur Abschätzung anthropogener Temperaturanomalien im Grundwasser,* 1988, ISBN 3-921694-67-1

68 Dittrich, Andreas; Westrich, Bernd: *Bodenseeufererosion, Bestandsaufnahme und Bewertung,* 1988, ISBN 3-921694-68-X, vergriffen

69 Huwe, Bernd; van der Ploeg, Rienk R.: *Modelle zur Simulation des Stickstoffhaushaltes von Standorten mit unterschiedlicher landwirtschaftlicher Nutzung,* 1988, ISBN 3-921694-69-8, vergriffen

70 Stephan, Karl: *Integration elliptischer Funktionen,* 1988, ISBN 3-921694-70-1

71 Kobus, Helmut; Zilliox, Lothaire (Hrsg.): *Nitratbelastung des Grundwassers, Auswirkungen der Landwirtschaft auf die Grundwasser- und Rohwasserbeschaffenheit und Maßnahmen zum Schutz des Grundwassers.* Vorträge des deutsch-französischen Kolloquiums am 6. Oktober 1988, Universitäten Stuttgart und Louis Pasteur Strasbourg (Vorträge in deutsch oder französisch, Kurzfassungen zweisprachig), 1988, ISBN 3-921694-71-X

72 Soyeaux, Renald: *Unterströmung von Stauanlagen auf klüftigem Untergrund unter Berücksichtigung laminarer und turbulenter Fließzustände,*1991,ISBN 3-921694-72-8

73 Kohane, Roberto: *Berechnungsmethoden für Hochwasserabfluß in Fließgewässern mit überströmten Vorländern,* 1991, ISBN 3-921694-73-6

74 Hassinger, Reinhard: *Beitrag zur Hydraulik und Bemessung von Blocksteinrampen in flexibler Bauweise,* 1991, ISBN 3-921694-74-4, vergriffen

75 Schäfer, Gerhard: *Einfluß von Schichtenstrukturen und lokalen Einlagerungen auf die Längsdispersion in Porengrundwasserleitern,* 1991, ISBN 3-921694-75-2

76 Giesecke, Jürgen: *Vorträge, Wasserwirtschaft in stark besiedelten Regionen; Umweltforschung mit Schwerpunkt Wasserwirtschaft,* 1991, ISBN 3-921694-76-0

77 Huwe, Bernd: *Deterministische und stochastische Ansätze zur Modellierung des Stickstoffhaushalts landwirtschaftlich genutzter Flächen auf unterschiedlichem Skalenniveau,* 1992, ISBN 3-921694-77-9, vergriffen

78 Rommel, Michael: *Verwendung von Kluftdaten zur realitätsnahen Generierung von Kluftnetzen mit anschließender laminar-turbulenter Strömungsberechnung,* 1993, ISBN 3-92 1694-78-7

79 Marschall, Paul: *Die Ermittlung lokaler Stofffrachten im Grundwasser mit Hilfe von Einbohrloch-Meßverfahren,* 1993, ISBN 3-921694-79-5, vergriffen

80 Ptak, Thomas: *Stofftransport in heterogenen Porenaquiferen: Felduntersuchungen und stochastische Modellierung,* 1993, ISBN 3-921694-80-9, vergriffen

81 Haakh, Frieder: *Transientes Strömungsverhalten in Wirbelkammern,* 1993, ISBN 3-921694-81-7

82 Kobus, Helmut; Cirpka, Olaf; Barczewski, Baldur; Koschitzky, Hans-Peter: *Versuchseinrichtung zur Grundwasser und Altlastensanierung VEGAS, Konzeption und Programmrahmen,* 1993, ISBN 3-921694-82-5

83 Zang, Weidong: *Optimaler Echtzeit-Betrieb eines Speichers mit aktueller Abflußregenerierung,* 1994, ISBN 3-921694-83-3, vergriffen

84 Franke, Hans-Jörg: *Stochastische Modellierung eines flächenhaften Stoffeintrages und Transports in Grundwasser am Beispiel der Pflanzenschutzmittelproblematik,* 1995, ISBN 3-921694-84-1

85 Lang, Ulrich: *Simulation regionaler Strömungs- und Transportvorgänge in Karstaquiferen mit Hilfe des Doppelkontinuum-Ansatzes: Methodenentwicklung und Parameteridentifikation,* 1995, ISBN 3-921694-85-X, vergriffen

86 Helmig, Rainer: *Einführung in die Numerischen Methoden der Hydromechanik,* 1996, ISBN 3-921694-86-8, vergriffen

87 Cirpka, Olaf: *CONTRACT: A Numerical Tool for Contaminant Transport and Chemical Transformations - Theory and Program Documentation* -, 1996, ISBN 3-921694-87-6

88 Haberlandt, Uwe: *Stochastische Synthese und Regionalisierung des Niederschlages für Schmutzfrachtberechnungen,* 1996, ISBN 3-921694-88-4

89 Croisé, Jean: *Extraktion von flüchtigen Chemikalien aus natürlichen Lockergesteinen mittels erzwungener Luftströmung,* 1996, ISBN 3-921694-89-2, vergriffen

90 Jorde, Klaus: *Ökologisch begründete, dynamische Mindestwasserregelungen bei Ausleitungskraftwerken,* 1997, ISBN 3-921694-90-6, vergriffen

91 Helmig, Rainer: *Gekoppelte Strömungs- und Transportprozesse im Untergrund - Ein Beitrag zur Hydrosystemmodellierung-*, 1998, ISBN 3-921694-91-4

92 Emmert, Martin: *Numerische Modellierung nichtisothermer Gas-Wasser Systeme in porösen Medien*, 1997, ISBN 3-921694-92-2

93 Kern, Ulrich: *Transport von Schweb- und Schadstoffen in staugeregelten Fließgewässern am Beispiel des Neckars*, 1997, ISBN 3-921694-93-0, vergriffen

94 Förster, Georg: *Druckstoßdämpfung durch große Luftblasen in Hochpunkten von Rohrleitungen 1997*, ISBN 3-921694-94-9

95 Cirpka, Olaf: *Numerische Methoden zur Simulation des reaktiven Mehrkomponententransports im Grundwasser*, 1997, ISBN 3-921694-95-7, vergriffen

96 Färber, Arne: *Wärmetransport in der ungesättigten Bodenzone: Entwicklung einer thermischen In-situ-Sanierungstechnologie*, 1997, ISBN 3-921694-96-5

97 Betz, Christoph: *Wasserdampfdestillation von Schadstoffen im porösen Medium: Entwicklung einer thermischen In-situ-Sanierungstechnologie*, 1998, ISBN 3-921694-97-3

98 Xu, Yichun: *Numerical Modeling of Suspended Sediment Transport in Rivers*, 1998, ISBN 3-921694-98-1, vergriffen

99 Wüst, Wolfgang: *Geochemische Untersuchungen zur Sanierung CKW-kontaminierter Aquifere mit Fe(0)-Reaktionswänden,* 2000, ISBN 3-933761-02-2

100 Sheta, Hussam: *Simulation von Mehrphasenvorgängen in porösen Medien unter Einbeziehung von Hysterese-Effekten*, 2000, ISBN 3-933761-03-4

101 Ayros, Edwin: *Regionalisierung extremer Abflüsse auf der Grundlage statistischer Verfahren*, 2000, ISBN 3-933761-04-2, vergriffen

102 Huber, Ralf: *Compositional Multiphase Flow and Transport in Heterogeneous Porous Media*, 2000, ISBN 3-933761-05-0

103 Braun, Christopherus: *Ein Upscaling-Verfahren für Mehrphasenströmungen in porösen Medien*, 2000, ISBN 3-933761-06-9

104 Hofmann, Bernd: *Entwicklung eines rechnergestützten Managementsystems zur Beurteilung von Grundwasserschadensfällen,* 2000, ISBN 3-933761-07-7

105 Class, Holger: *Theorie und numerische Modellierung nichtisothermer Mehrphasenprozesse in NAPL-kontaminierten porösen Medien,* 2001, ISBN 3-933761-08-5

106 Schmidt, Reinhard: *Wasserdampf- und Heißluftinjektion zur thermischen Sanierung kontaminierter Standorte*, 2001, ISBN 3-933761-09-3

107 Reinhold Josef:, *Schadstoffextraktion mit hydraulischen Sanierungsverfahren unter Anwendung von grenzflächenaktiven Stoffen*, 2001, ISBN 3-933761-10-7

108 Schneider, Matthias: *Habitat- und Abflussmodellierung für Fließgewässer mit unscharfen Berechnungsansätzen*, 2001, ISBN 3-933761-11-5

109 Rathgeb, Andreas: *Hydrodynamische Bemessungsgrundlagen für Lockerdeckwerke an überströmbaren Erddämmen*, 2001, ISBN 3-933761-12-3

110 Lang, Stefan: *Parallele numerische Simulation instätionärer Probleme mit adaptiven Methoden auf unstrukturierten Gittern*, 2001, ISBN 3-933761-13-1

111 Appt, Jochen; Stumpp Simone: *Die Bodensee-Messkampagne 2001, IWS/CWR Lake Constance Measurement Program 2001*, 2002, ISBN 3-933761-14-X

112 Heimerl, Stephan: *Systematische Beurteilung von Wasserkraftprojekten*, 2002, ISBN 3-933761-15-8

113 Iqbal, Amin: *On the Management and Salinity Control of Drip Irrigation*, 2002, ISBN 3-933761-16-6

114 Silberhorn-Hemminger, Annette: *Modellierung von Kluftaquifersystemen: Geostatistische Analyse und deterministisch-stochastische Kluftgenerierung*, 2002, ISBN 3-933761-17-4

115 Winkler, Angela: *Prozesse des Wärme- und Stofftransports bei der In-situ-Sanierung mit festen Wärmequellen*, 2003, ISBN 3-933761-18-2

116 Marx, Walter: *Wasserkraft, Bewässerung, Umwelt - Planungs- und Bewertungsschwerpunkte der Wasserbewirtschaftung*, 2003, ISBN 3-933761-19-0

117 Hinkelmann, Reinhard: *Efficient Numerical Methods and Information-Processing Techniques in Environment Water*, 2003, ISBN 3-933761-20-4

118 Samaniego-Eguiguren, Luis Eduardo: *Hydrological Consequences of Land Use / Land Cover and Climatic Changes in Mesoscale Catchments*, 2003, ISBN 3-933761-21-2

119 Neunhäuserer, Lina: *Diskretisierungsansätze zur Modellierung von Strömungs- und Transportprozessen in geklüftet-porösen Medien*, 2003, ISBN 3-933761-22-0

120 Paul, Maren: *Simulation of Two-Phase Flow in Heterogeneous Poros Media with Adaptive Methods*, 2003, ISBN 3-933761-23-9

121 Ehret, Uwe: *Rainfall and Flood Nowcasting in Small Catchments using Weather Radar*, 2003, ISBN 3-933761-24-7

122 Haag, Ingo: *Der Sauerstoffhaushalt staugeregelter Flüsse am Beispiel des Neckars - Analysen, Experimente, Simulationen -,* 2003, ISBN 3-933761-25-5

123 Appt, Jochen: *Analysis of Basin-Scale Internal Waves in Upper Lake Constance,* 2003, ISBN 3-933761-26-3

124 Hrsg.: Schrenk, Volker; Batereau, Katrin; Barczewski, Baldur; Weber, Karolin und Koschitzky, Hans-Peter: *Symposium Ressource Fläche und VEGAS - Statuskolloquium 2003, 30. September und 1. Oktober 2003,* 2003, ISBN 3-933761-27-1

125 Omar Khalil Ouda: *Optimisation of Agricultural Water Use: A Decision Support System for the Gaza Strip,* 2003, ISBN 3-933761-28-0

126 Batereau, Katrin: *Sensorbasierte Bodenluftmessung zur Vor-Ort-Erkundung von Schadensherden im Untergrund*, 2004, ISBN 3-933761-29-8

127 Witt, Oliver: *Erosionsstabilität von Gewässersedimenten mit Auswirkung auf den Stofftransport bei Hochwasser am Beispiel ausgewählter Stauhaltungen des Oberrheins,* 2004, ISBN 3-933761-30-1

128 Jakobs, Hartmut: *Simulation nicht-isothermer Gas-Wasser-Prozesse in komplexen Kluft-Matrix-Systemen*, 2004, ISBN 3-933761-31-X

129 Li, Chen-Chien: *Deterministisch-stochastisches Berechnungskonzept zur Beurteilung der Auswirkungen erosiver Hochwasserereignisse in Flussstauhaltungen,* 2004, ISBN 3-933761-32-8

130 Reichenberger, Volker; Helmig, Rainer; Jakobs, Hartmut; Bastian, Peter; Niessner, Jennifer: *Complex Gas-Water Processes in Discrete Fracture-Matrix Systems: Upscaling, Mass-Conservative Discretization and Efficient Multilevel Solution,* 2004, ISBN 3-933761-33-6

131 Hrsg.: Barczewski, Baldur; Koschitzky, Hans-Peter; Weber, Karolin; Wege, Ralf: *VEGAS - Statuskolloquium 2004,* Tagungsband zur Veranstaltung am 05. Oktober 2004 an der Universität Stuttgart, Campus Stuttgart-Vaihingen, 2004, ISBN 3-933761-34-4

132 Asie, Kemal Jabir: *Finite Volume Models for Multiphase Multicomponent Flow through Porous Media*. 2005, ISBN 3-933761-35-2

133 Jacoub, George: *Development of a 2-D Numerical Module for Particulate Contaminant Transport in Flood Retention Reservoirs and Impounded Rivers*, 2004, ISBN 3-933761-36-0

134 Nowak, Wolfgang: *Geostatistical Methods for the Identification of Flow and Transport Parameters in the Subsurface,* 2005, ISBN 3-933761-37-9

135 Süß, Mia: *Analysis of the influence of structures and boundaries on flow and transport processes in fractured porous media*, 2005, ISBN 3-933761-38-7

136 Jose, Surabhin Chackiath: *Experimental Investigations on Longitudinal Dispersive Mixing in Heterogeneous Aquifers*, 2005, ISBN: 3-933761-39-5

137 Filiz, Fulya: *Linking Large-Scale Meteorological Conditions to Floods in Mesoscale Catchments*, 2005, ISBN 3-933761-40-9

138 Qin, Minghao: *Wirklichkeitsnahe und recheneffiziente Ermittlung von Temperatur und Spannungen bei großen RCC-Staumauern*, 2005, ISBN 3-933761-41-7

139 Kobayashi, Kenichiro: *Optimization Methods for Multiphase Systems in the Subsurface - Application to Methane Migration in Coal Mining Areas*, 2005, ISBN 3-933761-42-5

140 Rahman, Md. Arifur: *Experimental Investigations on Transverse Dispersive Mixing in Heterogeneous Porous Media*, 2005, ISBN 3-933761-43-3

141 Schrenk, Volker: *Ökobilanzen zur Bewertung von Altlastensanierungsmaßnahmen*, 2005, ISBN 3-933761-44-1

142 Hundecha, Hirpa Yeshewatesfa: *Regionalization of Parameters of a Conceptual Rainfall-Runoff Model*, 2005, ISBN: 3-933761-45-X

143 Wege, Ralf: *Untersuchungs- und Überwachungsmethoden für die Beurteilung natürlicher Selbstreinigungsprozesse im Grundwasser*, 2005, ISBN 3-933761-46-8

144 Breiting, Thomas: *Techniken und Methoden der Hydroinformatik - Modellierung von komplexen Hydrosystemen im Untergrund*, 2006, 3-933761-47-6

145 Hrsg.: Braun, Jürgen; Koschitzky, Hans-Peter; Müller, Martin: *Ressource Untergrund: 10 Jahre VEGAS: Forschung und Technologieentwicklung zum Schutz von Grundwasser und Boden,* Tagungsband zur Veranstaltung am 28. und 29. September 2005 an der Universität Stuttgart, Campus Stuttgart-Vaihingen, 2005, ISBN 3-933761-48-4

146 Rojanschi, Vlad: *Abflusskonzentration in mesoskaligen Einzugsgebieten unter Berücksichtigung des Sickerraumes,* 2006, ISBN 3-933761-49-2

147 Winkler, Nina Simone: *Optimierung der Steuerung von Hochwasserrückhaltebeckensystemen*, 2006, ISBN 3-933761-50-6

148 Wolf, Jens: *Räumlich differenzierte Modellierung der Grundwasserströmung alluvialer Aquifere für mesoskalige Einzugsgebiete*, 2006, ISBN: 3-933761-51-4

149 Kohler, Beate: *Externe Effekte der Laufwasserkraftnutzung*, 2006, ISBN: 3-933761-52-2

150 Hrsg.: Braun, Jürgen; Koschitzky, Hans-Peter; Stuhrmann, Matthias: *VEGAS-Statuskolloquium 2006,* Tagungsband zur Veranstaltung am 28. September 2006 an der Universität Stuttgart, Campus Stuttgart-Vaihingen, 2006, ISBN: 3-933761-53-0

151 Niessner, Jennifer: *Multi-Scale Modeling of Multi-Phase - Multi-Component Processes in Heterogeneous Porous Media*, 2006, ISBN: 3-933761-54-9

152 Fischer, Markus: *Beanspruchung eingeerdeter Rohrleitungen infolge Austrocknung bindiger Böden*, 2006, ISBN: 3-933761-55-7

153 Schneck, Alexander: *Optimierung der Grundwasserbewirtschaftung unter Berücksichtigung der Belange der Wasserversorgung, der Landwirtschaft und des Naturschutzes*, 2006, ISBN 3-933761-56-5

154 Das, Tapash: *The Impact of Spatial Variability of Precipitation on the Predictive Uncertainty of Hydrological Models*, 2006, ISBN: 3-933761-57-3

Die Mitteilungshefte ab dem Jahr 2005 stehen auch als pdf-Datei über die Homepage des Instituts: www.iws.uni-stuttgart.de zur Verfügung.